TURBULENT TRANSPORT OF HEAT AND MOMENTUM IN A BOUNDARY LAYER SUBJECT TO DECELERATION, SUCTION AND VARIABLE WALL TEMPERATURE

By

A. F. Orlando, R. J. Moffat and W. M. Kays

Report No. HMT-17

Prepared with Support from

The Office of Naval Research
N00014-67-A-0112-0072

and

The National Aeronautics and Space Administration
NASA NGR-05-020-134

Thermosciences Division
Department of Mechanical Engineering
Stanford University
Stanford, California

May 1974

TURBULENT TRANSPORT OF HEAT AND MOMENTUM IN A BOUNDARY LAYER SUBJECT TO DECELERATION, SUCTION AND VARIABLE WALL TEMPERATURE

By

A. F. Orlando, R. J. Moffat and W. M. Kays

Report No. HMT-17

Prepared with Support from

The Office of Naval Research
N00014-67-A-0112-0072

and

The National Aeronautics and Space Administration

NASA NGR-05-020-134

Thermosciences Division
Department of Mechanical Engineering
Stanford University
Stanford, California

May 1974

ACKNOWLEDGMENTS

This research was made possible by assistance from three sources, each of which contributed in an important way.

First, the National Aeronautics and Space Administration whose funds (NASA NGR-05-020-134) supported the basic research facility, HMT-1: the smooth porous plate heat transfer apparatus. The interest of Dr. Robert W. Graham of the NASA Lewis Laboratories is gratefully acknowledged.

Second, the Office of Naval Research which provided funds (N00014-67-A-0112-0072) for the instrumentation needed to make these detailed studies of turbulent structure, and for operating costs during the program. The support of Mr. James Patton and Dr. Ralph Roberts, in this fundamental study, made these detailed measurements possible. It is hoped that the techniques developed herein will continue to be of use.

Finally, but of great personal importance to the first author; the National Research Council of Brazil (CONSELHO NACIONAL DE PESQUISAS) provided the financial support for him during his stay at Stanford University. This sponsorship is appreciated for having contributed, in a significant way, to his professional profile.

The authors appreciate the experienced counsel of Dr. J. P. Johnston who made available his expertise in turbulent boundary layer modeling and served as a critical reviewer of the work.

Mr. Marcos Pimenta must be singled out, among colleagues of the Heat and Mass Transfer Group, for his tireless efforts both during the conceptual development of the material, and during the final writing and production of this report.

Robin Birch developed the design of the rotatable probe holders and fabricated the probes and supports with infinite care.

In the last hectic days of assembling this report both Jan Moffat and Ruth Korb worked late into the night to make the deadlines --- far beyond the call of duty.

ABSTRACT

The objective of this work was the study of the relationship between the turbulent transport of heat and momentum in an adverse pressure gradient boundary layer. An experimental study was conducted of turbulent boundary layers subject to strong adverse pressure gradients with suction. Near-equilibrium flows were attained, evidenced by outer-region similarity in terms of defect temperature and defect velocity profiles.

The relationship between Stanton number and enthalpy thickness was shown to be the same as for a flat plate flow both for constant wall temperature boundary conditions and for steps in wall temperature. The superposition principle used with the step-wall-temperature experimental result was shown to accurately predict the Stanton number variation for two cases of arbitrarily varying wall temperature.

The Reynolds stress tensor components were measured for strong adverse pressure gradient conditions and different suction rates. Two peaks of turbulence intensity were found: one in the inner and one in the outer regions. The outer peak is shown to be displaced outward by an adverse pressure gradient and suppressed by suction.

The correlation coefficient and the ratio between the turbulent shear stress and the turbulent kinetic energy are shown to be constant and independent of pressure gradient and transpiration rate in the outer region of the boundary layer under nearly equilibrium conditions.

Temperature fluctuation and turbulent heat transfer were measured directly using the same probe used for the velocity fluctuations. The turbulent Prandtl number was then calculated directly from the turbulence and the mean profile measurements without the usual position error sensitivity. High values at the wall and low values in the outer region were measured, in accordance therefore, with some accepted studies.

A new procedure was developed to estimate the turbulent Prandtl number at the wall based on extrapolations of data near the wall. An adverse pressure gradient is shown to increase the turbulent Prandtl number at the wall while suction, on the other hand, is shown to decrease it.

Table of Contents

Table of Contents (cont.)

Table of Contents (cont.)

List of Figures

List of Figures (cont.)

Chapter 6

List of Figures (cont.)

LIST OF TABLES

NOMENCLATURE

A	Van Driest length scale.
A^+	Van Driest length scale (dimensionless) = Au_τ/ν.
A_G	Cross section area of gold plated portion of wire.
A_T	Cross section area of tungsten wire.
B	Heat transfer length scale
B^+	Heat transfer length scale = Bu_τ/ν.
B_f	Blowing parameter = $F/(C_f/2) = \rho_\infty v_o U_\infty/\tau_o$.
B_h	Heat transfer blowing parameter = F/St
C_p	Specific heat at constant pressure
$C_f/2$	Friction coefficient $\tau_o/\rho_\infty U_\infty^2$.
D	Diameter of wire.
D_G	Diameter of the gold plated portion of the wire
D_T	Diameter of the tungsten wire.
E	Output from anemometer.
e'	Fluctuating value, output from anemometer.
F	Blowing fraction = v_o/U_∞.
G	Clauser shape factor, Eq. 2.4.
G_h	Δ_4/Δ_3.
h	Heat transfer coefficient.
κ	Karman constant.
K	Acceleration parameter = $(\nu/U_\infty^2)\times(dU_\infty/dx)$.
K_T	Thermal conductivity of tungsten wire.
K_G	Thermal conductivity of gold.
L	Length of wire
ℓ	Unheated length; also mixing-length.
P	Static pressure.
Pr	Molecular Prandtl number.
P_o	Free stream static pressure
$P+$	$\nu/\rho_\infty U_\tau^3 \times d\rho/dx$.
Pr_t	Turbulent Prandtl number, $\varepsilon_M/\varepsilon_H$.
$\dot{q}_o''$	Heat flux at the wall.
$\overline{q^2}$	Turbulent kinetic energy = $\overline{u'^2} + \overline{v'^2} + \overline{w'^2}$.
Re_{Δ_T}	Enthalpy thickness Reynolds number = $U_\infty\Delta_T/\nu$.

R	Wire resistance.
R_G	Resistance of gold plated part of the wire.
R_T	Resistance of tungsten wire.
R_w	Average resistance of wire.
St	Stanton number = $\dot{q}_o''/\rho_\infty U_\infty (T_w - T_\infty) c_p$.
St_o	Stanton number, no transpiration.
St_T	Stanton number, isothermal plate.
St_{o_T}	Stanton number, isothermal plate, no transpiration.
T_w	Wire temperature, wall temperature.
T	Mean local temperature.
T_∞	Free stream temperature.
T^+	$\overline{T}\sqrt{C_f/2}/St$.
$\overline{T}$	$(T-T_w)/(T_\infty - T_w)$.
T_τ	$(T_o - T_\infty) St/\sqrt{C_f/2}$.
t'	Fluctuating temperature.
t'_∞	Fluctuating free stream temperature.
t'_m	Fluctuating average wire temperature.
T_m	Average wire temperature.
t	Time.
u	Local velocity, instantaneous value.
$\overline{u}$	Local velocity, average value.
U_∞	Free stream velocity.
u_τ	Friction velocity = $U_\infty \sqrt{C_f/2}$.
u'	Fluctuating longitudinal velocity.
$\overline{u'v'}$	Turbulent shear stress.
U_{eff}	Effective velocity (the velocity the wire "sees").
u^+	u/u_τ .
$\overline{u't'}$	Longitudinal velocity-temperature correlation.
$\overline{u'w'}$	Longitudinal-tangential velocity correlation.
U'_{eff}	Fluctuating effective velocity.

v	Normal velocity, instantaneous value.
$\bar{v}$	Normal velocity, average value.
v_o	Normal velocity at the wall.
v'	Fluctuating normal velocity.
$\overline{v't'}$	Normal velocity-temperature correlation.
v_o^+	v_o/u_τ .
$\overline{v'w'}$	Normal-tangential velocity correlation.
x	Stream wise coordinate.
x_o	Virtual origin of momentum boundary layer.
w	Tangential velocity, instantaneous value.
$\bar{w}$	Tangential velocity, average value.
w'	Fluctuating tangential velocity.
$\overline{w't'}$	Tangential velocity-temperature correlation.
y	Normal coordinate.
y^+	yu_τ/ν .
z	Transverse coordinate.

<u>Greek</u>

α	Thermal diffusivity = $k/\rho c_p$
β	Eq. 2.5.
Δ	Clauser boundary layer thickness, Eq. 2.2.
Δ_T	Enthalpy thickness = $\int_o^\infty \frac{\rho\bar{u}}{\rho_\infty U_\infty} \frac{T - T_\infty}{T_w - T_\infty} dy$.
Δ_3	Eq. 2.8.
Δ_4	Eq. 2.8
δ	Momentum boundary layer thickness $\bar{u}(\delta) = 0.99\ U_\infty$.
δ_T	Thermal boundary layer thickness $(T-T_w)/(T_\infty-T_w) = 0.99$.
δ_1	Displacement thickness = $\int_o^\infty \left(1 - \frac{\bar{u}}{U_\infty}\right) dy$.
δ_2	Momentum thickness = $\int_o^\infty \frac{\rho\bar{u}}{\rho_\infty U_\infty}\left(1 - \frac{\bar{u}}{U_\infty}\right) dy$.
ε_M	Eddy diffusivity for momentum = $-\overline{u'v'}/(\partial\bar{u}/\partial y)$
ε_H	Eddy diffusivity for heat = $-v't'/(\partial T/\partial y)$.

μ	Dynamic viscosity.
ν	Kinematic viscosity = μ/ρ .
ρ	Local density.
ρ_∞	Free stream density.

CHAPTER 1

INTRODUCTION AND OBJECTIVES

It is presently not possible to predict, with the desired accuracy, boundary layers subjected to arbitrary variations of free stream velocity, wall temperature and transpiration. Much progress has been made in the past few years, with the increasing use of finite difference computer programs capable of predicting the velocity and temperature distributions inside the boundary layer. These programs require, for closure, a structural model of the turbulent mixing process and some function relating the transport of energy to the transport of momentum. One currently successful approach uses a mixing length model for turbulence and a turbulent Prandtl number function. Others use the turbulent kinetic energy to predict the mixing, still others deal directly with the effective "stresses" induced by the turbulence. These models can most easily be developed by examination of large bodies of coherent data: data taken by following a "rational path" through the wide field of possible combinations of velocity, transpiration and wall temperature. Popular paths include "constant velocity flows", "equilibrium decelerations", and "asymptotic accelerations". Transpiration is adjusted to provide either "uniform blowing parameter" or "uniform blowing velocity" along the surface. From such data sets are drawn the values of the constants used in the predictive programs. The test of the validity of the programs comes from attempting to predict results not included within the data sets which were used in evaluating the constants: runs with steps in wall temperature, non-equilibrium decelerations, and arbitrary variations in transpiration.

The Heat and Mass Transfer Group at Stanford has been engaged for some time in studies of the momentum and heat transfer behavior of turbulent boundary layers, aimed at generating data in both classes: predictive and "test cases". Moffat [1] built the experimental facility to allow measurements in two-dimensional boundary layers and obtained measurements of Stanton numbers for zero pressure gradient flows with both blowing and suction within the limits of boundary layer behavior. Simpson [2] studied the hydrodynamic behavior of zero pressure gradient flows and Whitten [3] the heat transfer behavior for variable transpiration and wall temperature conditions. Julien [4] and Thielbahr [6] investigated moderate accelerations (asymptotic boundary layer flows) and Loyd [5] and Kearney [7] studied strong accelerations. Most recently, attention was turned to decelerating flows with Andersen [8] and Blackwell [9] dealing with mild adverse pressure gradients. From all of this work has come a wealth of data for developing operational models for the turbulent transport of heat and momentum. Incorporated into a finite difference computer program based on the Spalding-Patankar method, these models have been refined by challenges from other data from pipe flows, and from rocket nozzle data, mostly from accelerating or, at most, mildly decelerating flows.

The area of adverse pressure gradients with transpiration has not been investigated previously except for one study by McLean [57]. McLean investigated strong adverse pressure gradients with blowing, with primary emphasis on the onset of separation. The free stream velocity in these experiments was decreased linearly in the streamwise direction. Velocity profiles were measured with pitot probes and skin friction determined using Stevenson's [58] law of the wall. Stanton numbers were reported, but no temperature profiles. Such a data set is useful as a check on the ability of a model to predict Stanton numbers but the absence of temperature profiles makes it difficult to use the data to refine the model. Stanton number data alone are not sufficient to resolve problems with most models. Since finite difference prediction schemes predict mean velocity and temperature profiles, such data are needed to confirm these predictions. If prediction schemes using more than simple mixing length theory for closure are to be developed, then additional information about the turbulent structure of the boundary layer is required to develop the new models.

The present study has three main objectives related to the general problem of predicting turbulent boundary layer heat transfer: (1) extension of the body of hydrodynamic and heat transfer data into the area of strong decelerations, (2) development of a model for predicting the effect of the adverse pressure gradient on the turbulent Prandtl number in the near wall region, and (3) development of an improved experimental technique for studying temperature and velocity fluctuations in the boundary layer.

Particular emphasis was placed upon the development of new experimental techniques for evaluating the turbulent transports of momentum and energy. It appears likely that the "next generation" of turbulence models will lean heavily upon the stationary statistical properties of the turbulence and such data are difficult to acquire. The "present generation" has great need of more reliable data regarding turbulent Prandtl number in the near wall region.

The intermediate steps for carrying out this program are as follows:

(1) Provide Stanton number data for constant wall and step in wall temperature conditions, for a nearly equilibrium flow behavior, that would be used as a reliable source of comparisons for turbulent boundary layer prediction methods.

(2) Develop a model that would allow one to predict the Stanton number under different free stream adverse pressure gradient and transpiration rate conditions, for an arbitrary variation of the wall temperature.

(3) Develop the technique to allow the simultaneous measurement of mean temperature and velocity, with just one probe.

(4) Provide data on mean temperature and velocity for flows under strong free stream adverse pressure gradient and transpiration rate conditions.

(5) Provide data and the analysis of the hydrodynamic turbulence structure of nearly equilibrium decelerating flows.

(6) Provide data and the analysis of the direct measurement of the turbulent heat transfer and temperature fluctuation for nearly equilibrium flow conditions.

(7) Develop a measurement procedure to allow the turbulent Prandtl number at the wall to be estimated and investigate its behavior in the neighborhood of the wall.

(8) Provide the turbulent Prandtl number data from direct measurement of the turbulent transport of momentum and heat.

CHAPTER 2

EXPERIMENTAL BOUNDARY CONDITIONS

The objective of the experimental part of this investigation was to examine the mechanisms of the transport of momentum and energy in a transpired turbulent boundary layer under strong adverse pressure gradient conditions, including some effects of an arbitrary wall temperature distribution.

The experimental program was carried out on the Stanford Heat and Mass Transfer apparatus, which has been modified by Andersen [8] and Blackwell [9] to permit the establishment and accurate control of an adverse pressure gradient. The wall temperature control, however, is the same as used by Moffat [1].

This investigation was limited to low-speed, nearly constant property flows, with the transpiration fluid the same as the free stream (air). Hydrodynamic boundary conditions leading to strong deviations from "equilibrium" (for example, steps in the pressure gradient or in the transpiration rate) were not considered, nor were adverse pressure gradient conditions strong enough to cause separation. The energy transport portion of the problem was studied, in part, by imposing strong departures from "thermal equilibrium": steps in wall temperature were applied and used to generate the kernel function for superposition solutions to the arbitrary wall temperature distribution problem. Only heat transfer coefficients were measured for this non-equilibrium condition -- no profiles. Extensive profile measurements, both mean and fluctuating, were taken for the constant wall temperature conditions. The wall-to-free-stream temperature difference used in the measurements was small (20-30°F) and, therefore, nearly constant property flows were obtained. The maximum free-stream-to-wall density ratio was about 1.04.

2.1 The Concept of Equilibrium Flows

Because the temperature field depends on the velocity field, it is natural to analyze the momentum boundary layer first when attention is given to the establishment of an equilibrium momentum and thermal boundary layer.

The outer 90% region of the turbulent boundary layer is known to react more slowly than the inner wall region to changes in the boundary conditions. In fact, the wall region may be considered to be always in equilibrium, in the sense that only local values of the pressure gradient and transpiration rate are important. The outer region, on the other hand, shows a pronounced history effect. Information from upstream stations is important in determining the hydrodynamic behavior in the outer region.

The constant pressure layer has been known, for a long time, to possess both inner and outer region similarity, respectively known as the "law of the wall" and the "velocity defect law".

The velocity defect, $-(U_\infty-\overline{u})/u_\tau$, is a similarity variable for the outer region of the constant pressure boundary layer if plotted against y/δ. The outer $\simeq$ 90% of the boundary layer has a unique shape (independent of the Reynolds number) when plotted this way. Thus,

$$- \frac{U_\infty-\overline{u}}{u_\tau} = F\left(\frac{y}{\delta}\right) \tag{2.1}$$

represents a defect law for the zero pressure gradient boundary layer (δ is the boundary layer thickness).

Clauser [27], in 1954, considered the problem of similarity in turbulent boundary layers. His idea was to extend the concept of similarity to include turbulent boundary layers in adverse pressure gradient. He succeeded in experimentally creating adverse pressure gradient boundary layers with a defect similarity just as in the case of the zero pressure gradient boundary layer -- "equilibrium boundary layers".

Clauser defined a new boundary layer thickness, Δ, such that

$$\Delta = \delta \int_0^1 \frac{U_\infty-\overline{u}}{u_\tau}\, d\left(\frac{y}{\delta}\right) . \tag{2.2}$$

When the boundary layer has outer region similarity, the Clauser thickness Δ is a constant factor times δ, the boundary layer thickness, which is difficult to measure. Because of the fact that Δ can be more precisely determined from experimental data than δ, the defect law will be written as

$$-\frac{U_\infty-\bar{u}}{u_\tau} = F\left(\frac{y}{\Delta}\right) \quad . \tag{2.3}$$

Clauser then defined a shape factor for equilibrium velocity profiles as

$$G = \frac{\delta}{\Delta}\int_0^1 \left[\frac{U_\infty-\bar{u}}{u_\tau}\right]^2 d\left(\frac{y}{\delta}\right) \tag{2.4}$$

and reasoned that in such flows the ratio of the wall shear force and the pressure force acting on the boundary layer is constant. This condition implies that

$$\beta = \frac{\delta_1}{\tau_o}\frac{dp}{dx} = \text{constant} \quad . \tag{2.5}$$

Bradshaw [28] found that such an adverse equilibrium pressure gradient flow corresponds, experimentally, to a decreasing free-stream velocity in which $U_\infty \propto x^m$ $(m < 0)$.

Anderson [8] extended the concept of equilibrium flows to include transpiration based on the momentum integral equation, written in Bradshaw's form as

$$\frac{d}{dx}\left(\delta_2 U_\infty^2\right) = \frac{\tau_o}{\rho}\,(1 + \beta + B_f) \quad . \tag{2.6}$$

The conditions to give equilibrium flows are constant β <u>and</u> constant B_f, where $B_f = 2F/C_f$ (the Blowing Parameter).

The constant β condition is satisfied by setting the free-stream velocity so that $U_\infty \propto x^m$. The constant B_f condition is satisfied by setting $F \propto x^{m_f}$, where $F = \rho_o v_o/\rho_\infty U_\infty$ and m_f is dependent on m. Boundary layers in flows adjusted in this way have been experimentally shown to display similarity (Anderson [8]).

Blackwell [9] approached the problem of equilibrium thermal boundary layers by defining a defect enthalpy law which can be written, for a constant properties flow, as:

$$T_\infty^+ - T^+ = f_2(y/\delta_T) \quad , \tag{2.7}$$

where δ_T is the thermal boundary layer thickness. Following the same line as Clauser [27], the thickness parameters Δ_3 and Δ_4 were defined

$$\begin{aligned} \Delta_3 &= \delta_T \int_0^1 \left(T_\infty^+ - T^+\right) d(y/\delta_T) \\ \Delta_4 &= \delta_T \int_0^1 \left(T_\infty^+ - T^+\right)^2 d(y/\delta_T) \quad . \end{aligned} \tag{2.8}$$

When the thermal boundary layer has an outer region similarity, the thickness Δ_3 is a constant times δ_T, which is as hard to measure as was δ. As in the case of momentum boundary layers, Δ_3 can be experimentally determined more accurately, and the defect enthalpy law will be written as

$$T_\infty^+ - T^+ = F_2(y/\Delta_3) \quad . \tag{2.9}$$

The defect enthalpy profile shape factor is then defined as

$$G_h = \frac{\Delta_4}{\Delta_3} \quad .$$

If outer-layer similarity exists, then G_h is approximately constant.

Blackwell [9] also investigated conditions leading to equilibrium thermal layers. The energy integral equation for two-dimensional incompressible flows can be written in terms of the enthalpy thickness, Δ_T, as:

$$\frac{d}{dx}\left(\rho_\infty U_\infty c_p (T_w - T_\infty)\Delta_T\right) = \dot{q}_o''(1 + B_h) \quad , \tag{2.10}$$

where $B_h = F/St$, the heat transfer parameter.

A necessary condition for thermal equilibrium is a constant B_h, which can be achieved, as shown by Blackwell [9], by setting $U_\infty \propto x^m$ and $F \propto x^{m_f}$.

2.2 Boundary Conditions on U_∞ and F for the Structural Studies

Two different velocity distributions and four different transpiration rates were used in the studies of the turbulence structure. Taking the free-stream velocity variations to be given as

$$U_\infty = \bar{u}_1 \left(\frac{x - x_o}{x_1 - x_o}\right)^m \tag{2.11}$$

and

$$F = F_1 \left(\frac{x - x_o}{x_1 - x_o}\right)^{m_F} , \tag{2.12}$$

the flows can be summarized as in Table 2.2.1 .

Table 2.2.1

Summary of the Boundary Conditions Used

m	$\bar{u}_1$ ft/sec	F_1	m_F	x_o (in)	x_1 (in)
0.000	31.5	0.00	0.00	–	–
-0.275	30.1	0.000	0.000	-3	-4
		-0.001	0.000		
		-0.002	0.000		
		-0.004	0.000		

Only two flows ($m = 0$, $F = 0$ and $m = -0.275$, $F = 0$) are truly in hydrodynamic equilibrium. Constant F flows such as these are not truly equilibrium flows but tend to behave very well, since B_f changes so slowly along the surface that a "local equilibrium" seems to prevail (Whitten [3]).

2.3 Boundary Conditions on T_{wall} and F for the Step Wall Temperature Studies

Mean temperature, velocity, and turbulent profiles were taken for constant wall temperature conditions for each of the previously tabulated sets of conditions. A separate series of conditions was used for the step wall temperature tests in which the step in wall temperature was fixed at plate 10 (38 inches downstream).

Several cases were examined, as indicated by Table 2.3.1.

Table 2.3.1

Nominal Pressure Gradient and Transpiration Rates Studied with a Step in Wall Temperature Applied at Plate 10 (38 inches)

m	F_1	m_f
0.00	0.000	---
	0.000	
-0.15	+0.001	0.00
	+0.002	
	+0.004	
	0.000	
-0.275	-0.001	0.000
	-0.002	
	-0.004	

Two additional cases ($m = -0.15$, $F_1 = 0$; $m = -0.275$, $F_1 = 0.004$) were run with an arbitrary wall temperature distribution to test predictive capability, using the information obtained from the step wall temperature cases.

2.4 Identification of the Boundary Conditions

From the previous sections, it is obvious that the three parameters (m, F_1, m_F) nominally describe the pressure gradient and transpiration boundary condition. Therefore, each run will be identified by these three parameters. The designation of m_F, however, will be omitted in these runs because no constant B_F flows were examined. The run designation (-0.275, -0.004) will indicate $U_\infty \sim x^{-0.275}$, $F_1 = -0.004$.

CHAPTER 3

EXPERIMENTAL APPARATUS, INSTRUMENTATION AND QUALIFICATION TESTS

The basic apparatus used in this study was an open loop wind tunnel first described by Moffat [1]. It was originally designed for zero pressure gradient studies of the transpired turbulent boundary layer, and the description of subsequent modifications can be found in References [2] - [9]. The most relevant modification consisted of a new design for the upper surface of the test channel for the study of decelerating flows, as described by Andersen [8] and Blackwell [9]. Only a brief description will be given below, references being made to Fig. 3.1.

3.1 Main Air Flow

The main air flow enters the filter box, made of a 0.7 micron retention felt-type material. The main air blower is of the centrifugal type and has a 2000 scfm capacity at 30 inches of water. The flow turning header was designed to provide a uniform velocity across the face of the heat exchanger. Honeycomb is placed both upstream and downstream of the heat exchanger which is supplied with cooling water from the Stanford University water system. Since this heat exchanger has a very high effectiveness, any fluctuations in cooling water temperature would cause fluctuations in the test section air temperature. It was found that during evenings and weekends, the drift in mainstream temperature was less than 0.1°F per hour. For the measurement of turbulent quantities, a four hour period was usually required and a drift of 0.3°F at most was observed, although some measurements were taken with only a 0.1°F drift.

After leaving the heat exchanger, the main flow air passes through a 1.5 in. thick honeycomb with 3/16 in. cell size. Following the honeycomb and located in a constant area section 23 x 23 inches there are six 32 x 32 mesh stainless steel screens. The function of this set of screens is to reduce spanwise non-uniformities in dynamic pressure. It is well known that even a slight crease in a screen can considerably affect the uniformity of the flow through the screen, so these screens received careful attention.

Following the screen pack, the flow enters a 4:1 contraction (over 26 inches) nozzle which provides an almost two dimensional contraction to the 6 x 20 inch outlet. The nozzle is symmetric about both the vertical and the horizontal planes, with the contraction taking place primarily in the vertical dimension. Andersen [8] and Blackwell [9] found a separation bubble in the inlet of the nozzle, and the nozzle shape was modified to provide an initial contracting angle of approximately 5° downstream of the last screen. This eliminated the separation.

At the exit of the nozzle, a 3/16 inch wide slot was cut through the bottom and the side walls of the nozzle. Since the static pressure in the tunnel is slightly above atmospheric, this acts as a suction slot and removes the boundary layer that develops in the nozzle. To insure a fully turbulent profile at the first test plate, a 1/32 inch high by 1/4 inch wide boundary layer trip was located upstream of the first test plate. There were no trips on the side or top walls.

3.2 Test Section

The test section consists of a 6 x 20 inch rectangular cross section duct 8 feet in length. The side walls are 1/2 inch plexiglass, the top is 5/16 inch aluminum tool plate, and the bottom wall (the actual test surface) is porous sintered bronze.

One of the side walls contains static pressure taps, which are used in conjunction with Kiel probes for free stream velocity determination. The side wall static pressure taps are 0.040 inch diameter with sharp edges and are spaced two inches apart in the streamwise direction. The distance above the bottom wall test surface is 1 inch. Every 12 inches in the streamwise direction four additional pressure taps are provided at 2,3,4, and 5 inches above the test surface, on each side wall. The function of these vertical columns of pressure taps is to check the static pressure uniformity in the vertical and transverse directions. The side-to-side static pressure variation was found to be less than 0.002 inches of water. The pressure variation in the vertical direction was less than 0.001 inches of water, which is also the accuracy of the pressure measuring system. The static pressure taps are evident in Fig. 3.2.

The bottom wall of the test section consists of 24 individual porous plates mounted in four separate aluminum base castings. Each plate is thermally isolated from the base casting and its neighboring plates. The physical characteristics of the plates are as follows:

Material - sintered bronze

Dimensions - 18.0 x 3.975 x 0.25 inches

Particles - spherical, varying in diameter in the range 0.002 - 0.007 inches

Porosity - approximately 40%, uniform within $\pm$ 6% in center 6-inch section

Roughness - maximum of 200 microinches (RMS) measured with a stylus of 0.0005 inch radius

Thermal Conductivity - 6.5 Btu/hr-ft-°F, minimum

Surface Emittance - 0.37 average

Plate temperatures are monitored by five iron/constantan thermocouples, each located 0.040 inches below the surface. The spacing of the plate thermocouples is shown in Fig. 3.3 . Each plate is electrically heated by nichrome wires located in grooves on the underside of the plate. The power supplied to each plate is individually controlled by a rheostat. This allows one to vary the power to each plate individually to maintain a uniform surface temperature.

The upper wall of the test section is used to control the pressure gradient. It consists of a series of 24 aluminum plates, each 5/6 inch thick by 3.5 inches wide. These plates are arranged on top of the side walls such that there is a 1/2 inch space (in the flow direction) between adjacent plates. Each of the 23 resulting 1/2 inch wide slots is partially covered by two 1/2 inch thick aluminum bars. One of these bars is permanently fixed to the 3.5 inch plate, while the other bar is allowed to move relative to the fixed bar. The result is to form a slot whose width can be varied between 0 and 0.4 inches. A side view of the tunnel with the slot arrangement is shown in Fig. 3.4 . The slot width can be set to the desired width within 0.001 inches. Wing nuts are used to keep the movable bar in place once the slot width has been set.

The test section is extended 14 inches past the last heated plate by a projecting shelf which plays no role in the experiment other than to present "clean" flow on the last plate. A movable gate slides up and down vertically across this extension piece. This gate, plus the throttle valve at the main stream air blower are used to control the main stream air flow rate. The function of this extension is to insure that the influence of the sliding gate valve is not appreciably felt at the last test station.

3.3 Transpiration Air System

The transpiration air system is quite similar to the main air system. The main difference is that after leaving the transpiration blower the air goes to a header and then to 24 individually calibrated pairs of rotameters. The air supplied to a given plate can be routed to one of two rotameters, depending on the magnitude of the flow rate. By using the two rotameters in parallel, flow rates in the range of 0.5 to 18 scfm can be measured. Each of these 48 rotameters was individually calibrated by Kearney [7]. A typical transpiration compartment and plate assembly is shown in Fig. 3.5 .

3.4 Pressure Measurement

All pressure measurements were made with a Statham PM-97 unbonded strain gauge differential pressure transducer for pressures in the range 0 - 1.4 inches of water. The Wheatstone bridge was excited by a stable Hewlett-Packard model 6213 DC power supply. The output voltage from the pressure transducer was read by an integrating digital voltmeter, Hewlett-Packard Model 2401C. An external quartz oscillator time base generator was used to give an integration time of 10 seconds. The transducer was calibrated at regular intervals against a MERIAM micromanometer model 34FB2. The calibration curve was found to be linear and stable to $\pm$ 0.001 inches of water.

3.5 Procedure for Setting Up a New Run

The setting-up of a new run to a specified free-stream velocity, transpiration boundary condition and wall temperature is an iterative procedure. For the first trial the flow field is left isothermal, that is, the plates are not heated. From a statement of the desired velocity distribution (given in terms of the values of free stream pressure gradient and the velocity at the beginning of the test section) a computer program, Slot [8], supplies the desired dynamic pressure distribution. The total and static pressure at $x = 2$ inches are held constant during the course of the iterations. The rotameter readings (in case transpiration is used) and the slot widths are reset at each iterative cycle, again with the help of the above mentioned computer program. On the basis of the measured distribution of dynamic pressures, the total pressure and the rotameter settings, a correction is computed so that resetting would result in attainment of the desired boundary conditions. As a practical matter the iterations were discontinued when Slot predicted changes in slot width of 0.001 inches or less. The acceleration parameter K, could be set at a desired value within about 3% by comparing the measured value to the desired value and iterating.

After having set up the rig for hydrodynamic conditions, the plates were heated and the power to them iteratively adjusted to obtain a constant plate temperature within $\pm$ 0.25°F. Due to the small wall-to-free-stream temperature difference (20-30°F), no significant deviation from the originally set up hydrodynamic conditions was observed within the uncertainty of the measurements. The hydrodynamic and thermal conditions were reset at the beginning of each data taking procedure, to compensate for any ambient condition drift.

All free stream velocities were measured with a pitot probe, and the free stream temperature was measured with a calibrated iron-constantan thermocouple. However, both velocity and temperature inside the boundary layer were measured with a resistance thermometry approach, as indicated in the following section.

3.6 Sequential Measurement of Mean Velocity and Temperature

Prior studies in this series have relied mainly upon isothermal hydrodynamic data used with temperature profile data from a nominally identical run, except for the heated wall. This has introduced problems of two sorts into the structural studies of turbulent heat transfer: first, the position uncertainty inherent in overlaying the two profiles and, second, the possibility of changes in the shapes of the profiles caused by variable properties effects. Most of the prior work in this series has used a 20 to 30°F difference between wall and free stream temperature. This corresponds typically to a maximum density ratio, $\overline{\rho}_\infty/\overline{\rho}_o$, of about 1.04 hence has required considerably care in combining the isothermal hydrodynamic data with the hot wall temperature profiles. Thielbahr [6] investigated both experimentally and numerically the question of which one of the following candidates would be most nearly preserved: $\overline{u}/U_\infty$, $\overline{\rho u}/\rho_\infty U_\infty$, or $\overline{\rho u^2}/\rho_\infty U_\infty^2$. He found that the minimum error in integral parameters was achieved by assuming the preservation of $\overline{u}/U_\infty$. Thus the variable properties effect is under reasonable control. The position uncertainty arises because of the need to interpolate in one of the two data sets (T or $\overline{u}$) to obtain corresponding data. The uncertainty in locating either probe can give appreciable errors, close to the wall. If the first data point is 0.005 inches from the wall, then an error of only 0.0005 inches yields a 10% position error. When y-derivatives are to be compared, such errors are important.

These problems were solved in the present program by measuring the velocity and temperature sequentially with the same hot wire probe: first, the velocity was measured using a constant temperature anemometer, then the temperature was measured by switching to a constant current anemometer using the same probe as a resistance thermometer.

This sequential measurement of velocity and temperature eliminated the need for overlaying an isothermal velocity profile onto the temperature profile.

The proposal seems straightforward and initially it was believed that the DISA 55D01 anemometer would be able to perform both measurements using one chassis since it can be operated in either the constant temperature mode (for velocity measurements) or the constant current mode (for temperature measurements). The amplifier drift in the constant current mode, however, limits the accuracy of mean temperature measurement, even though this does not constitute a problem for temperature fluctuation measurement. Equally important, however, is the fact that both modes of operation use the same Wheatstone bridge and different currents are used (40-60 ma for constant temperature, 3 ma for constant current). Because of the change in bridge current the re-stabilizing of the system after switching from one mode to the other, requires a long waiting time. This problem is particularly important when taking a 30-40 point profile: the waiting time can be prohibitive.

The solution to this problem is the use of two anemometers. A 55D01 system was used as a constant temperature anemometer with a 55M system operated in the constant current mode. This new 55M unit has a temperature controlled input transistor in the first stage of amplification, and both the noise level and the amplifier drift are greatly reduced. Very high gains can be used, increasing greatly the sensitivity for temperature measurements.

Very low probe currents (2 ma with a 5 micron tungsten wire; 0.1 ma with a 1 micron platinum wire) can be used and the velocity contamination in the anemometer response for mean temperature measurement can be virtually eliminated.

The final stage of the measuring system is the coupling between the two anemometers. The DISA 55D65 Probe selector with very low contact resistance can be used. This unit was initially designed to allow several probes to be used with one anemometer; an inversion of the connections had to be made to use two anemometers and just one probe.

3.7 Hot Wire Instrumentation - Choice of the Probe for Mean Temperature and Velocity Measurement

Ideally an infinitely long wire would be the indicated one for mean velocity and mean temperature measurements in a 2-dimensional flow. The wire diameter, however, must be small if a good frequency response is to be obtained. This limits the wire length for strength reasons. For velocity measurements, a short length of wire has the disadvantage that it responds to the aerodynamic interference of its supports [11]. In the temperature measuring mode, deviation from the calibration curve can be caused by a non-uniform temperature distribution along the wire, the deviation being a function of the fluid velocity and the wire current [10].

The DISA 55F04 5 micron boundary layer probe meets the requirement of minimum aerodynamic interference. The wire is 3 mm long, gold plated to a diameter of 6 times its sensitive portion (about 1.2 mm long) for strengthening reasons. Although this was not the original purpose, it can be used for temperature measurement. According to Maye [10], this larger portion has practically no influence on the measured resistance and therefore on the probe sensitivity. Being located on the same isotherm as the sensing wire and having a diameter smaller than the prong diameter it can contribute effectively towards lowering the conduction between the sensing wire and the prongs. Appendix A describes a conduction error analysis when the wire is operated at very low currents, and used as a resistance thermometer.

The sensitivity of the wire is another important factor for temperature measurement. The highest possible wire current must be chosen, but it cannot be large enough so that the heat loss from the wire becomes appreciable. With a high amplifier gain (3500) and a very low current (2 ma), a good signal was obtained with the 55M system with a very high signal-to-noise ratio and very low drift.

Another factor to be taken into consideration is the position of the probe prongs with respect to the mean flow direction. Thinh [12] reports that the inclination giving the correct values (minimum aerodynamic interference) corresponds to a support placed parallel to the direction of the mean flow. Maye [10] reports that the prongs must be long and pointed, and located in the isothermal plane passing through the wire, if minimum conduction errors are desired when measuring temperature.

The shape of the 5 micron boundary layer type probe used in this investigation permits measurements to be taken very close to the wall (0.005 in.) and meets the above requirements.

Mean velocity and mean temperature measurements were performed using the system described in Section 3.6. The output from the two anemometers was read by a VIDAR 5206 D-DAS Data Acquisition System employing a D.E.C. PDP 8/L computer. It uses a VIDAR digital voltmeter with a very high input impedance (larger than 10 megohms). The sampling period was 0.167 seconds and the data taking was programmed with a variable integration time to provide an average value of the signal from the anemometer which was steady to within $\pm$ 1 mv out of a 3 volt output. This corresponds, for velocity, to less than 0.1 ft/sec at the lowest sensitivity. For temperature, this corresponds to 0.02°F. Very close to the wall an integration time higher than 10 seconds was required; in the outer region only a few seconds were needed.

The hot wire probe and its support are sketched in Fig. 3.6. The only difference between it and Andersen's probe [8] is the wire element. The probe has a "wall stop" that effectively prevents the wire from accidentally being damaged by the wall. The wire distance from the wall, when the wall stop touches it, was measured by an optical comparator and set nominally to 0.005 inches. As observed by Andersen [8], the probe stem position may deviate up to $\approx$ 0.001 inches. It appears, however, that for a given x position (i.e. a given access hole) the distance from the wall to the wire is reproducible to a greater accuracy; this conclusion, according to Andersen [8] is based on repeated evaluation of the wall shear stress using the first data point for the computation of the velocity gradient near the wall.

In making boundary layer traverses, the wall is located in the following way. The probe is lowered down until, visually, the wall stop touches the wall. This is observed by lighting the region from the back of the probe, as viewed from the observer, and adjusting until no light passes between the wall stop and the wall. Then the probe is advanced 0.002 in. to compensate for the micrometer backlash. The micrometer is rotated in the opposite direction until the probe starts being displaced upwards. Readings are taken for both mean temperature and velocity every 0.001 in. in the direction perpendicular to the wall for a set of 5 to 10 points, and a procedure based on the constancy of the temperature difference between a point and its neighbor (approximately 1°F) is followed to complete the profile. After having reduced the data, the profile is visually inspected and the first points (usually 2 or 3) are discarded. The criterion is to eliminate points having the same or only slightly different values of velocity and temperature. This would indicate that the probe had not been displaced yet from its position, accounting for micrometer backlash. Also some spring effects of the trasversing mechanism were observed when pressing the wall stop against the wall. The above procedure also takes into account this factor. The first data point is then assigned a value of 0.005 in., as measured by the optical comparator. The uncertainty is estimated to be $\pm$ 0.001 in. Some points in the near neighborhood of the wall had to be eliminated in certain cases because the calibration was found to be unreliable for velocities below 2.5 ft/sec. This is discussed in Section 3.11.

This probe was also used for measuring the rms value of the axial velocity component and the temperature fluctuations. This matter is discussed in Section 3.9.

The horizontality of the wire with respect to the wall was measured by means of an optical comparator, and the difference between the ordinates of the two prong tips was found to be 0.001 in.

3.8 Hot Wire Instrumentation - The Measurement of Turbulent Quantities

The details of turbulence in isothermal flows are usually measured by means of two wires following an X configuration, usually in a plane perpendicular to the wall and parallel to the mean flow field. Two anemometer units, for adding and subtracting signals analogically, and a multiplier are necessary to measure $\overline{u'v'}$, $\overline{v'^2}$, $\overline{u'^2}$. If each wire in the X configuration is at 45° (absolute value) with respect to the mean flow direction, one of them will respond to the sum $u' + v'$, the other one to the difference $u'-v'$, to a first order approximation (if small fluctuations are involved in the problem). A simple algebraic manipulation of the signals can generate the desired quantities in a rather quick way. The drawback is, of course, the matching between the two wires. They are not usually alike and manipulations with the analog signals are necessary. Because of the fact that so many analogic operations are performed, care must be exercised to bring the errors inherent in the electronics to a minimum level. Several other variations have been used for this kind of measurement. Watts [13], for example, used an X wire banked at an angle of 45° with respect to the plane perpendicular to the wall and parallel to the mean flow field. The latter being two-dimensional, both $\overline{u'v'}$ and $q^2 (= \overline{u'^2} + \overline{v'^2} + \overline{w'^2})$ could be determined directly even by using wires with unequal sensitivities and with angles that possess departures of greater than 1° from the nominal 45° value.

Instead of an X-wire probe, Fujita and Kovasznay [14] used a single, rotatable wire. By using redundant data, a least squares fit gave the best estimate for $\overline{u'v'}$, $\overline{u'^2}$ and $\overline{v'^2}$ in two dimensional flows. According to their work the errors in the hot wire response are minimized by calibrating it in place for every measurement, without having to make use of predetermined and accepted hot wire correlations and parameters. The advantage of using only one wire is simplicity: only one anemometer is used and the matching problem between wires is avoided. However, because of the fact that the system may be sensitive to small errors in the rms values, a longer integration time is required and the procedure becomes time consuming. Therefore, the experimenter must be sure that the flow conditions do not change during the data taking procedure. On the other hand, several turbulent quantities can be measured, once a reliable rotating system is designed. This flexibility has tempted some experimenters to use it. Durst and Rodi [15], for example, claim they could use this system in highly turbulent flows (e.g., jet flows), for measuring the turbulent quantities very accurately, provided the mean velocity field is known. Andersen [8] used a rotating wire for measurements of Reynolds stress tensor components and his procedure, with some modifications, has been used in this investigation.

Figure 3.7 shows the probe and its rotating mechanism, used to measure $\overline{u'v'}$ and, in connection with the horizontal wire, $\overline{v'^2}$ and $\overline{w'^2}$. The chosen probe was a DISA 55F02 hot wire element. It is a nominal 45° slant wire having a total length of 3 mm with a 1.2 mm sensitive center position. The ends of the wire are gold plated. The wire is made of tungsten and has a diameter of 5 μm. The prongs are parallel to the mean flow direction at any position of its rotation. Both the horizontal and the slant wires were shown to be strong: no great care is needed to handle them. Andersen's work [8] and this investigation confirmed this point. Only one wire for each kind of measurement was used during the whole period of data taking.

The rotatable hot wire probe has a cable drive to permit it to be rotated while in position in the tunnel. The probe spindle incorporates a "lock-drum" which features six radially drilled holes spaced at 60°. A spring loaded "lock pin" which fits into the holes in the lock drum may be lifted by means of a lever located on top of the transversing mechanism. The arrangement permits turning of the probe to any of the six angular positions, $\phi_n = (2n-1)\frac{\pi}{6}$; $n = \pm1, \pm2, \pm3$, while operating in the tunnel. The probe is similar to Andersen's [8], which had to be modified to allow measurements to be taken in a plane parallel to the wall. This was dictated by the need of measuring the mean velocity at the point of shear stress measurement, and by the necessity of checking the two-dimensionality of the flow field. The choice of the angular positions is somewhat arbitrary. Watts [13] uses the X wire banked at 45°, which allows direct measurement of the turbulent kinetic energy. A later study in this investigation indicated theoretically that a single slant wire with an angle different from the nominal 45° could give the same results in a simpler operation. Manufacturing difficulties, however, prevented the testing of this system. Appendix C discusses the theoretical basis for the direct measurement of $\overline{u'v'}$ and $\overline{q^2}$ with a single rotating wire. The positioning of the slant wire in a plane perpendicular to the wall was concluded in this study to be the correct one when nothing is known about the two dimensionality of the turbulent field ($\overline{v'w'}$ and $\overline{u'w'}$ not zero). This matter is discussed in Appendix B, together with the measurement technique for turbulent quantities. Tests of two dimensionality indicated that in the examined cases $\overline{v'w'} = \overline{u'w'} = 0$. Therefore, it was concluded that the above configuration could be used to measure $\overline{u'v'}$ with the probe placed at two different positions $-\frac{\pi}{6}$, $+\frac{5\pi}{6}$, the minimum required in such a procedure. The sensitivity of the wire is higher when normal to the wall. The above angles were chosen for three main reasons: (1) Andersen's probe [8] was available and only small modifications would be required. (The manufacturing of this probe is time consuming and expensive, requiring a high degree of craftsmanship). (2) In isothermal two-dimensional flows errors due to non-zero size of the wire (non-uniform velocity distribution along it) are minimized by placing the probe the closest possible to the horizontal plane, where the two-dimensional assumption about the mean flow field allows the velocity to be uniform along the wire. (3) In non-isothermal flows the departure of the wire prongs from the isothermal plane generates a non-symmetric temperature distribution along the wire and as a consequence the response of the system to temperature fluctuations (e.g., measurement of $\overline{v't'}$) becomes more susceptible of having significant errors.

The spacing between the prongs was chosen to provide minimum aerodynamic interference. Dahm and Rasmussen's [11] results show that for a 3 mm spacing the error in measuring mean velocity profiles is reduced to 2%. Strohl and Comte-Bellot [16] show and recommend a prong spacing of 3 mm together with other probe features if the error in measuring $\overline{u'v'}$ is to be kept down to 2%.

The angle of the wire and prong system with respect to the wall was measured by means of a toolmaker's microscope. Initially, an optical comparator was chosen for this kind of measurement. However, the uncertainty in the measurement, due to the fact that the shadow of the object is projected onto a screen and amplified, made this system not reliable for measurement of small angles. A direct observation through the use of a toolmaker's microscope gave a maximum departure from the nominal positions of less than 1°. According to Strohl and Comte-Bellot [16], and also some calculations done in this investigation, a maximum error of 2.5% can be present in the measurement of $\overline{u'v'}$ for a 1° deviation. The wire angle with respect to the mean flow was measured to be 48° rather than the nominal 45°. This value was therefore used in the data reduction.

The alignment of the hot wire spindle with the mean flow direction was done by placing the wire in a horizontal plane and measuring at two symmetric positions in this plane. The transversing mechanism fits into the access holes in the top plates and is locked in place before running. A procedure based on the sensitivity of the hot wire to angles was preferred over a mechanical alignment. The spindle was rotated by moving the mechanism body until the difference between the two electrical signals was 2 mv. (out of a 3 volt signal, as measured by a precision integrating digital voltmeter). When measuring velocity, the deviation from its mean value due only to probe misalignment was therefore 1 mv. or 0.1 ft/sec at the lowest sensitivity. This procedure was naturally carried out in the free stream, so that the fluctuating field could not influence the probe alignment. The probe was then lowered down to the boundary layer and measurements taken. During the Reynolds stress measurement procedure the mean velocity measurement was required because the system sensitivity to velocity is not constant (the linearizer is not used). An integration time of 100 sec. was used and the contribution to the error in the velocity sensitivity is believed to be less than 1%.

The distance from the center of the wire to the wall was measured by means of an optical comparator. The reference point, for determining when the spindle touches the wall, is the interface circumference between the tapered and the straight portion of the spindle. A nominal value of 0.069 in. was assigned to this point and the error was estimated to be ± 0.002 in. To start the measurement procedure the probe was simply lowered down until no light could be seen between the reference line and the wall. The micrometer then was rotated in the opposite direction until a light beam could be seen between the two points. This location is assigned a value of 0.070 in., indicating the probe has already departed from the wall.

In non-isothermal flows, as in the case of the measurement of $\overline{v't'}$, a careful study of the hot wire response had to be done. Corrsin [17] analyzed in a theoretical way the general problem of the response of the hot wire to temperature, velocity and concentration fluctuations in two-dimensional flows. The procedure is basically to assume an expression for the hot wire response, namely

$$E^2 = (T_w - T)(A + B\, U_{eff}^{0.5}) \; .$$

E being the output signal, T_w the wire temperature, T the fluid temperature, U_{eff} an effective velocity (function of U and V),

Differentiation of the above expression gives

$$dE = \frac{\partial E}{\partial U}\, dU + \frac{\partial E}{\partial V}\, dV + \frac{\partial E}{\partial T}\, dT \tag{3.1}$$

Finally, for small fluctuations, the following is obtained:

$$e' = \frac{\partial E}{\partial U}\, u' + \frac{\partial E}{\partial V}\, v' + \frac{\partial E}{\partial T}\, t' \tag{3.2}$$

The rms value of the anemometer signal is

$$\overline{e'^2} = \left(\frac{\partial E}{\partial U}\right)^2 \overline{u'^2} + \left(\frac{\partial E}{\partial V}\right)^2 \overline{v'^2} + \left(\frac{\partial E}{\partial T}\right)^2 \overline{t'^2} + 2\,\frac{\partial E}{\partial U}\frac{\partial E}{\partial V}\,\overline{u'v'} + 2\,\frac{\partial E}{\partial U}\frac{\partial E}{\partial T}\,\overline{u't'} + 2\,\frac{\partial E}{\partial V}\frac{\partial E}{\partial T}\,\overline{v't'} \tag{3.3}$$

Measuring at two different symmetrical positions and subtracting one from the other $\overline{e_1'^2} - \overline{e_2'^2} = a\,\overline{u'v'} + b\,\overline{v't'}$, where a and b are functions of the sensitivity coefficients, the wire material, the directional properties, and geometry. If two different wire temperatures are also employed, then a system of linear equations can be solved to give values for $\overline{u'v'}$ and $\overline{v't'}$.

Corrsin [17] has estimated the magnitude of each term in the equations and showed the feasibility of the measurement procedure. Arya and Plate [18] applied this technique for measuring $\overline{u'v'}$ and $\overline{v't'}$ with a slant wire. The velocity and temperature sensitivity of the anemometer system, as defined by $\partial E/\partial U$ and $\partial E/\partial T$ respectively, were determined experimentally, without having to assume an expression for the variation of the hot wire signal as a function of velocity and temperature. This was done by measuring, for each calibration velocity, the output signal for different $(T_w - T_\infty)$ where T_w is the wire temperature and T_∞ is the fluid temperature at the measurement point. The set of curves was differentiated to give the sensitivities.

As pointed out by Arya and Plate [18], however, this procedure is subject to some scatter in $\overline{v't'}$ due to experimental errors in the required rms values of the anemometer signal. A least square fit procedure was therefore used to improve the accuracy of the system.

This procedure has the advantage of simplicity of operation, because only one anemometer and one wire are used. The complexity of calibration is reduced to a minimum level and the reliability of the system is improved because only one wire can be broken and replaced. The spatial resolution is another factor of consideration. The information comes from one wire and, therefore, from one location only. This factor becomes important when steep temperature and velocity gradients are present. However, the procedure is time consuming and due to the fact that the information for the measurement of $\overline{v't'}$ is obtained at different instants of time, the experimenter must be sure that the flow conditions do not change during the data taking procedure. Naturally, as in the case of isothermal flows, a good hot wire rotating system must be supplied for the measurement procedure.

This technique has been used by a few investigators to measure $\overline{u't'}$, by means of a horizontal sensor. Among them, one could mention Kudva and Sesonske [19] who used one hot film probe. Only one reference, Fulachier and Dumas [26] has been found, in which measurements of $\overline{v't'}$ are carried out by this procedure.

Another technique requires 3 wires. Two of them, in an X configuration, with the anemometers operated in the constant temperature mode, give directly v' . The third one, a very small diameter wire, horizontal, with the anemometer operated in the constant current mode, at a very small current, gives directly t' . The procedure is based on the fact that if two matched wires are placed in symmetrical positions (as in the case of X configuration) the subtraction of the two signals is directly proportional to v' , being independent of the temperature fluctuation in low turbulence level flows, as observed by Corrsin [17]. The multiplication of this signal by the one from the temperature wire, gives $\overline{v't'}$

after a time averaging procedure. The main advantage is that instantaneous values of $\overline{v't'}$ can be obtained, being particularly useful for spectral measurements. This procedure is not time consuming but requires a somewhat complex electronic set up. Three anemometers must be used. Two of them operated in the constant temperature mode, and the other one in the constant current mode. A subtracting and a multiplying circuit must be employed. The wires must be carefully arranged to give a good spatial resolution. The calibration is obviously more complex and in case of breaking one of them extreme care must be exercised to replace it.

Johnston [20] used this procedure to measure $\overline{v't'}$. He used two 0.00015 in. tungsten wires and one 0.00005 in. platinum wire. Bremhorst and Bullock [21] used this method for the measurement of $\overline{u't'}$, but did not report any $\overline{v't'}$ measurement. Bourke and Pulling [22], and Bradshaw [23] reported having used this technique for obtaining $\overline{v't'}$. Blom [24] however slightly modified it by replacing the temperature wire for a very thin platinum film.

Finally, Burchill and Jones [25] present a procedure to obtain directly u', v', t', $\overline{U}$, $\overline{T}$ by means of a number of hot film sensors.

3.9 Calibration for Mean and RMS Temperature Measurement

The calibration of the 5 μm gold plated tungsten wire was done in a variable temperature oil bath (Rosemount Engineering Co. Model 910A) the temperature controller being a Thermotrol Model 910-508 from the same company (a Shell development design), using a resistance thermometer as a sensor.

The oil bath temperature was measured by an HP Model DY-2801A quartz thermometer. Its calibration was checked by placing the sensor into three different calibration standards. The first one was a standard stirred ice bath (Rosemount Engineering Co. Model 911); the second one, a Leeds and Northrup Co. steam point apparatus; and the third, a Thermowells Inc. tin freezing point standard. Having set the thermometer at 0.00°C, in ice, the calibration was checked to within 0.02°F for the steam point and 0.04°F for the tin point.

The constant current Wheatstone bridge is a DISA 55M20. A gain of about 3500 was used in conjunction with a wire current of 2 ma. The measured rms of the noise was 2mv. The calibration of the wire showed that a 5mv variation in the output corresponds to a 0.1°F difference. The noise therefore is equivalent to 0.04°F which was deducted from the measured rms value of the temperature fluctuation, when reducing the data.

The output from the anemometer was measured by a HP Model 2401C integrating digital voltmeter. About 10 points were used in the calibration covering the range 60°F - 100°F, and the maximum departure from the fitted straight line was 0.1°F. Also, the resistance of the wire as a function of the temperature was measured by using the same anemometer, which employs a 0.8 ma current for its measurement. A linear expression $R = AT + B$ was fitted and the sensitivity A was found to be $0.0077\Omega/°F$ for this tungsten wire.

Although the system is very stable, as far as resistance variation is concerned, some contact resistance changes were observed during the operation of the system. Unplugging the cables, plus a small instability in the resistance of the connections combined to give a resistance variation of 0.004 ohms. Due to the small sensitivity A of the wire, this would mean a 0.5°F variation. This instability or lack of repeatability was identified by recalibrating the probe after having disconnected the cables. The resistance-temperature curve had the same slope, but shifted up or down at random indicating that the change was not due to drifts in wire properties.

The solution to this difficulty was an in-place temperature calibration using a calibrated iron constantan thermocouple very close to the hot wire probe in an isothermal region of the wind tunnel. This check was done before and after every data taking procedure, and no variation was observed during the run, although changes were observed from one day to the other one.

The relative accuracy of temperature measurement is estimated as ± 0.1°F. The absolute one, about ± 0.2°F.

The in-place calibration and the oil bath calibration were both performed with both the wire and the prongs at the same temperature (no heating from the very low wire current), hence no conduction errors should be expected, as described in Appendix A.

The calibration oil bath is in continuous movement, and the risk of breaking the wire would be large if the probe were placed directly into it. Besides that risk, the oil film deposited on the wire surface would have to be cleaned afterwards, otherwise the frequency response would be degraded (the working fluid is air). Freon is a good solvent and could be used for this purpose, though the risk of breaking the wire is great. To obviate the need for cleaning the wire it was decided, therefore, to put the wire inside a copper test tube, which was placed in the oil bath. The fluid inside the test tube was air, and it was isolated from the ambient air in order to prevent any air currents from convecting heat from or to the probe or generating a temperature gradient in the neighborhood of the wire. The test tube material was copper, so that the time constant of the system was kept small, and the time required for the calibration minimized. The aspect ratio of the tube (length to diameter ratio) was large, so that the region where the wire was placed would be nearly isothermal: in the present case the ratio is about 7/1 with the probe nearly at the bottom of the tube.

An experiment was carried on to check the existence of conduction errors. The probe was covered by an aluminum foil and placed inside the oil bath, in a region where the flow is already isothermal. The foil prevented the oil movement from damaging the wire. No change in calibration was observed. The probe naturally had to be cleaned afterwards.

3.10 The Use of a Linearizing Circuit for Processing the Output from the Anemometer

A linearizer circuit can be used to convert the non-linear output of the anemometer to a linear function of velocity. Its use in non-isothermal flows, however, makes the measurement procedure very cumbersome, since the linearizer parameters must be changed to suit each ambient temperature (unless a temperature compensating probe is used). With a compensating probe the system would lack spatial resolution due to the large size of the probes and the small dimensions of a boundary layer flow. The usual procedure for measuring the rms value of the velocity fluctuation is to assume a linear dependence between the output from the anemometer and the velocity fluctuation about the mean flow field. Sandborn [30] suggests that a linearizer circuit for the hot wire signal will not noticeably improve the accuracy of turbulence measurements unless the turbulent intensity is larger than 30 to 40% of the mean. This level of intensity is usually found only in the region very close to the wall in a boundary layer flow. In the present investigation, this region can only be reached by the horizontal wire ($\overline{u'^2}$ measurement) and small errors may be present in those data. The measurement of $u'v'$ is done in regions of much lower turbulence levels and negligible errors should be expected. Watts [13] measured the Reynolds stress tensor on a flat plate, with no free stream pressure gradient, and also concluded that the measurement of $\overline{u'v'}$ could be done without the use of the linearizer. Klebanoff [31] also obtained his flat plate data without using the linearizer. It was decided, therefore, not to use a linearizing circuit for processing the output from the anemometer.

3.11 Calibration of the Horizontal Wire for the Measurement of Mean and RMS Velocities

The gold plated tungsten wire was calibrated in the free stream of the wind tunnel test section. The velocity was measured by means of a pitot probe, and the air stream temperature by means of a calibrated iron-constantan thermocouple. Both were placed nearby the hot wire probe. An experimental investigation of the influence of the proximity of the probes to the hot wire showed that the perturbation of the flow field could be neglected. The dynamic pressure was read by a Statham PM-97 unbonded strain gauge differential pressure transducer, using an integrating digital voltmeter HP Model 2401C, in connection with an external quartz oscillator, to give an integration time of 10 seconds. The same voltmeter was used to read the output from the anemometer and the temperature of the free stream.

The operating wire resistance was set to a fixed value of 6 ohms, giving an overheating value in the neighborhood of 1.50 ohms in the range of temperature of the examined thermal boundary layers. The calibration was carried out at two different ambient temperatures, 30°F apart, approximately the upper and lower limit of the temperature range in question. The cold resistance of the wire was measured before each data point for velocity calibration, and the two calibration curves were correlated by means of the expression

$$E^2/(R_w - R_f) = f(U)$$

as seen in Fig. 3.8 . The departure of the data points with respect to the above calibration curve is less than 1%, probably the accuracy of mean velocity measurement. Lower overheating ratio (R_w = 5.40 ohms) was also satisfactory but higher overheating ratio (R_w = 7.50 ohms) was less satisfactory.

During the measurement procedure, the cold resistance of the wire, to be used in conjunction with the calibration curve, was calculated from the measurement of mean temperature (Section 3.6) and the calibrated resistance versus temperature curve (Section 3.9).

Several functional relationships $f(U)$ were tried to give the best estimate of the calibration curve in the least square sense.

a) $f(U) = A + BU^n$, where A , B and n were determined by means of a non-linear least square fit. The exponent n was found to be in the neighborhood of 0.45, as originally concluded by Collis and Williams [32].

b) $f(U) = A + B\sqrt{U} + CU$, where A , B , and C were determined by means of a linear least square fit. This expression was tried because of the observation of Davies and Patrick [33], according to which, the velocity sensitivity $\partial E/\partial U$ of the hot wire, when determined from this expression, is very close to the value obtained from the dynamic calibration of the wire, important for the rms measurement of the axial velocity U .

c) $f(U) = \sum_{i=1}^{n} (A_i + B_i U + C_i U^2 + D_i U^3)$, spline fit. Usually two or three intervals were tried (n = 2 or 3), with the constraint that the matching of the functions should be with respect to its value, its first and second derivatives at the matching point. This spline fit (in the least square sense) using the concept of contrained optimization (Langrange multipliers approach) gave the best fit of the calibration curve. The procedure is outlined by Klaus and Van Ness [34]. A higher number of cubics (one for every two points) was tried, and it proved to be useful only for the velocity sensitivity ($\partial E/\partial U$) determination in the lower velocity range (2.5 to 5 ft/sec).

The conclusion of this study is that the form of the functional relationship $f(U)$ is not important when the mean velocity measurement is the only required quantity since all forms tried were acceptable. For simplicity, the expression b) was chosen.

For the determination of the velocity sensitivity $\partial E/\partial U$, in the measurement of $\overline{u'^2}$ (see Appendix B), the choice of $f(U)$ turned out to be important. Expression b) and the spline fit with 2 or 3 cubics, and with a cubic for every two points were used. The results are shown in Fig. 3.9. It can be seen that in the range 5 to 32 ft/sec the departure from the average value of the derivative (obtained from the three procedures) is about 3% at most. The lower range, 2.5 to 5 ft/sec, however is critical and analysis had to be carried out to determine the best estimate of the derivative. A cubic for every two points was used for two main reasons: (1) it gave the best mean value fit in that region and, (2) the derivative as calculated from this procedure turned out to be nearly constant in the beginning of the region, as expected from the analysis of the heat transfer from wires.

The mean velocity was corrected for proximity from the wall according to Repik [35]. The maximum correction was in the order of 0.2 ft/sec for velocities of 2.5 or 3 ft/sec. Measured velocities below 2.5 ft/sec were considered unreliable due to uncertainties in calibration.

The measurement of mean velocity was done using a Vidar 5206 D-DAS Data Acquisition System, employing a DEC PDP 8/L computer. The anemometer output was read through a Vidar digital voltmeter with a very high impedance (higher than 10 megohms), and a variable integration time sufficient to give mean velocity to within 0.1 ft/sec. (This does not suggest the overall accuracy of velocity measurement.)

The measurement of the rms value of streamwise velocity was done by feeding the output from the anemometer to a DISA true rms meter, set at a time constant of 30 seconds, to guarantee that the low frequency oscillations were included. The rms meter was calibrated specially by DISA to give a 1% accuracy on the measured value at the midrange of the meter, and 2% at the end of the scale. This was done because most of the critical measurements were done in the mid-range of the rms meter. The usual accuracy being 1% full scale, it would make the measurement rather inaccurate in that range. The calibration was checked using standard sine waves with known rms values. The mean square output was chosen to be read for two reasons. Firstly, it is slightly more accurate than the rms output (the square root can be obtained numerically and very accurately if necessary). Secondly, the output was averaged over a certain period of time, and conceptually there is a difference between averaging the square root and extracting the square root of the averaged value.

The mean square output was read by an integrating digital voltmeter HP 2401C set to an integration time of 100 seconds by means of an external clock. The final figure was obtained by letting the rms meter integrate during 100 seconds, and then by feeding to the DVM and integrating over 100 seconds. During the procedure the rms meter was monitored visually to make sure no sudden flow perturbation occurred. This was particularly important when measuring shear stress and turbulent heat transfer; since many operations are done on the signals, amplifying any errors. Measurements were repeated when perturbations were observed. With this procedure, repeatable values to within 1% were obtained.

3.12 Calibration of the Slant Wire for the Measurement of Turbulence Quantities

The use of the slant wire for turbulence measurements is based on the principle that the wire responds to both temperature and velocity fluctuation. For small fluctuations, one can write

$$dE = \frac{\partial E}{\partial U_{eff}} dU_{eff} + \frac{\partial E}{\partial T} dT \quad . \tag{3.4}$$

However $dE \approx e'$, $dU_{eff} \approx u'_{eff}$, $dT \approx t'$. Therefore the following expression can be written

$$e' = \frac{\partial E}{\partial U_{eff}} u'_{eff} + \frac{\partial E}{\partial T} t' \tag{3.5}$$

Appendix B gives the following relationships

$$\frac{\partial E}{\partial U_{eff}} = \frac{\partial E}{\partial U} \frac{1}{\sqrt{A}} \tag{3.6}$$

$$u'_{eff} = \sqrt{A}\, u' + \frac{D}{2\sqrt{A}} v' + \frac{F}{2\sqrt{A}} w' \tag{3.7}$$

Finally

$$e' = \frac{\partial E}{\partial U} \left[u' + \frac{D}{2A} v' + \frac{F}{2A} w' \right] + \frac{\partial E}{\partial T} t' \tag{3.8}$$

where U is the mean streamwise velocity.

The calibration of the wire consists basically of obtaining experimentally $\frac{\partial E}{\partial U}$ and $\frac{\partial E}{\partial T}$.

a) Calibration for velocity

As indicated by Arya and Plate [18] the response of the wire can be thought of as a function of the velocity and the difference between the wire temperature and the ambient temperature. Therefore, if the cold resistance is measured, and a constant wire to mean ambient temperature is used, only one calibration curve can be applied to the data reduction, simplifying greatly the measurement procedure.

In the present investigation, however, the gold plated 5 μm slant tungsten wire (DISA 55F02) seems to be contaminated by a perceptible heat conduction to the prongs due to its relatively low L/D ratio ($\approx$ 240, sensitive length) and the adverse effect of the gold plating. As a matter of fact, the plating of the wire was done originally for strengthening purposes; reducing the aerodynamic interference from the prongs requires the use of a long wire. As pointed out in Appendix A, the gold plated region tends to be at the prong temperature level due to its large thermal inertia (as compared to the wire itself).

As a consequence of the heat conduction effect, there is also a slight dependence of the wire response on the ambient temperature. For measurements in isothermal conditions, the wire was calibrated for velocity at a constant wire to ambient temperature difference (corresponding to 1.50 ohms), at the approximate free stream temperature of the measurement. For non-isothermal conditions, the wire was calibrated at approximately the temperature of the so called logarithmic region of the boundary layer, the closest possible to the wall the measurement can be done. This corresponds to a temperature approximately 15°F higher than the free stream. A slight difference was then found between the two calibrations. The choice of the overheating ratio ($\sim$ 1.50 ohms) was dictated by reasons as outlined when calibrating the probe for temperature sensitivity (b).

The probe was calibrated in the free stream of the wind tunnel, aligned according to the method described in Section 3.8. The measurement of velocity was made with a pitot probe, placed near the wire. The precautions described in Section 3.11 were taken in order to avoid any aerodynamic interference from the pitot probe to the wire. The dynamic pressure was measured by a pressure transducer, and read by a digital voltmeter, as described in Section 3.11. The calculation of the velocity sensitivity was done by following the same procedure as used for the horizontal wire and also described in Section 3.11.

b) Calibration for temperature

Ideally the sensitivity to temperature would have to be measured at a constant velocity, by keeping the wire temperature constant, and varying the ambient temperature. This procedure, however, would be very time consuming and difficult. Arya and Plate [18] suggested that once the output of the anemometer for a constant velocity is only a function of the difference between the wire and ambient temperatures, the sensitivity of the wire to ambient temperature can be obtained by varying only the wire temperature and by using the following relationship:

$$-\frac{\partial E}{\partial T_\infty} = \frac{\partial E}{\partial (T_w - R_\infty)} \frac{\partial R_w}{\partial T_\infty} = \frac{\partial E}{\partial (R_w - R_\infty)} \frac{\partial R_\infty}{\partial T_\infty} = \frac{\partial E}{\partial (R_w - R_\infty)} \frac{\partial R}{\partial T} \qquad (3.9)$$

The cold wire resistance at ambient temperature was about 4.40 ohms, and fixed overheating values of 1.50 ohms and 0.50 ohms were used during the measurement. This was achieved by measuring the cold resistance of the wire before each measurement and adding the overheating value to obtain the hot wire resistance.

The procedure can only be effective if two wire temperatures can be chosen so that the signals are distinctly different. The lowest wire temperature gives the highest temperature sensitivity and the lowest velocity sensitivity. When going from $\left(R_w - R_\infty\right) = 0.50$ to $\left(R_w - R_\infty\right) = 1.50$ the temperature sensitivity is reduced to half its value, and the velocity sensitivity is doubled. This was concluded to be a good pair for the measurement of $\overline{v't'}$. For each velocity (20-26 data points) in the range 2.5 ft/sec to 30 ft/sec, the ambient temperature was kept constant and about 18 wire resistances (0.1 ohm apart) generated a function of $\left(R_w - R_\infty\right)$. The curve was differentiated by a spline least square fit procedure and the derivatives calculated at $\left(R_w - R_\infty\right) = 0.50$ and $\left(R_w - R_\infty\right) = 1.50$. The curve of resistance as a function of temperature was obtained experimentally the same way as outlined in Section 3.9. Applying Eq. (3.9), the temperature sensitivity was obtained.

A problem appeared when performing a static calibration of the wire. By static calibration it is meant that the oncoming temperature field is not fluctuating. The wire was placed in an oil bath, as described in Section 3.9 for the horizontal wire, and by varying the ambient temperature, keeping the wire temperature constant, the sensitivity was determined at $\left(R_w - R_\infty\right) = 0.50$ and $\left(R_w - R_\infty\right) = 1.50$. Surprisingly, for the highest overheating value the difference in the two sensitivity measurements was about 2% only; for the lowest one, 15%. This suggested that the finite length of the wire might be impairing its calibration. A detailed analysis of the anemometer had to be carried out. A variable temperature calibration device was designed to provide control of flow rate and temperature. Static calibrations of the wire for the two overheating ratios were performed at approximately 31 ft/sec. Again, the difference was approximately the same, suggesting that the output from the anemometer is a function of the velocity, the wire and ambient temperatures individually, and not only on their difference as supposed before.

It was concluded that two higher overheating ratios should be used to measure $\overline{u'v'}$ and $\overline{v't'}$ in non-isothermal flows. However, as the wire temperature increases its sensitivity to temperature decreases, and the measurement of $\overline{v't'}$ becomes more uncertain. The first idea was to use a very high overheating ratio, so that the wire would be only sensitive to velocity, and a direct measurement of $\overline{u'v'}$ would be possible. Sandborn [30] however, states that the anemometer output becomes proportional to $\overline{u'v'}$, with a 5% error, at wire temperatures of about 1000°C. It was concluded therefore that the use of the value for $\overline{u'v'}$, as determined from the correspondent isothermal flow together with the measurement at $\left(R_w - R_\infty\right) = 1.50$ would be the right approach for $\overline{v't'}$ measurement.

One question however arose as to the validity of the assumption that $\overline{u'v'}$ is the same for both isothermal and non-isothermal flows. Johnson [20] measured both isothermal and non-isothermal $\overline{u'v'}$ and found a small difference very close to the wall, and practically nothing in the outer region of a flat plate flow. Kudva and Sesonske [19] found a small difference in the outer region of a pipe flow at low Reynolds number. In the present investigation, the measured mean velocity at the point of $\overline{v't'}$ measurement was the same as in the isothermal profile to within 1 or 2%. The local temperature was at most 15°F above the free stream indicating the flow could be considered a constant property flow in the region of $\overline{v't'}$ measurement (the density variation is about 2%). This suggests that the $\overline{u'v'}$ profile may be the same as the isothermal one in the region of $\overline{v't'}$ measurement and the above hypothesis is justified. The accuracy of measurement can then be checked by comparison with the value obtained from the mean profile in a flat plate case.

Arya and Plate [18] suggested that small experimental errors can give inaccurate results for $\overline{v't'}$, and offered as a solution the measurements of several wire temperatures and not only the minimum required. According to him a 15% error may be expected when using this procedure. The abundant data is then curve fitted to give the best estimate of $\overline{v't'}$.

In the present investigation, it was preferred to curve fit the anemometer output and the $\overline{u'v'}$ profile, because the long integration time reduced the scatter greatly. The profiles presented in Chapter 6 were obtained by smoothing the above quantities. This system was preferred over Arya and Plate's for two reasons. Firstly, only one wire temperature is used; when a number of data points at each station has to be obtained, the use of several wire temperatures becomes prohibitive as far as time is involved. Secondly, the long integration time used in this investigation greatly reduced the scatter.

The conclusion of this method for the measurement of $\overline{v't'}$ is that great care should be exercised to eliminate the prong effect. This can probably be done by using a very small diameter (1 μm) wire (probably platinum). The L/D ratio is large, yet the spatial resolution remains excellent because a relatively short wire is used. By doing so, the static calibration approaches the dynamic calibration and lower wire temperatures can be used. Both $\overline{u'v'}$ and $\overline{v't'}$ can be measured directly and the scatter will be much smaller. This procedure was tried. However, manufacturing difficulties, related to the fragility of the wire, prevented this approach from being used in the present investigation. As a final conclusion to this study, it can be said that a gold plated wire does not seem to be the right choice in non-isothermal flows, and a further investigation should be carried out.

3.13 Qualification of the Apparatus

A series of tests was performed to qualify the basic characteristics of the apparatus and they must be referred to Blackwell [9]. No need of repeating them was necessary because the elapsed time between the present investigation and Blackwell's was very short. However, velocity and temperature measurements were performed under the same conditions as Blackwell's and excellent agreement was found. Stanton number measurements have been carried out, repeating several of Blackwell's cases and excellent agreement (to less than 1%) was obtained. They were conducted mainly as a base line for step in wall temperature conditions.

The tests basically consisted of (1) transpiration energy balance, (2) transverse uniformity of the mean velocity and temperature profiles, (3) boundary layer energy balances, and (4) repeatability of earlier studies by Blackwell [9].

3.14 Qualification of the Measurement Procedure for Mean Temperature and Velocity Profiles

The velocity and temperature measurement system was checked on a flat plate case reported earlier by Andersen [8] and Blackwell [9]. The data are compared in Figs. 3.10 and 3.11, and show the accuracy of the measurement procedure. The cold wall data from Andersen [8] are well matched by the hot wall measurements made with the present technique. Similarly, the temperature profiles obtained with the present hot wire anemometer method agree with Blackwell's [9] thermocouple probe data, obtained using a carefully designed boundary layer thermocouple. Also, the mean velocity profile is seen to be invariant with respect to the temperature field for the low wall to free-stream temperature difference (≈25°F) used in this investigation. This conclusion has also been important for the measurement procedure employed in obtaining values of $\overline{v't'}$, described in Section 3.12 .

3.15 Qualification of the Procedure for Turbulence Measurements

As described in Appendix B , the procedure for obtaining turbulence quantities requires that $\overline{u'w'}$ and $\overline{v'w'}$ be zero. A test was carried out by measuring at symmetric positions of the probe. The difference between the signals gave a 1.5% error in the very neighborhood of the wall and 0.5% in the fully turbulent region. It can be suggested that there is perhaps a very small three dimensionality in the inner region;

however, this might also be attributed to experimental error, since the accuracy of the RMS meter is 1% of the measured signal. This test was carried out for all examined flows and was conducted during the measurement of $\overline{v't'}$ with similar conclusions. The basis for this criterion is discussed in Appendix B.

The next step was the measurement of $\overline{u'v'}$ in a known flow field. The calibration flow was a fully developed channel flow where the turbulent shear stress should be linear in the turbulent core. Figure 3.12 presents the experimental results plotted against the theoretical values. The friction velocity u_τ was obtained directly from pressure drop measurements. The experimental set-up used in this test is the same as described by Hussain [38] and a brief analysis is presented in Appendix C.

Finally, measurements of $-\overline{u'v'}/u_\tau^2$ and $\overline{v't'}/u_\tau T_\tau$ were performed in a flat plate flow and they were found to agree with the values obtained from the mean profiles. This is discussed in Chapter 6.

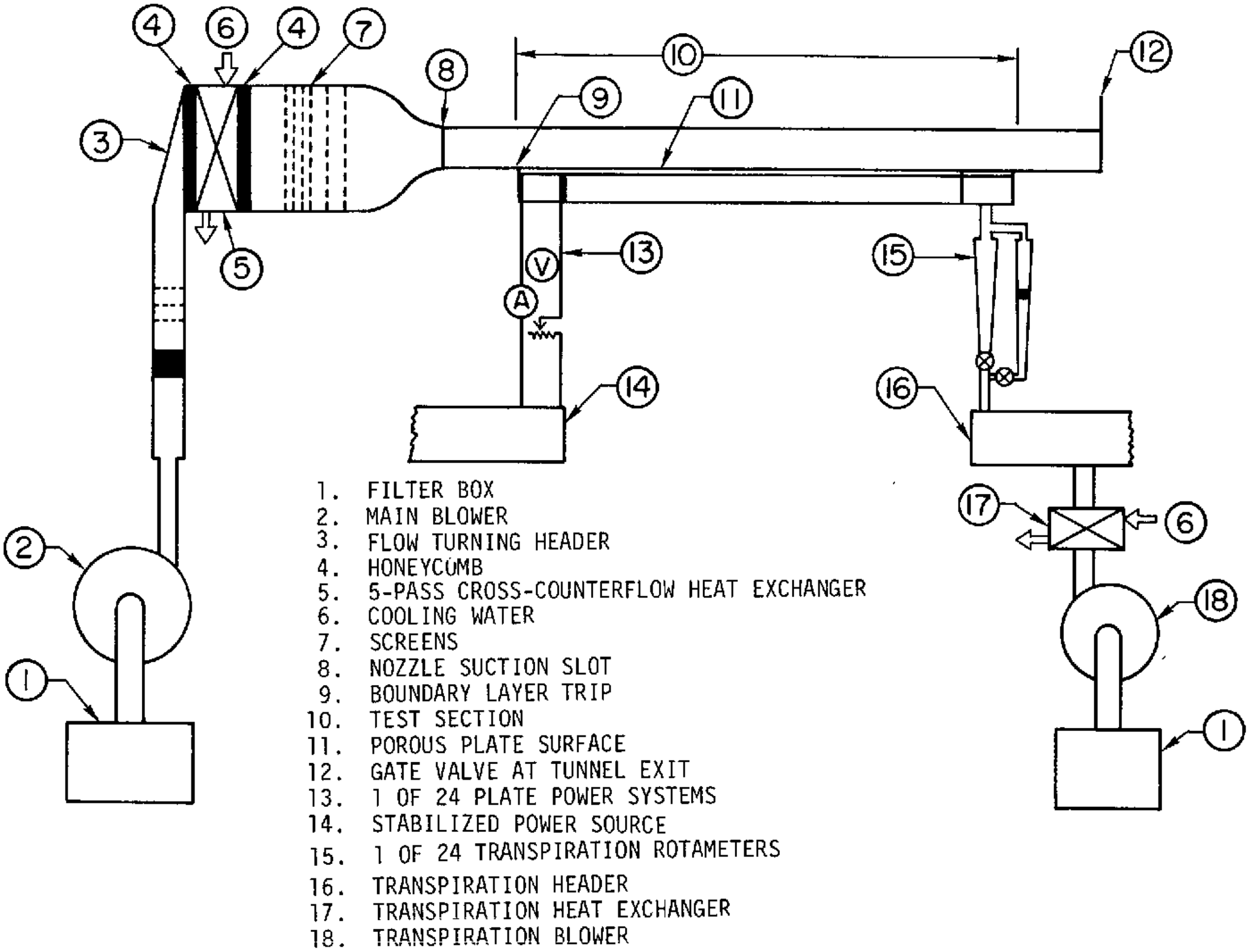

Fig. 3.1 Schematic of the test apparatus.

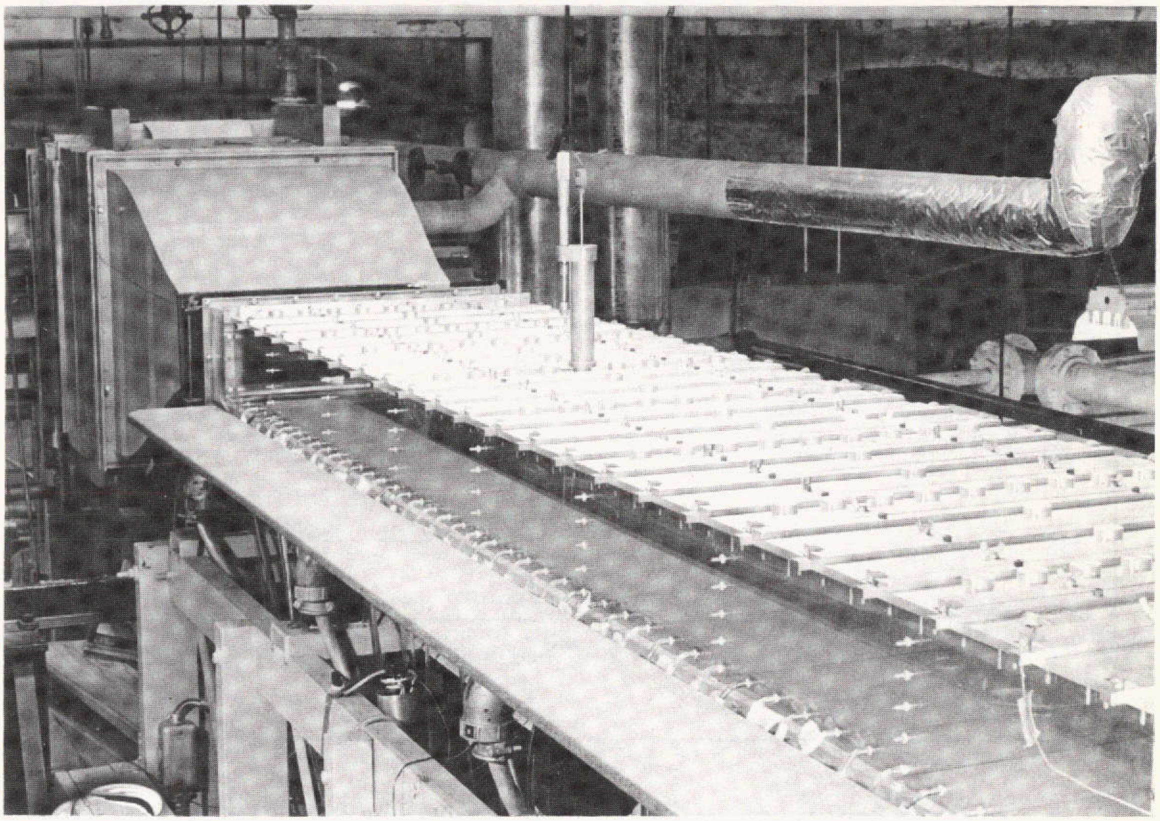

Fig. 3.2 Photograph of the test section with a traversing mechanism in position.

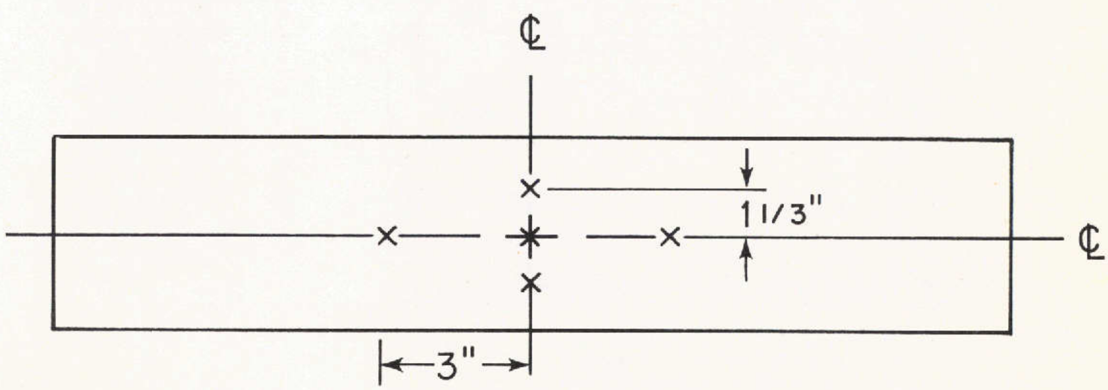

Fig. 3.3 Spacing of the plate thermocouples.

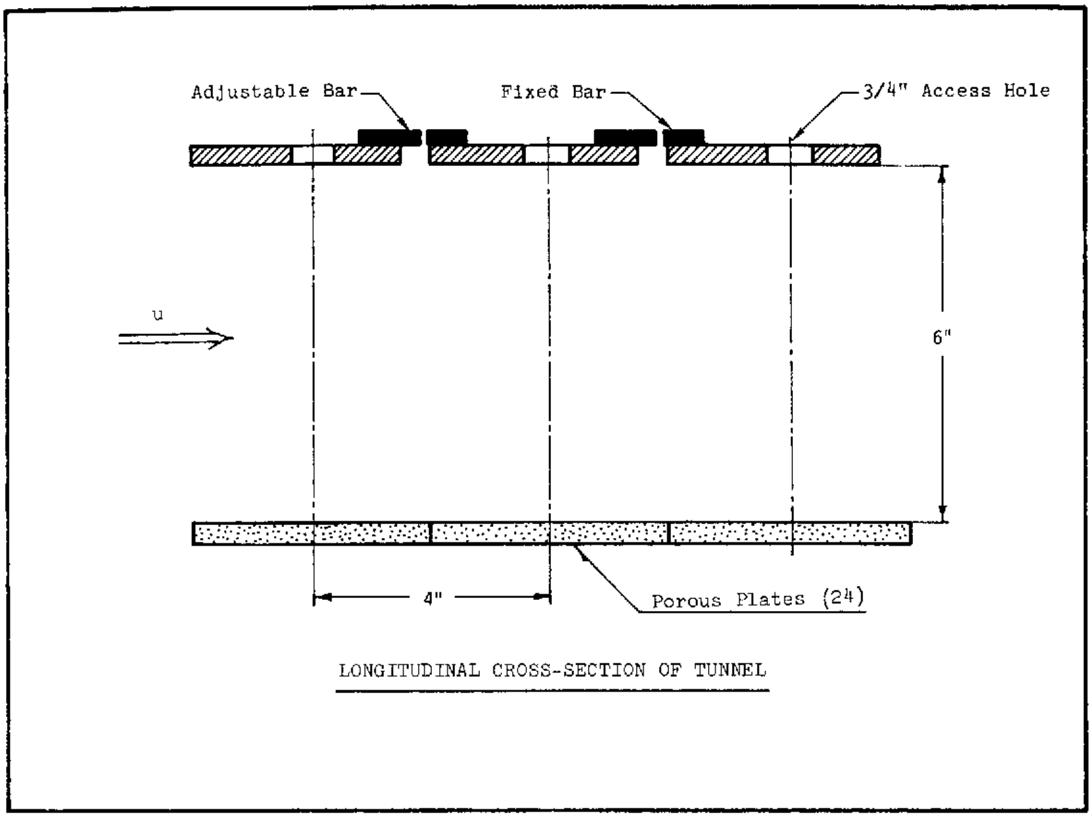

Fig. 3.4 A longitudinal cross section of the tunnel test section.

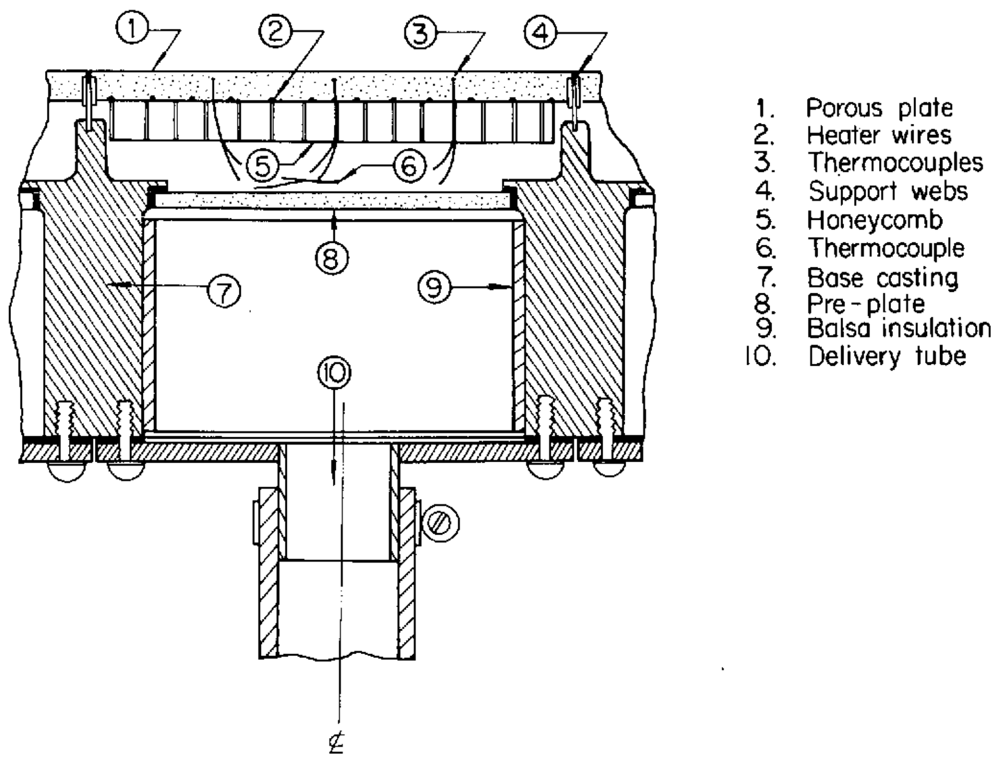

Fig. 3.5 Cross sectional view of a typical compartment.

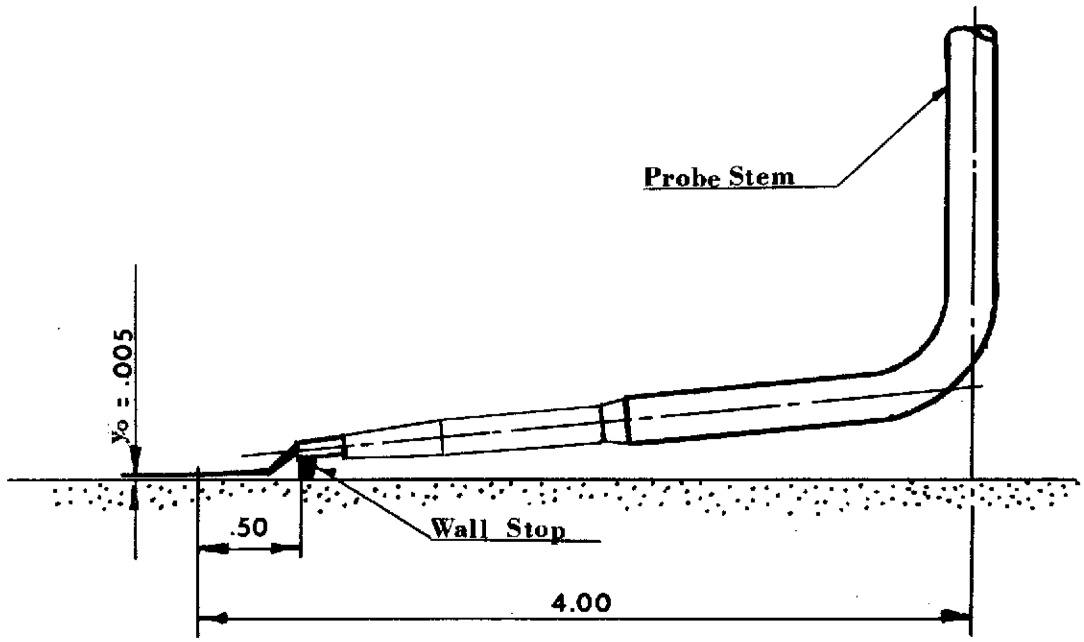

Fig. 3.6 The horizontal hot-wire probe.

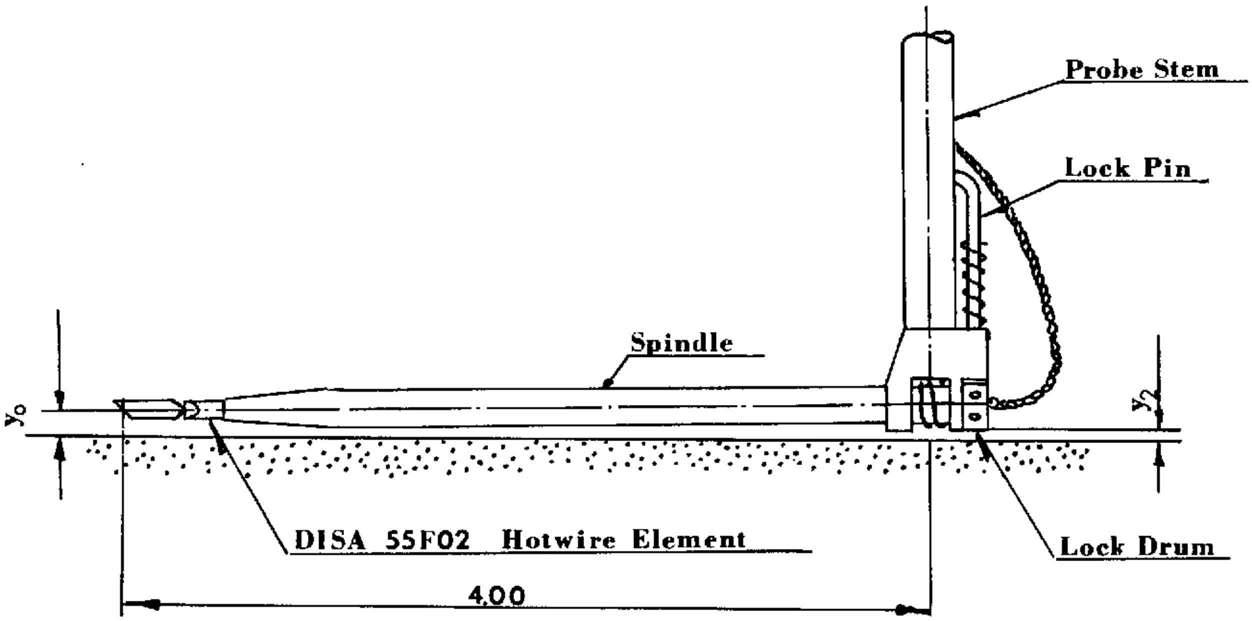

Fig. 3.7 The rotatable hot-wire probe.

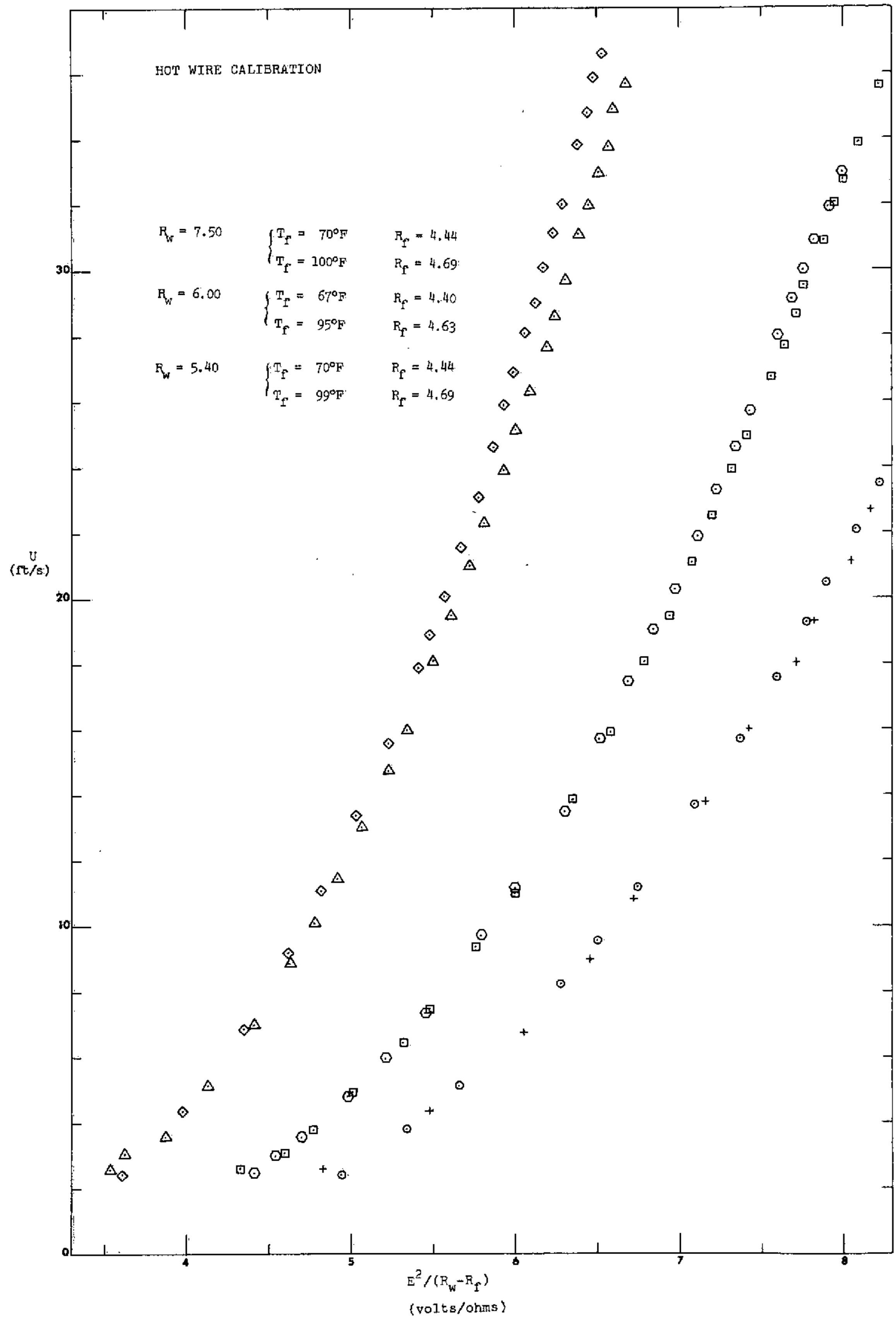

Fig. 3.8 The horizontal hot-wire calibration for different wire temperatures.

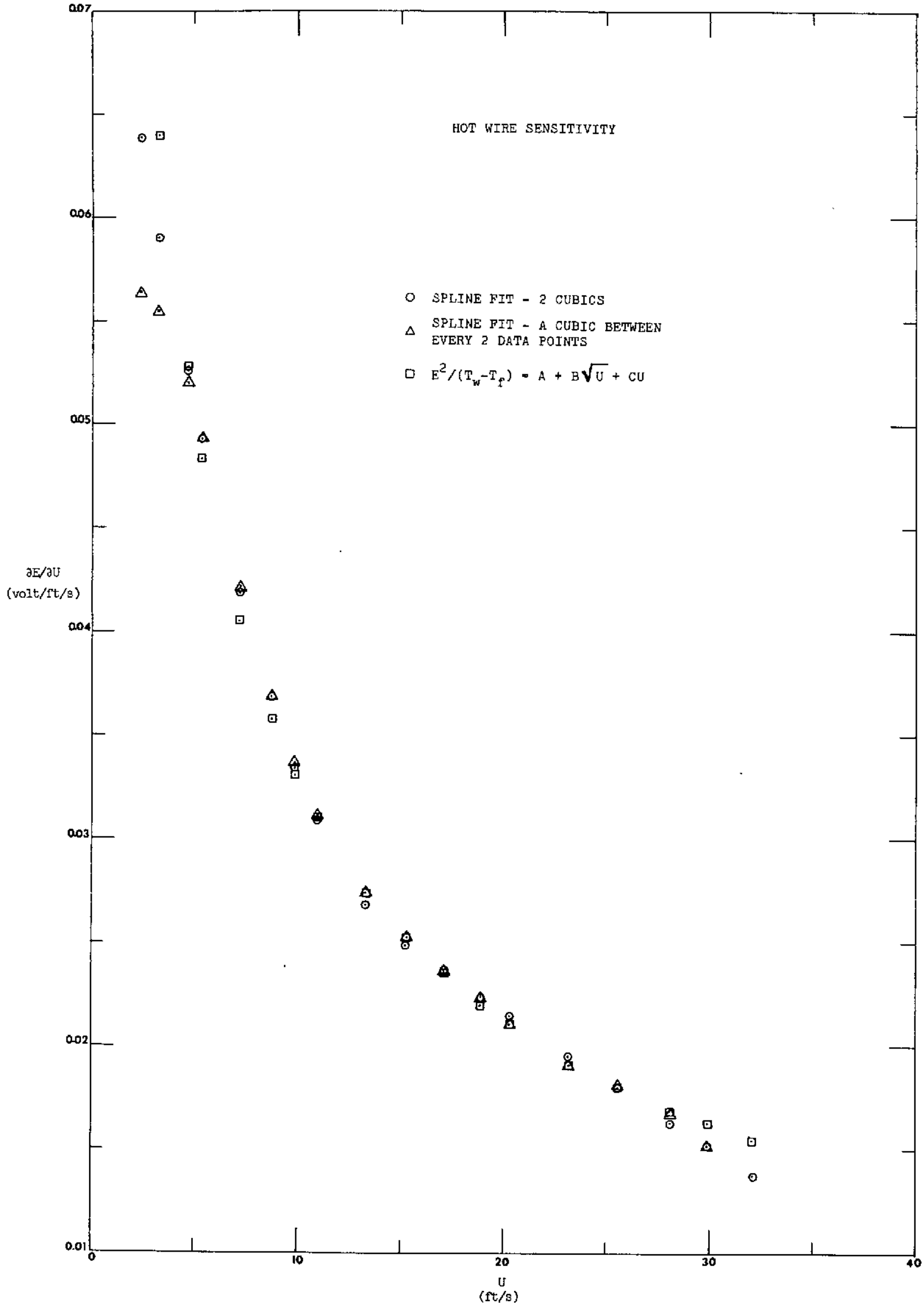

Fig. 3.9 The hot-wire sensitivity to velocity.

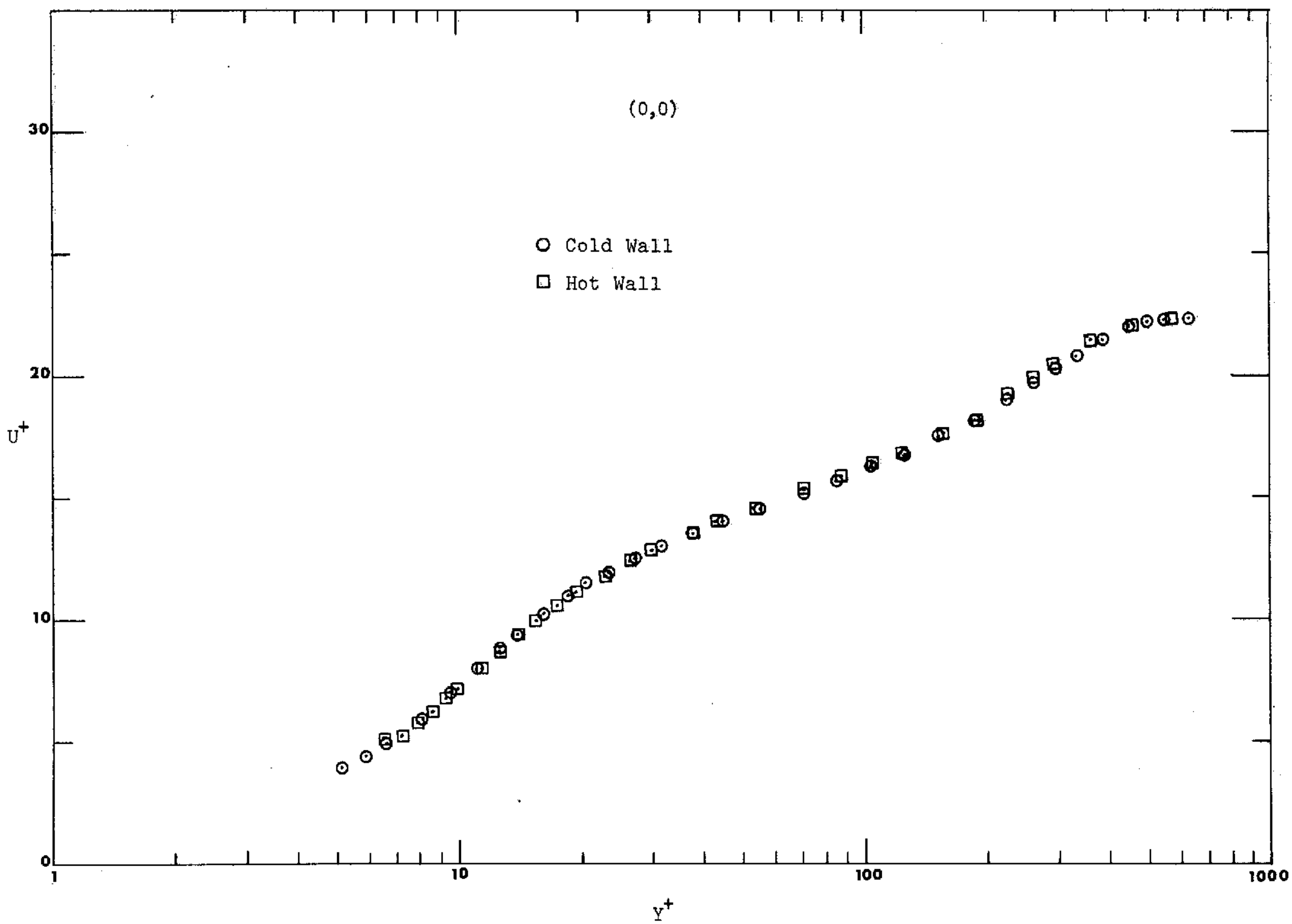

Fig. 3.10 Hot-wire measurements of velocity on a flat plate: cold wall vs. hot wall.

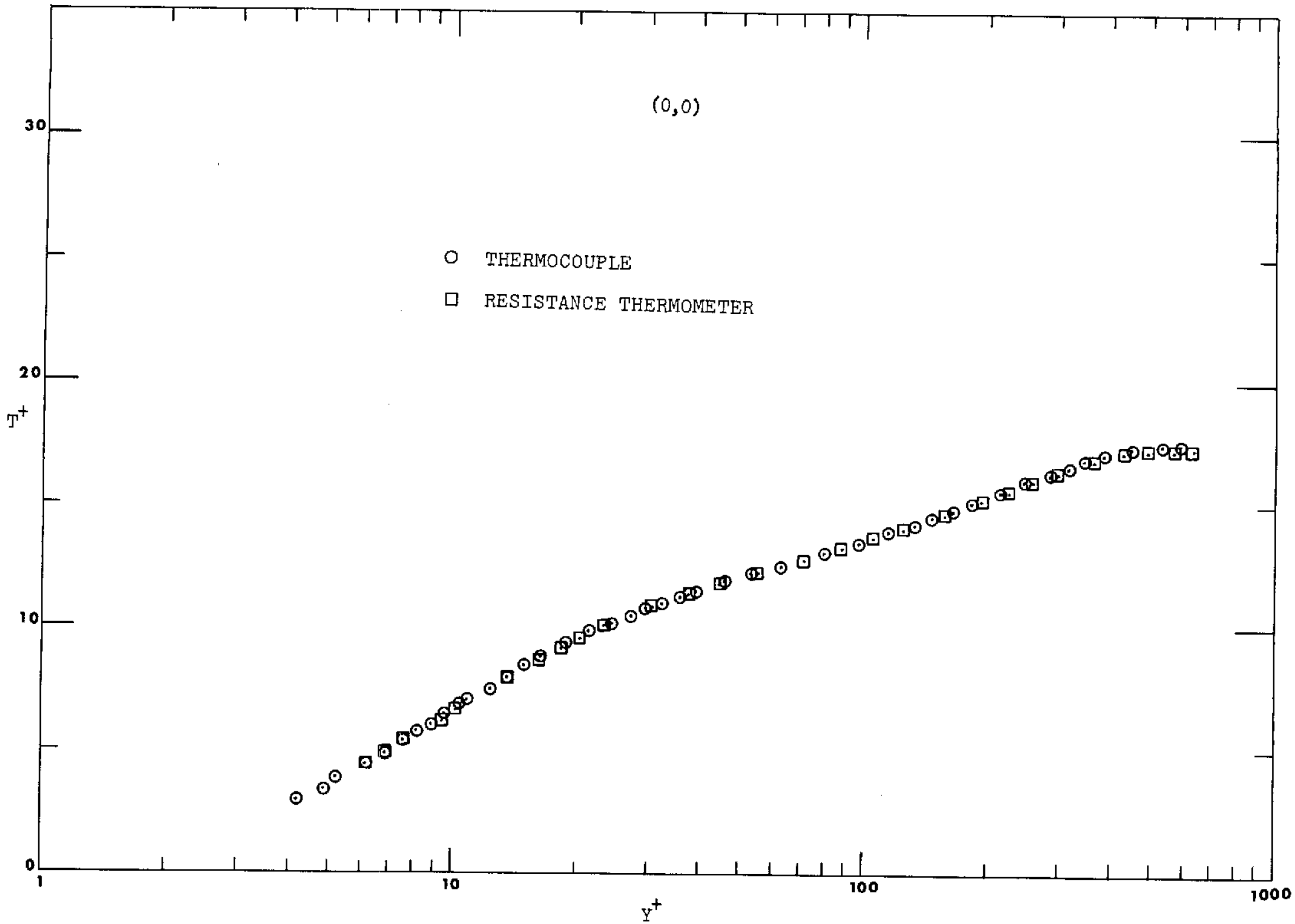

Fig. 3.11 Temperature measurements on a flat plate: thermocouple vs. resistance thermometer.

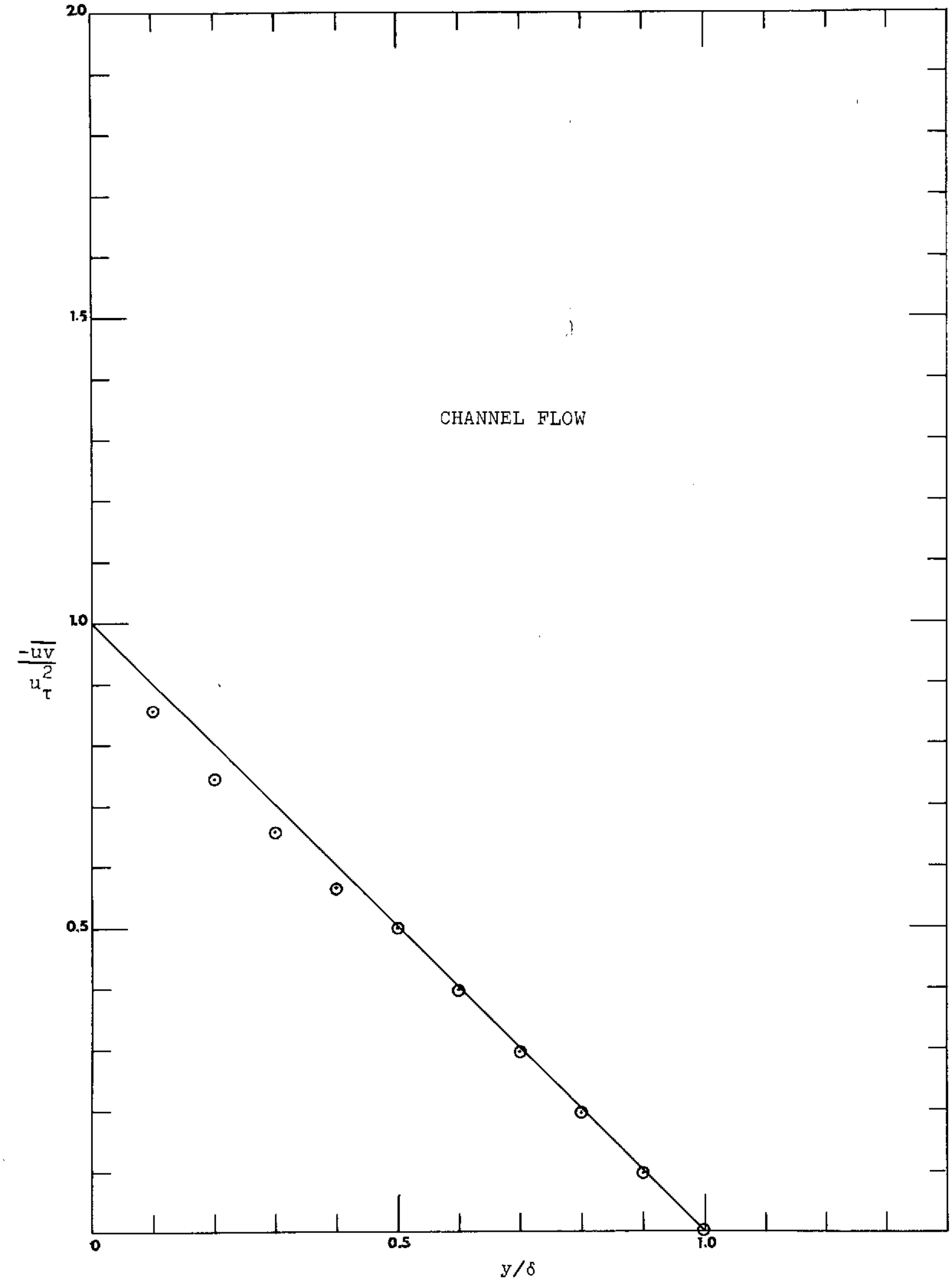

Fig. 3.12 Channel flow shear stress measurements: checking the hot-wire system.

CHAPTER 4

ANALYSIS OF STANTON NUMBER DATA

In this study, the analysis of Stanton number data consists of two parts: (1) constant wall temperature case, (2) step in wall temperature case.

For a given set of boundary conditions, the Stanton number data were taken twice to check the repeatability of the data. Also, several of Blackwell's [9] runs were repeated under exactly the same boundary conditions, and an excellent agreement, to within 1%, was found. The uncertainty of the data was estimated to be 3%, at most, by following the same procedure used by Blackwell [9]. For the step in wall temperature runs, the first plate downstream of the step does not give reliable data, due to conduction errors in the Stanton number determination procedure. That data point is listed, however, together with the data of all plates.

The Stanton number data are presented in the form of Stanton number vs. enthalpy thickness Reynolds number, Re_{Δ_T}. Values were measured for each of the 24 test plates, but the data from plates # 1, 2 and 24 will not be presented because of entrance and exit effects. Boundary layer measurements of enthalpy thickness Reynolds number are available for the locations at which the temperature and velocity profiles were measured (six stations). Blackwell [9] suggests that Re_{Δ_T} values obtained by integration of the two-dimensional boundary layer energy integral equation using the measured Stanton numbers may differ from the values obtained by probing the boundary layer for temperature and velocity profiles, due to streamline convergence or divergence. He has suggested that a better estimate for the enthalpy thickness Reynolds number could be obtained by curve-fitting the data from mean profiles and interpolating for the rest of the plates. This was tried during the present tests. The two procedures had an average difference of about 2%. In the worst case (strong suction) a maximum difference of 16% in Re_{Δ_T} was found, which gave a variation of 4% in St. However, only six temperature and velocity profiles were taken for each run, and, considering that Re_{Δ_T} as determined from profiles also has some uncertainty, it was decided to use the values from the energy equation method. Stanton number data were taken twice, and the average value chosen as representative of the flow.

4.1 Stanton Numbers for Constant Wall Temperature Conditions

Figure 4.1 shows Stanton number plots for a flat plate case and a strong adverse pressure gradient with different suction rates. From these data, it is concluded that an adverse pressure gradient has only a very small effect on Stanton numbers plotted as a function of Re_{Δ_T}. No difference is found between flat plate and the strong adverse pressure gradient data, to within the uncertainty of measurements. This same conclusion was also reached by Blackwell [9] for mild adverse pressure gradient flows.

Figure 4.2 plots Stanton number normalized by the unblown Stanton number, St_o, for the same enthalpy thickness Reynolds number as a function of the blowing parameter. The correlation used by Blackwell [9] and Whitten [3] is shown in the same figure by a solid line. The agreement is observed to be excellent, indicating that an adverse pressure gradient does not affect the Stanton number ratio as a function of the blowing parameter, for the same enthalpy thickness Reynolds number. It can be seen that even with strong suction and blowing the data deviate only slightly from this correlation.

The following expression, due to Whitten [3], is therefore recommended for mild and strong adverse pressure gradients, with transpiration:

$$\left.\frac{St}{St_o}\right|_{Re_{\Delta_T}} = \left(\frac{\ln(1+B_h)}{B_h}\right)^{1.25} (1 + B_h)^{.25} \quad , \qquad (4.1)$$

where the Stanton numbers are to be evaluated at the same enthalpy thickness Reynolds number. St_o is the Stanton number for zero transpiration and for the pressure gradient in question and $B_h = F/St$. Finally, from the evidence in Fig. 4.1, a flat plate Stanton number correlation could be used if data were not available for the pressure gradient in question.

The Reynolds analogy between heat and momentum transfer, as observed by Blackwell [9], is definitely not valid for adverse pressure gradient flows. While the adverse pressure gradient has only a very small effect on Stanton number, the skin friction coefficient varies over a wide range, as discussed in Chapter 5 (see Fig. 5.11).

The correlation expressed in Eqn. (4.1) was originally developed by Whitten [3] for constant B_h flows. The present investigation and Blackwell's [9] have verified it for slowly varying B_h: the case of constant F flows. The correlation statement can be written by means of the following expression:

$$\left.\frac{St}{St_o}\right|_{Re_{\Delta_T}} = f_1(B_h) \quad . \qquad (4.2)$$

Finally, it is interesting to note that the strongest suction run of this investigation approaches an asymptotic suction larger for $U_\infty \approx x^m$ flows (Fig. 4-1). The constant property, constant wall temperature energy integral equation can be written as

$$\frac{d\Delta_T}{dx} = St + F - \frac{m\Delta_T}{x-x_o} \quad , \qquad m < 0 \quad , \qquad (4.3)$$

For large values of x, the term $\Delta_T/(x-x_o)$ must approach zero, because Δ_T is approaching a constant value, which was verified in the present experiment. Thus, an asymptotic suction layer exists such that $St = - F$.

4.2 Stanton Numbers for Variable Wall Temperature Conditions

The purpose of this section is to present a step solution to be used with the superposition principle for calculating the Stanton number distribution resulting from an arbitrary wall temperature profile.

The superposition principle can be applied because the energy equation for constant-property, low-velocity flows is linear.

The step wall temperature boundary condition can be represented as

$$\begin{aligned} \Delta T &= 0 \quad , & x &< \ell \quad , \\ \Delta T &= \Delta T_o \quad , & x &> \ell \quad , \end{aligned} \qquad (4.4)$$

where ΔT is the difference between the wall and free-stream temperatures and ℓ is the unheated starting length along the x direction.

The effect on Stanton number of the unheated starting length can be expressed as the ratio of the non-isothermal to the isothermal Stanton number:

$$\phi(x;\ell) = \frac{St}{St_T} \quad . \tag{4.5}$$

This ratio is called the "step wall-temperature function" or "kernel" solution. It depends upon the flow conditions along the surface. Given this function, the total effect of any variation in wall temperature can be computed by the superposition principle.

In the present investigation, the wall temperature was varied in a stepwise manner and the total temperature difference at the i-th plate, $\Delta T(i)$, can be expressed as the sum of the steps in temperature ΔT_j, upstream of the plate:

$$\Delta T(i)(\text{local}) = \sum_{j=1}^{i} \Delta T_j(\text{upstream steps in } T_{wall}) \quad , \tag{4.6}$$

where

$$\begin{aligned} \Delta T(i) &= T_w(i) - T_\infty \quad , \\ \Delta T_j &= T_w(j) - T_w(j-1) \quad . \end{aligned} \tag{4.7}$$

For this case, the Stanton number correction resulting from all steps in T_w upstream of plate (i) is given by:

$$\phi(i) = \frac{St}{St_T} = \sum_{j=1}^{i} \phi_{ij} \frac{\Delta T_j}{\Delta T(i)} \quad , \tag{4.8}$$

where ϕ_{ij} is the kernel function, defined by Eqn. (4.5). As applied here, ϕ_{ij} is the effect on the Stanton number at plate (i), caused by a step in T_{wall} at an upstream plate (j). The function ϕ_{ij} can also be represented formally as $\phi(x_i;\ell_j)$.

The zero pressure gradient flows have already been well studied, and the expressions below for the kernels follow from Reynolds [37] and Whitten [3].

$$\phi_o(x;\ell;0) = \left[1 - \left(\frac{\ell}{x}\right)^{0.9}\right]^{-1/9} , \quad x > \ell , \tag{4.9}$$

$$\phi(x;\ell;F) = \frac{\exp\left[\frac{F}{St_{o_T}}\right] - 1}{\exp\left\{\frac{F}{St_{o_T}}\left[1 - \left(\frac{\ell}{x}\right)^{0.9}\right]^{1/9}\right\} - 1} \tag{4.10}$$

where the subscript o refers to the unblown case, and subscript T to the isothermal case.

The insensitivity to adverse pressure gradients of the Stanton number in the isothermal cases, shown in Section 4.1, suggested that the kernels would be valid in adverse pressure gradients. Analysis of the present step-wall temperature data showed agreement with these kernel functions to within 5% (even for the first plate downstream of the step) and two test cases with arbitrary wall temperature variations were chosen. These were mild adverse pressure gradient with no transpiration (-0.15,0) and strong adverse pressure gradient with strong suction (-0.275, -0.004). Fig. 4.3 shows the wall temperature profiles for the two test cases, while Fig. 4.4 shows the measured and calculated Stanton numbers.

4.3 Conclusions Regarding the Stanton Number Behavior

Two conclusions came out of this part of the study:

(1) The adverse pressure gradient, in the flows studied (nearly equlibrium flows), does not seem to have any influence on the relationship between the Stanton number and the enthalpy thickness Reynolds number, at least to within the uncertainty of measurements.

(2) The kernel functions as developed for the transpired flat plate cases with no pressure gradient are excellent approximations for adverse pressure gradient flows. They are, therefore, recommended for predicting Stanton number for an arbitrary wall temperature distribution. The no-transpiration, no-pressure gradient Stanton number correlation, well established in the literature, can be used as the unblown Stanton number

in the prediction scheme, and it is recommended according to the following expression:

$$St_o = 0.0154 \ (Re_{\Delta_T})^{-0.25} \quad . \tag{4.11}$$

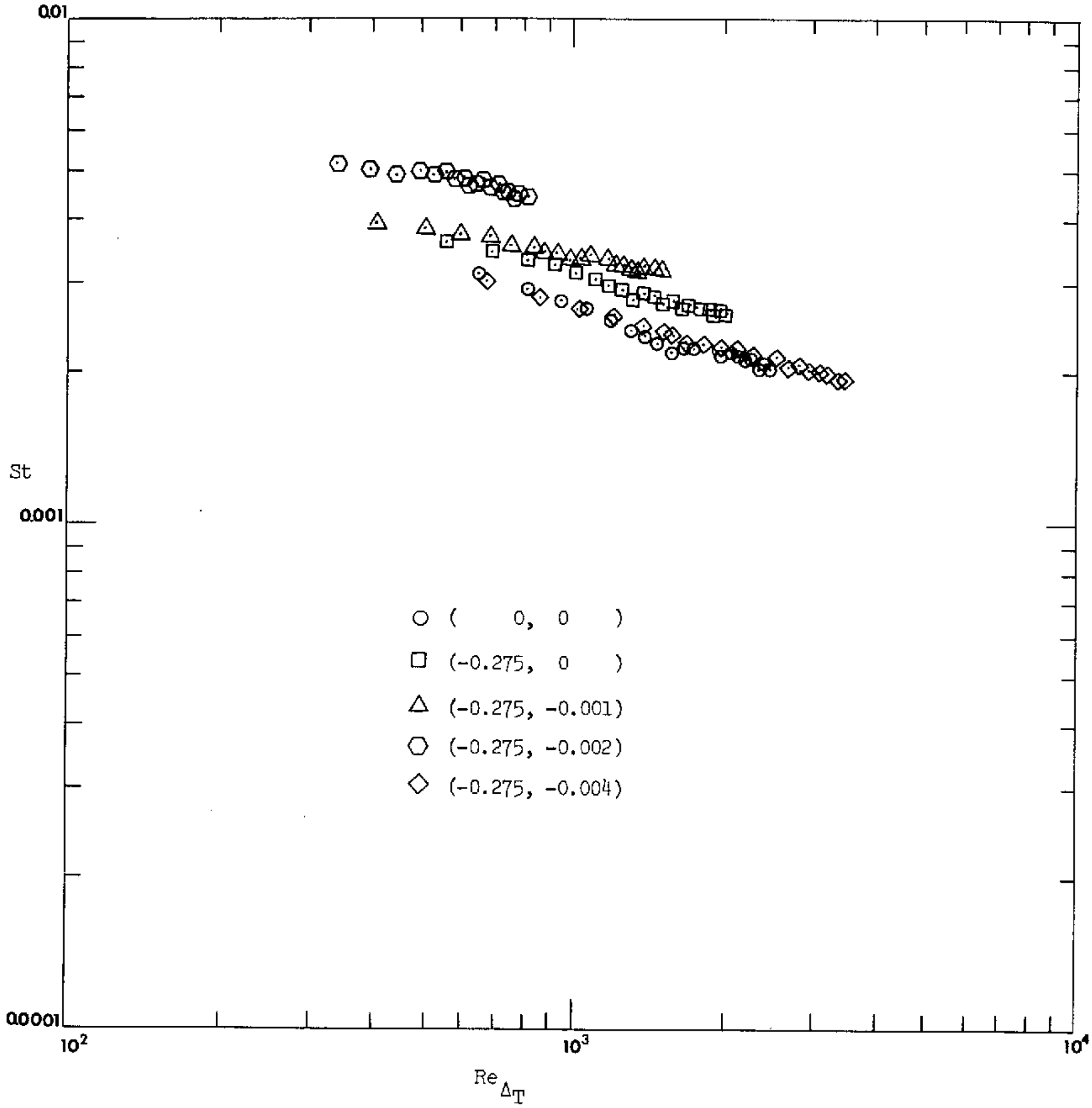

Fig. 4.1 Stanton number vs. enthalpy thickness Reynolds number -- strong adverse pressure gradient and flat plate values.

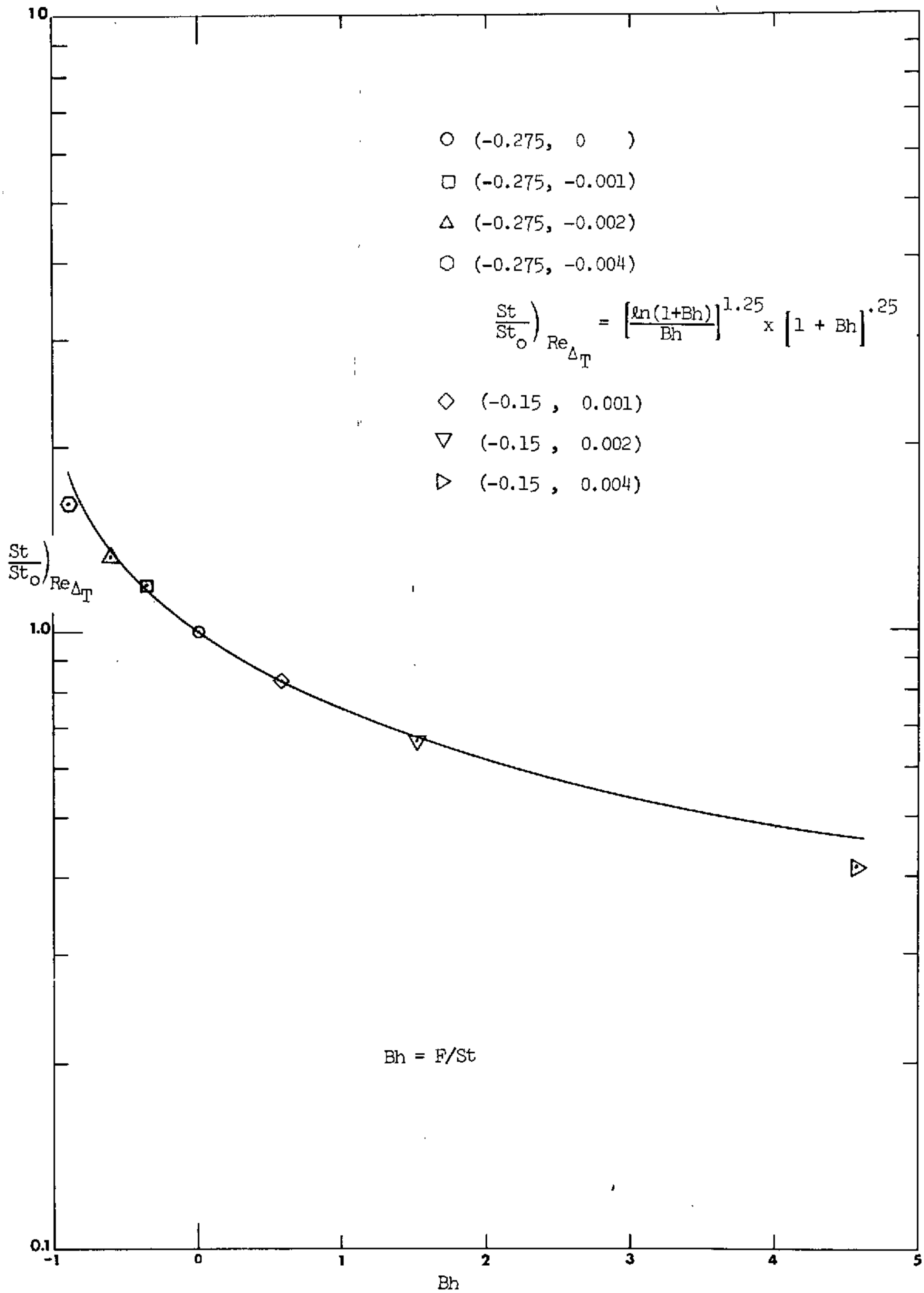

Fig. 4.2 The ratio between the actual Stanton number and its value with no transpiration at the same enthalpy thickness Reynolds number.

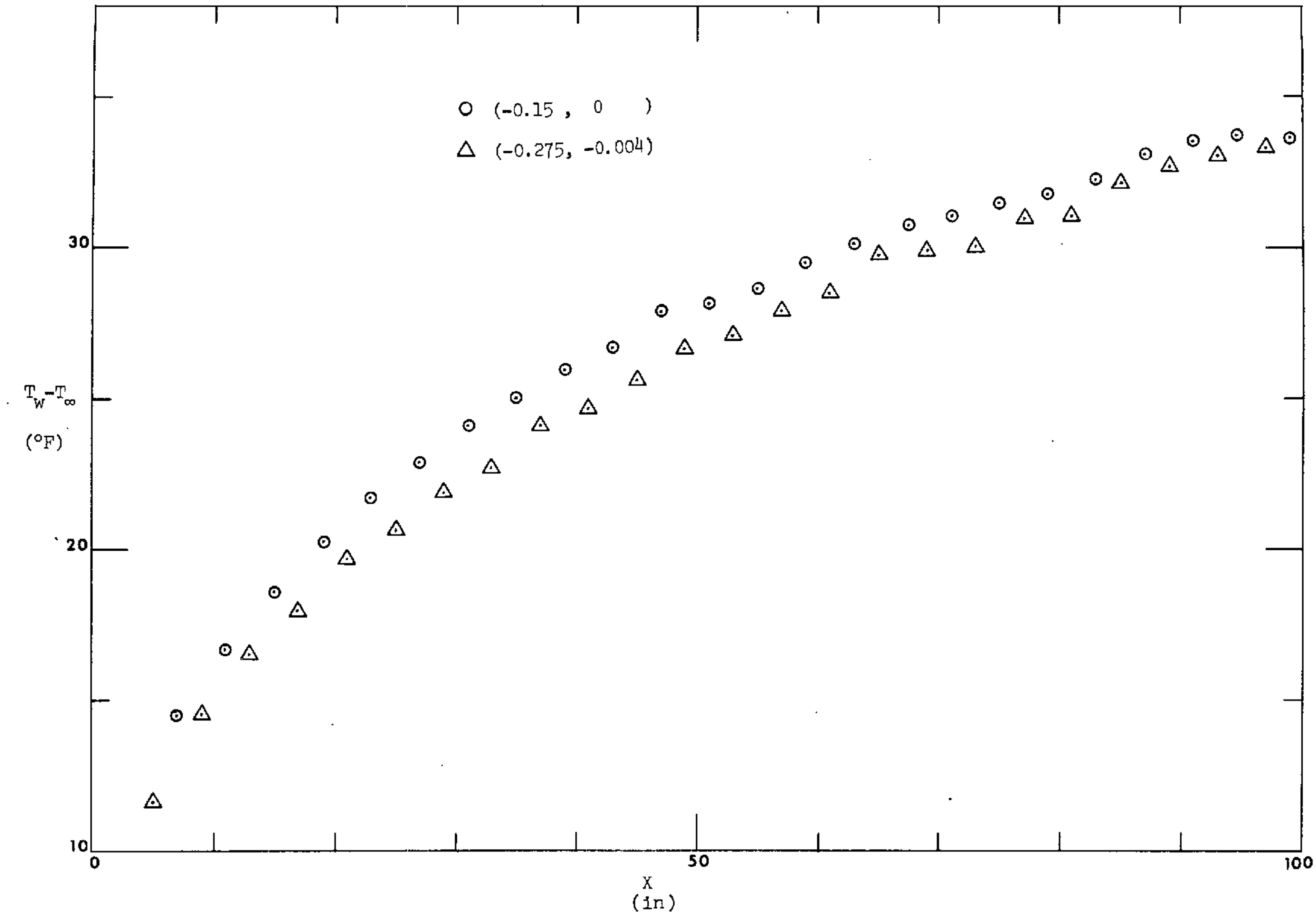

Fig. 4.3 Wall-temperature distributions for the variable temperature test cases (-0.15, 0) and (-0.275, -0.004).

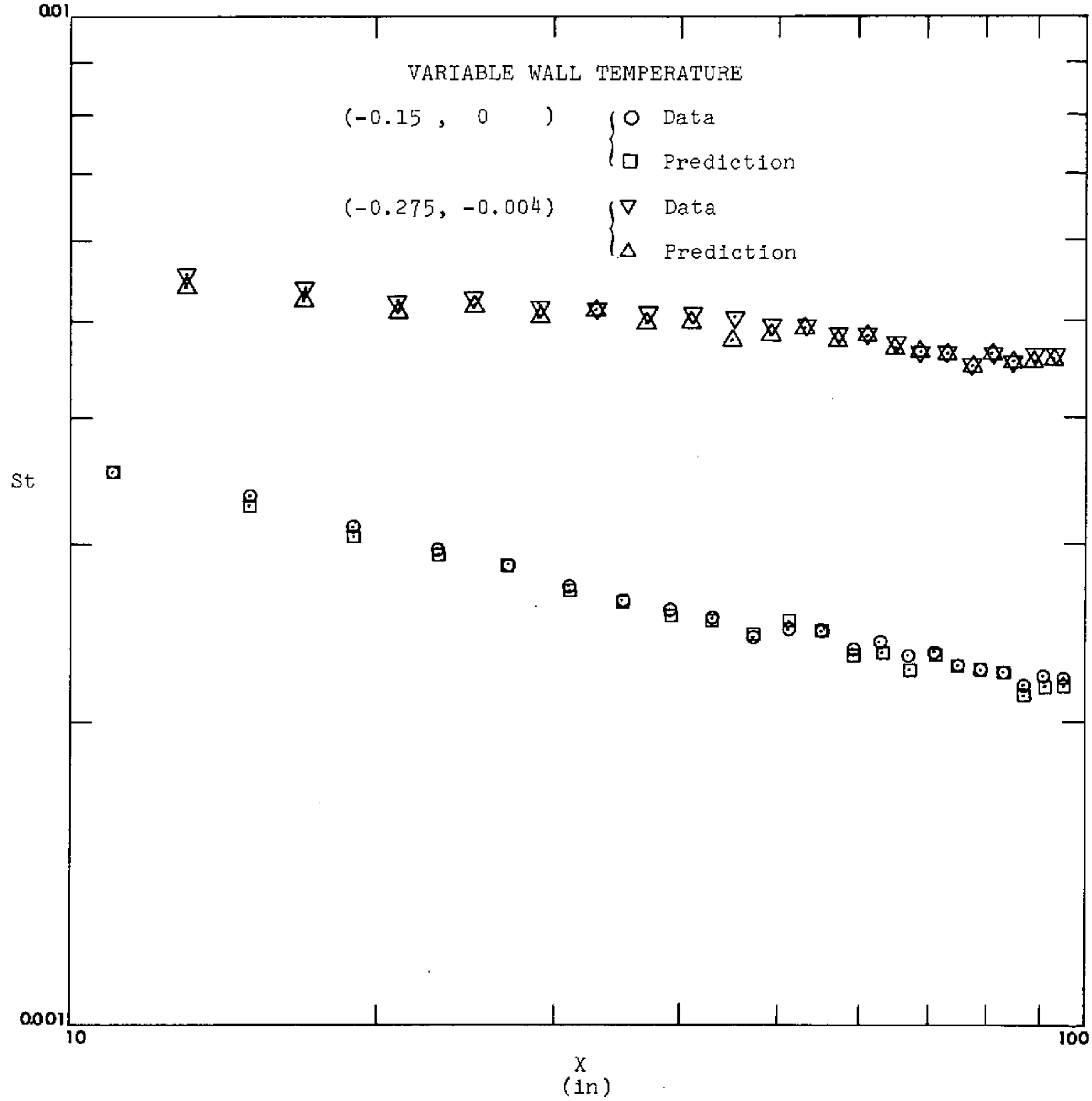

Fig. 4.4 Comparison of measured and predicted Stanton numbers for the variable wall temperature situations.

CHAPTER 5

ANALYSIS OF MEAN TEMPERATURE AND VELOCITY PROFILES

The mean velocity and temperature at each point in a boundary layer were measured sequentially with the same probe, as described in Chapter 3. Thus, no need exists for assuming a velocity profile from a "corresponding" isothermal flow. The uncertainties in the measurements are estimated to be ± 1% for velocity and ± 0.2°F for temperature.

The x-momentum equation, for incompressible flows, can be written as

$$\bar{u}\frac{\partial \bar{u}}{\partial x} + \bar{v}\frac{\partial \bar{u}}{\partial y} = -\frac{1}{\bar{\rho}}\frac{\partial \bar{p}}{\partial x} + \nu\frac{\partial^2 \bar{u}}{\partial x^2} + \nu\frac{\partial^2 \bar{u}}{\partial y^2} - \frac{\partial}{\partial x}(\overline{u'^2}) - \frac{\partial}{\partial y}(\overline{u'v'}) \quad (5.1)$$

The energy equation for low-velocity, constant-property flows can be written as

$$\bar{u}\frac{\partial T}{\partial x} + \bar{v}\frac{\partial T}{\partial y} = \alpha\frac{\partial^2 T}{\partial x^2} + \alpha\frac{\partial^2 T}{\partial y^2} - \frac{\partial}{\partial x}(\overline{u't'}) - \frac{\partial}{\partial y}(\overline{v't'}) \;. \quad (5.2)$$

The continuity equation for incompressible flows:

$$\frac{\partial \bar{u}}{\partial x} + \frac{\partial \bar{v}}{\partial y} = 0 \;. \quad (5.3)$$

5.1 Behavior of $\overline{u'v'}$ and Its Derivatives in the Region Very Close to the Wall

Expanding u' and v' in a Taylor series about $y = 0$,

$$u' = u'\Big|_o + \frac{u'}{y}\Big|_o y + \frac{\partial^2 u'}{\partial y^2}\Big|_o \frac{y^2}{2} + \ldots \;, \quad (5.4)$$

$$v' = v'\Big|_o + \frac{\partial v'}{\partial y}\Big|_o y + \frac{\partial^2 v'}{\partial y^2}\Big|_o \frac{y^2}{2} + \ldots \;, \quad (5.5)$$

but $u'\big|_o = 0$ and $v'\big|_o = 0$, and from continuity (5.6)

$$\underbrace{\left.\frac{\partial u'}{\partial x}\right|_o}_{0} + \left.\frac{\partial v'}{\partial y}\right|_o = 0 \quad , \tag{5.7}$$

so

$$\left.\frac{\partial v'}{\partial y}\right|_o = 0 \quad . \tag{5.8}$$

Therefore,

$$u' = \left.\frac{\partial u'}{\partial y}\right|_o y \tag{5.9}$$

$$v' = \left.\frac{\partial^2 v'}{\partial y^2}\right|_o \frac{y^2}{2} \quad . \tag{5.10}$$

So

$$\overline{u'v'} = \left.\overline{\frac{\partial u'}{\partial y}\frac{\partial^2 v'}{\partial y^2}}\right|_o \frac{y^3}{2} + \ldots \quad . \tag{5.11}$$

Therefore,

$$\left.\frac{\partial \overline{u'v'}}{\partial y}\right|_o = 0 \tag{5.12}$$

and

$$\left.\frac{\partial^2 \overline{u'v'}}{\partial y^2}\right|_o = 0 \quad . \tag{5.13}$$

5.2 Behavior of $\overline{v't'}$ and Its Derivatives in the Region Very Close to the Wall

Expanding t' in a Taylor series, about $y = 0$,

$$t' = t'\Big|_o + \left.\frac{\partial t'}{\partial y}\right|_o y + \left.\frac{\partial^2 t'}{\partial y}\right|_o \frac{y^2}{2} + \ldots \quad ; \tag{5.14}$$

but $t'\Big|_o = 0$, so

$$t' = \left.\frac{\partial t'}{\partial y}\right|_o y + \left.\frac{\partial^2 t'}{\partial y^2}\right|_o \frac{y^2}{2} \ . \tag{5.15}$$

Multiplying by (5.10) and time averaging,

$$\overline{v't'} = \left.\overline{\frac{\partial t'}{\partial y}\frac{\partial^2 v'}{\partial y^2}}\right|_o \frac{y^3}{2} + \ldots \ . \tag{5.16}$$

Therefore,

$$\left.\frac{\partial \overline{v't'}}{\partial y}\right|_o = 0 \tag{5.17}$$

and

$$\left.\frac{\partial^2 \overline{v't'}}{\partial y^2}\right|_o = 0 \ . \tag{5.18}$$

5.3 Validity of the Couette Flow Assumption in the Region Very Near the Wall

Expanding $\overline{u}$ in a Taylor series, about $y = 0$,

$$\overline{u} = \overline{u}\Big|_o + \left.\frac{\partial \overline{u}}{\partial y}\right|_o y + \left.\frac{\partial^2 \overline{u}}{\partial y^2}\right|_o \frac{y^2}{2} + \left.\frac{\partial^2 \overline{u}}{\partial y^3}\right|_o \frac{y^3}{6} + 0(y^4) \quad ; \tag{5.19}$$

but

$$\overline{u}\Big|_o = 0 \tag{5.20}$$

$$\left.\frac{\partial \overline{u}}{\partial y}\right|_o = \frac{u_\tau^2}{\nu} \ . \tag{5.21}$$

Evaluating the terms in the x-momentum equation, at $y = 0$, yields

$$\left.\frac{\partial^2 \overline{u}}{\partial y^2}\right|_o = v_o \frac{u_\tau^2}{\nu^2} + \frac{1}{\rho}\left.\frac{\partial \overline{p}}{\partial x}\right|_o \frac{1}{\nu} \ . \tag{5.21a}$$

Differentiating the x-momentum equation with respect to y, and evaluating the terms at $y = 0$,

$$\left.\frac{\partial^3 \bar{u}}{\partial y^3}\right|_o = \frac{v_o}{\nu}\left[\frac{v_o u_\tau^2}{\nu^2} + \frac{1}{\rho}\frac{\partial \bar{p}}{\partial x}\frac{1}{\nu}\right] + \frac{1}{\nu}\frac{\partial}{\partial y}\left(\frac{1}{\rho}\frac{\partial \bar{p}}{\partial x}\right) - \frac{\partial}{\partial y}\left(\frac{\partial^2 \bar{u}}{\partial x^2}\right)_o + \frac{\partial}{\partial y}\left(\frac{\partial \overline{u'^2}}{\partial x}\right)_o . \tag{5.22}$$

Thus,

$$\bar{u} = \frac{u_\tau^2 y}{\nu} + \left[v_o \frac{u_\tau^2}{\nu^2} + \frac{1}{\rho}\left.\frac{\partial \bar{p}}{\partial x}\right|_o\right]\frac{y^2}{2} + \left\{\frac{v_o}{\nu}\left[\frac{v_o u_\tau^2}{\nu^2} + \frac{1}{\rho}\left.\frac{\partial \bar{p}}{\partial x}\right|_o \frac{1}{\nu}\right] + \frac{1}{\nu}\frac{\partial}{\partial y}\left(\frac{1}{\rho}\frac{\partial \bar{p}}{\partial x}\right)_o - \frac{\partial}{\partial y}\left(\frac{\partial^2 \bar{u}}{\partial x^2}\right)_o + \frac{\partial}{\partial y}\left(\frac{\partial \overline{u'^2}}{\partial x}\right)_o\right\}\frac{y^3}{6} + \dots . \tag{5.23}$$

The conclusion is that the Couette flow assumption is valid in general to a second-order approximation very close to the wall and to a third-order approximation within the frame of the boundary layer assumptions. The expression for velocity can be written, therefore, in terms of dimensionless coordinates as

$$u^+ = y^+ + \left(p^+ + v_o^+\right)\frac{y^{+2}}{2} + v_o^+\left(v_o^+ + p^+\right)\frac{y^{+3}}{6} + 0\left(y^{+4}\right) . \tag{5.24}$$

Terms depending on the fluctuating quantities like $\overline{u'v'}$ and its derivatives are of higher orders.

The same conclusions can be reached for the temperature field, with respect to $\overline{v't'}$, and in dimensionless coordinates the temperature profile can be represented by

$$T^+ = \Pr y^+ + v_o^+ \Pr^2 \frac{y^{+2}}{2} + v_o^{+2} \Pr^3 \frac{y^{+3}}{6} + 0\left(y^{+4}\right) . \tag{5.25}$$

5.4 The Location of the First Data Point with Respect to the Wall

As seen in Chapter 3, the first data point position was measured by means of an optical comparator and by assuming that the same conditions of the measurement would hold during the data-taking procedure. Actually, this is not quite true, because small imperfections in the probe alignment can slightly change this distance. The uncertainty is estimated to be 0.001 in., but even this small variation can greatly change the profile in the region very near the wall. Blackwell [9] assumed that the Couette flow assumption was valid, and determined the position of the first point; he then shifted all others by the same amount. This can be a good procedure if Stanton number, as well as the local temperature, the wall temperature, and the free-stream temperature are each known with good accuracy, and the fluid properties are known, providing that the Couette flow assumption is really valid. This constitutes no problem, since a probing system is usually able to get very close to the wall. However, with so many uncertainties in the flow parameters, it is not really possible to decide whether the difference with respect to the Couette flow solution is due to uncertainties in the y-position or the flow parameters. Blackwell [9] had typically to shift upwards the position of his first data point by 0.0015 in. Analysis of the present data seems to indicate that the same trend would have to be followed.

It was decided, however, to keep the nominal value (as measured by the optical comparator) as representative of the position of the first point.

The velocity profile was corrected, in the neighborhood of the wall, for heat conduction losses from the probe according to Repik [35]. Typically, the correction amounted to 0.2 ft/sec at most.

The present procedure for measuring velocity and temperature sequentially gives a very smooth and accurate functional dependence of temperature upon the velocity, for the same y-position. In applications like the measurement of the turbulent Prandtl number where the ratio $(\partial T/\partial y)/(\partial \bar{u}/\partial y)$ has to be known, the direct differentiation $\partial T/\partial \bar{u}$ can be shown to be much more accurate, as far as numerical errors in the differentiation procedure are concerned.

5.5 Mean Velocity Profiles

As seen from Eqn. (5.24), the dimensionless velocity u^+ is a function not only of y^+, but also v_o^+ and P^+. If the same set of dimensionless coordinates is used to plot the data in the logarithmic region for all values of v_o^+ and P^+, no similarity between the profiles at different x-stations would be expected, since v_o^+ and P^+ vary from one station to the other.

Similarity may be recaptured by examining so-called "equilibrium flows." The concept of equilibrium layers as introduced by Clauser is related to an outer region similarity. This usually is referred to in graphs of mean velocity profiles shown in terms of non-dimensional defect velocity $(U_\infty - \bar{u})/u_\tau$ and y/Δ_2, where

$$\Delta_2 = \delta \int_0^1 \left[\frac{(U_\infty - \bar{u})}{u_\tau}\right]^2 d(y/\delta)$$

is the so-called Clauser boundary layer thickness.

Figures 5.1, 5.3, 5.5, 5.7 show, in these coordinates, the development of the turbulent boundary layer under a strong adverse pressure gradient with different transpiration rates. It can be seen that similarity holds, approximately, for the outer 70% of the boundary layer and that suction tends to expand this range.

Figure 5.9 presents the Clauser shape factor G, defined as

$$G = \Delta_2/\Delta \quad ,$$

where

$$\Delta = \delta \int_0^1 \left(\frac{U_\infty - \bar{u}}{u_\tau}\right) d(y/\delta)$$

for different x-stations and transpiration rates. As one can see, the desired "nearly equilibrium" condition is not achieved for all of the flows, since G is not constant with each flow. If one refers back to Figs. 5.1, 5.3, 5.5, 5.7, it can be seen that no inner region similarity exists, under the present conditions.

From these observations, plus the variation of G, one can deduce that the non-similarity of the inner region affects the value of G. The Clauser shape factor, G, is the resultant of an integration from the wall throughout the entire boundary layer. The velocity defect coordinates are appropriate only in the outer region. In flat-plate or mild adverse pressure gradients, the region of usefulness of the defect coordinates include the outer 90% of the boundary layer thickness and the contribution of the inner region to the value of G is thus negligible.

In strong adverse pressure gradients, however, the defect coordinate similarity holds only for the outer 70% of the boundary layer thickness, and the contribution of the inner region is not negligible. Thus we find relatively good outer similarity but, at the same time, a non-constant value of G.

5.6 Mean Temperature Profiles

Equation (5.25) shows that the dimensionless temperature profile T^+ is not a direct function of P^+. It is expected, therefore, that similarity, in defect coordinates, will hold over a larger portion of the boundary layer for the temperature profile than for the velocity profile. Figs. 5.2, 5.4, 5.6, 5.8 show the temperature defect plotted versus y/Δ_3 (defined below). The data confirm the expectations. The G_h shape factor, defined by Blackwell [9], can be written in terms of the temperature profile for a low-velocity, constant property flow as

$$G_h = \frac{\Delta_4}{\Delta_3} , \tag{5.26}$$

$$\Delta_4 = \delta_T \int_0^1 \left[\frac{(T_\infty - T)}{T_\tau}\right]^2 d(y/\delta_T) , \tag{5.27}$$

$$\Delta_3 = \delta_T \int_0^1 \left(\frac{T_\infty - T}{T_\tau}\right) d(y/\delta_T) . \tag{5.28}$$

Because of the extended similarity in the temperature case compared to the velocity case, the shape factor G_h is expected to have a much smaller scatter than G. This can be seen in Fig. 5.10. It can also be observed that this shape factor is not a function of the transpiration rate for the examined flows.

5.7 Determination of the Friction Coefficients

Friction coefficients were determined by Andersen's [8] shear stress method. The time-averaged x-momentum equation (boundary layer assumption) can be written as

$$\bar{u}\,\frac{\partial\bar{u}}{\partial x} + \bar{v}\,\frac{\partial\bar{u}}{\partial y} \;=\; -\frac{1}{\rho}\,\frac{\partial\bar{p}}{\partial x} + \nu\,\frac{\partial^2\bar{u}}{\partial y^2} - \frac{\partial}{\partial y}\,(\overline{u'v'}) \quad . \tag{5.29}$$

Integration of the equation from $y = 0$ to a point y somewhere in the inner region gives

$$\int_0^y \bar{u}\,\frac{\partial\bar{u}}{\partial x} + \bar{v}\,\frac{\partial\bar{u}}{\partial y}\;dy \;=\; -\frac{1}{\rho}\,\frac{\partial\bar{p}}{\partial x} + \nu\,\frac{\partial\bar{u}}{\partial y} - u_\tau^2 - \overline{u'v'} \quad . \tag{5.30}$$

The friction coefficient can be taken directly from the definition of $u_\tau^2 = U_\infty^2(C_f/2)$, and is given by

$$C_f/2 \;=\; \frac{\nu}{U_\infty^2}\,\frac{\partial\bar{u}}{\partial y} - \frac{\overline{u'v'}}{U_\infty^2} - \frac{1}{\rho}\,\frac{\partial\bar{p}}{\partial x}\,\frac{y}{U_\infty^2} - \frac{1}{U_\infty^2}\int_0^y \bar{u}\,\frac{\partial\bar{u}}{\partial x} + \bar{v}\,\frac{\partial\bar{u}}{\partial y}\;dy \;. \tag{5.31}$$

Once $\overline{u'v'}$ is measured at the particular y position, and mean velocity profiles have been taken at different x stations, then $C_f/2$ can be easily determined.

The friction coefficients were also determined by Andersen's law of the wall [8], but these values were found to be lower than the directly measured values. It is difficult to ascertain the cause of this discrepancy, but three candidates were examined. The first was the effect of three-dimensionality, not included in Eqn. (5.31). However, tests for 3-D effects were performed, as described in Chapter 3, Section 3.15, and the conclusion was that 3-D effects could be neglected. The second is related to the difficulty in determining the logarithmic region and its slope, when using Andersen's [8] law of the wall. The uncertainty can be high. Finally, during the course of the qualification procedure for the turbulent measurements, the skin friction was also measured for a zero pressure gradient, no transpiration case. Again, Andersen's law gave lower values, while the measured one was very close to Simpson's [2]. The measured skin friction was then preferred over the calculated one from Andersen's law of the wall.

Mean velocity and temperature profiles were taken at six stations for each run and the corresponding friction factor determined. Care was taken to avoid measurements in regions where the profile was not completely developed for the desired conditions (beginning of the test section), or in regions where end effects of the test section could influence the profile (end of the test section). Analysis of the data, however, shows that in the (-0.275, 0.000) run the profile is not completely developed at the first measured station (x = 22 in.); the last station (x = 82 in.), for each run, may still be disturbed by end effects.

Equation (5.31) for the friction coefficient can be cast in another form. If one uses the continuity Eqn. (5.3), the integral that appears in Eqn. (5.31) can be arranged so one gets (for constant density):

$$\frac{C_f}{2} = K\,\frac{U_\infty y}{\nu} + \frac{1}{U_\infty^2}\left(\nu\frac{\partial \bar{u}}{\partial y} - \overline{u'v'}\right) - \frac{1}{U_\infty^2}\frac{\partial}{\partial x}\int_0^y \bar{u}^2\,dy$$

$$- \frac{\bar{u}\,v_o}{U_\infty^2} + \frac{1}{U_\infty^2}\frac{\partial}{\partial x}\int_0^y \bar{u}\,dy \qquad (5.32)$$

Table E-1 shows the friction coefficients for the different runs of this investigation and, for comparison, the contribution of each term of Eqn. (5.32).

Figure 5.11 plots the friction coefficients as a function of momentum thickness Reynolds number. If we recall the discussion on Section 4.1, one can see that the friction coefficients are strongly influenced by the adverse pressure gradient and vary over a much wider range than do the Stanton numbers.

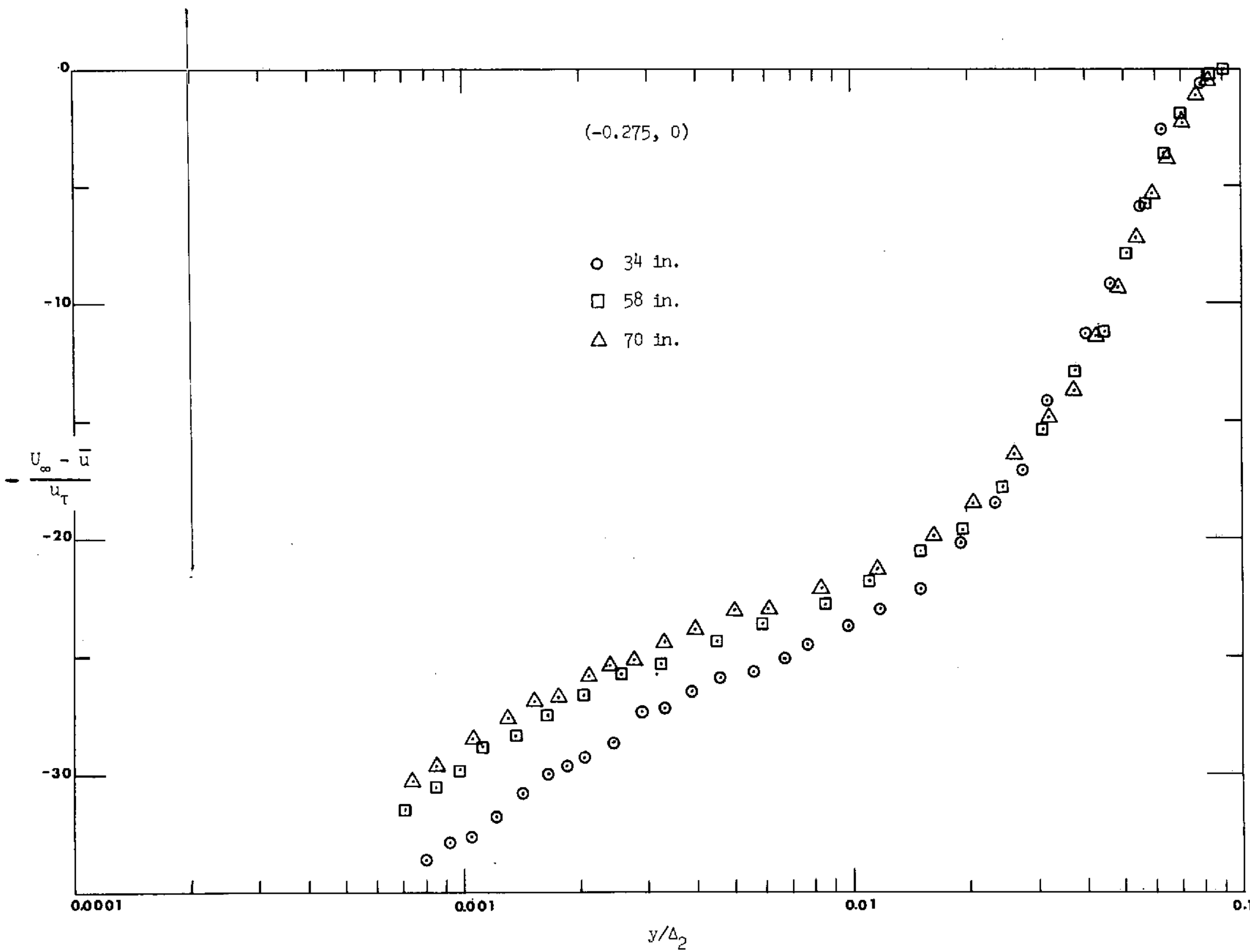

Fig. 5.1 Defect velocity profiles at different x-stations (-0.275, 0).

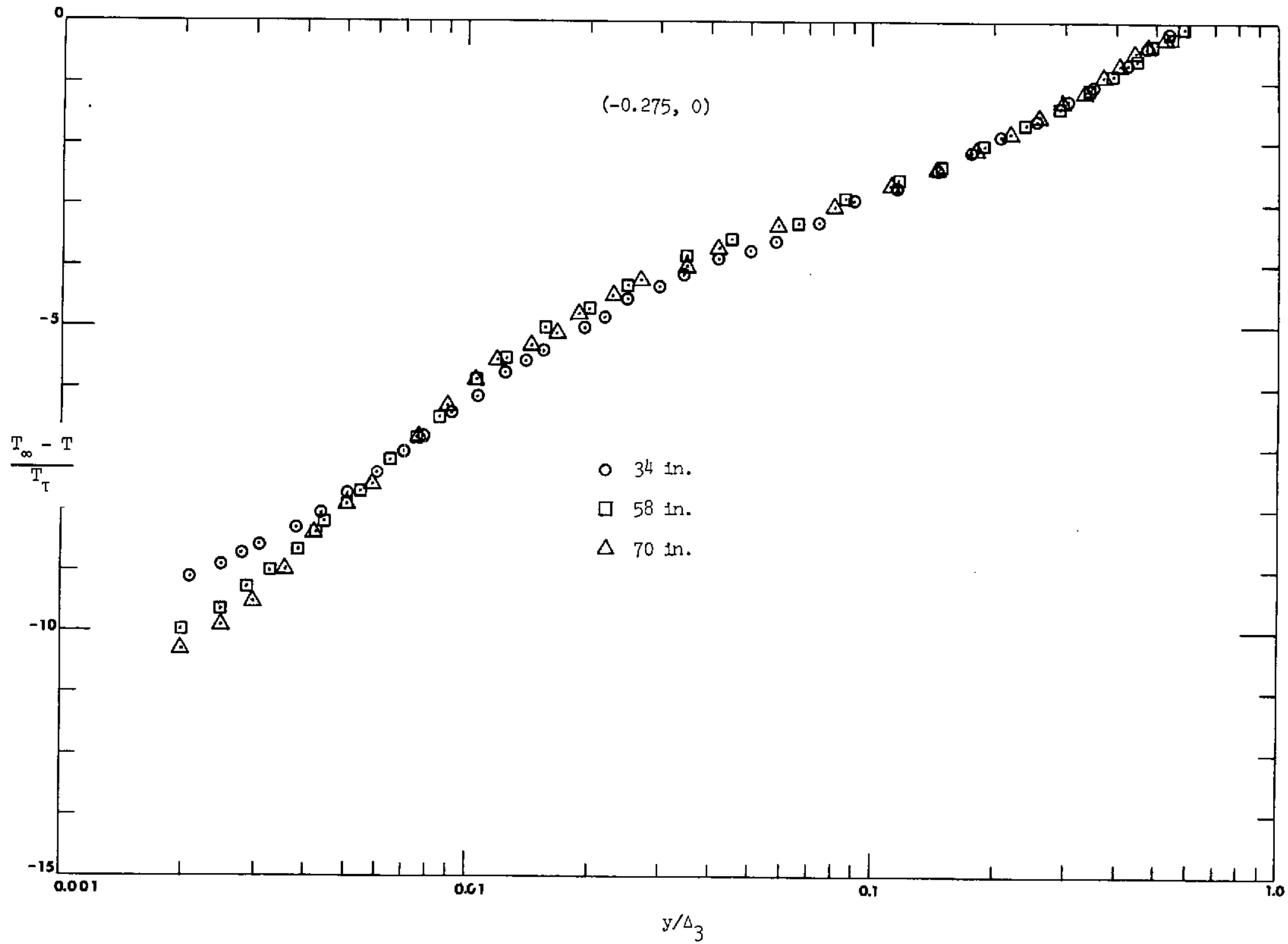

Fig. 5.2 Defect temperature profiles at different x-stations (-0.275, 0).

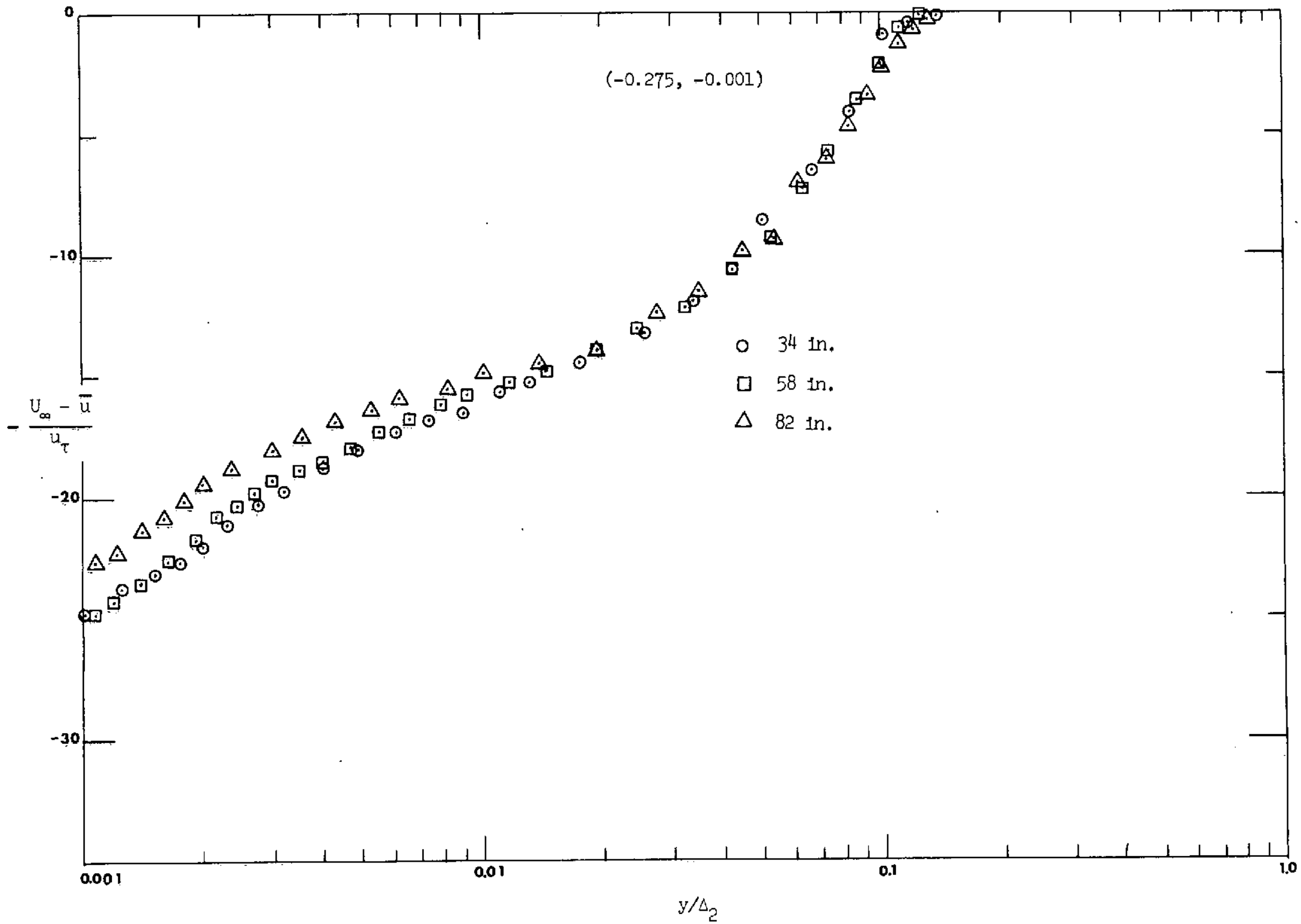

Fig. 5.3 Defect velocity profiles at different x-stations (-0.275, -0.001).

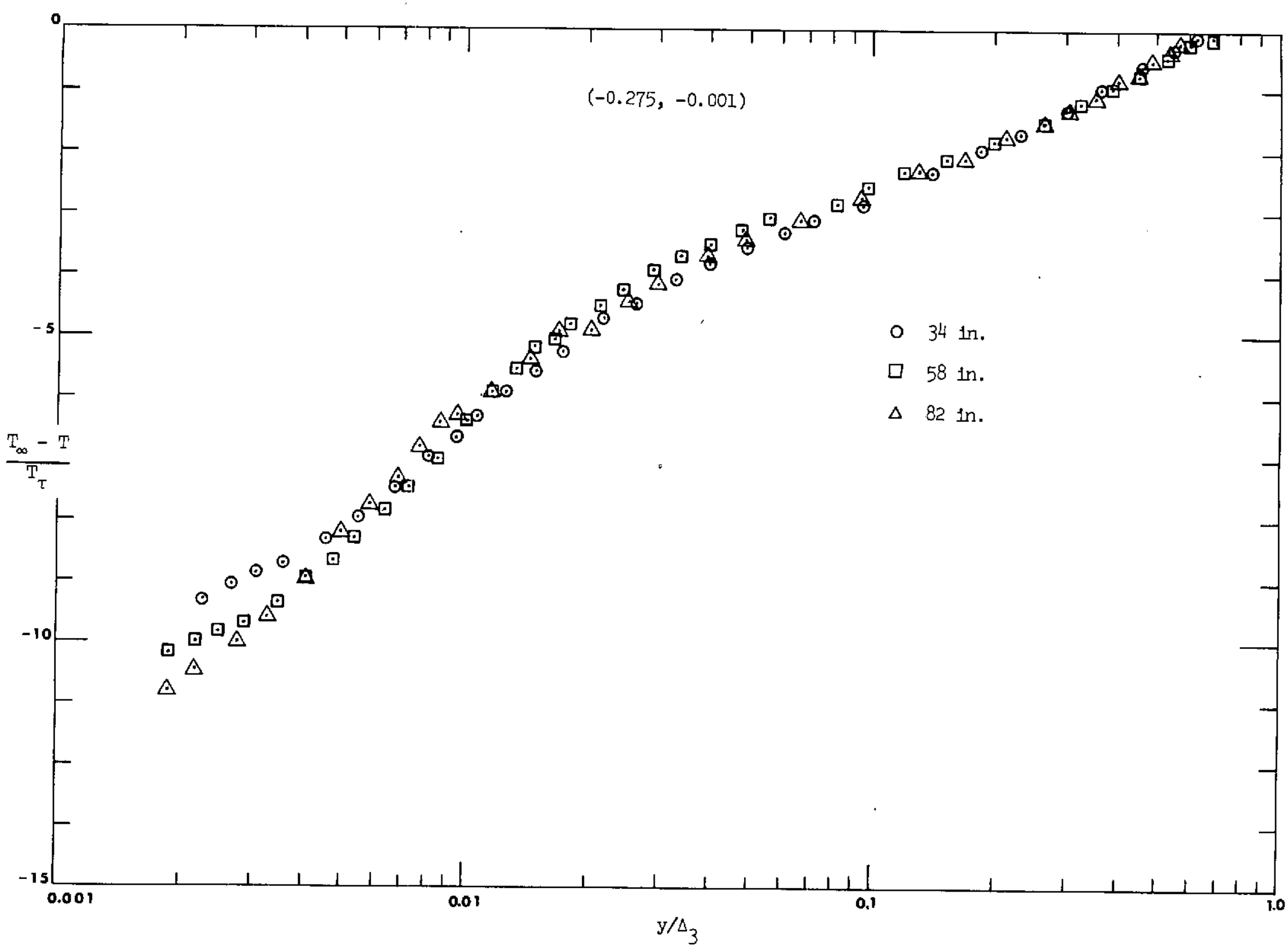

Fig. 5.4 Defect temperature profiles at different x-stations (-0.275, -0.001).

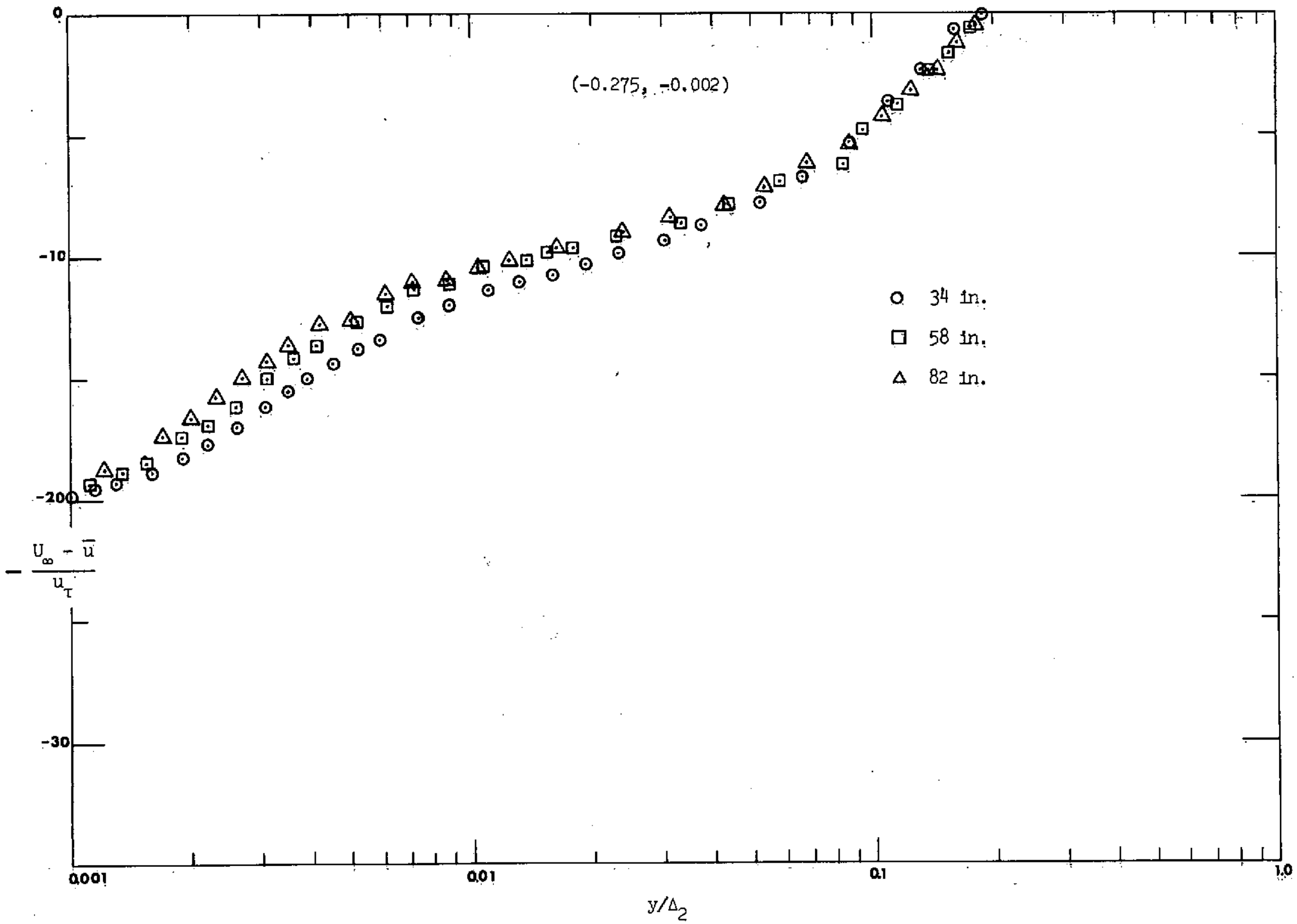

Fig. 5.5 Defect velocity profiles at different x-stations (-0.275, -0.002).

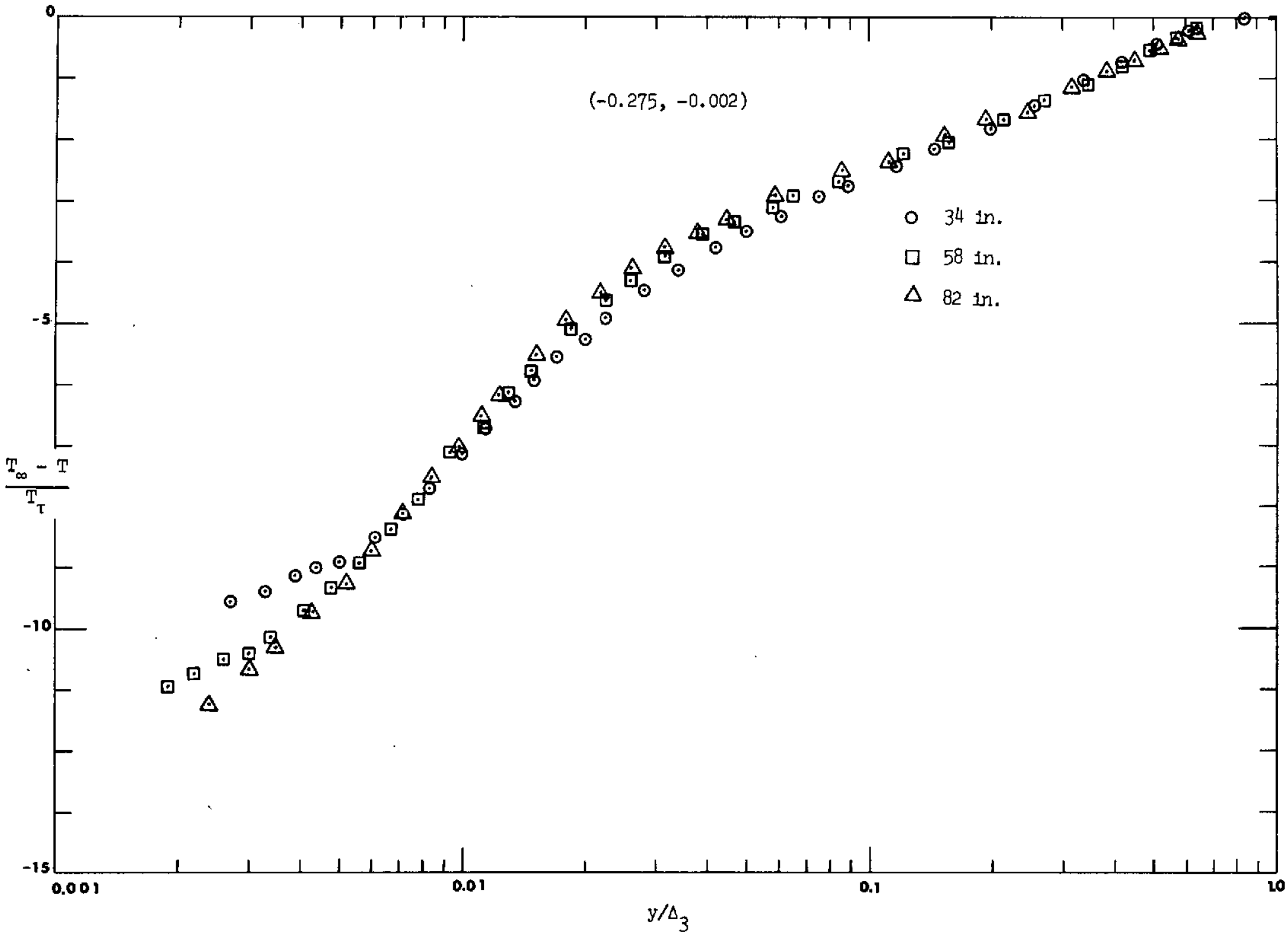

Fig. 5.6 Defect temperature profiles at different x-stations (-0.275, -0.002).

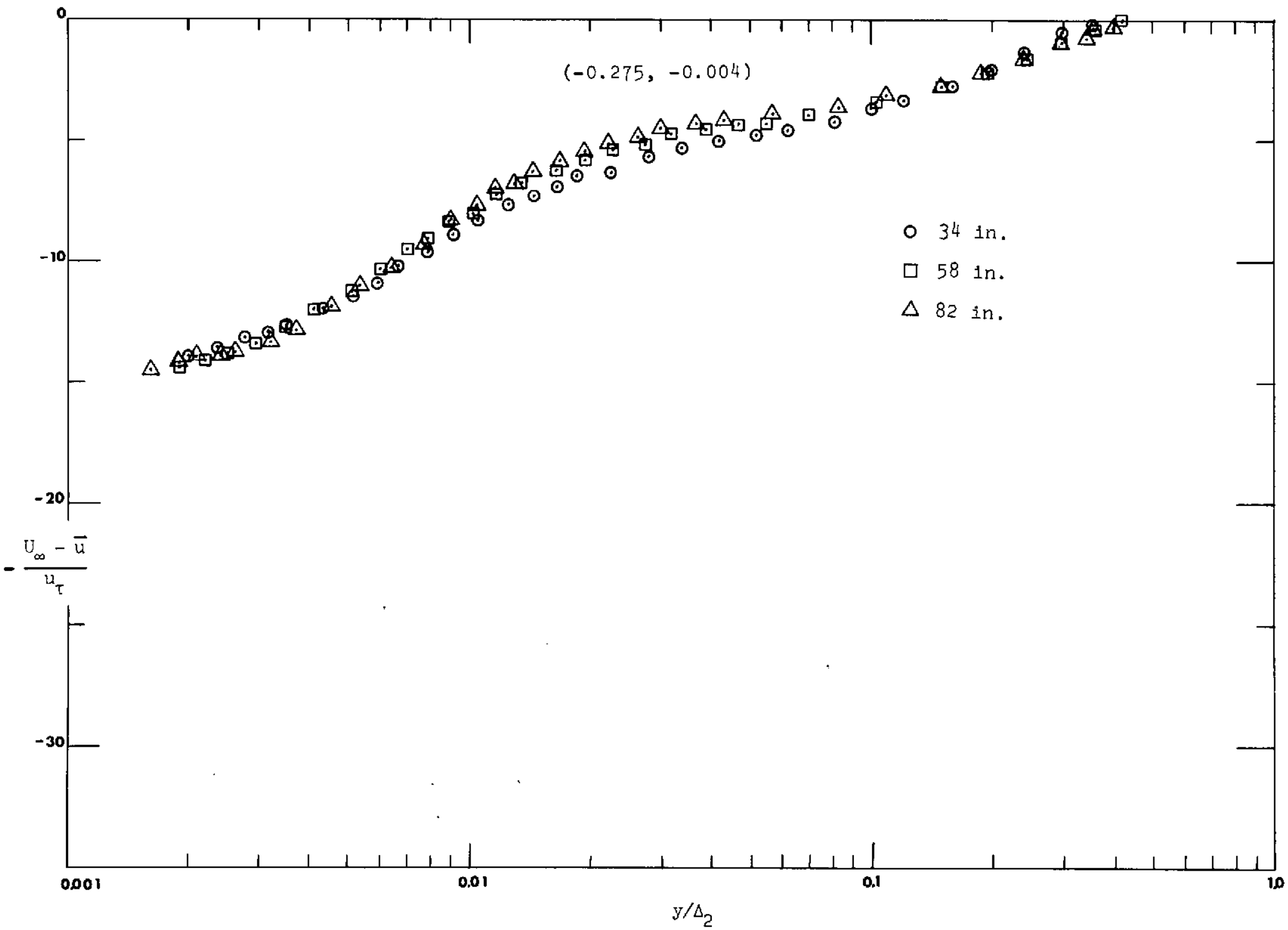

Fig. 5.7 Defect velocity profiles at different x-stations (-0.275, -0.004).

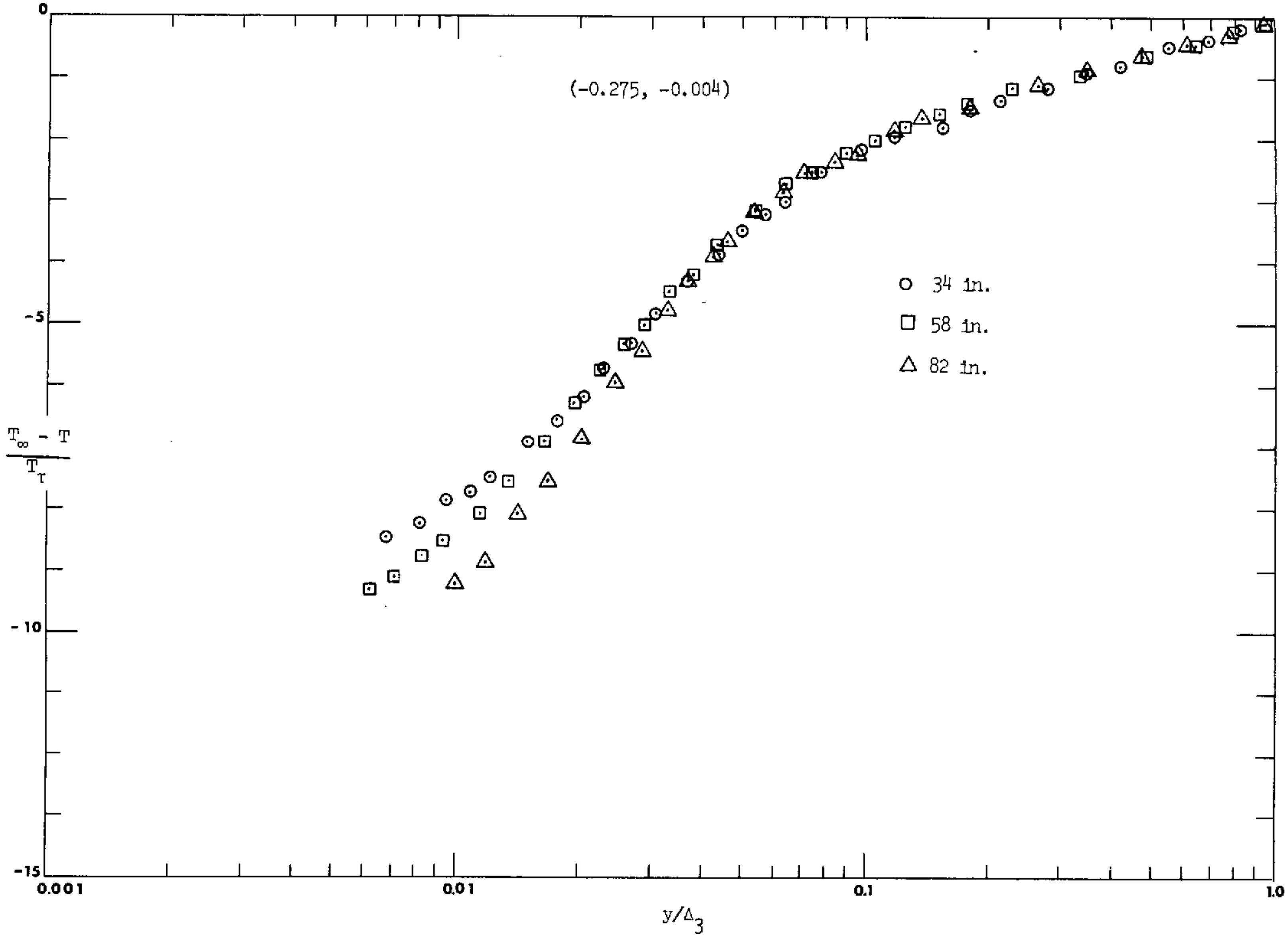

Fig. 5.8 Defect temperature profiles at different x-stations (-0.275, -0.004).

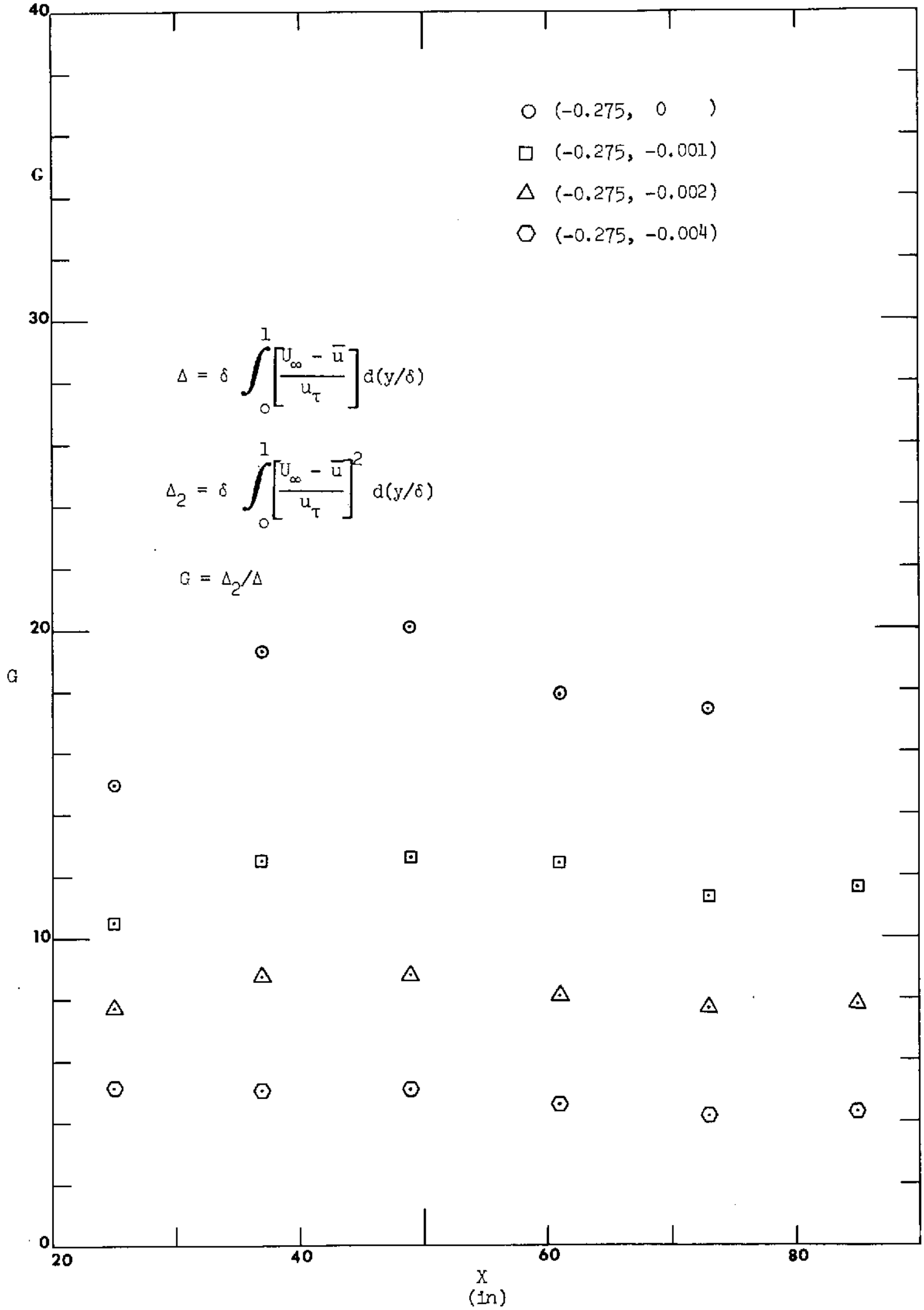

Fig. 5.9 Clauser shape factors for velocity as a function of x for different suction rates.

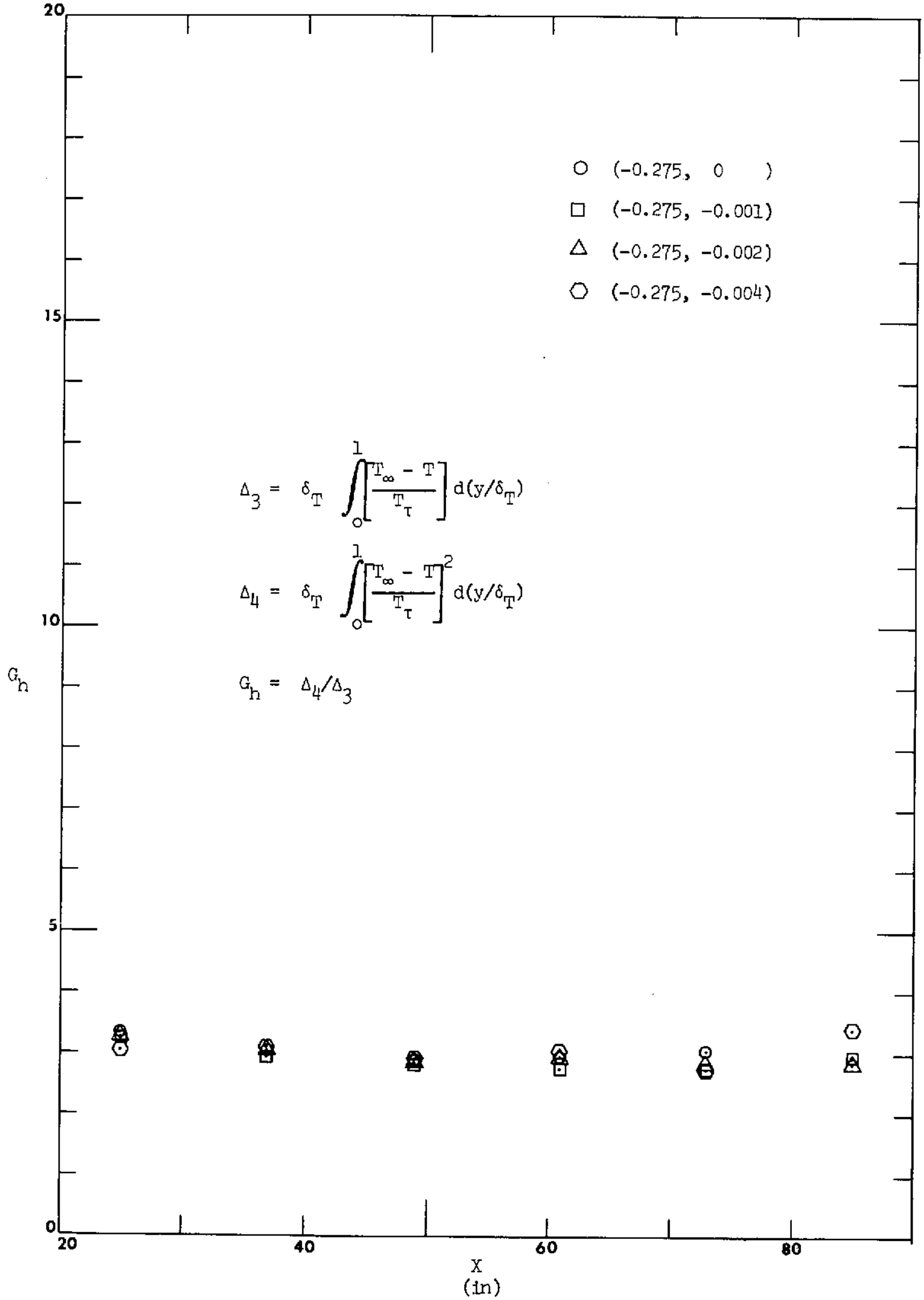

Fig. 5.10 Temperature shape factors as a function of x for different suction rates.

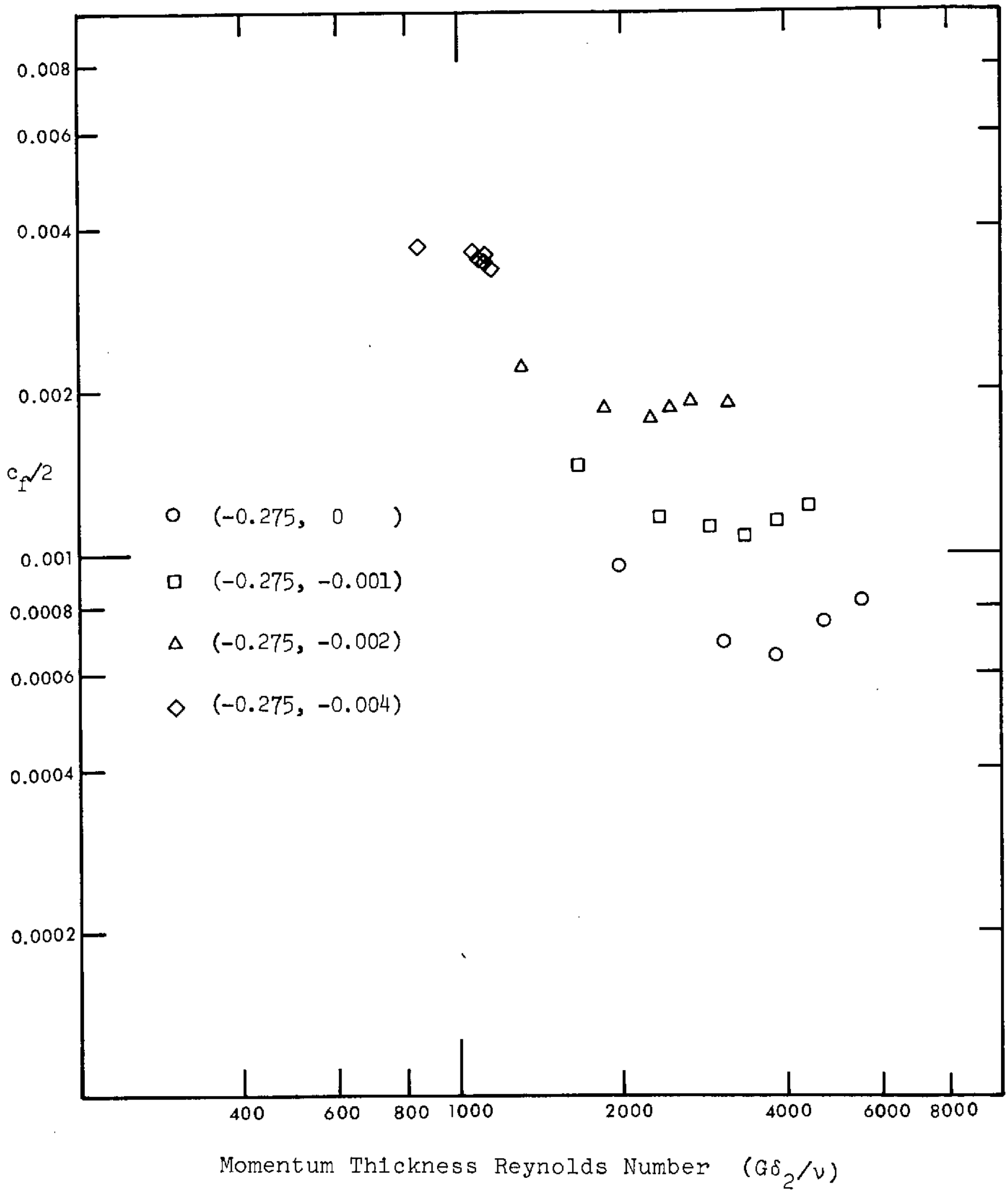

Fig. 5.11 Friction factor as a function of momentum thickness Reynolds number for strong adverse pressure gradient with suction.

CHAPTER 6

ANALYSIS OF THE TURBULENCE MEASUREMENTS

6.1 Hydrodynamics

Measurements of the turbulence quantities have previously been reported for zero pressure gradient boundary layers and completely developed pipe flows. Both spectral and Reynolds stress measurements are available for these cases. This investigation is concerned with Reynolds stress measurements in boundary layer flows subject to an adverse pressure gradient.

The zero pressure gradient flow has been well studied and several sets of measurements are available for reference. Klebanoff [31], for example, is considered a reliable source for a flat plate flow. Comparison is most fruitfully made in terms of similarity variables, as discussed in the following section.

6.1.1 Similarity variables for turbulence measurements

The x-momentum equation for a boundary layer flow can be written as

$$\bar{u}\frac{\partial \bar{u}}{\partial x} + \bar{v}\frac{\partial \bar{u}}{\partial y} = -\frac{1}{\bar{\rho}}\frac{\partial \bar{p}}{\partial x} + \nu\frac{\partial^2 \bar{u}}{\partial y^2} - \frac{\partial}{\partial y}\left(\overline{u'v'}\right) \quad . \tag{6.1}$$

In the inner region, however, the x-convective terms can be dropped and many experiments have shown that there is similarity of the mean flow when the following dimensionless coordinates are used:

$$u^+ = \frac{\bar{u}}{u_\tau} \quad \text{and} \quad y^+ = \frac{y u_\tau}{\nu} \tag{6.2}$$

where

$$u_\tau = U_\infty\sqrt{C_f/2}$$

Therefore, equation (6.1) can be written as:

$$v_o^+ \frac{du^+}{dy^+} = -P^+ + \frac{d^2u^+}{dy^{+2}} - \frac{d}{dy^+} \frac{\overline{u'v'}}{u_\tau^2} , \tag{6.3}$$

when the Couette flow assumption is used. This means that if there is to be inner region similarity of the mean flow field in terms of the above variables, the shear stress, $\overline{u'v'}$, must be normalized on u_τ^2, and the result should be a function only of y^+ in the inner region. As an extension to this similarity concept, the following dimensionless turbulent quantities, as functions of y^+, are offered as representative of flows which are similar in the inner region of a boundary layer:

$$\frac{\sqrt{\overline{u'^2}}}{u_\tau} , \quad \frac{\sqrt{\overline{v'^2}}}{u_\tau} , \quad \frac{\sqrt{\overline{w'^2}}}{u_\tau} , \quad \frac{-\overline{u'v'}}{u_\tau^2} . \tag{6.4}$$

In the outer region, when there is a mean flow field similarity, the following variables are used:

$$\frac{\bar{u}-U_\infty}{u_\tau} \quad \text{and} \quad y/\delta . \tag{6.5}$$

A similar reasoning would lead to analogous dimensionless turbulence quantities, as a function of y/δ, in the outer region of the boundary layer.

The dimensionless quantities (6.4) are used in this investigation for plotting the experimental data.

6.1.2 Comments on the measurement of turbulence quantities

The measurement of $\overline{u'v'}$ is usually done by means of two slant wires placed in a plane perpendicular to the wall and parallel to the mean flow direction. In regions of steep velocity gradients, it is expected that the non-uniform velocity distribution along each wire may cause some errors in the measurements, an effect which has been neglected by most investigators. Watts [13] measured $\overline{u'v'}$ with two slant wires located in planes parallel to the mean flow direction and banked 45° with respect to the wall. His measurements of $\overline{u'v'}$ were found to be higher

($\approx$ 6%) than the ones obtained by the usual procedure, with the wires in a plane perpendicular to the wall. Andersen [8] used just one rotatable slant wire, with the wire in a plane perpendicular to the wall. The present investigation used only a rotatable slant wire, with the measurements made in a plane inclined 60° with the wall, similar to that of Watts [13]. The present measurements of friction coefficient for a zero pressure gradient flow were found to be higher than Andersen's [8] by 8%, indicating again that the measured $\overline{u'v'}$ may be a function of wire orientation. A test was carried out by Pimenta [40], using the single rotatable wire procedure and the same difference was noticed. A further investigation on the hot-wire response is therefore necessary to resolve this difference. It is believed, however, that the banked position is the best one for this kind of measurement. Actually, the closest possible to the plane of constant velocity is recommended because the non-uniformity of the velocity distribution along the wire would be smaller. The sensitivity of the wire to the normal velocity, however, would be smaller, which limits the accuracy of the hot wire for $\overline{u'v'}$ measurement. The same kind of errors would also be present in the measurement of $\overline{v'^2}$ and $\overline{w'^2}$.

6.1.3 The zero pressure gradient flow

This flow has received a great deal of attention from investigators because of its relative simplicity. A few conclusions can be inferred from several experiments.

(1) The free stream turbulence intensity strongly influences the turbulence structure of the outer region of the boundary layer. Figure 6.1 shows a comparison between Klebanoff's [31] and the higher turbulence intensity data of the present investigation. The same effect was also noted, for accelerated flows, by Kearney [39]. The mean velocity field, however, does not seem to be much influenced by the turbulence. Sharan [41] discusses cases where the mean velocity is the same but the turbulence profiles are different. This suggests that the turbulence profiles should be functions of the free stream turbulence level and not simply functions of the mean velocity profile, as implied by the mixing-length theory.

(2) The fluctuation field seems to extend far beyond the edge of the momentum boundary layer (based on the mean velocity). Analysis of Watts' [13] and Klebanoff's [31] data shows that the free stream turbulence level is reached at $y/\delta \approx 1.4$. The observation is confirmed by the present investigation. This would suggest, therefore, that there is a region of the boundary layer which is characterized by the existence of turbulence in the absence of significant mean velocity deficit.

(3) The stream-wise normal velocity correlation, $-\overline{u'v'}/\sqrt{\overline{u'^2}}\ \sqrt{\overline{v'^2}}$ is found to be approximately equal to the Karman constant ($\kappa = 0.41 - 0.44$) in the outer region of the boundary layer ($0.2 < y/\delta < 0.8$). Klebanoff [31] reports a value in the neighborhood of 0.5.

(4) The ratio between the turbulent shear stress $-\overline{u'v'}$ and the kinetic energy of turbulence in the outer region of the boundary layer is found to be approximately constant and equal to 0.14, as already observed by other investigators (i.e., Townsend [42] and Bradshaw [43]).

6.1.4 Adverse pressure gradient flows

In the present study, measurements have been taken for all Reynolds stress tensor components in adverse pressure gradient flows with varying amounts of suction.

Comparisons to zero pressure gradient and mild adverse pressure gradient flows show that the production of turbulence increases when the pressure gradient increases. This can be verified by measuring the ratio between the rms value of the longitudinal velocity fluctuation and the local mean velocity, $\sqrt{\overline{u'^2}}/\overline{u}$.

A plot of $\sqrt{\overline{u'^2}}/u_\tau$ shows that the turbulence level profile has two peaks. The second one is located in the outer region of the boundary layer ($y/\delta \approx 0.5$) and can be seen in Fig. 6.2. Suction is observed to suppress the outer peak.

It is observed that when suction increases, the outer peak is reduced in magnitude much more than the inner one. This suggests that a mechanism is present which inhibits the diffusion of turbulent kinetic energy from the inner to the outer region of the boundary layer. This can be also verified by comparison to the zero pressure gradient and mild pressure gradient data of Andersen [8] and the strong adverse pressure gradient data of Bradshaw [43]. The outer layer peak is observed to be displaced outwards when the pressure gradient increases. This fact, associated with the observation that the production of turbulence is larger for a higher adverse pressure gradient, suggests that the diffusion of turbulent kinetic energy by pressure fluctuation may be important in the formation of the outer layer peak. The y-momentum boundary layer equation can be integrated to give the following expression:

$$\bar{p}_o = \bar{p} + \rho\overline{v'^2} \quad . \tag{6.6}$$

Suction reduces the turbulence level and $\overline{v'^2}$ becomes smaller. As a consequence, the local static pressure approaches the free stream static pressure and the local pressure fluctuations become smaller. In flows of relatively low turbulence level, the pressure fluctuation term is not probably large enough to generate a second peak.

Although measurements have been taken by other investigators for adverse pressure gradient flows, like, for example, Andersen [8] and Bradshaw [43], no mention of the presence of the second peak was found in the literature. It seems that a better understanding of this phenomenon would help to improve the predictive capability of turbulent flows. Figs. 6.3, 6.4, and 6.5 show, respectively, profiles for $\sqrt{\overline{v'^2}}/u_\tau$, $\sqrt{\overline{w'^2}}/u_\tau$, and the dimensionless shear stress $-\overline{u'v'}/u_\tau^2$. It can be concluded that a turbulence model used for predicting $\overline{u'v'}$ must not rely solely on the mean velocity field dependence. The peak of the $\overline{u'v'}$ profile in the outer region of the boundary layer cannot be explained by a mean field hypothesis, nor can the effects of the free stream turbulence. Some acknowledgment must be made of the turbulence. Many different approaches are possible. The Prandtl-Kolmogorov model, for example, uses both the turbulent kinetic energy and the mean velocity gradient as descriptors of the shear stress $\overline{u'v'}$, as follows:

$$-\overline{u'v'} = a\ \ell \sqrt{\overline{q^2}}\,\frac{d\bar{u}}{dy} \quad . \tag{6.7}$$

It has the potentiality of simulating, at least qualitatively, the turbulent process, when the mean flow pressure gradient is not zero.

For zero pressure gradient boundary layer flows, the use of an equation for the turbulent kinetic energy has been demonstrated to result in only a marginal improvement in mean velocity prediction. It seems likely, however, that its influence will be noticed more clearly when predicting flows under strong adverse pressure gradient and transpiration rate conditions, like some of Andersen's [8] flows.

Figures 6.6 and 6.7 show the correlation coefficients between the longitudinal and normal velocity components. The mild adverse pressure gradient of Andersen [8] and the strong one of this investigation demonstrate that, for equilibrium pressure gradients (defined as flows which have outer-region similarity), the correlation coefficient is approximately the same value as the Karman constant $\kappa(0.41-0.44)$. This indicates, therefore, similarities in the turbulent transport of momentum for these different equilibrium flows.

Figures 6.8 and 6.9 show the ratio between the shear stress and the kinetic energy of turbulence. For equilibrium adverse pressure gradient flows, it is concluded that in the outer region of the boundary layer an approximately constant value of 0.14 is appropriate. This fact has already been observed by Bradshaw [44], who employed a calculation procedure based on the constancy of this ratio for numerically predicting the mean flow field.

6.2 Temperature

Measurements of the temperature fluctuations and the turbulent heat transfer do not seem to be common in the literature. The lack of investigations in this area is due mainly to an experimental difficulty which makes the measurements complicated and time-consuming. Among the small number of measurements in the literature, only a few deal with $\overline{v't'}$ measurements, while several report $\overline{u't'}$ data.

6.2.1 Similarity variables for temperature and heat flux measurements

The energy equation for a low-velocity, constant property turbulent boundary layer flow can be written as

$$\bar{u}\,\frac{\partial T}{\partial x} + \bar{v}\,\frac{\partial T}{\partial y} = \alpha\,\frac{\partial^2 T}{\partial y^2} - \frac{\partial}{\partial y}\,(\overline{v't'}) \quad . \tag{6.8}$$

In the inner region, experiments have shown that there is a similarity of the mean temperature field when the following coordinates are used:

$$y^+ = \frac{yu_\tau}{\nu} \quad \text{and} \quad T^+ = \frac{T_w - T}{T_\tau} \quad , \tag{6.9}$$

where $T_\tau = (T_w - T_\infty)\mathrm{St}/\sqrt{C_f/2}$.

Equation (6.8) can be written as

$$v_o^+\,\frac{dT^+}{dy^+} = \frac{1}{Pr}\,\frac{d^2T^+}{{dy^+}^2} - \frac{d}{dy^+}\,\frac{\overline{v't'}}{u_\tau T_\tau} \quad , \tag{6.10}$$

when the Couette flow assumption is used. If there is similarity of the mean temperature field in terms of the above variables, then the velocity-temperature correlation must be normalized on the product $u_\tau T_\tau$. Further, from the fact that the mean temperature field is normalized on T_τ, the rms value of the temperature fluctuation should also be normalized on T_τ, leading to the set of dimensionless variables:

$$\frac{\sqrt{\overline{t'^2}}}{T_\tau} \;, \quad \frac{\overline{v't'}}{u_\tau T_\tau} \;, \quad \frac{T_w - T}{T_\tau} \;, \quad \text{and} \quad \frac{yu_\tau}{\nu} \;, \tag{6.11}$$

A similar reasoning would lead to analogous dimensionless turbulence quantities, as a function of y/δ_T, in the outer region of the boundary layer. However, it seems natural to compare the velocity and the temperature field, and this can be done more easily if y/δ (boundary thickness for the velocity field) is used as the independent variable. Naturally, this can only have a meaning when the momentum layer is approximately as thick as the thermal layer.

6.2.2 The zero pressure gradient flow

Only one reference was found in the literature for the measurement of $\sqrt{\overline{t'^2}}$, when the virtual origin of the momentum and thermal layers nearly coincide -- Fulachier and Dumas [26]. Fig. 6.10 shows a comparison between the flat plate measurements of this investigation and those of Fulachier and Dumas [26]. It can be seen that their values are higher in the outer region. It is not clear whether the comparison was made in inappropriate dimensionless variables or whether the free stream temperature turbulence level was different for the two experiments.

Figure 6.11 shows the dimensionless temperature fluctuation profile compared with the dimensionless longitudinal velocity fluctuation profile. It can be seen that the temperature peaks at a larger distance from the wall than does the velocity. The ratio is approximately 1.4 or the inverse of the molecular Prandtl number, if a generalization can be made upon this one observation. This fact naturally suggests that the thickness of the thermal sublayer is larger than the momentum one by the same amount. This is not totally unexpected; the mean values of the dimensionless temperature and velocity profiles in the sublayer can be written as

$$u^+ = y^+ \;, \qquad T^+ = \Pr y^+ \;. \tag{6.12}$$

Experiments have shown that the thermal sublayer extends farther away from the wall than the momentum sublayer. Eq. 6.12, therefore, suggests that the ratio between the sublayer thicknesses may be the molecular Prandtl number.

It is suggested, therefore, that any numerical scheme used for predicting the mean temperature profile and employing the sublayer thickness as a parameter (like van Driest's for the hydrodynamics), should have the temperature field related to the velocity field as above.

Cebeci [45] studied such a model for air (Pr = 0.73), and, by adjusting the value of the thermal sublayer thickness B^+ until the mean temperature profile could be predicted reasonably, obtained the following value:

$$B^+ \approx 35 \quad . \tag{6.13}$$

This compares favorably to the momentum sublayer thickness $A^+ = 26$, as above.

The normalized turbulent heat transfer $\overline{v't'}/u_\tau T_\tau$ was measured in this study for a constant wall temperature condition. No reference was found to compare exactly with the experimental data, although Johnston [20] and Blom [24] investigated the case of a stepwise discontinuity in wall temperature. The present data had to be evaluated by comparison with expected values obtained from mean temperature measurements. Equation (6.10) can be integrated from $y^+ = 0$ to a point in the logarithmic region of the boundary layer to give

$$v_o^+ T^+ = \frac{1}{Pr}\frac{dT^+}{dy^+} - 1 + \frac{\overline{v't'}}{u_\tau T_\tau} \quad . \tag{6.14}$$

For no transpiration $(v_o^+ = 0)$ and for a point in the logarithmic region where the y-derivative of the temperature is small, we should find

$$\frac{\overline{v't'}}{u_\tau T_\tau} \approx 1 \quad . \tag{6.15}$$

The experimental data are shown in Fig. 6.12.

6.2.3 Adverse pressure gradient flows

Measurements were taken of temperature fluctuations and turbulent heat transfer rates with suction and adverse pressure gradient. The dimensionless temperature fluctuation level (Fig. 6.13), as expected, decreases with suction, but not so much as the velocity fluctuation level. Following the same trend as the velocity field, its peak is displaced outwards for an increasing suction, indicating that the sublayer becomes thicker.

The temperature fluctuation profile is observed to have only one peak. If an analogy is made to the velocity field, a second peak might appear for an adverse free stream temperature gradient condition, as suggested by the following line of reasoning.

The temperature fluctuation equation can be written, from Tennekes and Lumley [46], for example, as

$$\bar{u}\frac{\partial}{\partial x}\left(\frac{\overline{t'^2}}{2}\right) + \bar{v}\frac{\partial}{\partial y}\left(\frac{\overline{t'^2}}{2}\right) = -\frac{\partial}{\partial x}\left[\frac{1}{2}\,\overline{t'^2u'} - \alpha\frac{\partial}{\partial x}\left(\frac{\overline{t'^2}}{2}\right)\right]$$
$$-\frac{\partial}{\partial y}\left[\frac{1}{2}\,\overline{t'^2v'} - \alpha\frac{\partial}{\partial y}\left(\frac{1}{2}\,\overline{t'^2}\right)\right] \tag{6.16}$$
$$-\overline{u't'}\,\frac{\partial T}{\partial x} - \overline{v't'}\,\frac{\partial T}{\partial y}$$
$$-\alpha\left[\overline{\left(\frac{\partial t'}{\partial x}\right)^2} + \overline{\left(\frac{\partial t'}{\partial y}\right)^2}\right] .$$

It can be seen that a free stream temperature gradient would influence directly the temperature fluctuation production term $\overline{u't'}\,\frac{\partial T}{\partial x}$ in the outer region of the boundary layer.

This indicates that for the same hydrodynamics, the turbulent Prandtl number, defined as the ratio between the eddy diffusivity for momentum and heat, would be a function of the temperature boundary conditions.

The temperature fluctuation profile is observed to peak at a larger distance from the wall than the velocity fluctuation profile. This ratio is approximately 1.4, or the inverse of the molecular Prandtl number, as for zero pressure gradient flows. This again suggests that the thermal sublayer is larger than the momentum one by the same amount. A numerical prediction scheme for the temperature field would, therefore, make use of this observation, as an extension of zero pressure gradient flows, to include the effects of pressure gradient.

Figure 6.14 plots the normalized $\overline{v't'}/u_\tau T_\tau$ profile, having y^+ as the independent variable. It can also be seen that it peaks in the outer region of the boundary layer and suction tends to suppress it. A comparison between the temperature fluctuation profile and the normal velocity fluctuation profile shows that the former peaks in the inner layer and the latter in the outer layer. Peaks of $\overline{v't'}$ are therefore expected to exist in between. This is actually the case, and Fig. 6-14 shows another feature: the $\overline{v't'}$ profile peaks also in the inner region. Because of the fact that $\sqrt{\overline{u'^2}}$ profile varies with suction more than $\sqrt{\overline{t'^2}}$ profile, it is expected that the hydrodynamics plays a more important role in the magnitude of this peak. For steep variations of $\sqrt{\overline{v'^2}}$, this inner peak can even be suppressed, as seems to be the case for no transpiration. The existence of the inner peak may be related to the observed decrease and then rise in the turbulent Prandtl number data of Blackwell [9] and of this investigation (Chapter 7) in the inner region of the boundary layer.

Figure 6.15 shows the correlation coefficient $\overline{v't'}/\sqrt{\overline{v'^2}}\sqrt{\overline{t'^2}}$ between the normal velocity and the temperature. It is observed that in the outer region high values of the coefficient are obtained, indicating that the phase shift between the normal velocity and the temperature fluctuations is small.

Finally, from experimental observation, it is apparent that the free stream temperature turbulence level is reached at a much higher distance from the wall than the thermal boundary layer thickness. This suggests that there is a region of the boundary layer which is characterized by the existence of a turbulent fluctuation in temperature without a measurable mean temperature deficit.

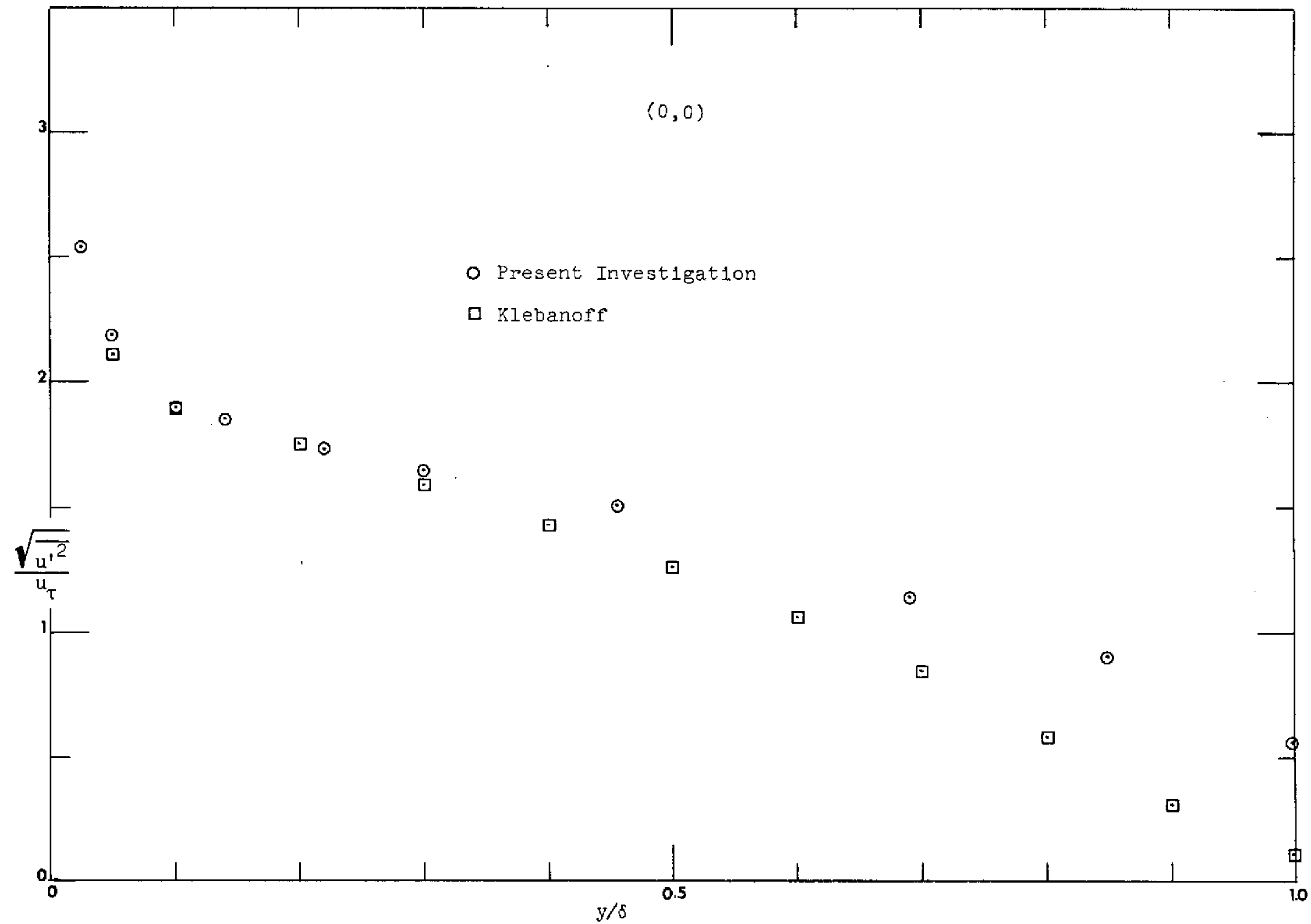

Fig. 6.1 Axial velocity fluctuation profiles -- comparison with the data of Klebanoff.

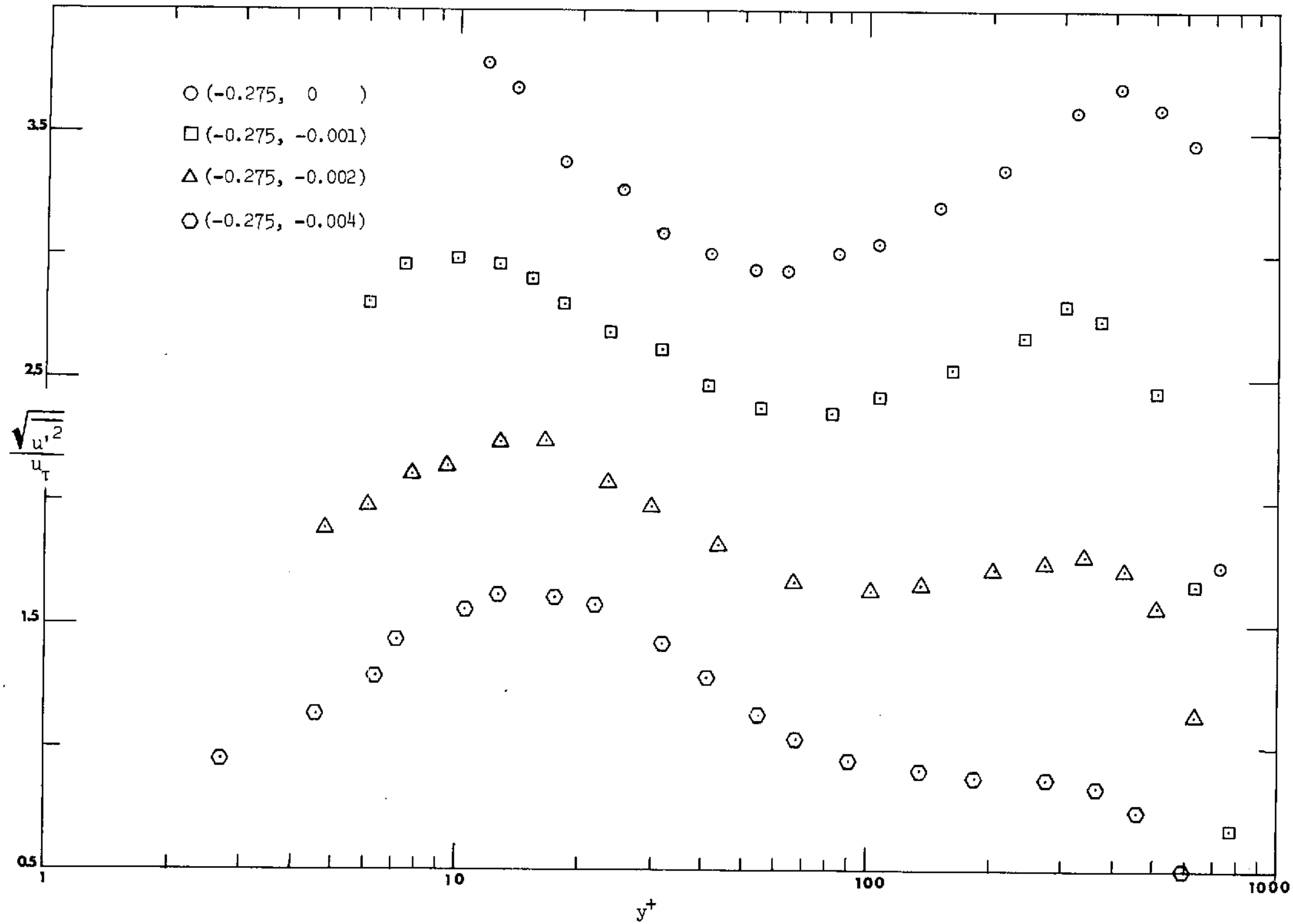

Fig. 6.2 Axial velocity fluctuation profiles for strong adverse pressure gradient flows with different suction rates.

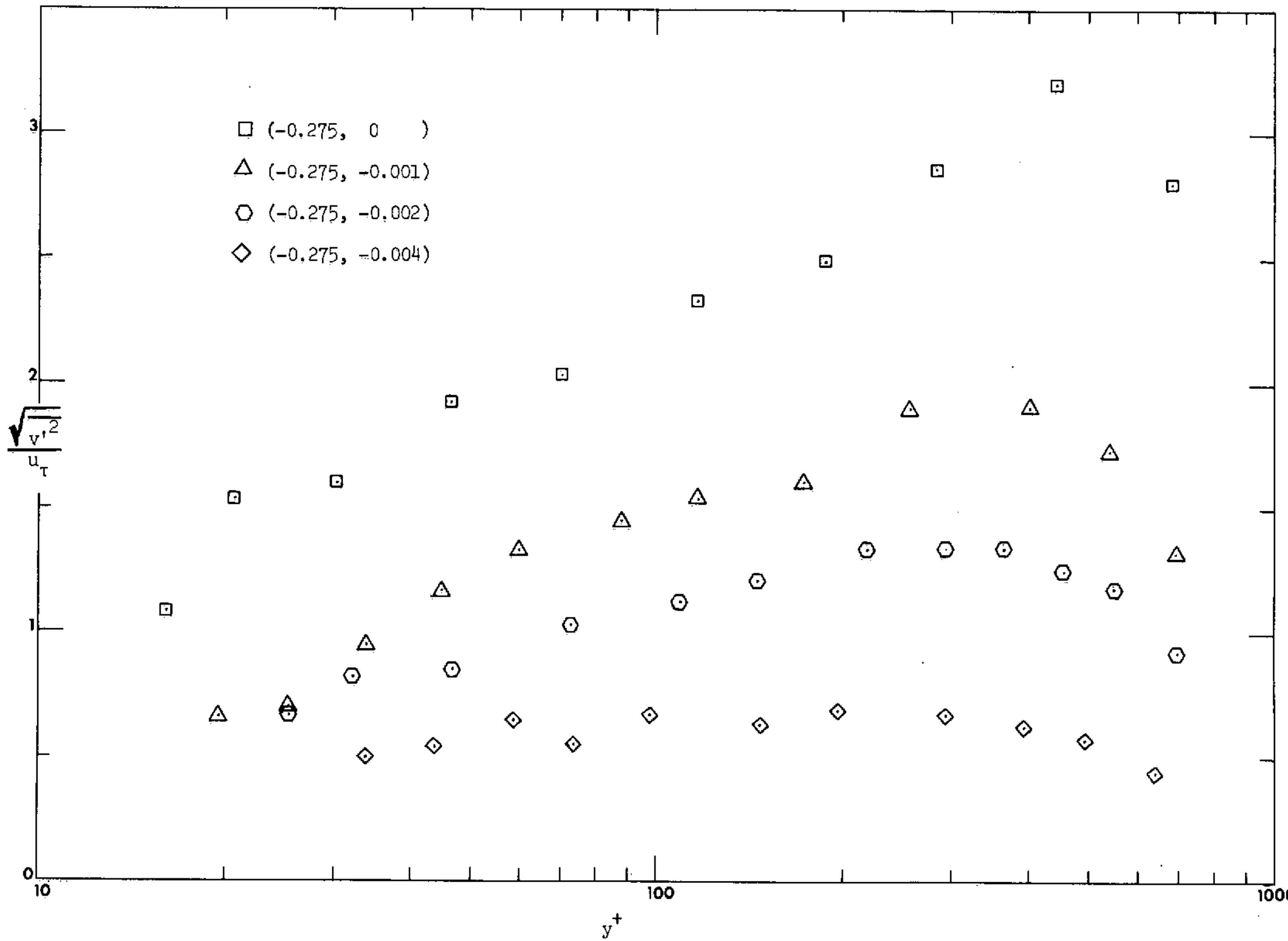

Fig. 6.3 Normal velocity fluctuation profiles for strong adverse pressure gradient flows with different suction rates.

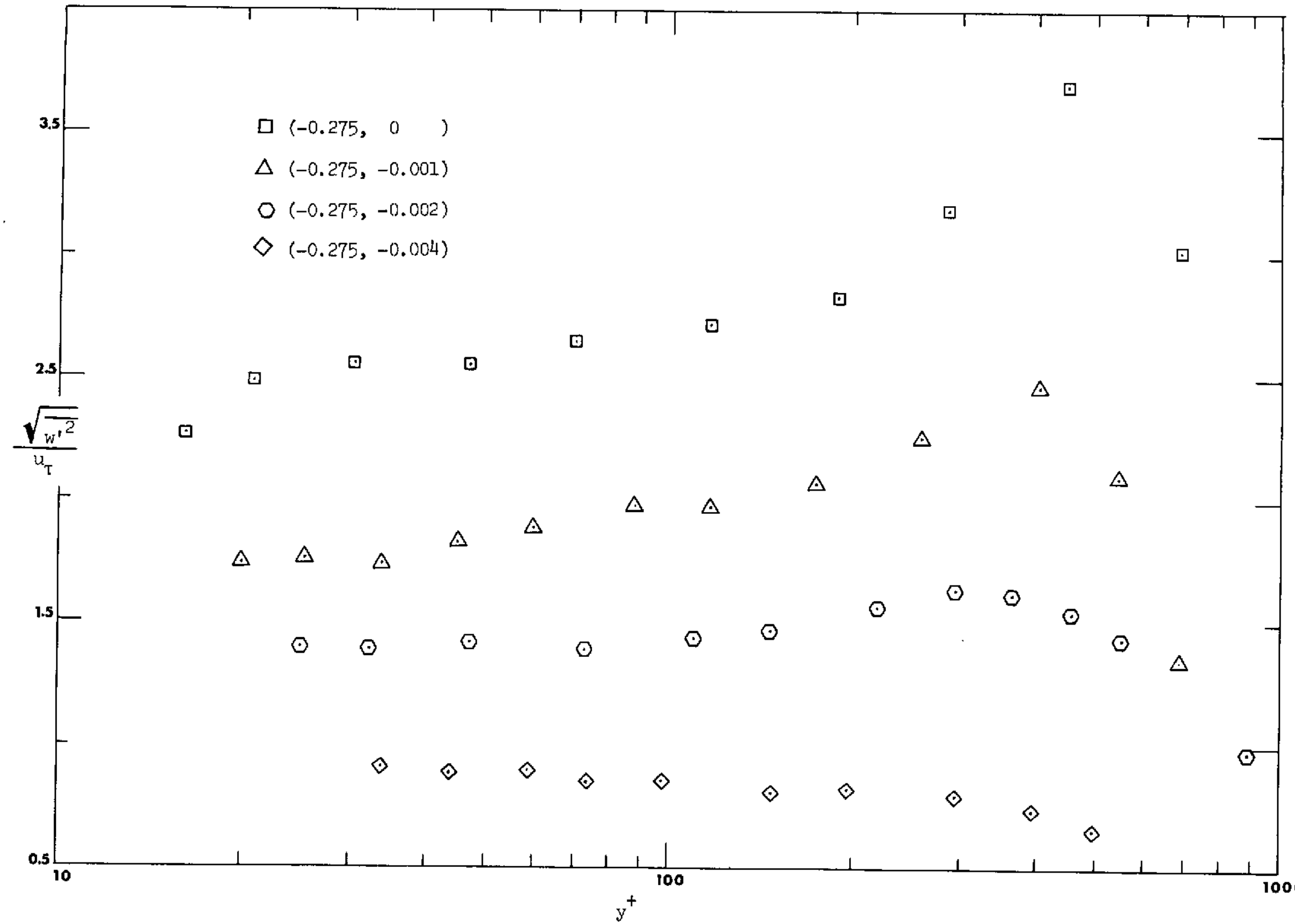

Fig. 6.4 Transverse velocity fluctuation profiles for strong adverse pressure gradients with different suction rates.

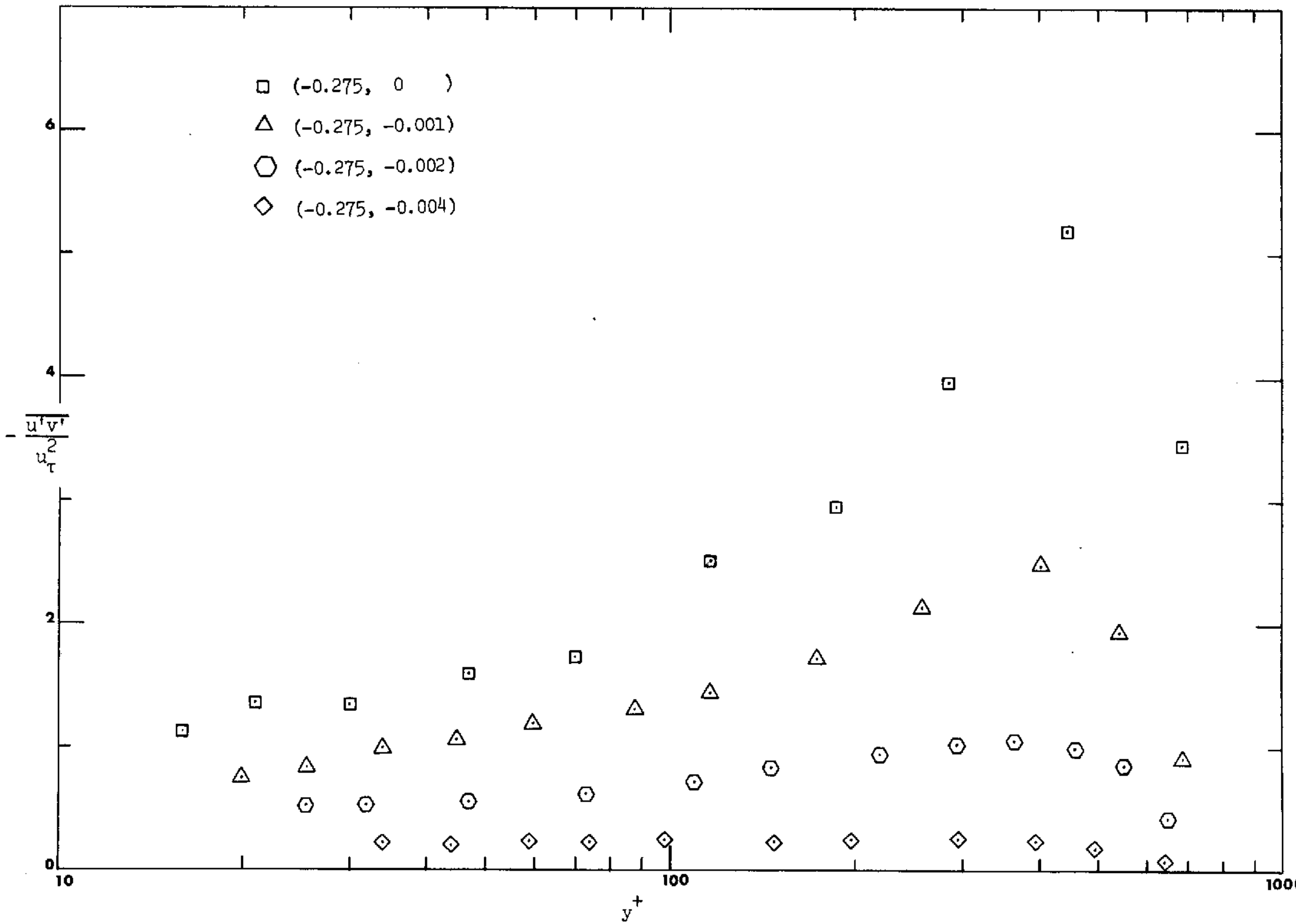

Fig. 6.5 Turbulent shear stress profiles for strong adverse pressure gradient with different suction rates.

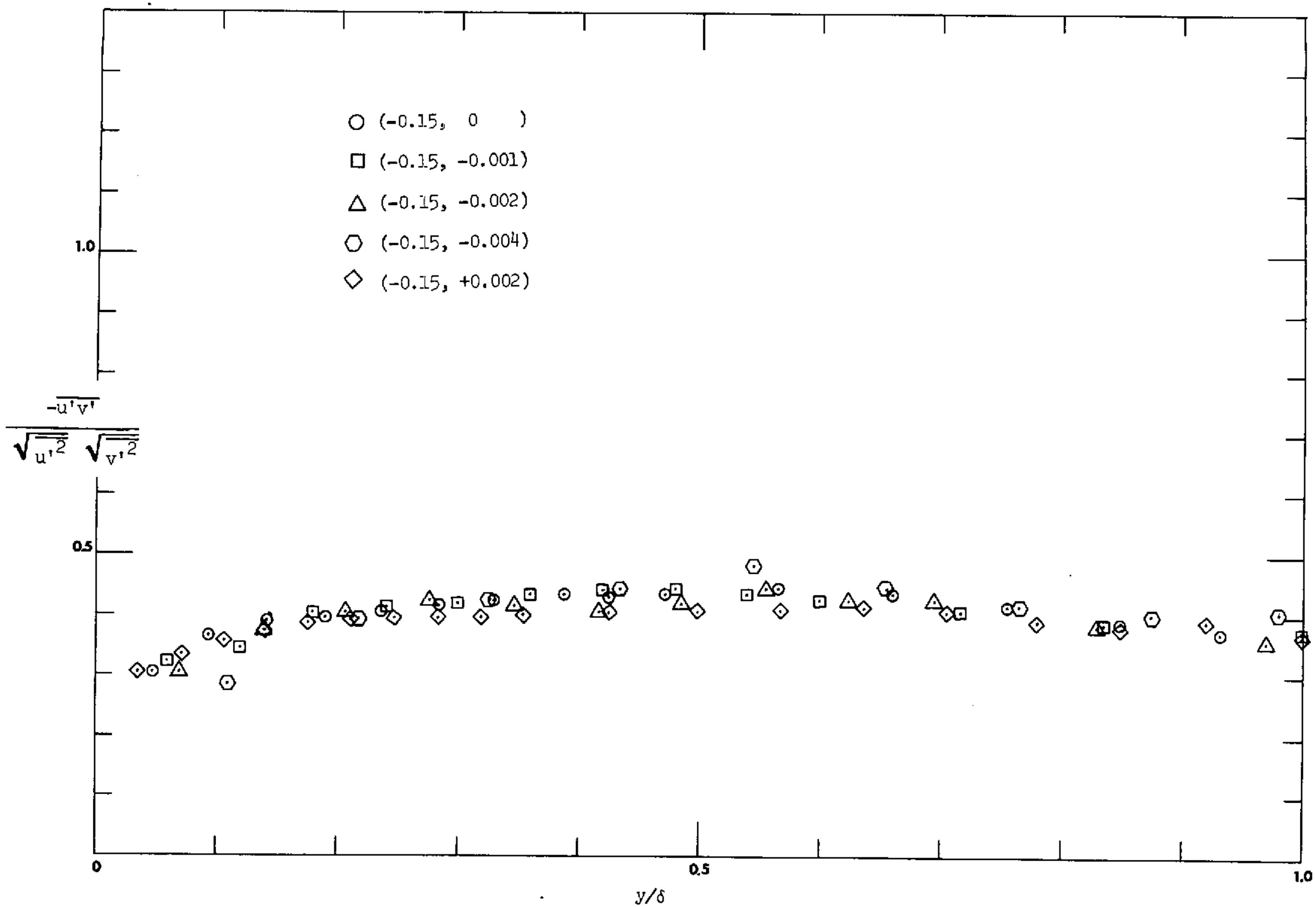

Fig. 6.6 Correlation coefficients between the longitudinal and normal velocities -- mild adverse pressure gradient.

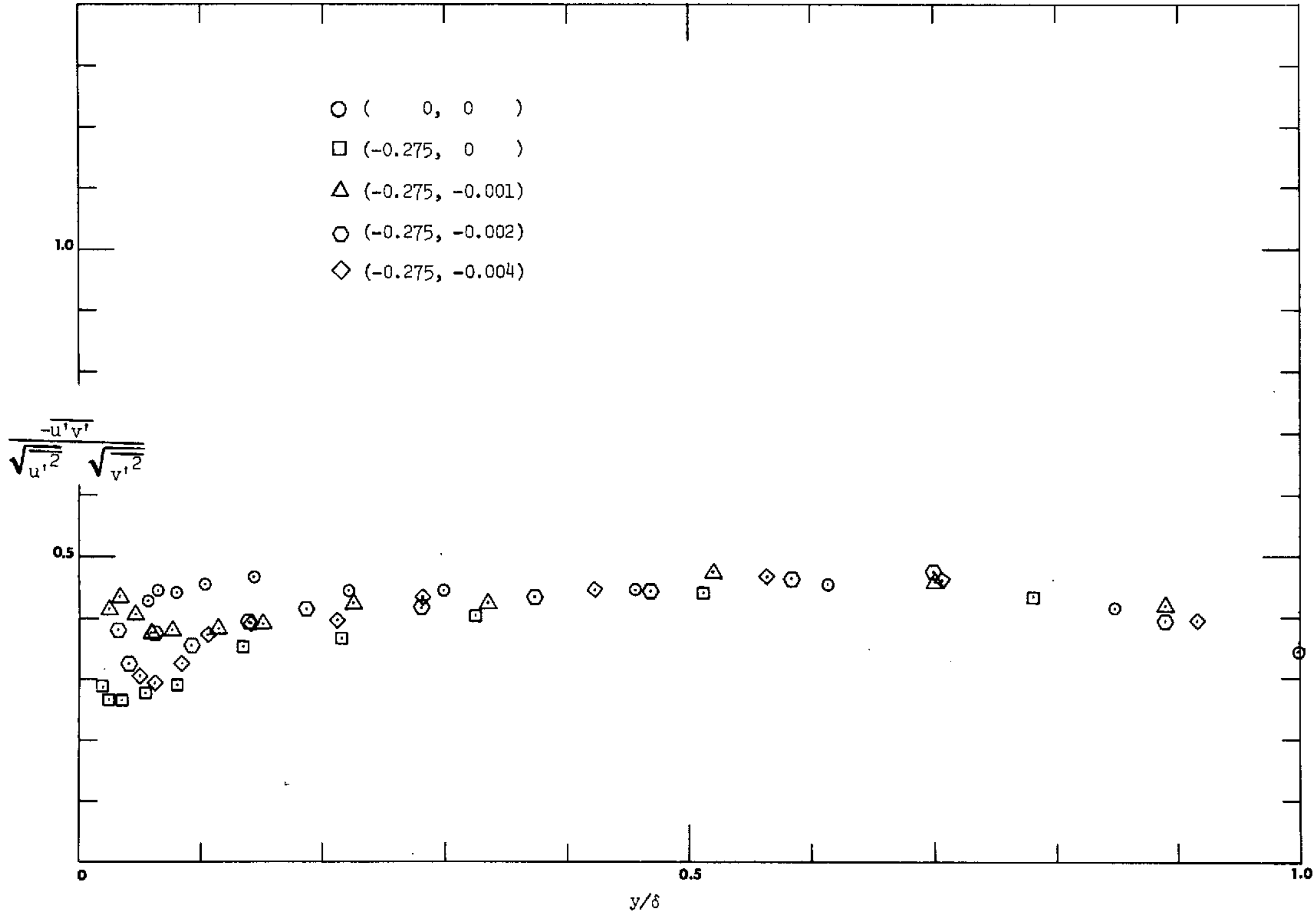

Fig. 6.7 Correlation coefficients between the longitudinal and normal velocities -- strong adverse pressure gradient.

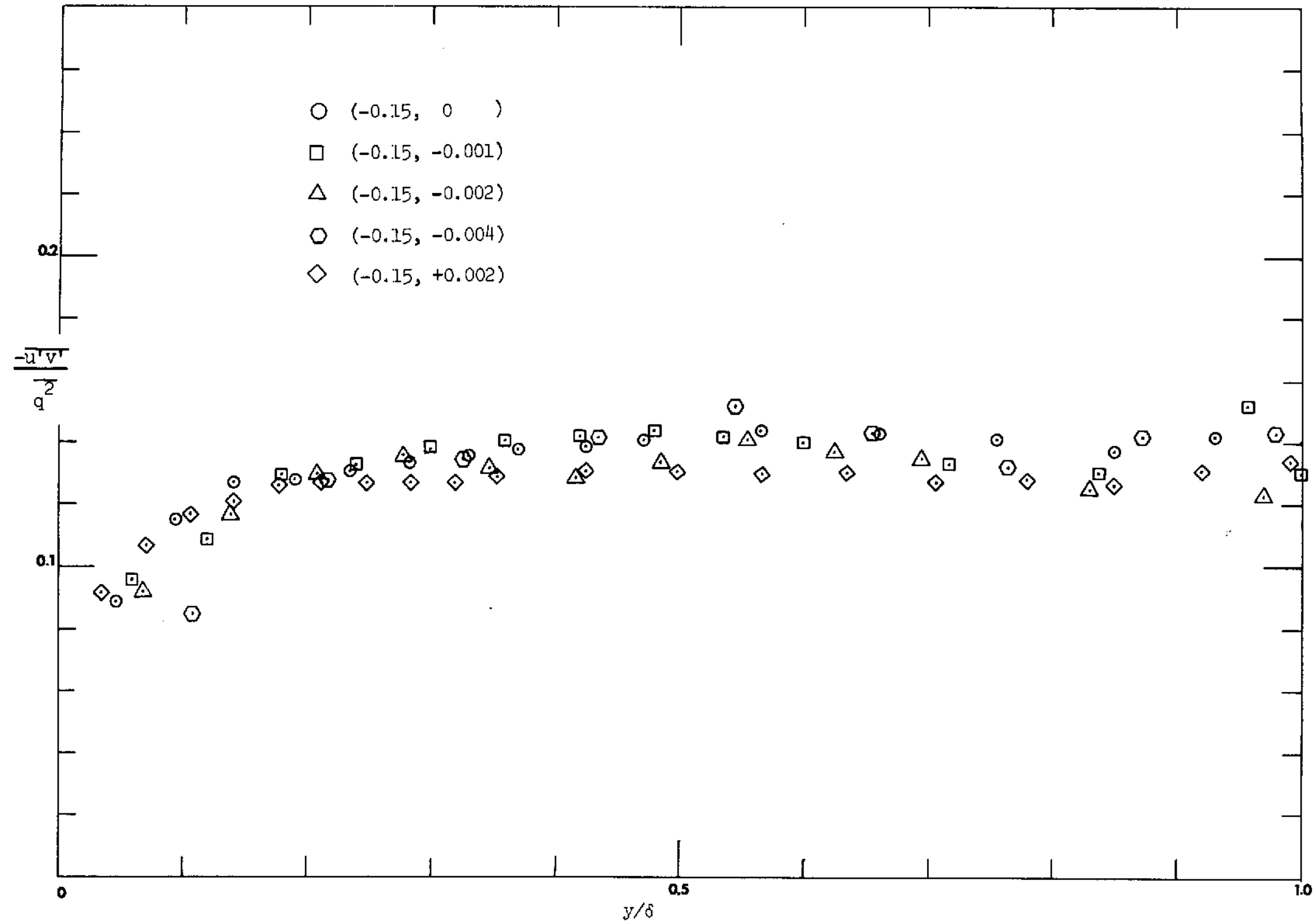

Fig. 6.8 The ratio between turbulent shear stress and turbulent kinetic energy -- mild adverse pressure gradient flows.

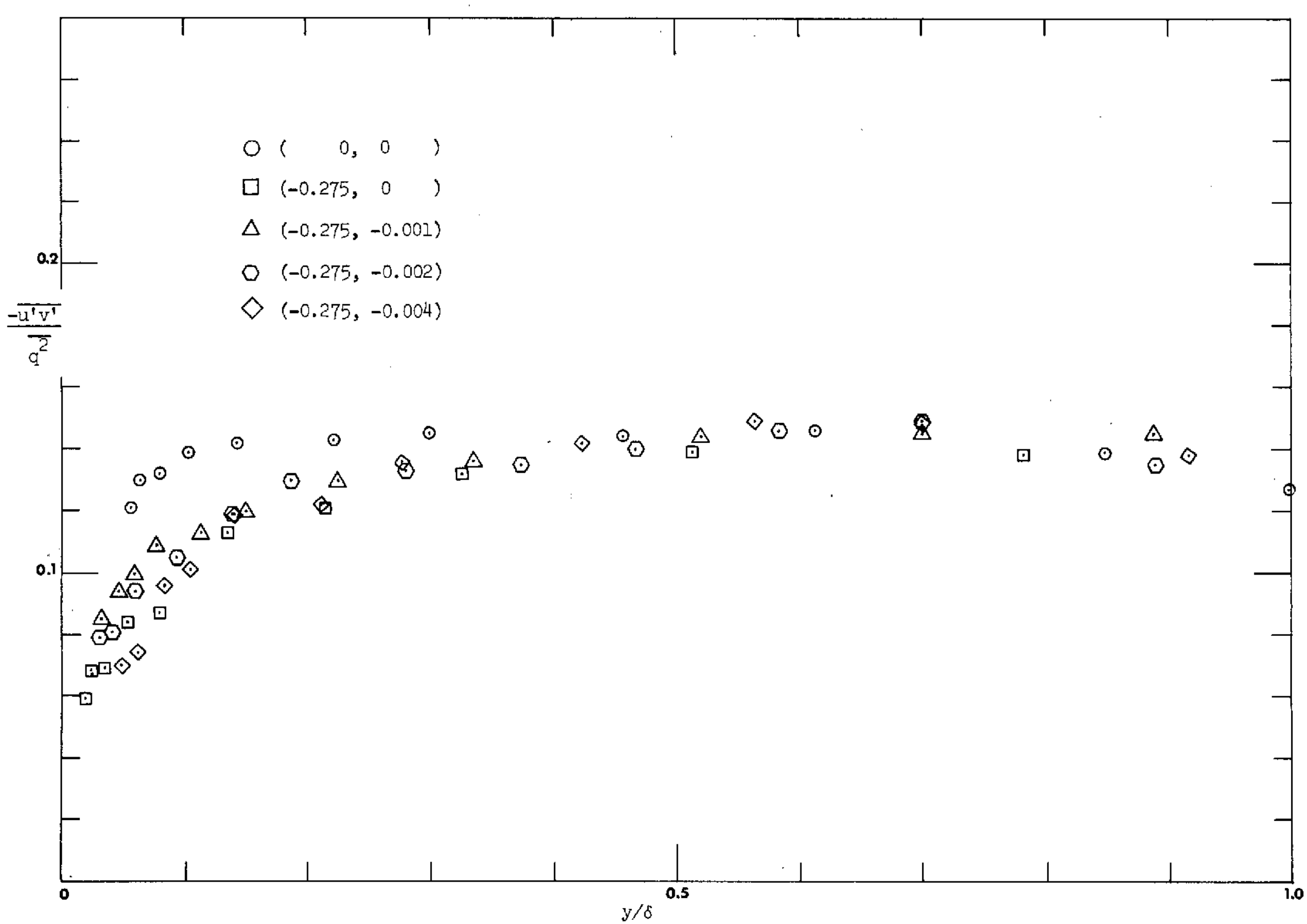

Fig. 6.9 The ratio between turbulent shear stress and turbulent kinetic energy -- strong adverse pressure gradient flows.

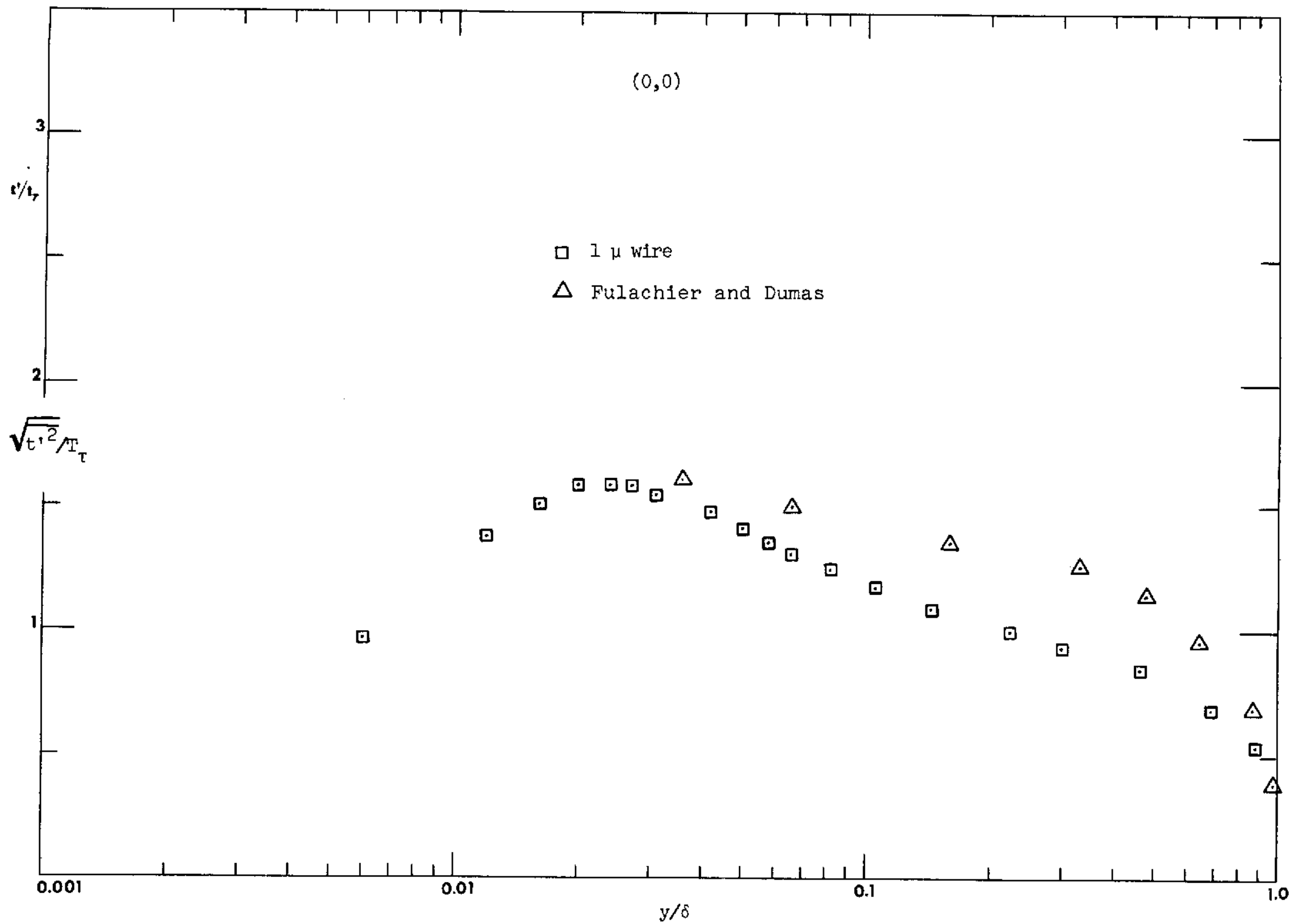

Fig. 6.10 Flat plate measurements of temperature fluctuations -- comparison with the data of Fulachier and Dumas.

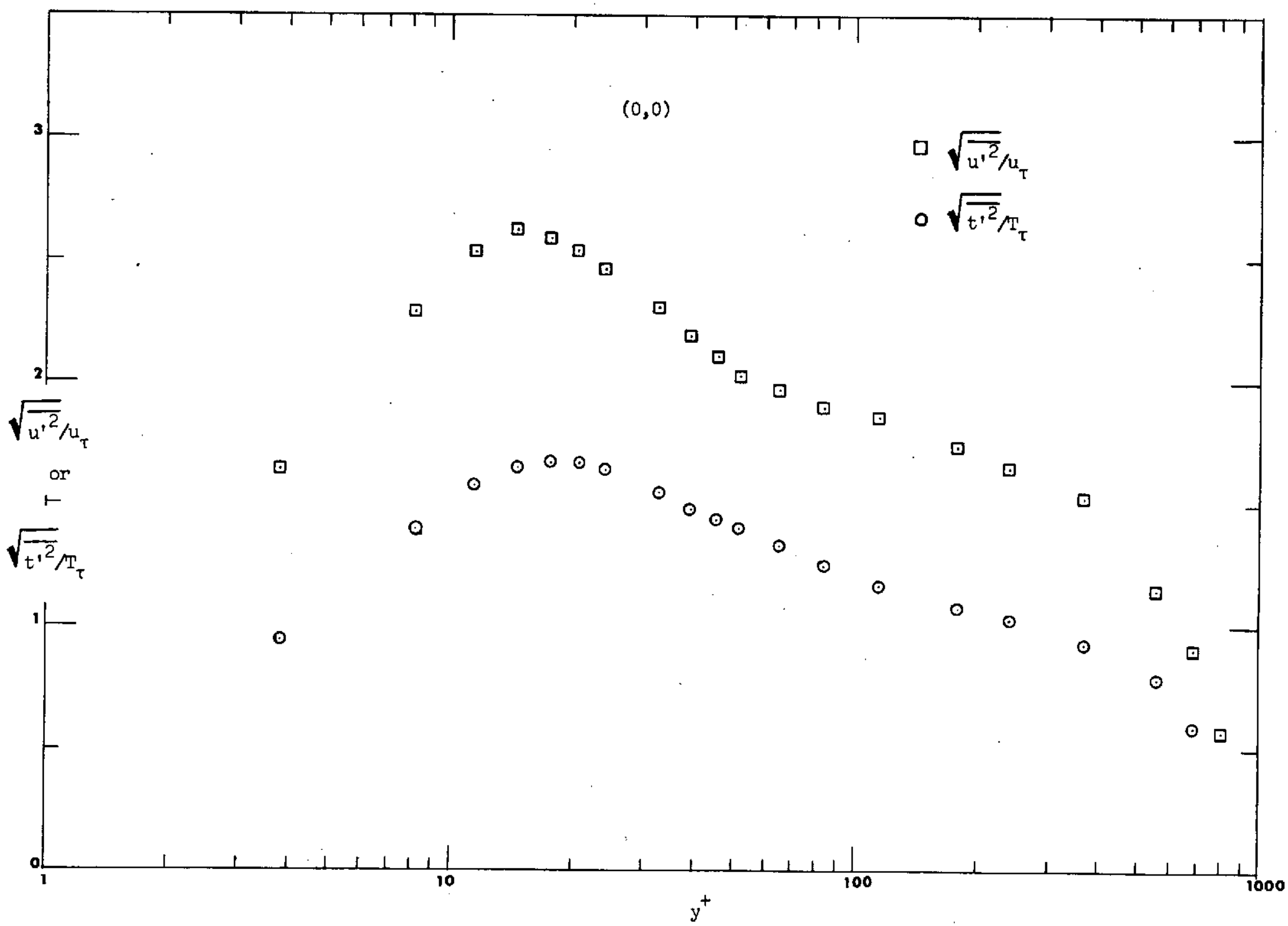

Fig. 6.11 The temperature fluctuation profile compared with the longitudinal velocity fluctuation profile -- flat plate data.

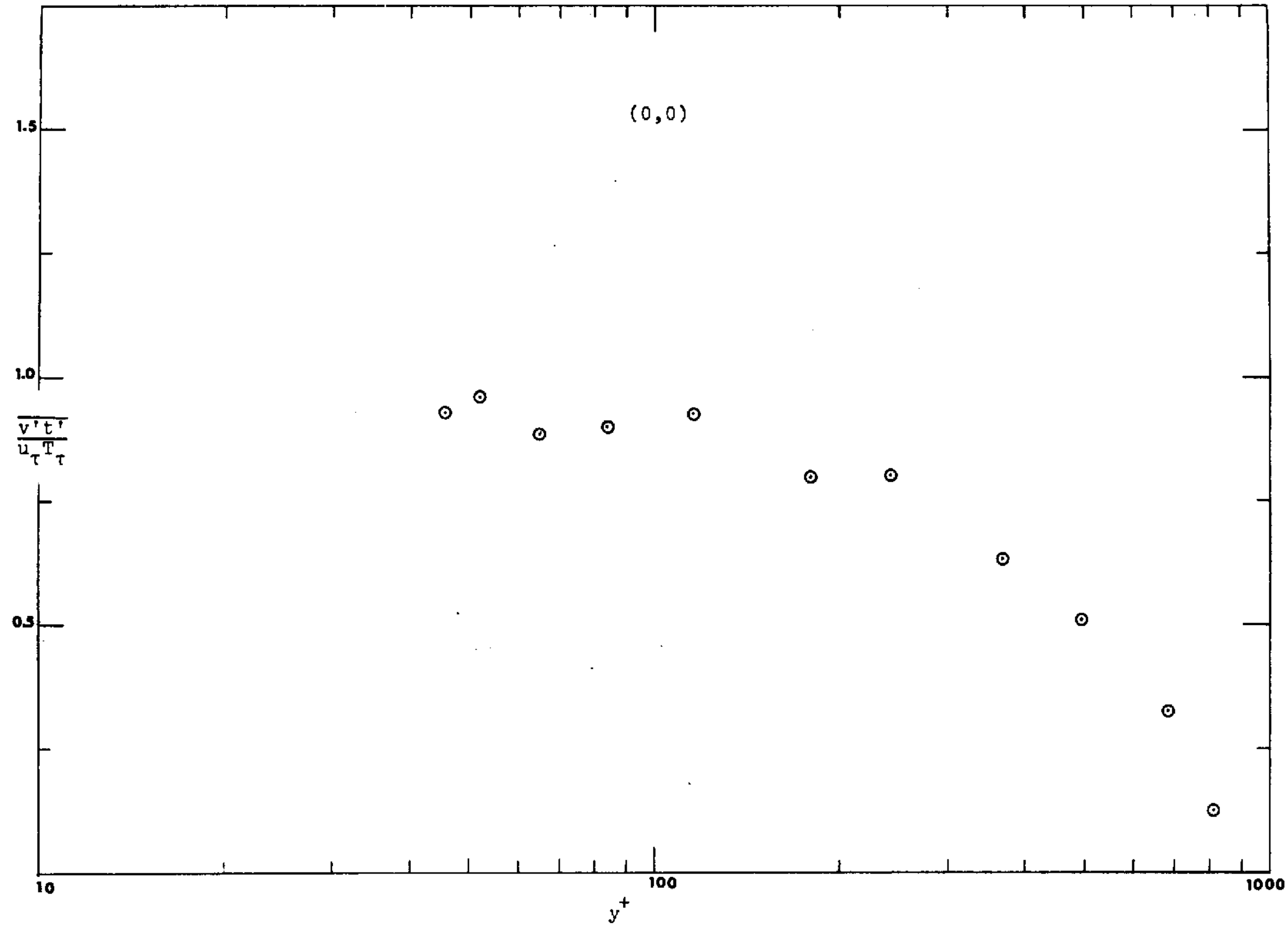

Fig. 6.12 Measured $\overline{v't'}$ profiles normalized on $u_\tau T_\tau$ -- flat plate.

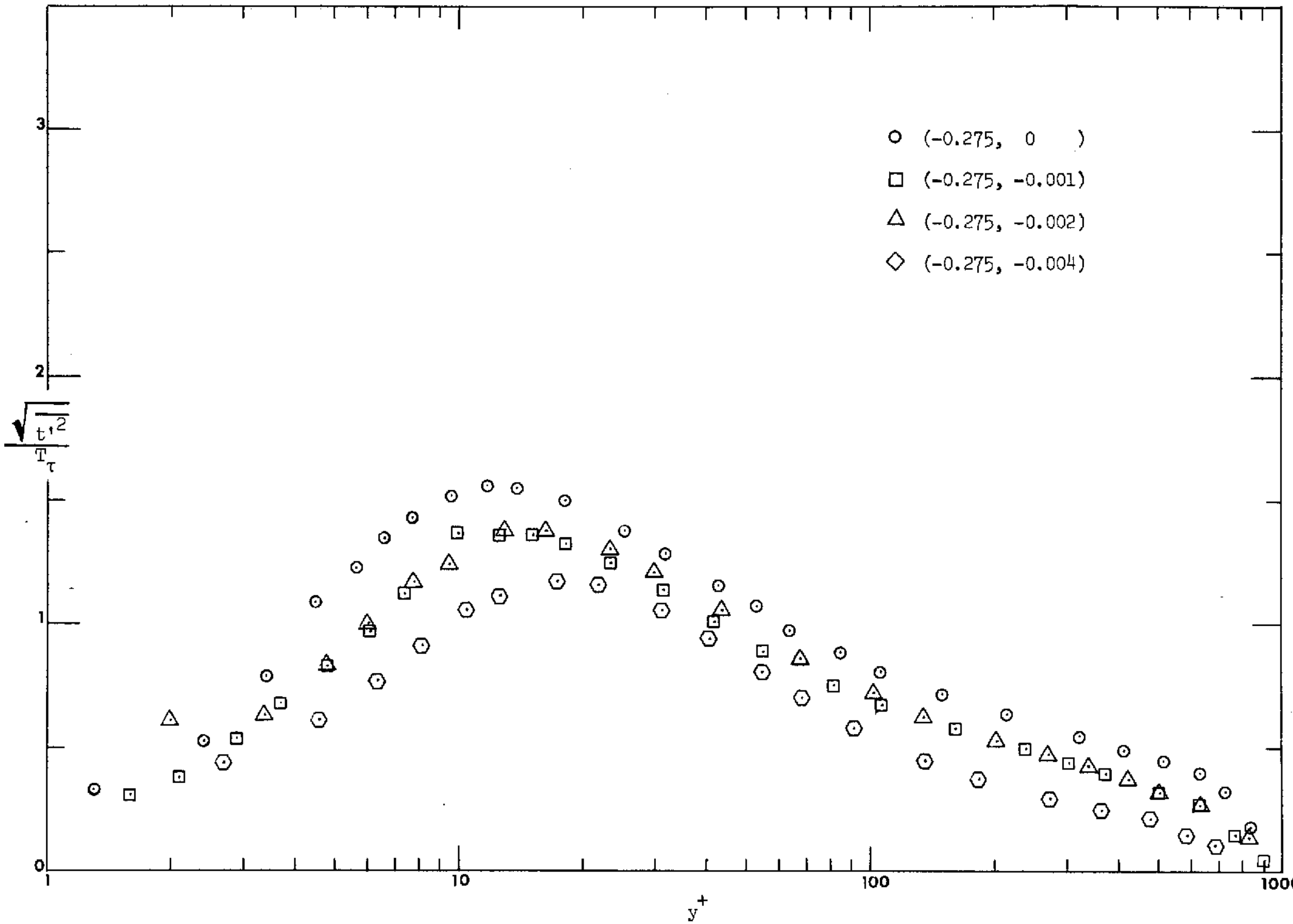

Fig. 6.13 The temperature fluctuation profiles in a strong adverse pressure gradient with different suction rates.

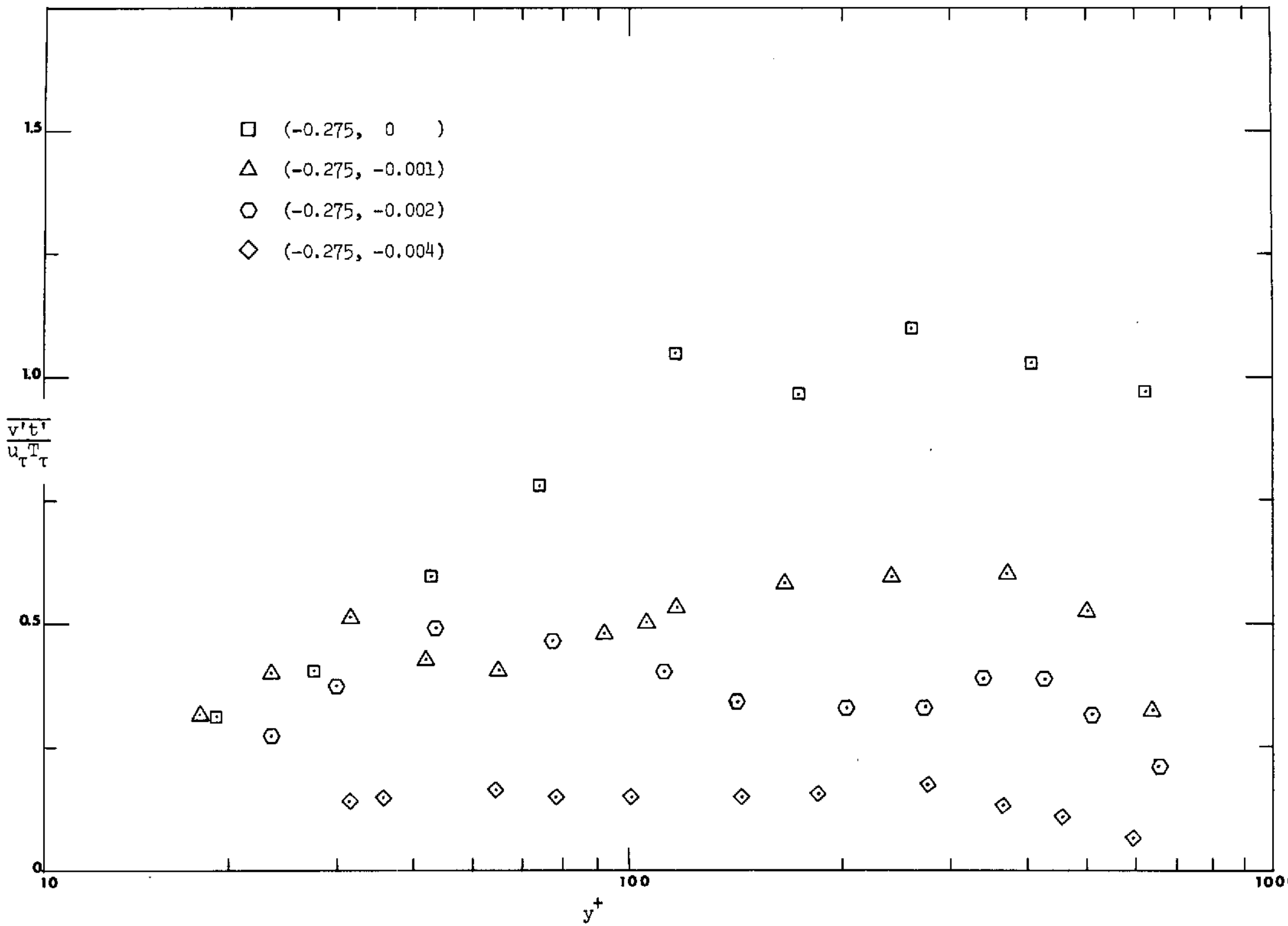

Fig. 6.14 The temperature-normal velocity correlation for a strong adverse pressure gradient with different suction rates.

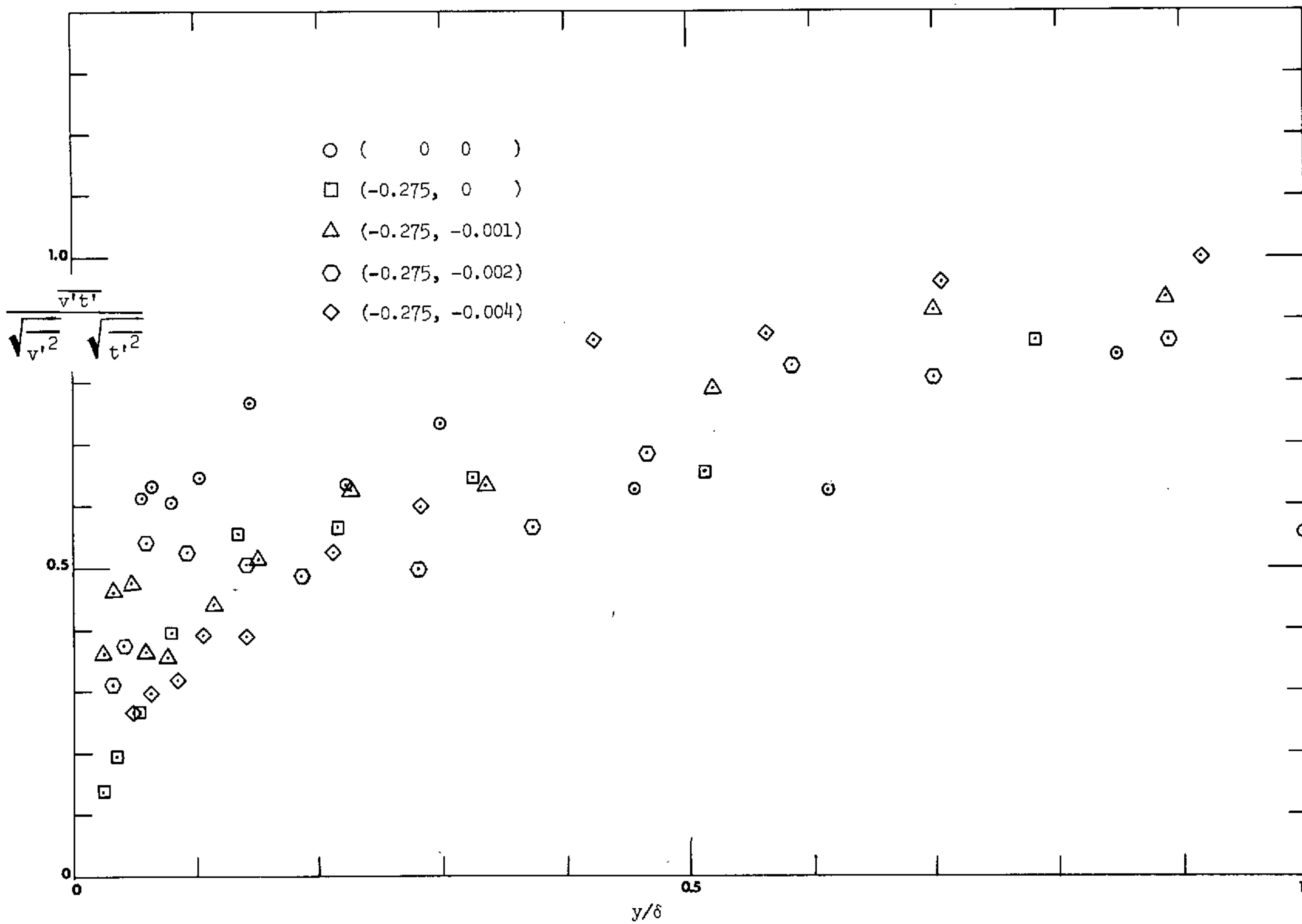

Fig. 6.15 The temperature-normal velocity correlation coefficient for a strong adverse pressure gradient with different suction rates.

CHAPTER 7

TURBULENT TRANSPORT OF HEAT AND MOMENTUM

There has been lately a considerable interest in predicting the behavior of the momentum and thermal boundary layers by numerical means. The details of the turbulence structure have become more and more important because the present numerical schemes for the solution of the boundary layer equations allow a high degree of sophistication for the specification of the turbulent terms. Elaborate schemes for the prediction of the hydrodynamic behavior of a turbulent boundary layer are presently available. The temperature counterpart of the problem, however, lacks the information necessary for the accurate prediction of the heat transfer coefficient and the temperature profile.

This chapter outlines the previous studies of the turbulent transport of heat and momentum and presents the results of turbulent heat transfer measurements together with a new experimental procedure for estimating the turbulent Prandtl number at the wall. The behavior in that region is then analyzed both analytically and experimentally, and it is shown that the turbulent Prandtl number must approach a constant value at the wall; i.e., $\partial Pr_t/\partial y = 0$ in the vicinity of the wall.

7.1 Previous Theoretical and Experimental Studies

The main objective of the study of turbulent transport of heat and momentum is the determination of the functional dependence of $\overline{u'v'}$ and $\overline{v't'}$ on the fluid flow parameters. This has been done by defining eddy diffusivities for momentum and heat respectively as

$$-\overline{u'v'} = \varepsilon_M \frac{\partial \bar{u}}{\partial y} \quad \text{and} \quad -\overline{v't'} = \varepsilon_H \frac{\partial T}{\partial y} \tag{7.1}$$

The next step is the introduction of the so-called turbulent Prandtl number, that is, the ratio $\varepsilon_M/\varepsilon_H$ between the eddy diffusivities for momentum and heat. Various assumptions have been made about this ratio in the past and several expressions have been proposed in attempts to predict the mean temperature profile and the heat transfer coefficient in the boundary layer. The simplest one of all is the Reynolds analogy, which implies a turbulent Prandtl number having a value of 1.0. The assumption is that heat and momentum are transferred by similar processes, which leads to the same values for the eddy diffusivities. The arguments which lead to this claim can be summarized as follows. Consider a mean velocity $\bar{u}$ and temperature T profile of a flowing fluid and suppose that a pulse of fluid is carried by a sudden cross-current fluctuation in the turbulent fluid from y_1 to y_2, normal to the wall. The enthalpy of this pulse of fluid before its sudden movement is c_pT, and accordingly the instantaneous excess of energy at the level y_2 is given by:

$$\text{excess of energy} = -(y_2-y_1)\frac{d}{dy}(c_pT) \quad , \tag{7.2}$$

assuming the wall is at a higher temperature than the free stream. The negative sign shows that there is actually an excess of energy which occurs at level y_2 owing to the sudden translation there of fluid from the higher energy level y_1.

Assuming that there is no loss of heat or any kind of energy during the movement, there is a sudden excess of temperature t' and enthalpy c_pt' at the new level y_2, i.e.,

$$c_pt' = -\Delta y\frac{d}{dy}(c_pT) \quad , \tag{7.3}$$

where t' will be positive. Multiplying by v' and averaging

$$-\overline{v't'} = \overline{v'\Delta y}\frac{dT}{dy} \quad . \tag{7.4}$$

Representing the rms values of the displacement Δy and the velocity fluctuation v' as ℓ and $\sqrt{\overline{v'^2}}$, respectively,

$$-\overline{v't'} = \ell\sqrt{\overline{v'^2}}\frac{dT}{dy} \quad . \tag{7.5}$$

Here ℓ is the mean distance of travel of the lumps of fluid before they lose their identities and are mixed into the fluid at the new position, and is referred to as the mixing length.

If an eddy diffusivity for heat is defined as

$$-\overline{v't'} = \varepsilon_H \frac{\partial T}{\partial y} \quad , \tag{7.6}$$

it can be seen, comparing (7.4) and (7.5), that

$$\varepsilon_H = \ell\sqrt{\overline{v'^2}} \quad . \tag{7.7}$$

But from the expression for the eddy diffusivity for momentum,

$$\varepsilon_H = \varepsilon_M = \ell\sqrt{\overline{v'^2}} \quad . \tag{7.8}$$

If the turbulent Prandtl number Pr_t is defined as

$$Pr_t = \frac{\varepsilon_M}{\varepsilon_H} \quad , \tag{7.9}$$

it can be seen that the hypothesis of no heat loss during the flight implies unity turbulent Prandtl number.

Momentum mixing length theory, however, was criticized by Taylor [36], who proposed that the eddy, during its flight, would preserve its vorticity rather than momentum. Taylor's predicted temperature profile in the wake region behind a cylinder compared favorably with experiments.

The assertion that the average value of the turbulent Prandtl number is near unity seems to hold well for boundary layer flows when the molecular Prandtl number is unity and there is no streamwise pressure gradient, because of the similarity of the momentum and energy equations.

Experimental data, however, have shown that the turbulent Prandtl number varies through the layer in a way which depends on both molecular Prandtl number and the flow field. Measurements have shown that the wall region is characterized by values of the turbulent Prandtl number higher than unity, falling to less than 1 in the outer region.

Measurements of $\overline{v't'}$ are usually obtained from mean temperature measurements and by means of the time averaged energy equation. However, as pointed out by Simpson [47] the uncertainty in the measurement of Pr_t becomes high in two regions.

(a) Inner region: $\overline{u'v'}$ and $\overline{v't'}$ are very small and then determination from subtraction of terms of nearly the same order of magnitude becomes uncertain.

(b) Outer region: the y-derivatives of temperature and velocity are very small and their determination becomes uncertain.

In the logarithmic region, though, there seems to be a better chance for accuracy in the determination of the turbulent Prandtl number. A number of experiments have shown that its value for zero pressure gradient flows (air as working fluid) is approximately 0.9 . Among them, one could mention Simpson [47], Blackwell [9], and Chen [48].

The outer region of zero pressure gradient flows seems to be characterized by values of the turbulent Prandtl number smaller than 1. Rotta [49] examined the no transpiration case and presented an expression for Pr_t as a function of y/δ in the outer region.

There remains only the inner region. Experimental difficulties have been responsible for the lack of a definite conclusion on its behavior. However, numerical experiments show that the temperature field is predicted reasonably only by assuming a value greater than 1 in that region. The same numerical experiments show that the inner region is very important for the description of the heat transfer and that in the range $10 < y^+ < 15$, the turbulent Prandtl number drops considerably from its high value at the wall to its low value in the log region.

It is obvious therefore, that the inner region has to be investigated in more detail owing to its importance on the description of the heat transfer.

Only a few direct measurements of $\overline{u'v'}$ and $\overline{v't'}$ for the study of the turbulent Prandtl number have been reported in the literature. This is probably due to the fact that the measurement of $\overline{v't'}$ is very difficult. Both Johnson [20] and Blom [24] measured Pr_t for a step in wall temperature condition. The purpose of their study was mainly to generate a kernel function used for the prediction of the heat transfer under a variable wall temperature condition. They found that Pr_t increased with y^+ close to the wall, reached a maximum of 0.8-1.2 in the range $y^+ = 50-80$ and then decreased. The trends are therefore different from the constant wall temperature case. This would then suggest that the turbulent Prandtl number is not only a function of the turbulent Peclet number Pe_t $(Pr \cdot \varepsilon_M/\nu)$, as usually assumed, but also on other parameters.

The dependence of the turbulent Prandtl number on the molecular Prandtl number, pressure gradient and transpiration rates has been discussed by several investigators, who try to prove that Pr_t has a universal profile as a function of certain dimensionless independent variables.

Mizushina, Ito and Ogino [50] examined the near wall region of a rectangular duct flow by means of a Mach-Zehnder interferometer technique for the range of $Pr \simeq 6-40$ and no dependence of the turbulent Prandtl number on the molecular Prandtl number was observed. Blom [24], on the other hand presents a survey of the experimental data available for Pr_t in which it is concluded that the molecular Prandtl number is important for the description of Pr_t. In general, the experimental results show an enormous scatter, leaving the general behavior of Pr_t an unsolved problem. Simpson [47] studied zero pressure gradient flows under different transpiration rates. The results again show a considerable scatter but to within the calculated uncertainty of measurements (which is high) no effect of blowing or suction could be observed. A definite trend was then observed: high values at the wall and low values in the outer region. Thielbahr [6] studied mild favorable pressure gradient flows and by numerical experiments, he found a direct pressure gradient dependence in the inner layer and a direct transpiration rate dependence in the outer layer, besides the dependence on the Reynolds number of turbulence ε_M/ν and the sublayer thickness A^+. Kearney [7] studied a strong favorable pressure gradient with different transpiration rates. He observed a large scatter in his data, but examination of the turbulent Prandtl number as a function of the Reynolds number of turbulence, ε_M/ν, does not show a definite trend towards the universality of the profile. Finally, Blackwell [9] studied mild adverse pressure gradient flows and obtained an expression for the turbulent Prandtl number as a function of local parameters of the velocity field, which depend on the pressure gradient, transpiration rate and the velocity profile itself.

It is not clear, therefore, whether the scatter in the data is a consequence of the uncertainty in the measurements or there is really no trend towards the universality of the turbulent Prandtl number profile. In that case, it would be a function of the pressure gradient, transpiration rate and boundary conditions for both velocity and temperature field, and it would throw some doubts on the usefulness of Pr_t. The usefulness of Pr_t is also challenged by Blom's results [24] showing Pr_t to be a function of the wall temperature distribution.

Different models for the turbulent Prandtl number have been proposed in the literature. All of them use a physical hypothesis as far as the nature of the turbulent heat transfer is concerned.

The simplest of all is the Prandtl theory which suggests that $Pr_t = 1$, as outlined in the beginning of this section.

Jenkins [51] was among the first ones to develop a model which allows an eddy during its flight to lose heat to the flow field. A universal dependence on the turbulent Peclet number ($Pr\ \varepsilon_M/\nu$) was then obtained. The eddies were assumed to be spheres having a radius equal to the mixing length. Their surface temperature was assumed to vary linearly during their movement from creation to destruction. The drawback of this model is that it always predicts values for the turbulent Prandtl higher than unity, which has been shown experimentally not to be the case. However, some investigators have been using this model in the inner region of the boundary layer.

Some other models assume a linear variation of the mean temperature field during the eddy flight and an expression for Pr_t is obtained as a function of Pe_t. Others like Wassel and Catton [52] are a mixture of this model and a curve fitting to predict the observed experimental data. By doing so Pr_t can be smaller than 1 in the outer region. Blackwell [9] for example used a similar formulation in the inner region and Rotta's modified expression in the outer region of the boundary layer.

Coefficients were adjusted as a function of local parameters of the velocity boundary layer and the temperature field was predicted quite reasonably for adverse pressure gradient flows and different transpiration rates. The Stanton number prediction however, was not so good. The reason is possibly that his model predicts an infinite turbulent Prandtl number at the wall. The present investigation proves that it must have a finite value at the wall.

Others like Cebeci [45] assume two mixing lengths, similar to the Van Driest formulation. The sublayer thickness B^+ would therefore have to be determined as suggested in Chapter 6. A complete formulation would rely on adjusting the constants to predict flows under adverse pressure gradient conditions and different transpiration rates.

Hinze [29] suggests that the diffusion of heat might be a combination of gradient and large eddy transport. Simpson [47] used his ideas to develop a model for Pr_t under zero pressure gradient conditions and different transpiration rates.

From this discussion it is concluded that there is no consensus as to the behavior of the turbulent Prandtl number very close to the wall. This thesis analyzes it both analytically and experimentally, by means of a new measurement procedure.

The turbulent Prandtl number throughout most of the boundary layer is deduced from sequential measurements of temperature and velocity using a hot-wire probe. Values at the wall are estimated analytically.

7.2 Behavior of the Turbulent Prandtl Number Close to the Wall

The turbulent Prandtl number can be written as

$$Pr_t = \frac{\overline{u'v'}}{\overline{v't'}} \; \frac{\partial T/\partial y}{\partial u/\partial y} \qquad (7.10)$$

In the neighborhood of the wall, from (5.11) and (5.16)

$$\overline{u'v'} = - \overline{\frac{\partial u'}{\partial y} \frac{\partial^2 v'}{\partial y^2}}\Bigg|_o \; \frac{y^3}{2} + \cdots\cdots = - a \frac{y^3}{2} \qquad (5.11)$$

$$\overline{v't'} = - \overline{\frac{\partial t'}{\partial y} \frac{\partial^2 v'}{\partial y^2}} \Bigg|_o \frac{y^3}{2} + \cdots = - b \frac{y^3}{2} \tag{5.16}$$

and the Pr_t can be written as

$$Pr_t = \frac{a}{b} \frac{\partial T/\partial y\big|_o}{\partial u/\partial y\big|_o} \tag{7.11}$$

It can be concluded therefore that Pr_t approaches a constant value at the wall. This analysis shows then that models requiring an infinite value for the turbulent Prandtl number at the wall cannot be correct

7.3 New Measurement Procedure for Estimating Pr_t at the Wall

The purpose of this procedure is to obtain data for analyzing Pr_t at the wall as a function of pressure gradient and transpiration rates.

The procedure is based on the premise that the correlation coefficients between each velocity component and the temperature can be written as

$$-\overline{u'v'} = c\sqrt{\overline{u'^2}}\sqrt{\overline{v'^2}} \tag{7.12}$$

$$-\overline{v't'} = d\sqrt{\overline{t'^2}}\sqrt{\overline{v'^2}} \tag{7.13}$$

Experimental data shows that both c and d should tend to small values close to the wall. The following analysis is intended to estimate the ratio c/d , as the wall is approached.

The flow visualization data of Runstadler, Reynolds and Kline [54] shows a streaky nature of the flow close to the wall, which appears to have a well defined transverse wavelength. The streaks are oriented so that their direction is in the flow direction. Periodically these streaks break away from the wall and disperse into the main flow. These large and highly coherent components retain their identity for a long time and thus a high correlation should be expected between the longitudinal velocity fluctuation and the temperature fluctuation

$$\frac{\overline{u't'}}{\sqrt{\overline{u'^2}}\ \sqrt{\overline{t'^2}}} \rightarrow 1.0 \tag{7.14}$$

As the wall is approached, the correlation coefficient becomes 1, indicating that there is no phase shift between u' and t'. As a consequence, the correlation coefficients c and d in (7.12) and (7.13) respectively become identical.

An experimental confirmation of this result was done by Bremhorst and Bullock [21] for fully developed pipe flow, together with the data of Johnson [20] and Morrison [53]. Bremhorst and Walker [55] used a new procedure for measuring $\overline{u'v'}$ very close to the wall, by sensing the wake of a hot wire with a cold one and obtained a model for the transport of momentum which successfully interprets these results.

The turbulent Prandtl number can be written by using Eq. (7.12) and (7.13), and the fact that the correlation coefficients are equal at the wall as:

$$Pr_{t_o} = \lim_{y \to o} \frac{\overline{u'v'}}{\overline{v't'}} \frac{\partial T/\partial y}{\partial u/\partial y} = \lim_{y \to o} \frac{\sqrt{\overline{u'^2}}}{\sqrt{\overline{t'^2}}} \frac{\partial T/\partial y}{\partial u/\partial y} \tag{7.15}$$

Writing Eq. (7.15) in terms of dimensionless coordinates

$$Pr_{t_o} = \lim_{y \to o} \frac{\sqrt{\overline{u'^2}}/u_\tau}{\sqrt{\overline{t'^2}}/T_\tau}\ Pr \tag{7.16}$$

The procedure used for estimating the turbulent Prandtl number at the wall consists of calculating the function

$$R = \frac{\sqrt{\overline{u'^2}}/u_\tau}{\sqrt{\overline{t'^2}}/T_\tau}\ Pr \tag{7.17}$$

near the wall and extrapolating it to the wall. The extrapolation does not constitute a problem because both $\sqrt{\overline{u'^2}}$ and $\sqrt{\overline{t'^2}}$ are linear with y near the wall. Actually, the function R (Eq. 7.17) does not change much for points near the wall, making the extrapolation procedure very easy.

There are some uncertainties associated with this procedure. First of all, expression (7.15) shows that the y-derivatives of velocity and temperature must be known so that the calculation of the function R can be carried out. As well known, these derivatives are very difficult to calculate, especially near the wall. This problem can be overcome by the knowledge that in the inner layer the similarity variables T^+, u^+, y^+ will describe the flow and a Couette flow function will fit the data.

The Couette flow function is sensitive to the value of Stanton number and friction factor and these are known, for several flow conditions, with good accuracy. The data for flat plate flows is the most certain. Figure 7.1 shows the turbulent Prandtl numbers deduced from the present measurements, for the flat plate case. The value at the wall is shown as 1.4 based on the present technique of extrapolating Eq. 7.17 to the wall. This value is approximately the inverse of the molecular Prandtl number for air, a relationship which has been noted by other investigators.

The data from the present work were used to generate Figs. 7.2, 7.3, 7.4, and 7.5, which show the turbulent Prandtl number profiles for a strong pressure gradient flow and different suction rates. The determination of the Stanton number, which is used in the extrapolation procedure, is believed to be accurate to within 5% as in the flat plate case. The friction coefficient was obtained by direct measurement of $\overline{u'v'}$ and the same procedure was used for all flows. The consistency of the measurement procedure provides, thus, a general trend of the influence of the pressure gradient and transpiration rate on the turbulent Prandtl number.

It is concluded, therefore, that an adverse pressure gradient increases the turbulent Prandtl number at the wall and the suction decreases it.

One could raise doubts as far as the usefulness of the present results are concerned to the prediction of heat transfer. As very well known, in the laminar sublayer, the turbulent quantities do not contribute much to the description of the mean profile. However, it has been proved in Section 7.2 that the derivative of the turbulent Prandtl number close to the wall is zero. This fact, together with the observation that both $\sqrt{\overline{u'^2}}$ and $\sqrt{\overline{t'^2}}$ are approximately linear with y in the sublayer, suggests that the turbulent Prandtl number varies little from the wall to the region where there is a sharp drop to its value in the logarithmic region. The present results should be used, therefore, as an upper limit for turbulent Prandtl number in the region which is believed to be the most important one for the turbulent heat transfer (for flat plate $y^+ < (10\text{-}15)$.

7.4 Analysis of the Turbulent Prandtl Number Data

Figure 7.1 shows the turbulent Prandtl number profile for zero pressure gradient flow. In the logarithmic region a value of approximately 0.9 is obtained, and approaches 0.5 in the outer region. This measurement constitutes an experimental confirmation of the analysis obtained from mean profile measurement. It can be done by assuming a Couette flow approximation in the inner region.

$$-\frac{\overline{u'v'}}{u_\tau^2} = 1 - \frac{du^+}{dy^+} \tag{7.18}$$

$$+\frac{\overline{v't'}}{u_\tau T_\tau} = 1 - \frac{dT^+}{dy^+}\frac{1}{Pr} \tag{7.19}$$

The turbulent Prandtl number can then be written as

$$Pr_t = \frac{\overline{u'v'}}{\overline{v't'}}\ \frac{\partial T/\partial y}{\partial u/\partial y} = -\frac{\overline{u'v'}/u_\tau^2}{\overline{v't'}/u_\tau T_\tau}\ \frac{dT^+}{du^+} \ . \tag{7.20}$$

Substituting (7.18) and (7.19) into (7.20) and by neglecting $\frac{du^+}{dy^+}$ and $\frac{dT^+}{dy^+}$ in the log region since they are small;

$$Pr_t = \frac{dT^+}{du^+} \tag{7.21}$$

This derivative has been calculated from experimental data and found to be approximately 0.9 in the logarithmic region.

Figures 7.2, 7.3, 7.4 and 7.5 show the turbulent Prandtl number profiles for adverse pressure gradient and different transpiration rates. It is observed that the adverse pressure gradient seems to decrease Pr_t in both the logarithmic and the outer regions. The same conclusion was reached by Blackwell [9] who obtained the turbulent Prandtl number profile for milder adverse pressure gradient flows from mean temperature and velocity measurements. His data, however, seem to indicate a higher dependence on pressure gradient.

Suction is observed to increase Pr_t in both logarithmic and outer regions. This is also confirmed by Blackwell [9], and sharply contrasts with the finding that Pr_t decreases with suction at the wall, as discussed in Section 7.3. This would indicate that the dominant terms in the turbulent transport of heat may be different for the near wall region and the rest of the boundary layer.

It can also be observed in the same figures that there is a region of the boundary layer where the turbulent Prandtl number drops and then rises to its value in the logarithmic region of the boundary layer. This was also observed in Blackwell's [9] data and is a result of a peak in the $\overline{v't'}$ profile in a different position from the peak in $\overline{u'v'}$ profile. This was discussed in Chapter 6.

Figure 7.6 shows the variation of $\partial T/\partial \bar{u}$ within an adverse pressure gradient boundary layer. This derivative can be evaluated throughout the boundary layer at any x holding all other parameters of the flow constant, since then both T and $\bar{u}$ are functions of y alone. We can write

$$\frac{\partial T}{\partial \bar{u}} = \frac{\partial T/\partial y}{\partial \bar{u}/\partial y} \tag{7.22}$$

It can be observed, by comparing the values of $\partial T/\partial \bar{u}$ from Fig. 7.6 with the values of Pr_t shown in Figs. 7.2 through 7.5, that in any boundary layer where $\partial T/\partial \bar{u}$ changes significantly, then Pr_t changes significantly. In boundary layers where $\partial T/\partial \bar{u}$ does not change much, then Pr_t is nearly constant. Examination of $\partial T/\partial \bar{u}$ throughout a boundary layer may serve to identify the trends of Pr_t which that boundary layer will exhibit. In particular, boundary conditions which affect $\partial T/\partial \bar{u}$ differently in the inner and outer regions will result in variations of turbulent Prandtl number within the layer. Thus, investigators seeking a "universal function" to describe Pr_t solely in terms of y^+ or the turbulent Peclet number may be doomed to failure.

Figure 7.7 shows turbulent Prandtl number as a function of y^+ for four different values of suction. Most nearly uniform are the values for $F = -0.004$ (strong suction). Reference to Fig. 7.6 shows $\partial T/\partial \bar{u}$ for that case to be nearly uniform. Most widely variable are the Prandtl number values for $F = 0.00$, and for that case $\partial T/\partial \bar{u}$ is also widely varying.

Figure 7.8 shows the turbulent Prandtl number data displayed as a function of turbulent Peclet number, $\frac{\varepsilon M}{\nu}$ Pr . Once again, the strong suction data are most nearly uniform, the unblown data least uniform. When pressure gradient effects and suction are present, there does not seem to be a good correlation. Simpson [47] and Kearney [7] found this same variation in data for turbulent Prandtl number in earlier studies. Different investigators have tried different techniques for accommodating the scatter, with more or less limited success. Blackwell [9] proposed a functional relationship between Pr_t and Pr $\frac{\varepsilon M}{\nu}$ with coefficients which were functions of the local hydrodynamic parameters. Simpson [9] followed Hinze's [29] suggestion that the diffusion of heat might be a combination of gradient and eddy transport.

The possibility exists, in view of the demonstrated variations of turbulent Prandtl number, that no universal correlation exists between Pr_t and Pr $\frac{\varepsilon M}{\nu}$ and that some more fundamental approach to the energy transport problem must be adopted.

7.5 Uncertainty Intervals

Review of the calibration data and consideration of the observed scatter in measurements made during the data taking has led to the following estimates for the stochastic (i.e. random) component of the uncertainty in the following measured quantities (expressed in relative terms):

$$\sqrt{\overline{u'^2}} = \pm 4\%$$

$$\sqrt{\overline{t'^2}} = \pm 4\%$$

$$\overline{u'v'} = \pm 8\%$$

$$v't' = \pm 14\%$$

$$\sqrt{\overline{v'^2}} = \pm 8\%$$

$$\sqrt{\overline{w'^2}} = \pm 8\%$$

$$\frac{dT}{dU} = \pm 4\%$$

$$u_\tau = \pm 5\%$$

$$T_\tau = \pm 8\%$$

Based on these estimates and the defining equations for Pr_t and Pr_{t_o}, the following uncertainties were estimated by a propagation at constant probability (Root Sum Square Combination)

$$Pr_t = \pm 17\%$$

$$Pr_{t_o} = \pm 11\%$$

These intervals are shown in the figures as vertical bars thru the data points.

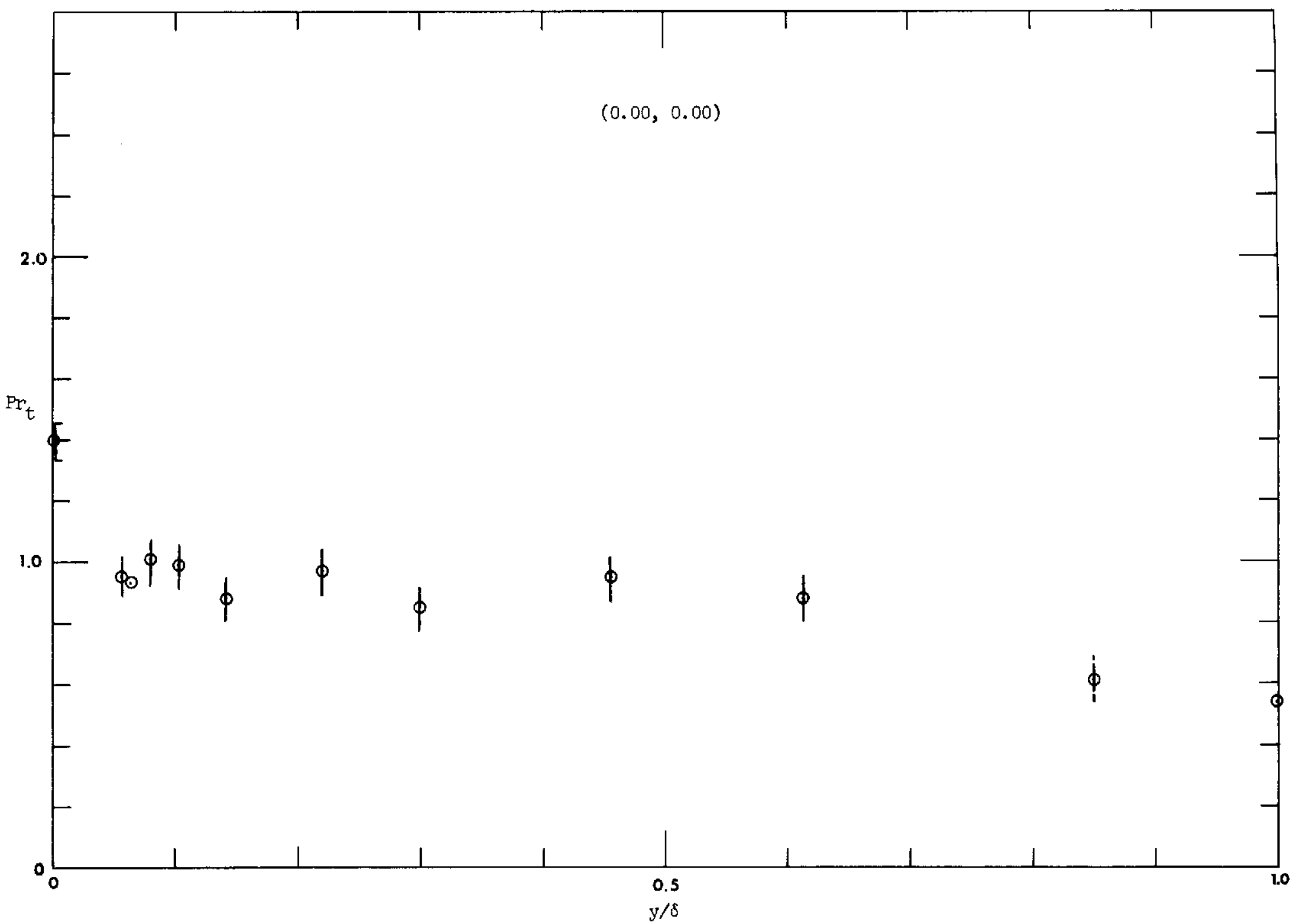

Fig. 7.1 The turbulent Prandtl number distribution in a flat plate boundary layer (0, 0).

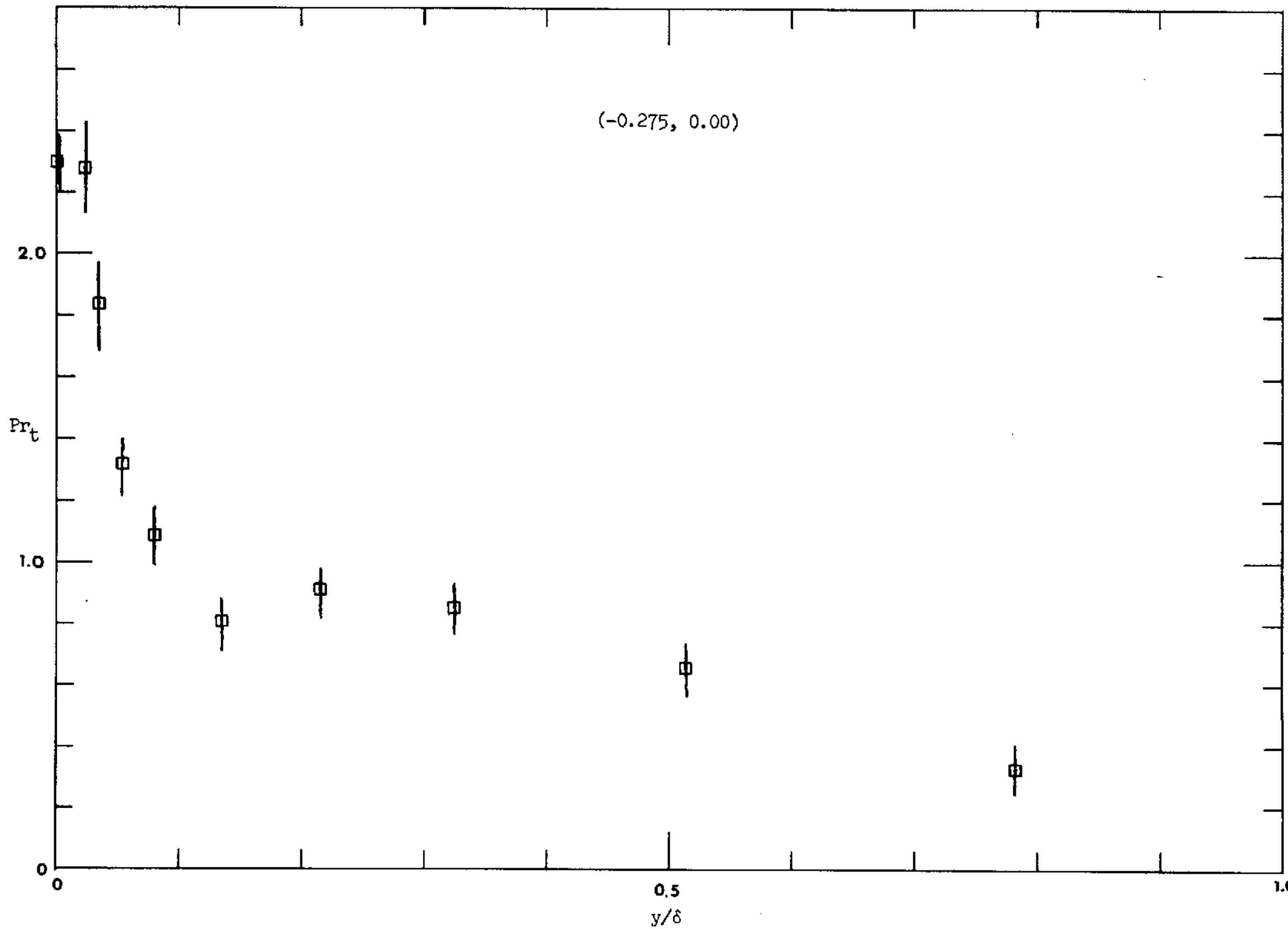

Fig. 7.2 The turbulent Prandtl number distribution in an adverse pressure gradient (-0.275, 0).

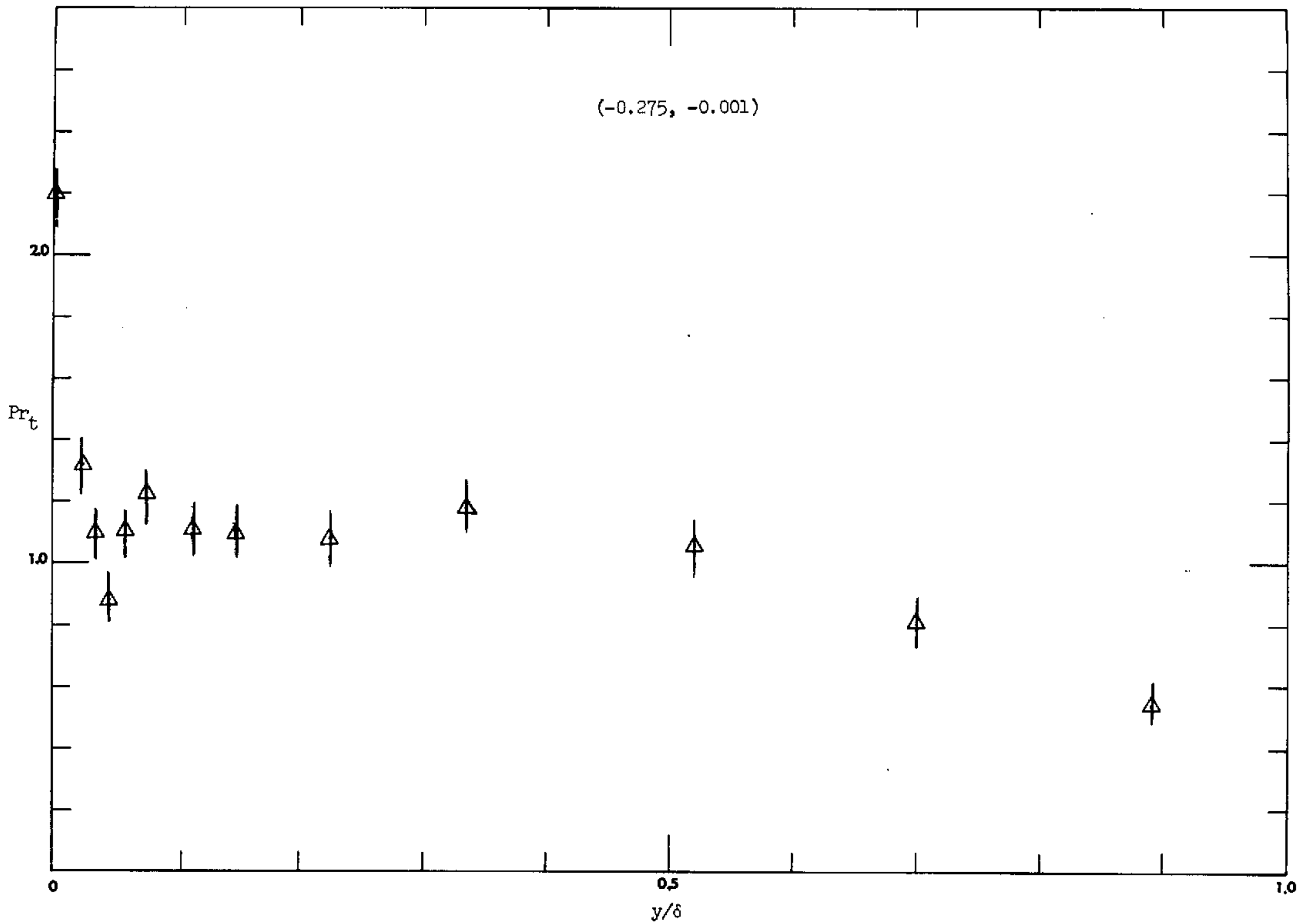

Fig. 7.3 The turbulent Prandtl number distribution in an adverse pressure gradient with mild suction (-0.275, -0.001).

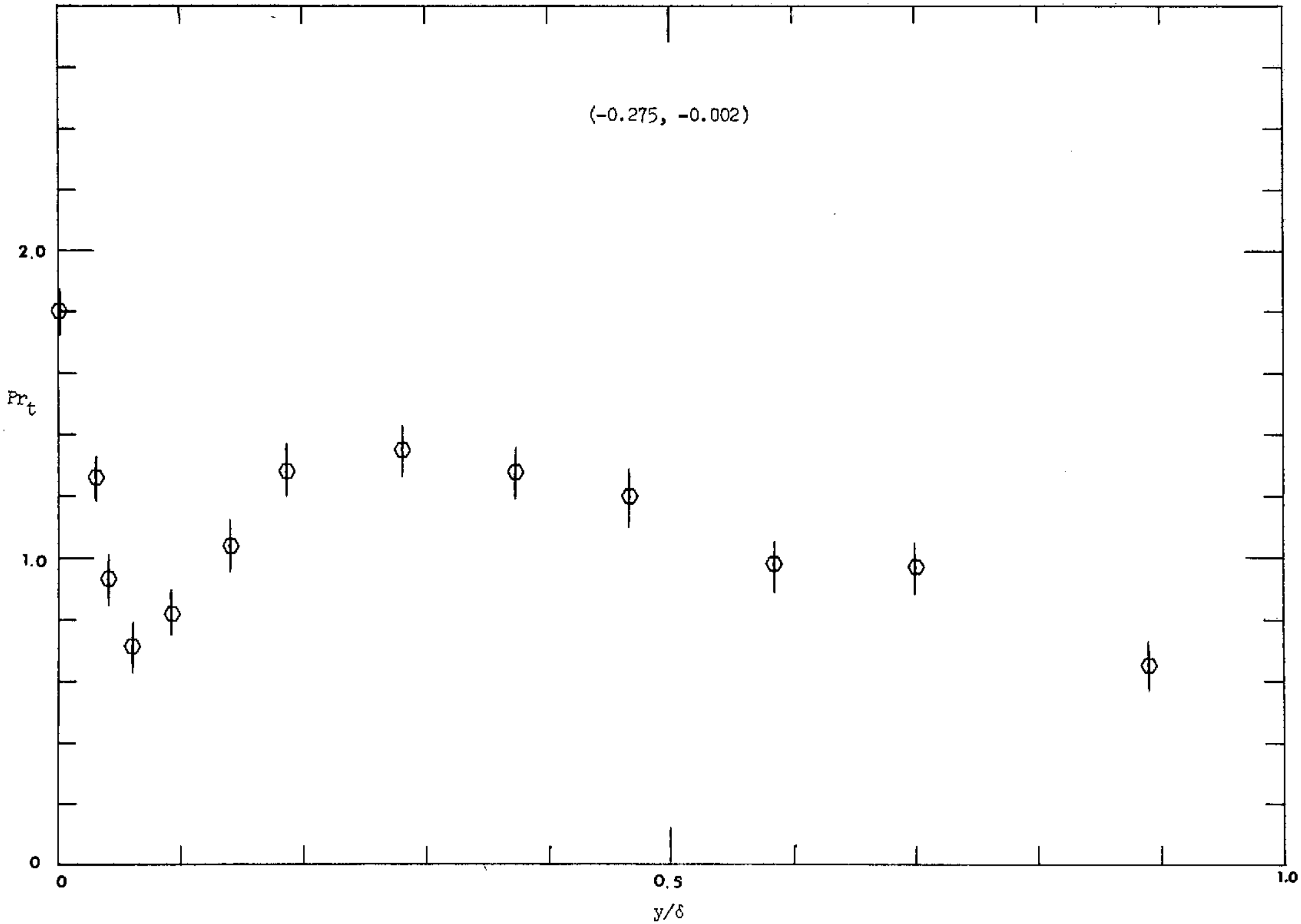

Fig. 7.4 The turbulent Prandtl number distribution in an adverse pressure gradient with suction (-0.275, -0.002).

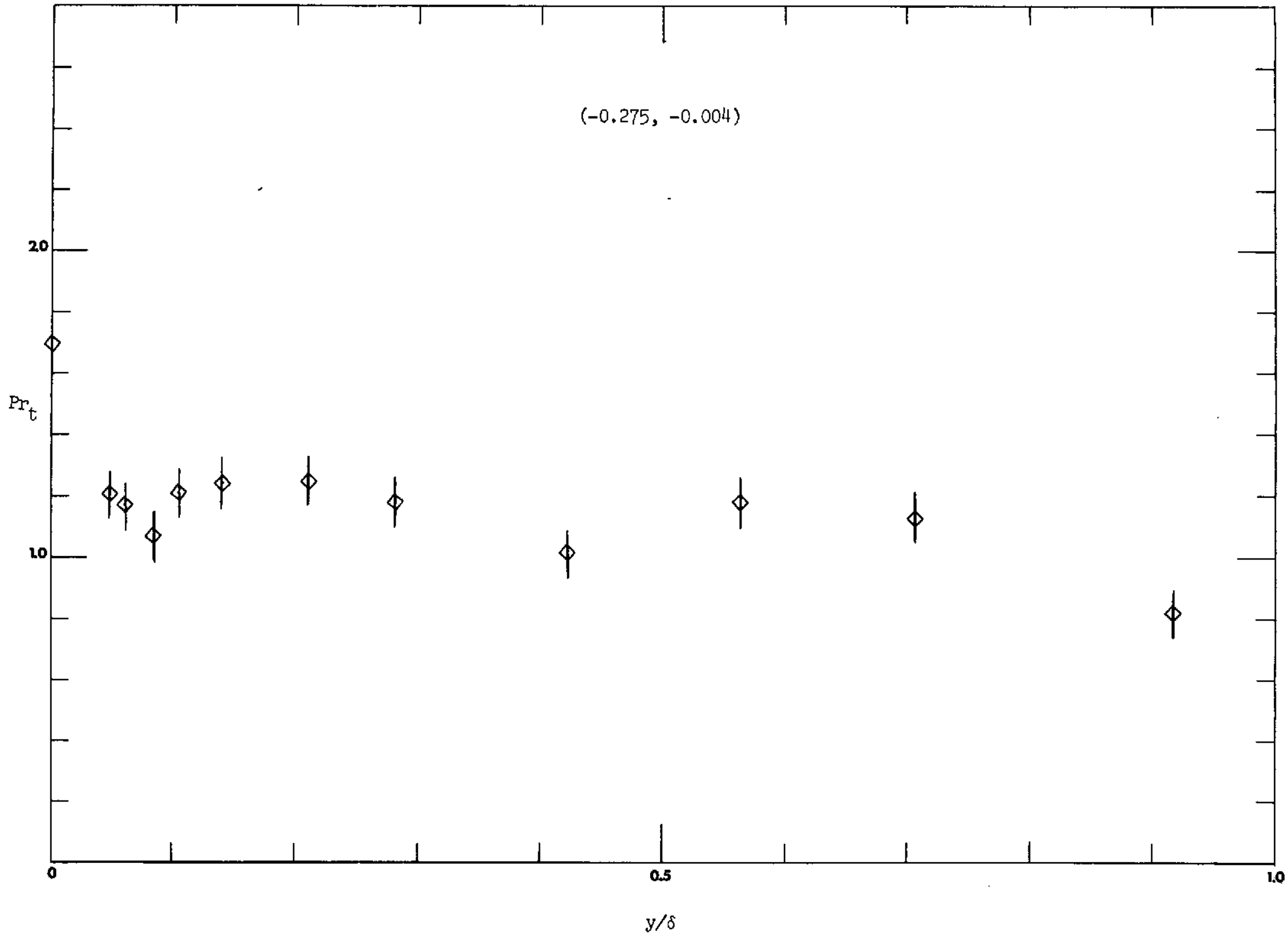

Fig. 7.5 The turbulent Prandtl number distribution in an adverse pressure gradient with strong suction (-0.275, -0.004).

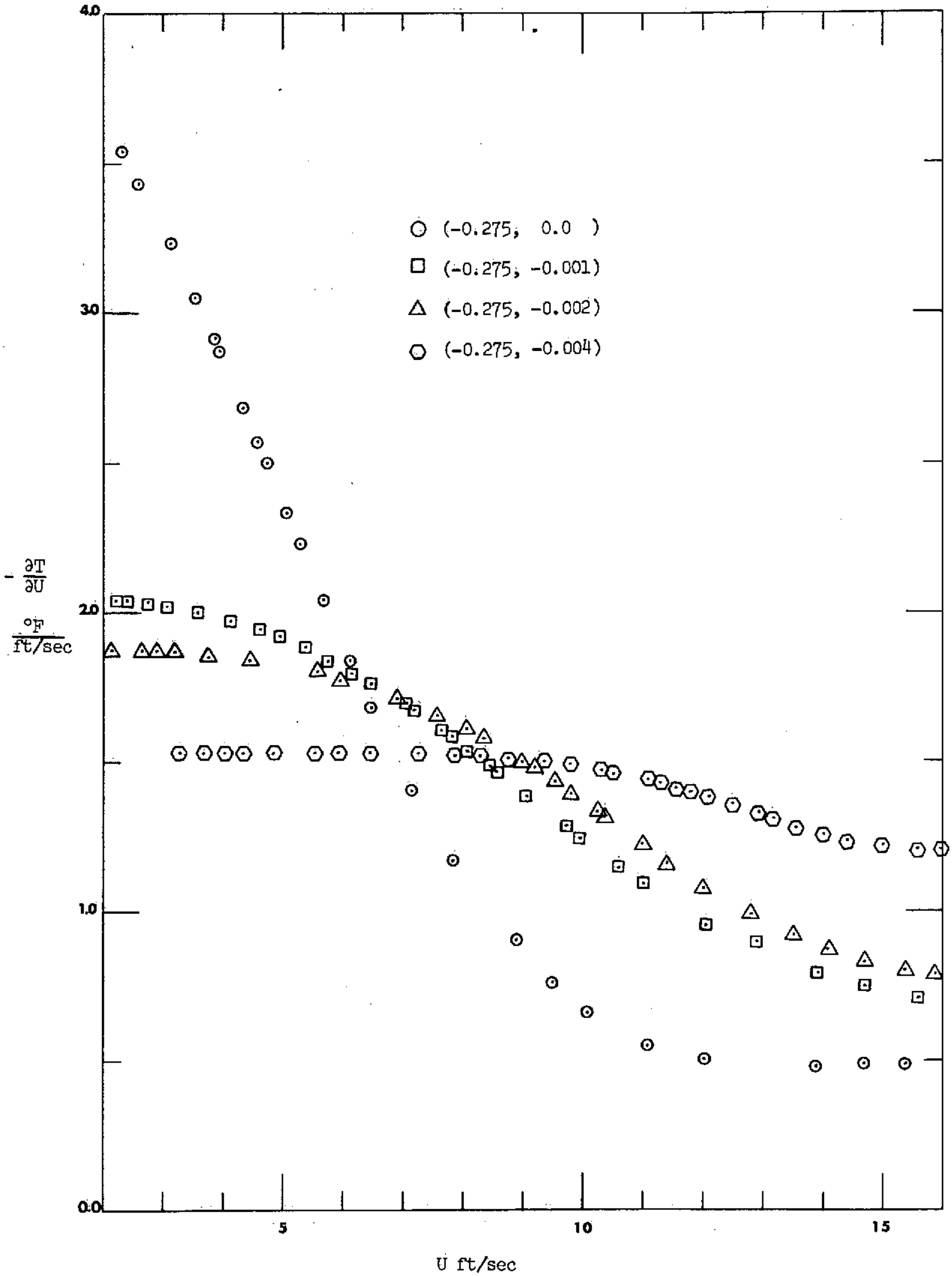

Fig. 7.6 The ratio $\partial T/\partial U$ within boundary layers subject to strong adverse pressure gradient with different suction rates.

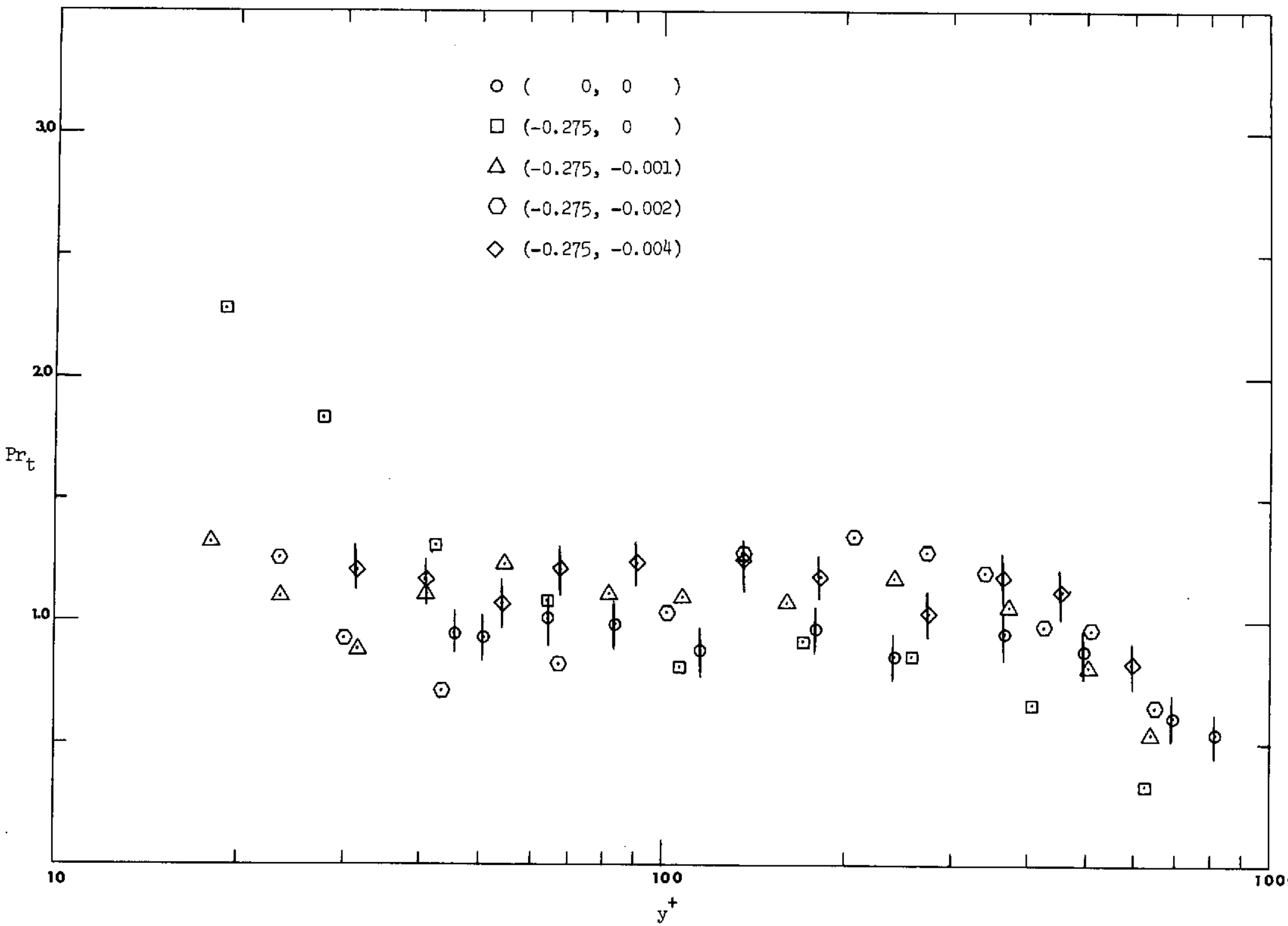

Fig. 7.7 Turbulent Prandtl number as a function of y^+; strong adverse pressure gradients with suction.

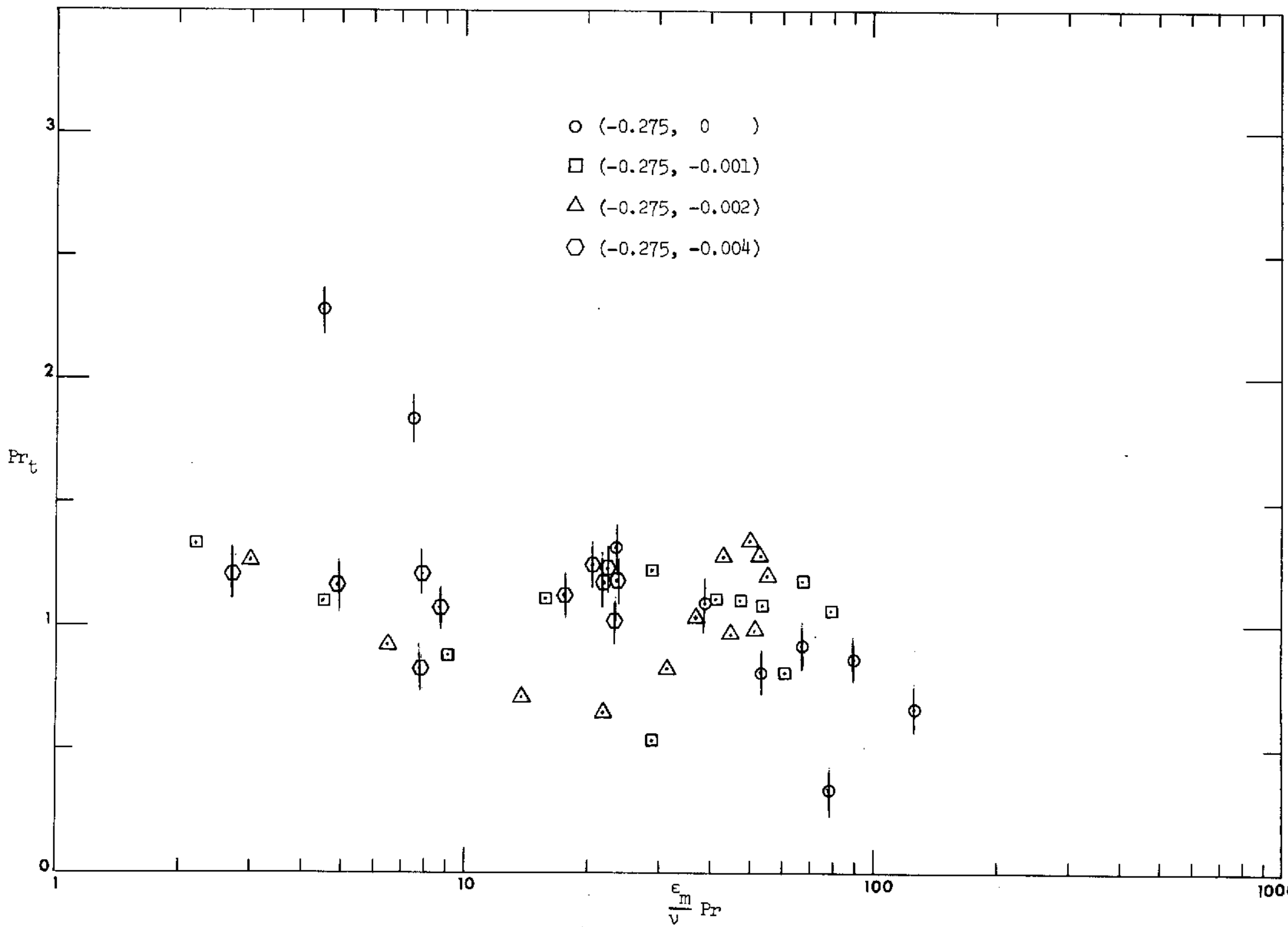

Fig. 7.8 Turbulent Prandtl number as a function of the turbulent Péclét number; strong adverse pressure gradients with suction.

CHAPTER 8

SUMMARY AND CONCLUSIONS

The behavior of near equilibrium turbulent boundary layers, under strong adverse pressure gradient conditions and with different suction rates has been examined with emphasis on the determination of the Stanton number and on the behavior of the turbulent Prandtl number.

The free stream velocity variation in this investigation may be described by an equation of the form

$$U_{\infty} \propto x^{m} \text{ , where } m \leq 0 \qquad (8.1)$$

The transpiration boundary condition, when expressed in terms of the blowing fraction F , is kept constant along the test section. Both constant and variable wall temperature conditions are examined. Chapter 2 summarizes the boundary conditions of this investigation.

The following are the results and conclusions drawn from the experimental results of this thesis:

1. Mean temperature and velocity profiles were measured sequentially by using only one probe. The friction coefficient was obtained by means of the direct measurement of $\overline{u'v'}$.

2. Direct measurements of the turbulent heat transfer and the temperature fluctuations have been made, and the turbulent Prandtl number calculated from the data for the turbulent transport of heat and momentum.

3. A new procedure has been developed to estimate the turbulent Prandtl number at the wall. It is shown from limited data that an adverse pressure gradient increases and suction decreases it.

4. The Stanton number for uniform wall temperature is shown to be the same function of enthalpy thickness Reynolds number

and blowing parameter in mild and strong adverse pressure gradients as it is in flat plate flows. The relationship between Stanton number for a given transpiration rate and the corresponding Stanton number for the no transpiration case (at the same enthalpy thickness Reynolds number) is, therefore, independent of pressure gradient and only a function of the blowing parameter B_h.

5. The Stanton number following a step in wall temperature in an adverse pressure gradient region is shown to be related to the isothermal Stanton number by the same function of relative position which describes the flat plate behavior for a step in wall temperature.

6. The analysis of the hydrodynamic turbulence structure of equilibrium flows shows that an adverse pressure gradient tends to increase the turbulence level. The $\overline{u'^2}$ profile is shown to develop two peaks. The second one is located in the outer region of the boundary layer ($y/\delta \sim 0.5$) and is displaced outward, when the pressure gradient increases. Suction is shown to suppress this second peak. The correlation coefficient between u' and v' is shown to have a constant value (approx. equal to the Karman constant) in the outer region of near equilibrium flows. The same constancy is observed for the ratio between the shear stress and the turbulent kinetic energy, which takes a value of approximately 0.14. It is shown that when simulating $\overline{u'v'}$ the outer layer peak can be predicted, in principle, by models like the Prandtl-Kolmogorov, which employs the turbulent kinetic energy as a descriptor for the eddy diffusivity for momentum.

7. Analysis suggests that the turbulent Prandtl number should tend to a constant value in the region near the wall.

8. In the logarithmic region adverse pressure gradient decreases

and suction increases the turbulent Prandtl number. Once again, it has been confirmed that Pr_T has a high value at the wall and reaches approximately 0.5 in the outer edge of the boundary layer.

References

1. Moffat, R. J., and Kays, W. M., "The Turbulent Boundary Layer on a Porous Plate: Experimental Heat Transfer with Uniform Blowing and and Juction," Report No. HMT-1, Thermosciences Division, Dept. of Mech. Engrg., Stanford Univ. (1967) PhD Thesis.

2. Simpson, R. L., Kays, W. M., and Moffat, R. J., "The Turbulent Boundary Layer on a Porous Plane: An Experimental Study of the Fluid Dynamics with Injection and Juction," Report No. HMT-2, Thermosciences Division, Dept. of Mech. Engrg., Stanford Univ. (1967) PhD Thesis.

3. Whitten, D. G., Kays, W. M., and Moffat, R. J., "The Turbulent Boundary Layer on a Porous Plate: Experimental Heat Transfer with Variable Suction, Blowing and Surface Temperature," Report No. HMT-3, Thermosciences Division, Dept. of Mech. Engrg., Stanford Univ. (1967) PhD Thesis.

4. Julien, H. L., Kays, W. M., and Moffat, R. J., "The Turbulent Boundary Layer on a Porous Plate: Experimental Study of the Effects of a Favorable Pressure Gradient, "Report No. HMT-4, Thermosciences Division, Dept. of Mech. Engrg., Stanford Univ. (1969) PhD Thesis.

5. Loyd, R. J., Moffat, R. J., and Kays, W. M., "The Turbulent Boundary Layer on a Porous Plate: An Experimental Study of the Fluid Dynamics with Strong Favorable Pressure Gradients and Blowing," Report No. HMT-13, Thermosciences Division, Dept. of Mech. Engrg., Stanford Univ. (1970) PhD Thesis.

6. Thielbahr, W. H., Kays, W. M., and Moffat, R. J., "The Turbulent Boundary Layer: Experimental Heat Transfer with Blowing, Suction, and Favorable Pressure Gradient," Report No. HMT-5, Thermosciences Division, Dept. of Mech. Engrg., Stanford Univ. (1969) PhD Thesis.

7. Kearney, D. W., Moffat, R. J., and Kays, W. M., "The Turbulent Boundary Layer: Experimental Heat Transfer with Strong Favorable Pressure Gradients and Blowing," Report No. HMT-12, Thermosciences Division Dept. of Mech. Engrg., Stanford Univ. (1970) PhD Thesis.

8. Andersen, P. S., Kays, W. M., and Moffat, R. J., "The Turbulent Boundary Layer on a Porous Plate: An Experimental Study of the Fluid Mechanics for Adverse Free-Stream Pressure Gradients," Report No. HMT-15, Thermosciences Division, Dept. of Mech. Engrg., Stanford Univ. (1972) PhD Thesis.

9. Blackwell, B. F., Kays, W. M., and Moffat, R. J., "The Turbulent Boundary Layer on a Porous Plate: An Experimental Study of the Heat Transfer Behavior with Adverse Pressure Gradients," Report No. HMT-16, Thermosciences Division, Dept. of Mech. Engrg., Stanford Univ. (1972) PhD Thesis.

10. Maye, F. P., "Error Due to Thermal Conduction Between the Sensing Wire and Its Supports when Measuring Temperatures with a Hot Wire Anemometer Used as a Resistance Thermometer," DISA Information No. G, February 1970, pp. 22-26.

11. Dahm, M. and Rasmussen, C. G., "Effect of Wire Mounting System on Hot-wire Probe Characteristics," DISA Information No. 7, January 1970, pp. 19-24.

12. Thinh, Nguyen Van, "On Some Measurements Made by Means of a Hot Wire in a Turbulent Flow Near a Wall," DISA Information No. 7, January 1970, pp. 13-18.

13. Watts, K. C., "The Development of Asymptotic Turbulent, Transitional, and Laminar Boundary Layers Induced by Suction," Ph.D. Thesis, Department of Mechanical Engineering, University of Waterloo, June 1972.

14. Fujita, H. and Kovasznay, L. S. G., "Measurement of Reynolds Stress by a Jingle Rotated Hot Wire Anemometer," The Review of Scientific Instruments, Volume 39, No. 9, September 1968.

15. Durst, F. and Rodi, W., "Evaluation of Hot Wire Signals in Highly Turbulent Flows," Fluid Dyn. Meas. in Ind. and Med. Envir., Proc., Disc. Conf., New York, Humanities Press, 1972.

16. Strohl, A. and Comte-Bellot, G., "Aerodynamic Effects Due to Configuration of X-Wire Anemometers," ASME paper No. 73-APM-P.

17. Corrsin, S., "Extended Applications of the Hot-wire Anemometer" NACA Technical Note No. 1864, April 1949.

18. Arya, S. P. S. and Plate, E. J., "Hotwire Measurements in Non-Isothermal Flow," Instruments & Control Systems, p. 87, March 1969.

19. Xuova, A. K. and Sesonsk F. A., "Structure of Turbulent Velocity and Temperature Fields in Ethylene Glycol Pipe Flow at Low Reynolds Number," International Journal of Heat and Mass Transfer, Vol. 15, pp. 127-145, 1972.

20. Johnson, D. S., "Velocity and Temperature Fluctuation Measurements in a Turbulent Boundary Layer Downstream of a Stepwise Discontinuity in Wall Temperature," Journal of Applied Mechanics, ASME, September 1959, p. 325.

21. Bremhorst, K. and Bullock, K. J., "Spectral Measurements of Temperature and Longitudinal Velocity Fluctuations in Fully Developed Pipe Flow," International Journal of Heat and Mass Transfer, Vol. 13, pp. 1313-1329, 1970.

22. Bourke, P. J. and Pulling, D. J., "A Turbulent Heat Flux Meter and Some Measurements of Turbulence in Air Flow Through a Heated Pipe," International Journal of Heat and Mass Transfer, Vol. 13, pp. 1331-1338, 1970.

23. Bradshaw, P. "An Introduction to Turbulence and its Measurement," The Commonwealth and International Library of Science Technology Engineering and Liberal Studies, Pergamon Press, 1971.

24. Blom, J. "Experimental Determination of the Turbulent Prandtl Number in a Developing Temperature Boundary Layer," Fourth International Heat Transfer Conference Paris-Versailles, Volume II, 1970.

25. Burchill, W. E. and Jones, B. G., "Interpretation of Hot-Film Anemometer Response in a Non-Isothermal Field," Proceedings of Symposium on Turbulence on Liquids, October 4-6, 1971. Department of Chemical Engineering, University of Missouri-Rolla.

26. Fulachier, L. and Dumas, R., "Repartitions Spectrales des Fluctuations Thermiques dans une Couche Limite Turbulent," Agard Conference Proceedings No. 93 on Turbulent Shear Flows, Paper 4, January 1972.

27. Clauser, F. H., "Turbulent Boundary Layers in Adverse Pressure Gradients," Journal of Aero Sci., 21, 91 (1954).

28. Bradshaw, P., "The Turbulence Structure of Equilibrium Boundary Layers," Journal of Fluid Mechanics, Vol. 29, Part 4, pp. 625-645, (1967).

29. Hinze, J. O., "Turbulence, An Introduction to its Mechanism and Theory," McGraw Hill, (1959).

30. Sandborn, V. A., "Hotwire Anemometer Measurements in Large-Scale Boundary Layers," Advances in Hotwire Anemometry, Proceedings of The International Symposium on Hotwire Anemometry, held at University of Maryland, (1967).

31. Klebanoff, P. S., "Characteristics of Turbulence in a Boundary Layer with Zero Pressure Gradient," NACA Report 1247, (1955).

32. Collis, D. C. and Williams, M. J., "Two-Dimensional Convection from Heated Wires at Low Reynolds Numbers," Journal of Fluid Mechanics, Vol. 6, p. 357, (1959).

33. Davies, T. W. and Patrick, M. A., "A Simplified Method of Improving the Accuracy of Hotwire Anemometry," Fluid Dyn. Meas. in Ind. and Med. Envir., Proc., Disc. Conf., New York, Humanities Press, (1972).

34. Dlaus, R. L. and Van Ness, H. C., "An Extension of the Spline Fit Technique and Applications to Thermodynamic Data," AIChE Journal, Vol. 13, Nov. 1967, p. 1132.

35. Repik, Y. E. U. and Ponomareva, V. S., "The Effect of Proximity of Walls on the Readings of a Hotwire Anemometer in Turbulent Boundary Layers," Heat Transfer-Soviet Research, Vol. 2, No. 4, July 1970.

36. Taylor, G. I., "The Transport of Vorticity and Heat Through Fluids in Turbulent Motion," The Scientific Papers of G. I. Taylor, Vol. II, Cambridge University Press, (1960).

37. Reynolds, W. C., Kays, W. M., and Kline, S. J., "Heat Transfer in the Turbulent Incompressible Boundary Layer with a Step Wall Temperature Distribution," Stanford University Report, Part II, Stanford, California, July 1957.

38. Hussain, K. M. F. and Reynolds, W. C., "The Mechanics of a Perturbation Wave in Turbulent Shear Flow," Report FM-6, Mech. Eng. Dept., Stanford University, May 1970.

39. Kearney, D. W., Kays, W. M., Moffat, R. J., Loyd, R. J., "The Effect of Free-Stream Turbulence on Heat Transfer to a Strongly Accelerated Turbulent Boundary Layer," Report HMT-9, Mech. Eng. Dept., Stanford, Feb. 1970. PhD Thesis.

40. Pimenta, M. M., Private Communication, Heat and Mass Transfer Group, Mechanical Engineering Dept., Stanford University.

41. Sharan, V. Kr., "On the Importance of Turbulence in Boundary Layer Simulation," Int. J. Mech. Sci., Vol. 15, pp. 643-640, (1973).

42. Townsend, A. A., "The Structure of Turbulent Shear Flow," Cambridge University Press, (1956).

43. Bradshaw, P., Ferris, O. H. and Atwell, N. P., "Calculation of Boundary Layer Development Using the Turbulent Energy Equation," Journal of Fluid Mechanics, Vol. 28, Part 3, pp. 593-616, (1967).

44. Bradshaw, P., "The Turbulence Structure of Equilibrium Boundary Layers," NPL Aero Report 1184, (1966).

45. Cebeci, T., "A Model for Eddy Conductivity and Turbulent Prandtl Number," ASME Paper No. 72-WA/HT-13.

46. Tennekes, H. and Lumley, J. L., "A First Course in Turbulence," The MIT Press, (1972).

47. Simpson, R. L., Whitten, D. G., and Moffat, R. J., "An Experimental Study of the Turbulent Prandtl Number of Air with Injection and Suction," Int. Journal Heat Mass Transfer, Vol. 13, pp. 125-143, (1970).

48. Chen, Che Pen, "Détermination Expérimentâle du Nombre de Prandtl Turbulent près d'une Paroi Lisse," International Journal of Heat and Mass Transfer, Vol. 16, pp. 1849-1862, October 1973.

49. Rotta, J. C., "Turbulent Boundary Layers in Incompressible Flows," Progress in Aeronautical Sciences, Edited by A. Ferri, D. Kuchemann and L. Sterne, Vol. 2, pp. 1-219, Macmillan, New York, (1962).

50. Mizushina, T., Ito, R. and Ogino, F., "Eddy Diffusivity Distribution Near the Wall," 4th International Heat Transfer Conference Paris-Versailles, Volume II, (1970).

51. Jenkins, R., "Variation of the Eddy Conductivity with Prandtl Modulus and its use in Prediction of Turbulent Heat Transfer Coefficients," Heat Transfer and Fluid Mechanics Institute, Stanford University Press, Stanford, California, p. 147, (1952).

52. Wassel, A. T. and Cotton, I., "Calculation of Turbulent Boundary Layers over Flat Plates with Different Phenomenological Theories of Turbulence and Variable Turbulent Prandtl Number," International Journal of Heat and Mass Transfer, Vol. 16, pp. 1547-1563, (1973).

53. Morrison, R. B., "Two Dimensional Frequency Wave Number Spectra and Narrow Band Shear Stress Correlations in Turbulent Pipe Flow," Ph.D. Thesis, University of Queensland, Australia, (1969).

54. Runstadler, T. W., Kline, S. J. and Reynolds, W. C., "An Experimental Investigation of the Flow Structure of the Turbulent Boundary Layer," Stanford University, Mech. Eng. Dept., Thermosciences Div., Report MD-8, (1963).

55. Bremhorst, K. and Walker, T. B., "Spectral Measurements of Turbulent Momentum Transfer in Fully Developed Pipe Flow," Journal of Fluid Mechanics, Vol. 61, part 1, pp. 173-186, (1973).

56. Jorgensen, F. E., "Directional Sensitivity of Wire and Hot Film Probes," DISA Information No. 11, (1971).

57. McLean, J. D., "The Transpired Turbulent Boundary Layer in an Adverse Pressure Gradient," PhD Thesis, Department of Aerospace and Mechanical Sciences, Princeton University, (1970).

58. Stevenson, T. N., "A Law of the Wall for Turbulent Boundary Layers with Suction or Injection," The College of Aeronautics, Cranfield, Aero Report No. 166 (1963).

59. Friehe, C. A. and Schwartz, W. H., "Deviations from the Cosine Law for Yawed Cylindrical Anemometer Sensors," Trans. ASME, 35E, 655 (1968).

APPENDIX A

ANALYSIS OF A RESISTANCE THERMOMETER RESPONSE TO MEAN AND FLUCTUATING TEMPERATURE

The use of a hot wire probe as a resistance thermometer for temperature measurement is dictated by the necessity of using a transducer with excellent temporal resolution. For boundary layer measurements it seems to be the best transducer available: its small size allows measurements of mean and fluctuating temperature even in regions of moderately sharp temperature gradients.

A parasitic effect caused by thermal conduction between the sensing element and its support can give incorrect results, however. The following analysis is intended to estimate the errors, and follows from Maye [10] and Hinze [29].

A 5 μm gold plated tungsten wire, DISA model 55F04 is used in this investigation. The probe was originally designed for reducing aerodynamic interference and has a gold plated portion for strengthening purposes. It turns out, however, that it can contribute towards lowering the heat conduction to the prongs. The analysis can be done by considering an effective resistance to heat transfer of the gold tungsten composite region, as seen in Fig. A.1.

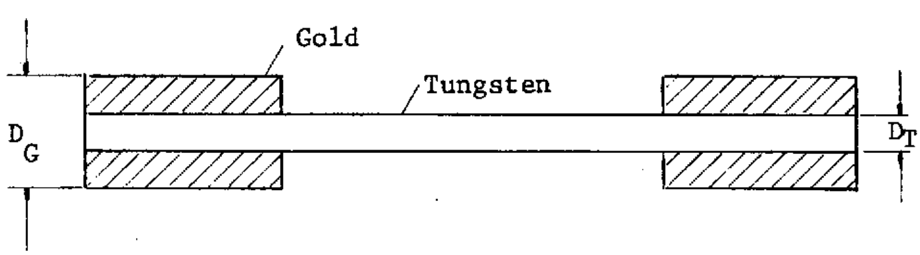

Figure A.1. Gold plated tungsten wire ($D_G/D_T = 6$).

The axial conduction resistance to heat transfer in this gold plated region can be seen as two resistances in parallel.

The first one, R_T , is due to tungsten; the second one, R_G , is due to gold. It follows that

$$R = \frac{R_G R_T}{R_G + R_T} \tag{A-1}$$

but $$R_G = \frac{L}{K_G A_G} \quad \text{where} \quad A_G = \frac{\pi}{4}(D_G^2 - D_T^2) \tag{A-2}$$

and $$R_T = \frac{L}{K_T A_T} \quad \text{where} \quad A_T = \frac{\pi}{4} D_T^2 \tag{A-3}$$

Substituting back into the expression for the resistance R ,

$$R = \frac{L}{K_G A_G + K_T A_T} = \frac{L}{K_T A_T}\left(1 + \frac{K_G}{K_T}\left(\frac{D_G^2}{D_T^2} - 1\right)\right)^{-1} \tag{A-4}$$

In order to estimate the magnitude of the resistance, the following values are assumed:

$$D_G/D_T = 6$$

$$K_G = 170 \text{ BTU/(hr) ft°F (Gold)}$$

$$K_T = 94 \text{ BTU/(hr) ft°F (Tungsten)}$$

$$\text{Thus,} \quad R = \frac{L}{K_T A_T} \; 0.0155 \tag{A-5}$$

This means that the resistance to heat transfer of the composite region is much smaller than if only the tungsten wire were present. As a result, the temperature will be nearly uniform in that region. However, in order to take advantage of this feature the prongs must be in the isothermal plane passing through the wire, because the gold plated portion follows nearly the prong temperature. A discussion of this point is made at the end of this appendix.

Maye [10] reports that conduction errors can be important in resistance thermometry. An analysis was carried out assuming that the total wire length is made of tungsten (3 mm, therefore).

Consider an element of wire placed in an isothermal plane for temperature measurement. The conservation of energy principle gives the following expression, as indicated in Fig. A.2.

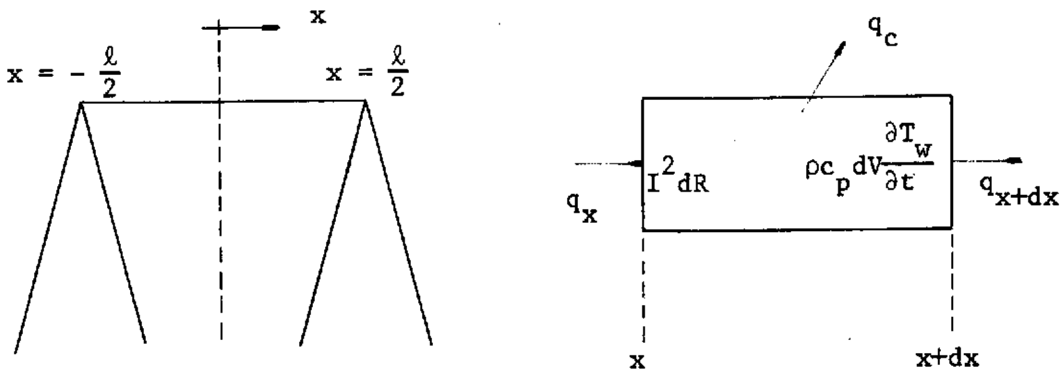

Figure A.2. Analysis of the wire.

$$q_x - q_{x+dx} - q_c + I^2 R \frac{dx}{\ell} = \rho\, c_p\, dV \frac{\partial T_w}{\partial t} \qquad (A.6)$$

$$\frac{\pi D^2}{4} \frac{\partial}{\partial x}\left(K \frac{\partial T_w}{\partial x}\right) dx - h\pi D dx (T_w - T_\infty) + I^2 R \frac{dx}{\ell} = \rho\, c_p \frac{\pi D^2}{4} dx \frac{\partial T_w}{\partial t} \qquad (A.7)$$

Assuming constant properties, which is quite reasonable for the temperature difference between the wire and the free stream, and integrating from $x = -\ell/2$ to $x = +\ell/2$

$$\frac{\pi D^2}{4} K \left.\frac{\partial T_w}{\partial x}\right|_{x = \frac{\ell}{2}} - h\pi D (T_m - T_\infty) + I^2 \frac{R_m}{\ell} = \rho\, c_p \frac{\pi D^2}{4} \frac{\partial T_m}{\partial t} \qquad (A.8)$$

where T_m and R_m are respectively the average wire temperature and resistance.

The first term to the left represents the thermal conduction along the wire. The non-uniformity of the temperature distribution along the wire is smaller for a low wire current and for small differences between prong and ambient temperature.

The second term represents the heat convection between the wire and the free stream. Under ideal circumstances, i.e., zero wire current and zero thermal inertia, it is zero. The wire temperature is uniform and therefore $T_m = T_\infty$. This is the ultimate objective of the resistance thermometry approach, i.e., to measure the fluid temperature by means of the wire temperature.

The third term represents the heat generation by the wire current. This contributes towards increasing the non-uniformity of the wire temperature, and therefore the heat conduction term.

Finally, the term to the right represents the thermal inertia of the wire.

In practice, ideal conditions are not attainable. The heat transfer coefficient h is velocity dependent, and the temperature of the wire is a function of the fluid velocity.

This dependence can be minimized by using a very small current, so that an acceptable error in the fluid temperature measurement is obtained.

In order to analyze the thermal inertia term, consider the ideal case of negligible heat conduction, with a cosinusoidal variation of the fluid temperature. The equation becomes

$$- h\pi D(T_m - T_\infty) = \rho\ c_p\ \frac{\pi D^2}{4}\frac{dT_m}{dt} \tag{A.9}$$

where $T_\infty = T_o \cos(\omega t)$

$$\text{then,}\quad \frac{T_{mo}}{T_o} = \frac{1}{[1 + (\omega \cdot \tau_c)^2]^{1/2}} \qquad \text{where}\quad \tau_c = \frac{\rho c_p D}{4h} \tag{A.10}$$

Assuming a tungsten wire

$\rho = 1208\ \mathrm{lb/ft^3}$

$c_p = 0.0321\ \mathrm{BTU/lb°F}$

$D = 5 \times 10^{-6}\ \mathrm{m}$

$h = 1182$ BTU/hr ft°F (30 ft/sec, 68°F)

$\tau_c = 0.484$ msec

For $\frac{T_{mo}}{T_o} = 0.90$, $\omega = 159$ hertz .

However, the frequencies encountered in the examined flows are higher. The DISA 55M20 temperature bridge employs a compensating network in the feedback loop of the amplifier to account for the low frequency response of the wire; according to the specifications, for a 1 μm platinum wire, the system has a flat response up to 3 Kh_z .

Assuming the thermal inertia can be taken care of by the compensating network (this is discussed in another section)

$$\frac{d^2T_w}{dx^2} - \frac{4h}{KD}(T_w - T_\infty) + \frac{I^2R}{\ell} \Big/ \frac{\pi D^2 K}{\ell} = 0 \qquad (A.11)$$

but $R = AT_w + B$ so

$$\frac{d^2T_w}{dx^2} - \omega^2 T_w + \lambda = 0 \qquad (A.12)$$

where $$\omega^2 = \frac{4h}{KD} - \frac{I^2}{\ell}\frac{4}{\pi D^2 K} A$$

$$\lambda = \frac{4h}{KD} T_\infty + \frac{I^2}{\ell}\frac{4}{\pi D^2 K} B = \omega^2 T_\infty + \frac{I^2}{\ell}\frac{4}{\pi D^2 K} R_\infty = \omega^2 T_\infty + \alpha$$

The solution of the above equation, subject to the following boundary conditions:

$$T_w = T_p \quad \text{at} \quad x = \pm \frac{\ell}{2}$$

$$\frac{dT_w}{dx} = 0 \quad \text{at} \quad x = 0$$

is $$\frac{T_w - \lambda/\omega^2}{T_p - \lambda/\omega^2} = \frac{\cosh \omega x}{\cosh \omega \ell/_2} \tag{A.13}$$

Then, the average wire temperature becomes:

$$T_m = \frac{2}{\ell} \int_o^{\ell/2} T_w dx$$

$$\frac{T_m - \lambda/\omega^2}{T_p - \lambda/\omega^2} = \frac{2}{\omega \ell} \tanh \frac{\omega \ell}{\alpha} = \nu \tag{A.14}$$

or $$T_\infty = \frac{T_m}{1-\nu} - \frac{\nu}{1-\nu} T_p - \frac{\alpha}{\omega^2}$$

An estimate of the magnitude of the terms can be done by assuming the following values:

$I = 2$ ma

$A = 0.0124\ \Omega/°C$

Kwire = 94 BTU/hr ft°F

$\ell = 3$ mm

$R_\infty = 4.5\ \Omega$

At a typical velocity of 10 ft/sec, and 85°F, the terms are:

$$\frac{4h}{K_w D} = 2.09 \times 10^6 \text{ sec}^{-1}$$

$$\frac{I^2 4A}{\ell \pi D^2 K} = 0.48 \times 10^3 \text{ sec}^{-1}$$

$$\omega^2 T_\infty = 1.77 \times 10^8 \text{ °F/sec}$$

$$\frac{I^2 4R_\infty}{\ell\pi D^2 K} = 3.15 \times 10^5 \ \text{°F/sec}$$

Therefore, for this low current of 2 ma , the 5 micron tungsten wire response can be treated as though there were no current through it, and as analyzed by Maye [10]

$$T_\infty = T_m + \frac{\nu}{1-\nu}(T_m - T_p) \tag{A.15}$$

where $\nu = \frac{2}{\omega\ell} \tanh \frac{\omega\ell}{2}$

$$\omega^2 = \frac{4h}{KD}$$

The response of the wire to the mean temperature can be analyzed by means of Equation (A.8). The gold plated portion makes the wire temperature nearly uniform in that region. Further, due to its large thermal inertia as compared to the sensitive region, its temperature fluctuates with very low amplitude about the mean temperature of the fluid. According to Maye [10] this can only be true for a low ν probe. A small variation of the prong temperature (i.e., when they are not placed in the isothermal plane of the wire) will not be felt appreciably by the sensing portion of the wire.

Table A.1 shows values of ν for different velocities ($\ell/D = 600$, $D = 5\mu m$). This should be viewed as a lower limit for the gold plated probe in question. Naturally the placing of the prongs in a non-isothermal plane will increase the heat conduction and therefore the value of ν .

	U(ft/sec)	0	3	10	15	20	30
Probe 55F02	ν	0.24	0.17	0.14	0.13	0.13	0.12
Probe 55F01	ν	0.21	0.17	0.16	0.15	0.15	0.15

Table A.1 Values of ν as a function of velocity for the DISA 55F02 5 μm tungsten probe and DISA 55F01 1 μm platinum probe.

Assuming the prongs in the isothermal plane of the wire, and time averaging Equation (A.8)

$$\frac{\pi D^2}{4} K \left.\frac{\partial T_w}{\partial x}\right|_{\ell/2} - h\pi D(T_w - T_\infty) + \frac{I^2 R_m}{\ell} = 0 \tag{A.16}$$

where bars mean time average value of the quantities. However

$$\begin{aligned} \left.\frac{\partial T_w}{\partial x}\right|_{\ell/2} &\approx 0 \qquad \text{(gold plating)} \\ \frac{I^2 R_m}{\ell} &\approx 0 \qquad \text{(very low current)} \end{aligned} \tag{A.17}$$

Thus $\overline{T}_m \approx \overline{T}_\infty$

An experiment to determine the value of ν seems to be a very difficult one. Maye [10] reports that lower values as compared to the calculated ones were obtained by him. This would place the present calculation on the safer side of error prediction. In the present experiments, the probe was placed in the free stream of the wind tunnel and the independence from the fluid velocity was confirmed to a nominal $\pm$ 0.05°F. This only means that actually the probe current is very small and its heating effect is negligible. Nothing can be said about the influence on ν because the whole system was isothermal. The actual operation would be in a temperature gradient field where the departure from isothermality is evident.

Maye [10] recommends the present probe for mean temperature measurements. The response of the wire to temperature fluctuations requires some further analysis. Equation (A.15) can be used for this purpose. By assuming that T_p is nearly time independent due to large inertia of the prongs:

$$t'_\infty = \frac{1}{1-\nu} t'_m \tag{A.18}$$

where $$\nu = \frac{2}{\ell\omega} \tanh \frac{\omega\ell}{2}$$

Referring to Table A.1, it can be seen that the actual rms value of the fluid temperature can differ from the measured one by 31% at zero velocity and by 13% at 30 ft/sec. It can also be seen that both probes (1 μm and 5 μm) can have similar performance as far as heat conduction is concerned. However, the 1 μm probe has a much smaller thermal inertia. The 55M anemometer is compensated for frequencies up to 3Khz when the 1 μm platinum wire is used. This upper limit must be reduced when the 5 μm wire is used. Figure A.3 shows the same flat plate case as measured by the two probes. It can be seen that the performances are similar, although the 5 μm probe is in error due to its larger thermal inertia. It is seen that in the outer region where the time scales are larger, there is a much better agreement between the two measurements, indicating that the frequency response of the system may be different for the two probes.

In the above analysis, it has been assumed that the prongs are in the isothermal plane of the wire. This configuration could be ideally achieved by placing them parallel to the wall. However, in regions where the temperature gradient is steeper, i.e., very close to the wall, the prongs can be at a different temperature. In the present set-up, the wall is hotter than the free stream, hence approaching from above the prongs will be colder than the wire. The gold plating follows nearly the prong temperature. Therefore the conduction will be higher and the measured value of the temperature will be below the fluid temperature.

The 1 μm platinum wire has one main advantage over the 5 μm tungsten wire for mean temperature measurement: its frequency response is better. The magnitude of ν does not increase in regions of steep temperature gradient (a higher heat conduction tends to increase ν). If a 5 μm wire is to be used, a better compensating network has to be used.

The accuracy of measurement of mean temperature with the 5 μm tungsten wire has been checked by measuring a flat plate case. Excellent agreement to Blackwell's data [9] has been achieved and is discussed in Section 3.14.

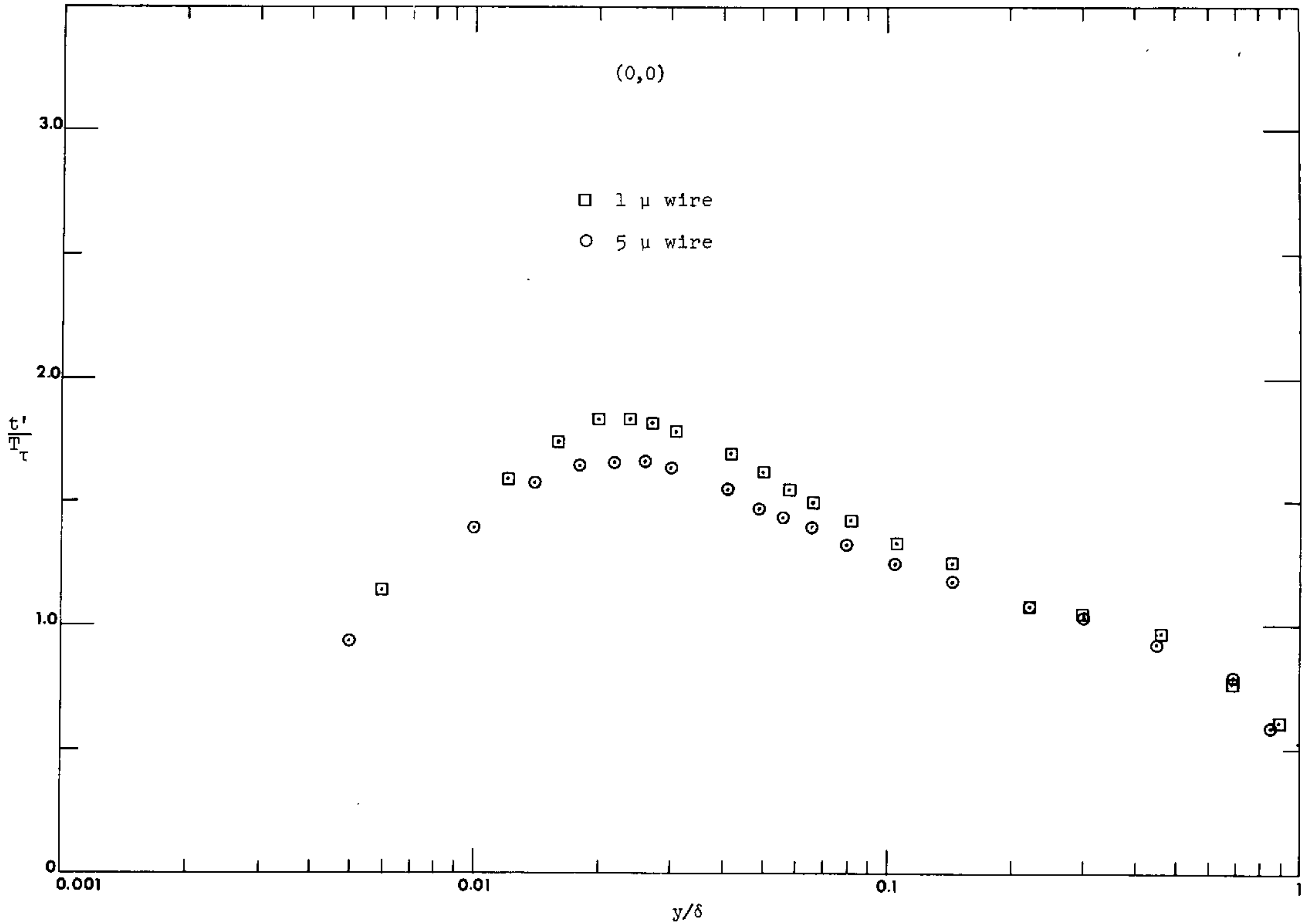

Fig. A.3   Flat plate temperature fluctuations: comparison between the 1 μm and the 5 μm wires.

APPENDIX B

THE MEASUREMENT OF TURBULENCE QUANTITIES

The measurement of the turbulence quantities is done by means of the directional properties of the hot wire to velocity and temperature.

Let E be the output from the hot wire anemometer; U_{eff} an effective velocity as felt by the wire and a function of the velocity components u, v, w; T the ambient temperature.

A small variation of the anemometer signal will be related to the temperature and velocity field by:

$$dE = \frac{\partial E}{\partial U_{eff}} dU_{eff} + \frac{\partial E}{\partial T} dT \tag{B.1}$$

For small fluctuations,

$$e' = \frac{\partial E}{\partial U_{eff}} u'_{eff} + \frac{\partial E}{\partial T} t' \tag{B.2}$$

If the measurement is referred to a system of coordinates in such a way that only the streamwise velocity component has a value different from zero, Eq. (B.2) can be written as:

$$e' = \frac{\partial E}{\partial U} \frac{\partial U}{\partial U_{eff}} u'_{eff} + \frac{\partial E}{\partial T} t' \tag{B.3}$$

where the sensitivities $\frac{\partial E}{\partial U}$ and $\frac{\partial E}{\partial T}$ are determined directly from a calibration procedure. There remains only the determination of the relationship between the effective velocity and the velocity components.

1. Directional Sensitivity of the Hot Wire

The directional sensitivity of the hot wire to velocity components, as shown by Jorgensen [56] can be approximated by

$$U_{eff}^2 = U_2^2 + k_1^2 V_2^2 + k_2^2 W_2^2 \tag{B.4}$$

where U_2 , V_2 , and W_2 are the velocity components in the coordinate system of the wire: V_2 is the velocity component parallel to the wire, W_2 is perpendicular to the wire and to the wire supports and U_2 is perpendicular to the wire and lies in the plane of the wire supports. k_1 and k_2 are constants which depend upon the probe design (i.e., wire length and diameter, prong interference etc.) and have been determined by some investigators for the probe used in this experiment to be:

$$k_1 = 0.2 \qquad k_2 = 1.02 \tag{B.5}$$

Figure B.1 shows the geometry and position of the hot wire probe for the present analysis

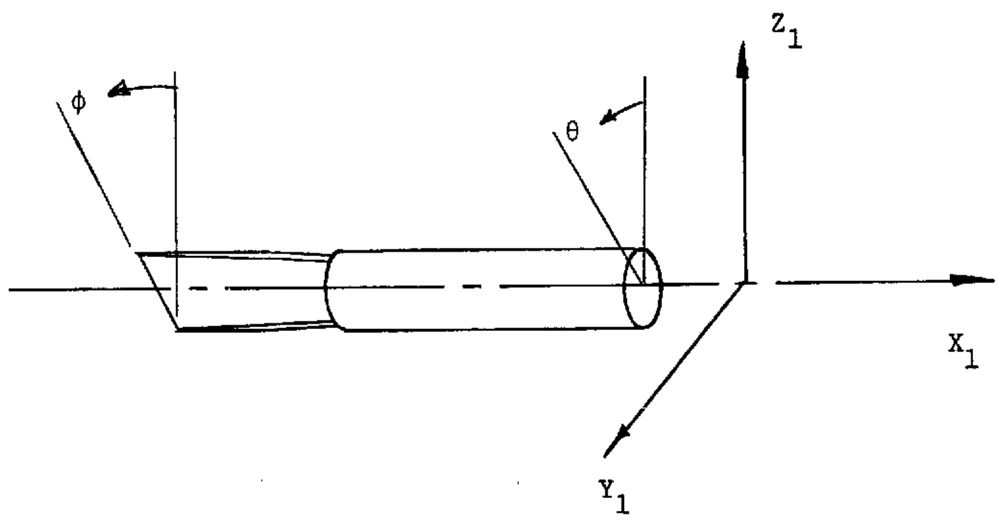

B.1 The geometry and coordinates of the slant wire.

The angle ϕ measures the inclination of the wire with respect to a plane perpendicular to the probe axis: for a "slant" wire, $\phi \neq 0$.

The present analysis follows from Andersen [8] and only the final results will be given.

Writing the effective velocity as a function of the velocity components in the frame of the laboratory (U_1 , V_1 , W_1)

$$U_{eff}^2 = A\ U_1^2 + B\ V_1^2 + C\ W_1^2 + D\ U_1 V_1 + E\ V_1 W_1 + F\ U_1 W_1 \qquad (B.6)$$

where

$$A = \cos^2\phi + k_1^2 \sin^2\phi$$

$$B = (\sin^2\phi + k_1^2 \cos^2\phi)\cos^2\theta + k_2^2 \sin^2\theta$$

$$C = (\sin^2\phi + k_1^2 \cos^2\phi)\sin^2\theta + k_2^2 \cos^2\theta$$

$$D = (1-k_1^2)\sin^2\phi \cos\theta$$

$$E = (\sin^2\phi + k_1^2 \cos^2\theta - k_2^2)\sin 2\theta$$

$$F = (1-k_1^2)\sin 2\phi \sin\theta$$

The velocity components in the "mean flow" frame of reference may be expressed as follows, presuming that the mean velocity is aligned with the axis of the probe:

$$\begin{aligned} U_1 &= \overline{u} + u' \\ V_1 &= v' \\ W_1 &= w' \end{aligned} \qquad (B.7)$$

Expanding U_{eff} in Taylor series about $(\overline{u}, 0, 0)$

$$U_{eff} = \sqrt{A}\,\overline{u} + \sqrt{A}\,u' + \frac{D}{2\sqrt{A}} v' + \frac{F}{2\sqrt{A}} w'$$

$$+ \left(\frac{B}{\sqrt{A}} - \frac{D^2}{4A\sqrt{A}}\right)\frac{v'^2}{2u} + \left(\frac{C}{\sqrt{A}} - \frac{F^2}{4A\sqrt{A}}\right)\frac{w'^2}{2u}$$

$$+ \left(\frac{E}{\sqrt{A}} - \frac{DF}{2A\sqrt{A}}\right)\frac{v'w'}{2u} + 0(3) \qquad (B.8)$$

Define $U'_{eff} = U_{eff} - \sqrt{A}\ \overline{u}$ from B.8 . (B.9)

Note that $\overline{U'_{eff}}$ is zero to 0(1) in the fluctuations, satisfying the requirement for a fluctuation term. Squaring U'_{eff}, time averaging, and discarding terms of higher order than 0(2) yields the working expression for $\overline{U'^2_{eff}}$:

$$\overline{U'^2_{eff}} = A\ \overline{u'^2} + \frac{D^2}{4A}\ \overline{v'^2} + \frac{F^2}{4A}\ \overline{w'^2} + D\ \overline{u'v'} + \frac{DF}{2A}\ \overline{v'w'} + F\ \overline{u'w'} + 0(3) \tag{B.10}$$

Therefore, the mean square value of the effective velocity fluctuation can be related to the velocity components in the frame of the mean flow by (B.10) and can be used to measure all the components of the Reynolds stress tensor.

2. <u>Test for Three Dimensional Effects on the Flow Field</u>

The probe system design used in this investigation allows measurements to be taken for a $\phi = 48°$ probe at $\theta = 0°$, $\pm 30°$, $\pm 90°$, $\pm 150°$.

At $\theta = +90$, Eq. (B-10) can be written as

$$\overline{U'^2_{eff}}\Big|_{\theta=90} = A\ \overline{u'^2} + \frac{F^2}{4A}\ \overline{w'^2} + F\ \overline{u'w'} \tag{B.11}$$

At $\theta = -90$

$$\overline{U'^2_{eff}}\Big|_{\theta=-90} = A\ \overline{u'^2} + \frac{F^2\overline{w'^2}}{4A} - F\ \overline{u'w'} \tag{B.12}$$

Measurements for all examined strong adverse pressure gradient flows were taken at different y-locations of the boundary layer (normal to the wall) and for $\theta = +90°$ and $\theta = -90°$. Very small differences between the anemometer signals were observed, indicating that $\overline{u'w'}$ was really very close to zero.

Measurements were also taken at $\theta = \pm 30°$ and $\theta = \pm 150°$ and it was concluded that $\overline{v'w'}$ was also very close to zero.

The 2-D hypothesis about the flow field was therefore proved to be true and the analysis that follows will therefore be based on $\overline{u'w'} = \overline{v'w'} = 0$.

3. <u>The Measurement of the Axial Velocity Component in Isothermal Flows</u>

The measurement of the axial velocity component in isothermal flows is obtained by using a horizontal wire ($\phi = 0°$, $\theta = 90°$).

Equation (B.10) can then be written as:

$$\overline{U'^2_{eff}} = \overline{u'^2} + 0(3) \tag{B.13}$$

and to a second order approximation, the measurement of $\overline{u'^2}$ can be done with a horizontal wire. The probe used for obtaining this profile has the advantage, due to its design, of obtaining measurements very close to the wall (0.005 in.), which cannot be obtained directly by means of a slant wire.

4. <u>The Measurement of the Reynolds Stress Tensor Components in Isothermal Flows</u>

Equation (B.10), with the 2-D hypothesis about the flow field ($\overline{u'w'} = \overline{v'w'} = 0$) can be written as:

$$\overline{U'^2_{eff}} - A\,\overline{u'^2} = \frac{D^2}{4A}\,\overline{v'^2} + \frac{F^2}{4A}\,\overline{w'^2} + D\,\overline{u'v'} + 0(3) \tag{B.14}$$

In Eq. (B.14) it is assumed that the axial velocity fluctuation component $\overline{u'^2}$ is known from the horizontal wire measurement. In principle, if data are obtained for 3 different probe angles θ ($\phi = 48°$ is constant along the path of the probe support rotation), a system of equations can be solved to obtain directly $\overline{v'^2}$, $\overline{w'^2}$ and $\overline{u'v'}$. This has been done for $\theta = -30°, -90°, -150°$ using a fixed $\phi = 48°$.

5. <u>The Measurement of $\overline{v't'}$</u>

The term $\frac{\partial U}{\partial U_{eff}}$ in Eq. (B.3) can be obtained by differentiating Eq. (B.9) and neglecting the fluctuating components. Then, it follows that

$$\frac{\partial U}{\partial U_{eff}} = \frac{1}{\sqrt{A}} \tag{B.15}$$

Squaring and averaging Eq. (B.3), and using (B.15)

$$\overline{e'^2} = \left(\frac{\partial E}{\partial U}\,\frac{1}{\sqrt{A}}\right)^2 \overline{U'^2_{eff}} + \left(\frac{\partial E}{\partial T}\right)^2 \overline{t'^2} + \left(2\,\frac{\partial E}{\partial U}\,\frac{\partial E}{\partial T}\,\frac{1}{\sqrt{A}}\right)\overline{u'_{eff}t'} \qquad \text{(B.16)}$$

If measurements are taken at $\theta = -30°$ and $\theta = -150°$ two equations are obtained. Introducing the definition of U'_{eff} (Eq. B.9), subtracting, discarding terms above $O(2)$:

$$\overline{e'^2}\Big|_{\theta=-30} - \overline{e'^2}\Big|_{\theta=-150} = \left(\frac{\partial E}{\partial U}\right)^2 \frac{2D}{A}\,\overline{u'v'} + \left(\frac{\partial E}{\partial U}\,\frac{\partial E}{\partial T}\right)\frac{2D}{A}\,\overline{v't'} \qquad \text{(B.17)}$$

From knowledge of $\overline{u'v'}$, a value for $\overline{v't'}$ can be obtained; however, the value of $\overline{u'v'}$ can be also obtained at the same time by using two more measurements at the same θ positions at different wire temperatures. The solution of a system of two linear equations will give $\overline{u'v'}$ and $\overline{v't'}$ both from this pair of values.

6. The Measurement of $\overline{t'^2}$

This measurement can be obtained by means of a resistance thermometry approach and was discussed in Appendix A.

APPENDIX C

THE MEASUREMENT OF SHEAR STRESS IN COMPLETELY DEVELOPED RECTANGULAR CHANNEL FLOW

The present analysis is intended as a baseline for the measurement of the Reynolds stress tensor components in the adverse pressure gradient flows of this investigation.

A completely developed rectangular channel flow was used for checking the new hot wire system because the shear stress is known to follow a theoretically established equation, which is developed in this appendix.

Figure C.1 shows the channel flow and the system of coordinates to be used in this analysis.

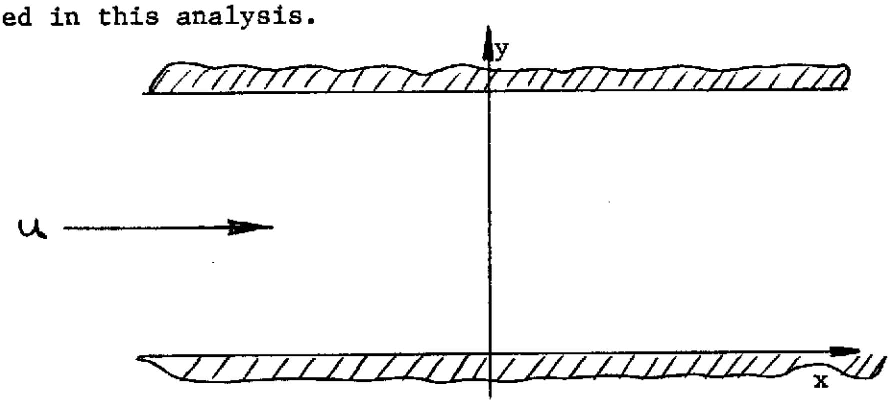

Figure C.1 Channel flow and the system of coordinates.

The continuity equation for a two dimensional, constant density flow can be written as

$$\frac{\partial \overline{u}}{\partial x} + \frac{\partial \overline{v}}{\partial y} = 0 \tag{C.1}$$

Because of the fact that the flow is completely developed, $\frac{\partial \overline{u}}{\partial x} = 0$. As a consequence, $\overline{v} = 0$ because at the wall $v_o = 0$.

The Navier Stokes equation for 2-D completely developed flows, after having dropped the x-derivatives of the velocity components and by setting $\overline{v} = 0$, is:

$$0 = -\frac{1}{\overline{\rho}}\frac{\partial\overline{p}}{\partial x} + \nu\frac{\partial^2\overline{u}}{\partial y^2} - \frac{\partial}{\partial y}(\overline{u'v'}) \qquad (C.2)$$

Integration of (C.2) with respect to y , and setting $u_\tau^2 = \nu \left.\frac{\partial\overline{u}}{\partial y}\right|_o$ gives

$$0 = -\frac{1}{\overline{\rho}}\frac{\partial\overline{p}}{\partial x}y + \nu\frac{\partial\overline{u}}{\partial y} - \overline{u'v'} - u_\tau^2 \qquad (C.3)$$

At the centerline ($y = \delta$), however, $\frac{\partial\overline{u}}{\partial y} = 0$, $\overline{u'v'} = 0$ hence by using (C.3)

$$u_\tau^2 = -\frac{1}{\rho}\frac{\partial\overline{p}}{\partial x}\delta \qquad (C.4)$$

Equation (C.3) can therefore be written as

$$\tau^+ = \frac{1}{u_\tau^2}\left(\nu\frac{\partial\overline{u}}{\partial y} - \overline{u'v'}\right) = (1-\frac{y}{\delta}) \qquad (C.5)$$

It is therefore concluded that the total stress τ^+ is a linear function of the distance from the wall. Far away from the wall, the laminar contribution to the total stress is very small and the turbulent stress can be written as

$$-\frac{\overline{u'v'}}{u_\tau^2} = 1 - \frac{y}{\delta} \qquad (C.6)$$

The determination of the friction velocity u_τ can be made directly by pressure drop measurements along the channel; thus the shear stress $\overline{u'v'}$ can be known accurately and compared to the value obtained with the new hot wire system.

APPENDIX D

THE DIRECT MEASUREMENT OF THE TURBULENT KINETIC ENERGY AND THE SHEAR STRESS BY MEANS OF A SINGLE SLANT, ROTATABLE HOT WIRE PROBE

As shown in Appendix B, the measurement of the Reynolds stress tensor components can be done by using a single rotatable wire, which provides measurements at different positions of the probe. The solution of a system of linear equations will thus give the value of each component separately.

There has been lately, however, a great interest in the turbulent kinetic energy profile in order to provide a closure for the turbulent flow system of equations. Turbulent kinetic energy can be found by adding up the three components of the mean square values of the velocity fluctuation vector to give the turbulent kinetic energy defined as

$$\overline{q^2} = \overline{u'^2} + \overline{v'^2} + \overline{w'^2} \tag{D.1}$$

The uncertainties of the measurement of each component, however, add up to give an even higher uncertainty in $\overline{q^2}$. In some applications where only the value of $\overline{q^2}$ is required, its calculation based on the sum of each component becomes time consuming and an unnecessary procedure.

A measurement procedure is proposed, to give directly the value of $\overline{q^2}$ and $\overline{u'v'}$ by means of a single rotating slant wire.

Equation (B.14), in Appendix B, shows that the hot wire response in a two-dimensional flow field can be written in the reference frame of the mean flow as

$$\overline{u_i'^2} = A\,\overline{u'^2} + \frac{D^2}{4A}\,\overline{v'^2} + \frac{F^2}{4A}\,\overline{w'^2} + D\,\overline{u'v'} + O(3) \tag{B.14}$$

where A, D, F depend on the angles of the wire and the probe design.

If a combination of the parameters is chosen such that

$$A = \frac{D^2}{4A} = \frac{F^2}{4A} \quad . \tag{D.2}$$

Equation (B.14) can be written as

$$\overline{u_1'^2} = A\,\overline{q^2} + D\,\overline{u'v'} \quad . \tag{D.3}$$

Two measurements are therefore sufficient to give $\overline{q^2}$ and $\overline{u'v'}$.

The values of A, D, F can be used from (B.6) to solve a system of equations and give θ and ϕ .

The first relationship, $\frac{D^2}{4A} = \frac{F^2}{4A}$ gives

$$D = \pm F \tag{D.4}$$

or

$$(1 - k_1^2)\sin 2\phi \cos\theta = \pm (1 - k_1^2)\sin 2\phi \sin\theta \tag{D.5}$$

which gives

$$\theta = (2K + 1)\frac{\pi}{4} , \quad K = 0, \pm 1 , \pm 2 \ldots \tag{D.6}$$

This means that the direct measurement can only be done in particular positions given by (D.6).

The second relationship $A = \frac{D^2}{4A}$

gives

$$D = \pm 2A \quad \text{or} \tag{D.7}$$

$$(1 - k_1^2)\sin 2\phi \cos\theta = \cos^2\phi + k_1^2 \sin^2\phi \quad . \tag{D.8}$$

This non-linear equation can be solved for ϕ , using $\theta = \pm 45°$ and the functional dependence of k_1 on ϕ and θ , as indicated by Friehe and Shwartz [59] to give a wire angle of approximately $\phi \approx 57°$. This angle is different from the usual 45° slant wire; the probe would thus have to be built under these specifications and the comparison between its direct measurement of $\overline{q^2}$ and the value obtained from adding up the components from a slanted probe would check its accuracy.

Unfortunately, manufacturing difficulties prevented such a probe from being built. Another trial will be made in a future program.

The probe would be basically a 57° gold plated slant wire, diameter of 5 μm , with provisions for the rotating mechanism to stop at every 45°. This probe would be the indicated one for measurements in isothermal flows.

Appendix E

TABULATIONS OF EXPERIMENTAL DATA

Table E-1. Friction Factor Data

Table E-1.1 Friction Factor Data (-0.275, 0.0)

	x = 22	x = 34	x = 46	x = 58	x = 70	x = 82
$\kappa\left(\frac{u_\infty y}{\nu_\infty}\right)$	-0.00075	-0.00050	-0.00038	-0.00031	-0.00027	-
$\nu\frac{\partial u}{\partial y}$	0.0687	0.0637	0.0460	0.0545	0.0499	-
$-\overline{u'v'}$	0.773	0.402	0.296	0.269	0.239	-
$\frac{1}{u_\infty^2}\left(\nu\frac{\partial u}{\partial y}-\overline{u'v'}\right)$	0.00178	0.00126	0.00107	0.00108	0.00104	-
$-\frac{1}{\rho_\infty u_\infty^2}\frac{\partial}{\partial x}\int_o^y \rho u^2 dy$	0.00001	0.	0.	0.	0.	-
$-\frac{uv_o}{u_\infty^2}$	0.	0.	0.	0.	0.	-
$\frac{1}{\rho_\infty u_\infty^2}u\frac{\partial}{\partial x}\int_o^y \rho u dy$	-0.00009	-0.00008	-0.00005	-0.	-0.00004	-
$c_f/2$	0.00096	0.00069	0.00065	0.00076	0.00081	-
$c_f/2$ (Andersen)	0.00079	0.00055	0.00047	0.00053	0.00048	-
Re_{δ_2}	1991	3061	3844	4695	5517	-

Table E-1.2 Friction Factor Data (-0.275, -0.001)

	x = 22	x = 34	x = 46	x = 58	x = 70	x = 82
$\kappa\left(\frac{u_\infty y}{\nu_\infty}\right)$	-0.00075	-0.00050	-0.00037	-0.00030	-0.00027	-0.00024
$\nu\frac{\partial u}{\partial y}$	0.0788	0.0653	0.0647	0.0587	0.0662	0.0611
$-\overline{u'v'}$	0.833	0.457	0.3190	0.2450	0.236	0.208
$\frac{1}{u_\infty^2}\left(\nu\frac{\partial u}{\partial y}-\overline{u'v'}\right)$	0.00184	0.00136	0.00120	0.00103	0.00105	0.00105
$-\frac{1}{\rho_\infty u_\infty^2}\frac{\partial}{\partial x}\int_o^y \rho u^2 dy$	0.00001	0.	0.	0.	0.	0.
$-\frac{uv_o}{u_\infty^2}$	0.00048	0.00041	0.00038	0.00039	0.00039	0.00035
$\frac{1}{\rho_\infty u_\infty^2}u\frac{\partial}{\partial x}\int_o^y \rho u dy$	-0.00010	-0.00010	-0.00008	-0.00005	0.	-0.00004
$c_f/2$	0.00146	0.00118	0.00114	0.00108	0.00116	0.00121
$c_f/2$ (Andersen)	0.00123	0.00097	0.00093	0.00103	0.00114	0.00097
Re_{δ_2}	1658	2392	2939	3351	3846	4494

Table E-1.3 Friction Factor Data (-0.275, -0.002)

	x = 22	x = 34	x = 46	x = 58	x = 70	x = 82
$\kappa\left(\frac{u_\infty y}{\nu_\infty}\right)$	-0.00075	-0.00050	-0.00037	-0.00030	-0.00026	-0.00021
$\nu \frac{\partial u}{\partial y}$	0.0793	0.0707	0.0648	0.0717	0.0754	0.0724
$-\overline{u'v'}$	0.878	0.482	0.347	0.299	0.261	0.217
$\frac{1}{u_\infty^2}\left(\nu \frac{\partial u}{\partial y} - \overline{u'v'}\right)$	0.00199	0.00148	0.00130	0.00126	0.00121	0.00114
$-\frac{1}{\rho_\infty u_\infty^2} \frac{\partial}{\partial x} \int_o^y \rho u^2 dy$	0.00001	0.00001	0.	0.	0.	0.
$-\frac{u v_o}{u_\infty^2}$	0.00110	0.00100	0.00096	0.00099	0.00098	0.00094
$\frac{1}{\rho_\infty u_\infty^2} u \frac{v_o}{u_\infty} \int_o^y \rho u dy$	-0.00014	-0.00014	-0.00012	-0.00008	-0.00003	-0.00003
$c_f/2$	0.00221	0.00185	0.00178	0.00187	0.00191	0.00190
$c_f/2$ (Andersen)	0.00170	0.00147	0.00146	0.00166	0.00176	0.00158
Re_{δ_2}	1312	1868	2283	2430	2678	3144

Table E-1.4 Friction Factor Data (-0.275, -0.0004)

	x = 22	x = 34	x = 46	x = 58	x = 70	x = 82
$\kappa\left(\frac{u_\infty y}{\nu_\infty}\right)$	-0.00076	-0.00050	-0.00038	-0.00031	-0.00027	-0.00023
$\nu \frac{\partial u}{\partial y}$	0.0649	0.0635	0.0611	0.0605	0.0502	0.0618
$-\overline{u'v'}$	0.568	0.376	0.253	0.203	0.201	0.162
$\frac{1}{u_\infty^2}\left(\nu \frac{\partial u}{\partial y} - \overline{u'v'}\right)$	0.00136	0.00121	0.00103	0.00092	0.00094	0.00093
$-\frac{1}{\rho_\infty u_\infty^2} \frac{\partial}{\partial x} \int_o^y \rho u^2 dy$	0.00043	0.00043	0.00036	0.00023	0.00007	0.00011
$-\frac{u v_o}{u_\infty^2}$	0.00287	0.00278	0.00273	0.00278	0.00281	0.00263
$\frac{1}{\rho_\infty u_\infty^2} u \frac{\partial}{\partial x} \int_o^y \rho u dy$	-0.00019	-0.00020	-0.00018	-0.00013	-0.00007	0.
$c_f/2$	0.00370	0.00371	0.00357	0.00349	0.00350	0.00323
$c_f/2$ (Andersen	0.00269	0.00256	0.00265	0.00265	0.00296	0.00290
Re_{δ_2}	834	1072	1124	1211	1255	1364

E-2 Experimental Stanton Number at a Constant Wall Temperature Condition

The runs are tabulated below and, with the help of the special nomenclature, should be self-explanatory.

Date	m	F
012973	-0.275	0
021273	-0.275	-0.001
030473	-0.275	-0.002
031273	-0.275	-0.004

Special Nomenclature

Symbol	Explanation	Unit
TAMB	Ambient temperature	°F
TBASE	Casting base temperature	°F
TGAS	Free stream static temperature	°F
TCOV	Wind tunnel cover (top) temperature	°F
PBAR	Barometric pressure	in Hg
RHUM	Relative humidity	-
PL	Plate number	-
X	Stream-wise coordinate	in
UINF	Free stream velocity, U_∞	ft/sec
TO	Plate temperature	°F
F	$\dot{m}''/\rho_\infty U_\infty$ (negative for suction)	-
ST	Stanton number	-
RED2	Enthalpy thickness Reynolds number	-
STO	Stanton number for F = 0 (same RED2)	-
BH	F/St	-

STANTON NUMBER - CONSTANT WALL TEMPERATURE

DATE = 012973 (-0.275,0.)

TAMB = 71.9 TBASE = 76.1 TGAS = 59.0
TCOV = 70.0 PBAR = 30.32 RHUM = 0.80

PL	X	UINF	TO	F	ST	RED2	ST/STO	BH
3	10.	25.7	91.5	0.00000	0.00315	650.	1.082	0.000
4	14.	24.1	91.3	0.00000	0.00293	814.	1.065	0.000
5	18.	22.6	91.4	0.00000	0.00278	954.	1.051	0.000
6	22.	21.3	91.4	0.00000	0.00269	1081.	1.049	0.000
7	26.	20.3	91.5	0.00000	0.00253	1195.	1.012	0.000
8	30.	19.4	91.3	0.00000	0.00241	1306.	0.986	0.000
9	34.	18.8	91.4	0.00000	0.00235	1397.	0.977	0.000
10	38.	18.3	91.3	0.00000	0.00229	1494.	0.969	0.000
11	42.	17.9	91.5	0.00000	0.00218	1573.	0.934	0.000
12	46.	17.5	91.2	0.00000	0.00227	1670.	0.987	0.000
13	50.	17.2	91.3	0.00000	0.00226	1749.	0.994	0.000
14	54.	16.9	91.4	0.00000	0.00217	1823.	0.965	0.000
15	58.	16.7	91.2	0.00000	0.00223	1915.	1.004	0.000
16	62.	16.5	91.4	0.00000	0.00217	1984.	0.985	0.000
17	66.	16.3	91.3	0.00000	0.00221	2063.	1.013	0.000
18	70.	16.0	91.3	0.00000	0.00217	2138.	1.004	0.000
19	74.	15.7	91.3	0.00000	0.00214	2215.	0.999	0.000
20	78.	15.4	91.2	0.00000	0.00215	2287.	1.011	0.000
21	82.	15.1	91.3	0.00000	0.00203	2353.	0.962	0.000
22	86.	14.9	91.3	0.00000	0.00210	2415.	1.001	0.000
23	90.	14.7	91.4	0.00000	0.00204	2477.	0.979	0.000

STANTON NUMBER - CONSTANT WALL TEMPERATURE

DATE = 021273 (-0.275,-0.001)

TAMB = 72.7 TBASE = 77.9 TGAS = 63.7
TCOV = 70.8 PBAR = 30.20 RHUM = 0.68

PL	X	UINF	TO	F	ST	RED2	ST/STO	BH
3	10.	26.0	88.7	-0.00099	0.00358	559.	1.184	-0.277
4	14.	24.4	88.7	-0.00098	0.00345	695.	1.205	-0.284
5	18.	22.9	88.8	-0.00099	0.00331	811.	1.202	-0.299
6	22.	21.6	88.7	-0.00100	0.00325	922.	1.218	-0.308
7	26.	20.6	88.7	-0.00101	0.00310	1018.	1.191	-0.326
8	30.	19.7	88.7	-0.00102	0.00305	1107.	1.197	-0.334
9	34.	19.0	88.8	-0.00103	0.00296	1183.	1.181	-0.348
10	38.	18.4	88.8	-0.00103	0.00291	1258.	1.179	-0.354
11	42.	18.0	88.9	-0.00103	0.00276	1324.	1.133	-0.373
12	46.	17.6	88.7	-0.00103	0.00286	1398.	1.190	-0.360
13	50.	17.3	88.8	-0.00102	0.00283	1462.	1.190	-0.360
14	54.	17.1	88.8	-0.00100	0.00274	1527.	1.165	-0.365
15	58.	16.9	88.8	-0.00102	0.00280	1590.	1.203	-0.364
16	62.	16.6	88.7	-0.00100	0.00268	1654.	1.163	-0.373
17	66.	16.5	88.8	-0.00100	0.00273	1709.	1.194	-0.366
18	70.	16.3	89.0	-0.00099	0.00269	1757.	1.185	-0.368
19	74.	16.1	88.8	-0.00099	0.00267	1830.	1.188	-0.371
20	78.	15.8	88.7	-0.00100	0.00264	1887.	1.184	-0.379
21	82.	15.4	88.8	-0.00100	0.00258	1935.	1.164	-0.388
22	86.	15.1	88.7	-0.00103	0.00266	1993.	1.209	-0.387
23	90.	14.7	88.8	-0.00103	0.00274	2041.	1.253	-0.376

STANTON NUMBER - CONSTANT WALL TEMPERATURE

DATE = 030473 (-0.275,-0.002)

TAMB = 67.8 TBASE = 79.5 TGAS = 64.2
TCOV = 70.4 PBAR = 30.30 RHUM = 0.63

PL	X	UINF	TO	F	ST	RED2	ST/STO	BH
3	10.	26.0	88.5	-0.00199	0.00398	409.	1.218	-0.500
4	14.	24.4	88.4	-0.00196	0.00386	511.	1.248	-0.508
5	18.	22.9	88.6	-0.00198	0.00378	598.	1.272	-0.524
6	22.	21.6	88.6	-0.00199	0.00374	681.	1.300	-0.532
7	26.	20.6	88.5	-0.00201	0.00361	756.	1.288	-0.557
8	30.	19.7	88.6	-0.00204	0.00359	820.	1.307	-0.568
9	34.	19.0	88.5	-0.00204	0.00347	881.	1.286	-0.588
10	38.	18.4	88.7	-0.00205	0.00351	932.	1.319	-0.584
11	42.	17.9	88.6	-0.00206	0.00334	987.	1.274	-0.617
12	46.	17.5	88.5	-0.00205	0.00340	1040.	1.313	-0.603
13	50.	17.3	88.5	-0.00206	0.00342	1088.	1.336	-0.602
14	54.	17.0	88.5	-0.00202	0.00332	1136.	1.311	-0.608
15	58.	16.8	88.5	-0.00201	0.00335	1184.	1.337	-0.600
16	62.	16.6	88.5	-0.00200	0.00324	1227.	1.304	-0.617
17	66.	16.5	88.5	-0.00199	0.00329	1273.	1.337	-0.605
18	70.	16.3	88.4	-0.00199	0.00323	1320.	1.324	-0.616
19	74.	16.1	88.6	-0.00199	0.00318	1352.	1.312	-0.626
20	78.	15.8	88.6	-0.00202	0.00326	1393.	1.355	-0.620
21	82.	15.5	88.6	-0.00202	0.00319	1432.	1.335	-0.633
22	86.	15.1	88.5	-0.00204	0.00322	1475.	1.357	-0.634
23	90.	14.8	88.6	-0.00203	0.00321	1507.	1.361	-0.632

STANTON NUMBER - CONSTANT WALL TEMPERATURE

DATE = 031273 (-0.275,-0.004)

TAMB = 70.7 TBASE = 81.1 TGAS = 63.4
TCOV = 71.2 PBAR = 30.25 RHUM = 0.58

PL	X	UINF	TO	F	ST	RED2	ST/STO	BH
3	10.	25.9	87.0	-0.00411	0.00520	341.	1.520	-0.790
4	14.	24.3	86.9	-0.00405	0.00507	398.	1.540	-0.799
5	18.	22.9	87.0	-0.00402	0.00493	446.	1.541	-0.815
6	22.	21.7	86.8	-0.00413	0.00503	492.	1.612	-0.821
7	26.	20.7	86.8	-0.00423	0.00491	527.	1.620	-0.862
8	30.	19.8	86.7	-0.00434	0.00501	558.	1.656	-0.866
9	34.	19.1	86.9	-0.00423	0.00484	580.	1.616	-0.874
10	38.	18.4	86.9	-0.00431	0.00485	604.	1.636	-0.889
11	42.	18.0	86.9	-0.00423	0.00467	622.	1.587	-0.906
12	46.	17.6	86.8	-0.00417	0.00471	644.	1.614	-0.885
13	50.	17.3	86.9	-0.00423	0.00480	662.	1.656	-0.881
14	54.	17.1	86.8	-0.00414	0.00466	683.	1.621	-0.888
15	58.	16.9	86.8	-0.00416	0.00471	703.	1.650	-0.883
16	62.	16.7	86.8	-0.00413	0.00457	721.	1.611	-0.904
17	66.	18.6	86.9	-0.00408	0.00454	734.	1.608	-0.899
18	70.	16.4	86.7	-0.00410	0.00454	756.	1.619	-0.903
19	74.	16.1	86.9	-0.00399	0.00440	763.	1.573	-0.907
20	78.	15.9	86.8	-0.00422	0.00457	773.	1.642	-0.923
21	82.	15.5	86.9	-0.00405	0.00447	789.	1.612	-0.906
22	86.	15.2	86.8	-0.00406	0.00447	804.	1.619	-0.908
23	90.	14.8	86.8	-0.00420	0.00452	818.	1.644	-0.929

E-3 Experimental Stanton Numbers: Step in Wall Temperature Condition

The runs are tabulated below and, with the help of the special nomenclature and the one from E-2, the data tabulation should be self-explanatory. It should be noted that the step is present at plate 10. Before and after that plate the wall temperature is constant.

Date	m	F
122272	0	0
122872	-0.15	0
010273	-0.15	0.001
010473	-0.15	0.004
012973	-0.275	0
021973	-0.275	-0.001
030173	-0.275	-0.002
031273	-0.275	-0.004

Special Nomenclature

Symbol	Explanation	Unit
ST	Stanton number at a plate for a step condition	-
STT	Stanton number at a plate for a constant wall temperature condition (same hydrodynamics)	-
STC	Predicted Stanton number at a plate for a step condition	-

STANTON NUMBER - STEP IN WALL TEMPERATURE

DATE = 122272 (0.,0.)

TAMB = 75.4   TBASE = 76.3   TGAS = 65.0
TCOV = 71.1   PBAR = 30.52   RHUM = 0.67

PL	X	UINF	TO	STT	ST	STC
3	29.	31.1	65.6	0.00304		
4	33.	31.1	65.6	0.00282		
5	37.	31.0	65.6	0.00269		
6	41.	31.0	65.7	0.00261		
7	45.	31.1	65.8	0.00249		
8	49.	31.1	65.9	0.00241		
9	53.	31.1	67.0	0.00230		
10	57.	31.1	86.2	0.00232	0.00407	0.00341
11	61.	31.0	86.8	0.00225	0.00287	0.00295
12	65.	31.1	87.1	0.00225	0.00280	0.00280
13	69.	31.1	86.7	0.00218	0.00263	0.00263
14	73.	31.1	86.8	0.00210	0.00250	0.00248
15	77.	31.1	86.8	0.00215	0.00248	0.00249
16	81.	31.0	86.8	0.00205	0.00235	0.00235
17	85.	31.0	86.8	0.00208	0.00234	0.00236
18	89.	31.0	86.8	0.00202	0.00226	0.00227
19	93.	31.1	86.7	0.00201	0.00222	0.00224
20	97.	31.0	86.7	0.00200	0.00223	0.00222
21	101.	31.0	86.5	0.00193	0.00212	0.00212
22	105.	31.0	86.6	0.00194	0.00214	0.00213
23	109.	31.0	86.6	0.00193	0.00211	0.00210

STANTON NUMBER - STEP IN WALL TEMPERATURE

DATE = 122872 (-0.15,0)

TAMB = 70.6   TBASE = 73.5   TGAS = 64.5
TCOV = 69.3   PBAR = 30.37   RHUM = 0.50

PL	X	UINF	TO	STT	ST	STC
3	15.	26.4	65.0	0.00312		
4	19.	25.5	65.1	0.00289		
5	23.	24.6	65.1	0.00277		
6	27.	24.1	65.2	0.00269		
7	31.	23.6	65.4	0.00255		
8	35.	23.1	65.5	0.00250		
9	39.	22.8	67.3	0.00242		
10	43.	22.4	90.1	0.00239	0.00425	0.00340
11	47.	22.0	90.4	0.00235	0.00290	0.00299
12	51.	21.8	90.4	0.00238	0.00292	0.00288
13	55.	21.5	90.4	0.00232	0.00278	0.00273
14	59.	21.2	90.5	0.00221	0.00262	0.00255
15	63.	21.0	90.7	0.00225	0.00263	0.00255
16	67.	20.8	90.6	0.00217	0.00251	0.00243
17	71.	20.6	90.6	0.00222	0.00248	0.00247
18	75.	20.4	90.5	0.00216	0.00239	0.00238
19	79.	20.3	90.5	0.00213	0.00238	0.00233
20	83.	20.1	90.5	0.00214	0.00232	0.00233
21	87.	20.0	90.5	0.00203	0.00224	0.00220
22	91.	19.8	90.5	0.00209	0.00228	0.00225
23	95.	19.7	90.4	0.00208	0.00226	0.00223

STANTON NUMBER - STEP IN WALL TEMPERATURE

DATE = 010273 (-0.15,0.001)

TAMB = 67.6   TBASE = 71.8   TGAS = 65.0
TCOV = 68.5   PBAR = 30.43   RHUM = 0.57

PL	X	UINF	TO	STT	ST	STC
3	15.	26.4	66.4	0.00270		
4	19.	25.4	66.5	0.00246		
5	23.	24.6	66.5	0.00232		
6	27.	24.0	66.6	0.00226		
7	31.	23.6	66.9	0.00217		
8	35.	23.1	67.0	0.00200		
9	39.	22.7	68.6	0.00192		
10	43.	22.3	88.9	0.00200	0.00365	0.00304
11	47.	22.0	89.0	0.00192	0.00253	0.00256
12	51.	21.7	89.0	0.00193	0.00244	0.00243
13	55.	21.4	89.0	0.00187	0.00227	0.00228
14	59.	21.2	89.1	0.00174	0.00212	0.00207
15	63.	21.0	89.1	0.00181	0.00214	0.00211
16	67.	20.7	89.1	0.00175	0.00206	0.00202
17	71.	20.6	89.1	0.00176	0.00202	0.00200
18	75.	20.4	89.0	0.00170	0.00194	0.00192
19	79.	20.3	89.1	0.00168	0.00192	0.00188
20	83.	20.1	89.1	0.00175	0.00197	0.00194
21	87.	20.0	89.2	0.00162	0.00182	0.00179
22	91.	19.9	89.1	0.00160	0.00181	0.00176
23	95.	19.7	89.0	0.00159	0.00176	0.00174

STANTON NUMBER - STEP IN WALL TEMPERATURE

DATE = 010473 (-0.15,0.004)

TAMB = 68.2   TBASE = 69.8   TGAS = 63.9
TCOV = 67.1   PBAR = 30.51   RHUM = 0.62

PL	X	UINF	TO	STT	ST	STC
3	15.	26.4	67.2	0.00168		
4	19.	25.4	67.3	0.00130		
5	23.	24.6	67.5	0.00113		
6	27.	24.0	67.6	0.00114		
7	31.	23.5	67.9	0.00107		
8	35.	23.1	68.0	0.00090		
9	39.	22.7	69.3	0.00087		
10	43.	22.3	86.9	0.00089	0.00194	0.00172
11	47.	22.0	87.3	0.00061	0.00100	0.00097
12	51.	21.8	87.1	0.00076	0.00103	0.00110
13	55.	21.5	87.0	0.00070	0.00097	0.00097
14	59.	21.3	87.1	0.00070	0.00090	0.00094
15	63.	21.1	87.0	0.00072	0.00094	0.00093
16	67.	20.9	87.0	0.00072	0.00088	0.00092
17	71.	20.7	87.1	0.00068	0.00082	0.00085
18	75.	20.6	87.0	0.00058	0.00076	0.00071
19	79.	20.4	87.1	0.00051	0.00065	0.00062
20	83.	20.3	87.1	0.00068	0.00081	0.00081
21	87.	20.1	87.2	0.00060	0.00072	0.00072
22	91.	20.0	87.1	0.00060	0.00072	0.00071
23	95.	19.9	87.0	0.00051	0.00063	0.00060

STANTON NUMBER - STEP IN WALL TEMPERATURE

DATE = 012973 (-0.275,0.)

TAMB = 72.3 TBASE = 76.1 TGAS = 66.8
TCOV = 72.5 PBAR = 30.32 RHUM = 0.69

PL	X	UINF	TO	STT	ST	STC
3	13.	25.9	67.4	0.00315		
4	17.	24.2	67.4	0.00293		
5	21.	22.7	67.5	0.00278		
6	25.	21.4	67.6	0.00269		
7	29.	20.4	67.9	0.00253		
8	33.	19.6	68.2	0.00241		
9	37.	18.9	70.8	0.00235		
10	41.	18.4	95.0	0.00229	0.00400	0.00324
11	45.	18.0	95.4	0.00218	0.00276	0.00270
12	49.	17.6	95.4	0.00227	0.00285	0.00274
13	53.	17.3	95.3	0.00226	0.00269	0.00265
14	57.	17.1	95.5	0.00217	0.00254	0.00249
15	61.	16.8	95.3	0.00223	0.00256	0.00252
16	65.	16.6	95.4	0.00217	0.00243	0.00242
17	69.	16.4	95.4	0.00221	0.00248	0.00245
18	73.	16.1	95.2	0.00217	0.00238	0.00238
19	77.	15.8	95.1	0.00214	0.00235	0.00233
20	81.	15.5	95.3	0.00215	0.00234	0.00233
21	85.	15.3	95.5	0.00203	0.00219	0.00219
22	89.	15.0	95.5	0.00210	0.00230	0.00226
23	93.	14.8	95.3	0.00204	0.00219	0.00218

STANTON NUMBER - STEP IN WALL TEMPERATURE

DATE = 021973 (-0.275,-0.001)

TAMB = 74.4 TBASE = 76.6 TGAS = 64.5
TCOV = 72.5 PBAR = 30.46 RHUM = 0.61

PL	X	UINF	TO	STT	ST	STC
3	13.	25.9	64.9	0.00361		
4	17.	24.3	65.0	0.00346		
5	21.	22.8	64.0	0.00334		
6	25.	21.5	64.1	0.00327		
7	29.	20.5	64.3	0.00311		
8	33.	19.6	64.5	0.00306		
9	37.	18.9	67.3	0.00298		
10	41.	18.3	87.7	0.00293	0.00483	0.00385
11	45.	17.9	88.2	0.00278	0.00340	0.00330
12	49.	17.5	88.1	0.00287	0.00338	0.00331
13	53.	17.3	88.0	0.00285	0.00322	0.00318
14	57.	17.0	88.1	0.00274	0.00311	0.00305
15	61.	16.8	88.1	0.00280	0.00314	0.00309
16	65.	16.6	88.0	0.00268	0.00297	0.00292
17	69.	16.4	88.1	0.00279	0.00298	0.00291
18	73.	16.2	88.1	0.00272	0.00291	0.00287
19	77.	16.0	88.0	0.00267	0.00286	0.00285
20	81.	15.7	87.9	0.00268	0.00286	0.00276
21	85.	15.4	87.9	0.00259	0.00276	0.00272
22	89.	15.0	88.0	0.00267	0.00281	0.00280
23	93.	14.7	88.1	0.00264	0.00278	0.00278

STANTON NUMBER - STEP IN WALL TEMPERATURE

DATE = 030173 (-0.275,-0.002)

TAMB = 74.8 TBASE = 76.3 TGAS = 64.7
TCOV = 72.6 PBAR = 30.52 RHUM = 0.57

PL	X	UINF	TO	STT	ST	STC
3	13.	25.9	64.8	0.00396		
4	17.	24.3	64.8	0.00384		
5	21.	22.8	64.9	0.00374		
6	25.	21.6	64.9	0.00372		
7	29.	20.6	65.0	0.00359		
8	33.	19.7	65.2	0.00356		
9	37.	18.9	66.7	0.00348		
10	41.	18.3	87.1	0.00349	0.00570	0.00446
11	45.	17.9	87.5	0.00332	0.00405	0.00390
12	49.	17.5	87.4	0.00338	0.00402	0.00385
13	53.	17.2	87.4	0.00341	0.00391	0.00379
14	57.	17.0	87.6	0.00331	0.00376	0.00363
15	61.	16.8	87.5	0.00336	0.00375	0.00361
16	65.	16.6	87.6	0.00324	0.00363	0.00347
17	69.	16.4	87.6	0.00327	0.00358	0.00353
18	73.	16.3	87.5	0.00321	0.00350	0.00344
19	77.	16.0	87.6	0.00318	0.00344	0.00336
20	81.	15.7	87.5	0.00325	0.00349	0.00343
21	85.	15.4	87.6	0.00319	0.00341	0.00333
22	89.	15.1	87.5	0.00322	0.00344	0.00336
23	93.	14.7	87.6	0.00322	0.00340	0.00334

STANTON NUMBER - STEP IN WALL TEMPERATURE

DATE = 031273 (-0.275,-0.004)

TAMB = 68.8 TBASE = 75.6 TGAS = 63.3
TCOV = 70.1 PBAR = 30.25 RHUM = 0.62

PL	X	UINF	TO	STT	ST	STC
3	13.	25.9	63.4	0.00521		
4	17.	24.3	63.5	0.00508		
5	21.	22.9	63.5	0.00494		
6	25.	21.7	63.5	0.00504		
7	29.	20.7	63.6	0.00491		
8	33.	19.8	63.6	0.00500		
9	37.	19.1	64.8	0.00485		
10	41.	18.4	85.2	0.00486	0.00732	0.00566
11	45.	18.0	85.5	0.00467	0.00532	0.00513
12	49.	17.6	85.7	0.00471	0.00524	0.00508
13	53.	17.3	85.4	0.00480	0.00513	0.00511
14	57.	17.1	85.5	0.00466	0.00504	0.00491
15	61.	16.9	85.5	0.00471	0.00506	0.00494
16	65.	16.7	85.5	0.00456	0.00481	0.00475
17	69.	16.6	85.5	0.00455	0.00484	0.00473
18	73.	16.4	85.4	0.00454	0.00479	0.00470
19	77.	16.1	85.6	0.00439	0.00453	0.00453
20	81.	15.9	85.6	0.00458	0.00473	0.00472
21	85.	15.5	85.6	0.00446	0.00460	0.00458
22	89.	15.2	85.6	0.00447	0.00465	0.00458
23	93.	14.8	85.6	0.00452	0.00467	0.00462

E-4 Mean Temperature and Velocity Profiles

The runs are tabulated below and, with the help of the special nomenclature, the data tabulation should be self-explanatory.

Date	m	F	Number of profiles (x-wise)
013073	-0.275	0	5
021573	-0.275	-0.001	6
030473	-0.275	-0.002	6
031173	-0.275	-0.004	6

It should be noted that the above dates correspond to the date of the first profile out of a number indicated to the right of the table. The x-wise position of the profile is indicated in the tabulation.

Special Nomenclature

Symbol	Explanation	Unit
RUN	Date and run number	-
PLATE	Plate number	-
X(IN)	X-wise coordinate in inches	in
Z(IN)	Z-wise coordinate (distance from centerline)	in
POINTS	Number of points of the profile (different y)	-
UINF	Free stream velocity, U_∞	ft/sec
TWALL	Wall temperature	°F
DC	Clauser boundary layer thickness (Eq. 2.2) Δ	in
DEL3	Δ_3 (Eq. 2.8)	in
TGAS	Free stream temperature	°F
K	Acceleration parameter	-
BETA	β (Eq. 2.5)	-
BF	Blowing parameter for velocity $(F/(C_f/2))$	-
F	Blowing fraction (v_o/U_∞)	-
BH	Heat transfer blowing parameter (F/St)	-
CF/2	Friction coefficient	-
ST	Stanton number	-
PPLUS	$(\nu/\rho u_\tau^3)d\bar{p}/dx$	-
VOPLUS	v_o/u_τ	-

REY.NO	Reynolds number	-
DELM	Momentum boundary layer thickness, δ	in
DEL1M	Displacement thickness, δ_1	in
DEL2M	Momentum thickness, δ_2	in
REM	Momentum thickness Reynolds number	-
H	Shape factor, δ_1/δ_2	-
DELH	Temperature boundary layer thickness, δ_T	in
DEL2H	Enthalpy thickness, Δ_T	in
REH	Enthalpy thickness Reynolds number	-
GH	Heat transfer shape factor, (Eq. 2.8 Δ_4/Δ_3)	-
GF	Clauser shape factor (Eq. 2.4)	-
I	Profile point number	-
Y	Normal to the wall coordinate	in
YPLUS	yu_τ/ν	-
U	Local velocity	ft/sec
UPLUS	$\overline{u}/u_\tau$	-
UDE	Defect velocity $(\overline{u}-U_\infty)/u_\tau$	-
UBAR	$\overline{u}/U_\infty$	-
T	Local temperature	F
TPLUS	$(T_w-T)/T_\tau$	-
TBAR	$(T_w-T)/(T_w-T_\infty)$	-
TDE	Defect temperature $(T^+ - T^+_\infty)$	-

ADVERSE PRESSURE GRADIENT (-0.275,0.)

RUN =	13073-1	UINF	= 21.5	K	=-0.970E-06	CF/2	= 0.00096	DELM	= 1.070	DELH	= 1.068
PLATE =	6	TWALL	= 96.0	BETA =	3.755	ST	= 0.00269	DEL1M =	0.331	DEL2H =	0.0825
X(IN) =	22.	DC	= 10.697	BF =	0.000	PPLUS =	0.03274	DEL2M =	0.178	REH =	923.
Z(IN) =	0.	DEL3	= 1.888	F =	0.00000	VDPLUS=	0.00000	REM =	1991.	GH =	3.315
POINTS=	43	TGAS	= 65.5	BH =	0.000	REY.NO=0.302E 06		H =	1.862	GF =	14.950

I	Y	YPLUS	Y/DELM	Y/DC	U	UPLUS	UDE	UBAR	Y/DELH	Y/DEL3	T	TPLUS	TDE	TBAR
1	0.000	0.0	0.0000	0.00000	0.00	0.00	-32.32	0.000	0.0000	0.0000	96.00	0.00	-11.50	0.000
2	0.005	1.6	0.0047	0.00047	1.62	2.44	-29.88	0.075	0.0047	0.0026	90.85	2.01	-9.49	0.175
3	0.006	1.9	0.0056	0.00056	1.72	2.59	-29.73	0.080	0.0056	0.0032	90.42	2.18	-9.32	0.189
4	0.007	2.2	0.0065	0.00065	1.84	2.77	-29.55	0.086	0.0066	0.0037	90.06	2.32	-9.18	0.202
5	0.008	2.5	0.0075	0.00075	2.00	3.01	-29.31	0.093	0.0075	0.0042	89.46	2.55	-8.95	0.222
6	0.009	2.8	0.0084	0.00084	2.25	3.38	-28.94	0.105	0.0084	0.0048	89.01	2.73	-8.77	0.237
7	0.010	3.1	0.0093	0.00093	2.32	3.49	-28.83	0.108	0.0094	0.0053	88.39	2.97	-8.53	0.258
8	0.011	3.5	0.0103	0.00103	2.51	3.77	-28.55	0.117	0.0103	0.0058	87.99	3.13	-8.37	0.272
9	0.013	4.1	0.0122	0.00122	2.82	4.24	-28.08	0.131	0.0122	0.0069	86.98	3.52	-7.98	0.306
10	0.015	4.7	0.0140	0.00140	3.28	4.93	-27.39	0.153	0.0140	0.0079	86.13	3.85	-7.65	0.335
11	0.017	5.4	0.0159	0.00159	3.68	5.53	-26.79	0.171	0.0159	0.0090	85.45	4.12	-7.38	0.358
12	0.019	6.0	0.0178	0.00178	3.97	5.97	-26.35	0.185	0.0178	0.0101	84.43	4.52	-6.98	0.393
13	0.021	6.6	0.0196	0.00196	4.31	6.48	-25.84	0.200	0.0197	0.0111	83.92	4.72	-6.78	0.410
14	0.023	7.2	0.0215	0.00215	4.72	7.10	-25.22	0.220	0.0215	0.0122	83.19	5.00	-6.50	0.435
15	0.025	7.9	0.0234	0.00234	4.87	7.32	-25.00	0.227	0.0234	0.0132	82.86	5.13	-6.37	0.446
16	0.028	8.8	0.0262	0.00262	5.40	8.12	-24.20	0.251	0.0262	0.0148	82.03	5.45	-6.04	0.474
17	0.031	9.8	0.0290	0.00290	5.87	8.82	-23.49	0.273	0.0290	0.0164	81.78	5.55	-5.94	0.483
18	0.034	10.7	0.0318	0.00318	6.17	9.27	-23.04	0.287	0.0318	0.0180	81.05	5.84	-5.66	0.507
19	0.037	11.6	0.0346	0.00346	6.33	9.52	-22.80	0.294	0.0346	0.0196	80.56	6.03	-5.47	0.524
20	0.041	12.9	0.0383	0.00383	6.80	10.22	-22.10	0.316	0.0384	0.0217	80.12	6.20	-5.30	0.539
21	0.045	14.2	0.0421	0.00421	7.07	10.63	-21.69	0.329	0.0421	0.0238	79.51	6.44	-5.06	0.560
22	0.050	15.7	0.0467	0.00467	7.32	11.00	-21.32	0.340	0.0468	0.0265	79.20	6.56	-4.94	0.570
23	0.055	17.3	0.0514	0.00514	7.54	11.33	-20.98	0.351	0.0515	0.0291	78.70	6.75	-4.74	0.587
24	0.065	20.5	0.0608	0.00608	7.95	11.95	-20.37	0.370	0.0609	0.0344	77.91	7.06	-4.43	0.614
25	0.075	23.6	0.0701	0.00701	8.35	12.55	-19.77	0.388	0.0702	0.0397	77.31	7.29	-4.20	0.634
26	0.090	28.3	0.0841	0.00841	8.72	13.11	-19.21	0.406	0.0843	0.0477	76.61	7.57	-3.93	0.658
27	0.105	33.1	0.0981	0.00982	9.15	13.75	-18.56	0.426	0.0983	0.0556	76.12	7.76	-3.74	0.675
28	0.125	39.3	0.1168	0.01169	9.56	14.37	-17.95	0.445	0.1170	0.0662	75.56	7.98	-3.52	0.694
29	0.150	47.2	0.1402	0.01402	9.80	14.73	-17.59	0.456	0.1405	0.0795	74.89	8.24	-3.26	0.716
30	0.175	55.1	0.1636	0.01636	10.27	15.44	-16.88	0.478	0.1639	0.0927	74.30	8.47	-3.02	0.736
31	0.225	70.8	0.2103	0.02103	11.07	16.64	-15.68	0.515	0.2107	0.1192	73.62	8.74	-2.76	0.760
32	0.275	86.6	0.2570	0.02571	11.74	17.65	-14.67	0.546	0.2575	0.1457	72.67	9.11	-2.39	0.792
33	0.325	102.3	0.3038	0.03038	11.90	17.89	-14.43	0.553	0.3043	0.1721	72.24	9.28	-2.22	0.806
34	0.400	125.9	0.3739	0.03739	13.47	20.25	-12.07	0.627	0.3745	0.2119	71.40	9.60	-1.89	0.835
35	0.475	149.5	0.4440	0.04440	14.71	22.11	-10.21	0.684	0.4448	0.2516	70.62	9.91	-1.59	0.861
36	0.575	181.0	0.5374	0.05375	15.82	23.78	-8.54	0.736	0.5384	0.3046	69.49	10.35	-1.15	0.900
37	0.675	212.5	0.6309	0.06310	17.33	26.05	-6.27	0.806	0.6320	0.3575	68.92	10.57	-0.93	0.919
38	0.775	243.9	0.7244	0.07245	18.53	27.85	-4.46	0.862	0.7257	0.4105	68.10	10.89	-0.61	0.947
39	0.925	291.2	0.8646	0.08647	20.29	30.50	-1.82	0.944	0.8661	0.4899	67.32	11.20	-0.30	0.973
40	1.075	338.4	1.0048	0.10049	21.32	32.05	-0.27	0.992	1.0066	0.5694	66.81	11.40	-0.11	0.991
41	1.225	385.6	1.1450	0.11451	21.53	32.36	0.05	1.001	1.1470	0.6488	66.49	11.52	0.02	1.002
42	1.425	448.5	1.3319	0.13321	21.50	32.32	0.00	1.000	1.3343	0.7548	66.42	11.55	0.05	1.004
43	1.625	511.5	1.5188	0.15191	21.50	32.32	0.00	1.000	1.5216	0.8607	66.54	11.50	-0.00	1.000

ADVERSE PRESSURE GRADIENT (-0.275,0.)

RUN	= 13073-2	UINF	= 19.0	K	=-0.729E-06	CF/2	= 0.00069	DELM	= 1.978	DELH	= 1.793
PLATE	= 9	TWALL	= 96.3	BETA	= 6.581	ST	= 0.00235	DEL1M	= 0.626	DEL2H	= 0.1332
X(IN)	= 34.	DC	= 23.894	BF	= 0.000	PPLUS	= 0.04044	DEL2M	= 0.309	REH	= 1319.
Z(IN)	= 0.	DEL3	= 3.162	F	= 0.00000	VOPLUS	= 0.00000	REM	= 3061.	GH	= 3.027
POINTS	= 40	TGAS	= 66.8	BH	= 0.000	REY.NO	= 0.386E 06	H	= 2.027	GF	= 19.326

I	Y	YPLUS	Y/DELM	Y/DC	U	UPLUS	UDE	UBAR	Y/DELH	Y/DEL3	T	TPLUS	TDE	TBAR
1	0.000	0.0	0.0000	0.00000	0.00	0.00	-38.14	0.000	0.0000	0.0000	96.31	0.00	-11.16	0.000
2	0.005	1.2	0.0025	0.00021	0.97	1.94	-36.20	0.051	0.0028	0.0016	91.45	1.83	-9.32	0.164
3	0.006	1.4	0.0030	0.00025	1.08	2.16	-35.98	0.057	0.0033	0.0019	91.06	1.98	-9.17	0.178
4	0.007	1.7	0.0035	0.00029	1.13	2.26	-35.87	0.059	0.0039	0.0022	90.84	2.06	-9.09	0.185
5	0.008	1.9	0.0040	0.00033	1.25	2.51	-35.63	0.066	0.0045	0.0025	90.33	2.26	-8.90	0.202
6	0.009	2.1	0.0046	0.00038	1.39	2.79	-35.35	0.073	0.0050	0.0028	89.89	2.42	-8.73	0.217
7	0.010	2.4	0.0051	0.00042	1.42	2.85	-35.29	0.075	0.0056	0.0032	89.50	2.57	-8.58	0.230
8	0.012	2.8	0.0061	0.00050	1.62	3.25	-34.89	0.085	0.0067	0.0038	88.63	2.90	-8.26	0.260
9	0.014	3.3	0.0071	0.00059	1.79	3.59	-34.55	0.094	0.0078	0.0044	88.01	3.13	-8.02	0.281
10	0.016	3.8	0.0081	0.00067	1.97	3.95	-34.19	0.104	0.0089	0.0051	87.27	3.41	-7.74	0.306
11	0.019	4.5	0.0096	0.00080	2.28	4.57	-33.57	0.120	0.0106	0.0060	86.39	3.75	-7.41	0.336
12	0.022	5.2	0.0111	0.00092	2.62	5.25	-32.89	0.138	0.0123	0.0070	85.39	4.12	-7.03	0.370
13	0.025	5.9	0.0126	0.00105	2.78	5.57	-32.57	0.146	0.0139	0.0079	84.77	4.36	-6.80	0.391
14	0.029	6.8	0.0147	0.00121	3.16	6.33	-31.81	0.166	0.0162	0.0092	83.76	4.74	-6.41	0.425
15	0.034	8.0	0.0172	0.00142	3.62	7.26	-30.88	0.190	0.0190	0.0108	83.13	4.98	-6.18	0.446
16	0.039	9.2	0.0197	0.00163	4.06	8.14	-30.00	0.213	0.0218	0.0123	82.02	5.40	-5.76	0.484
17	0.044	10.4	0.0222	0.00184	4.27	8.56	-29.58	0.224	0.0245	0.0139	81.56	5.57	-5.58	0.499
18	0.049	11.6	0.0248	0.00205	4.44	8.90	-29.24	0.233	0.0273	0.0155	81.07	5.75	-5.40	0.516
19	0.059	13.9	0.0298	0.00247	4.78	9.58	-28.56	0.251	0.0329	0.0187	79.98	6.17	-4.99	0.553
20	0.069	16.3	0.0349	0.00289	5.41	10.84	-27.30	0.284	0.0385	0.0218	79.54	6.33	-4.82	0.568
21	0.079	18.6	0.0399	0.00331	5.45	10.92	-27.22	0.286	0.0441	0.0250	78.80	6.61	-4.54	0.593
22	0.094	22.2	0.0475	0.00393	5.79	11.60	-26.54	0.304	0.0524	0.0297	78.33	6.79	-4.36	0.609
23	0.109	25.7	0.0551	0.00456	6.10	12.23	-25.91	0.321	0.0608	0.0345	77.86	6.97	-4.18	0.624
24	0.134	31.6	0.0678	0.00561	6.26	12.55	-25.59	0.329	0.0747	0.0424	77.14	7.24	-3.91	0.649
25	0.159	37.5	0.0804	0.00665	6.51	13.05	-25.09	0.342	0.0887	0.0503	76.70	7.41	-3.75	0.664
26	0.184	43.4	0.0930	0.00770	6.80	13.63	-24.51	0.357	0.1026	0.0582	76.31	7.55	-3.60	0.677
27	0.234	55.2	0.1183	0.00979	7.21	14.45	-23.69	0.379	0.1305	0.0740	75.45	7.88	-3.27	0.706
28	0.284	67.0	0.1436	0.01189	7.56	15.15	-22.99	0.397	0.1584	0.0898	74.62	8.19	-2.96	0.734
29	0.359	84.7	0.1815	0.01502	8.02	16.07	-22.07	0.421	0.2002	0.1135	74.04	8.41	-2.74	0.754
30	0.459	108.3	0.2321	0.01921	9.00	18.04	-20.10	0.473	0.2560	0.1452	73.29	8.69	-2.46	0.779
31	0.559	131.9	0.2826	0.02340	9.79	19.62	-18.52	0.514	0.3118	0.1768	72.47	9.00	-2.15	0.807
32	0.659	155.5	0.3332	0.02758	10.50	21.04	-17.10	0.552	0.3675	0.2084	71.73	9.28	-1.87	0.832
33	0.809	190.8	0.4091	0.03386	12.01	24.07	-14.07	0.631	0.4512	0.2559	71.04	9.54	-1.61	0.855
34	0.959	226.2	0.4849	0.04014	13.32	26.70	-11.44	0.700	0.5348	0.3033	70.26	9.84	-1.31	0.882
35	1.109	261.6	0.5607	0.04641	14.48	29.02	-9.12	0.761	0.6185	0.3507	69.53	10.11	-1.04	0.906
36	1.309	308.8	0.6619	0.05478	16.14	32.35	-5.79	0.848	0.7300	0.4140	68.54	10.49	-0.67	0.940
37	1.509	356.0	0.7630	0.06315	17.65	35.37	-2.77	0.927	0.8416	0.4772	67.92	10.72	-0.43	0.961
38	1.709	403.2	0.8641	0.07152	18.80	37.68	-0.46	0.988	0.9531	0.5405	67.29	10.96	-0.20	0.982
39	1.909	450.3	0.9652	0.07989	18.74	37.56	-0.58	0.985	1.0647	0.6037	66.73	11.17	0.01	1.001
40	2.109	497.5	1.0664	0.08827	19.03	38.14	0.00	1.000	1.1762	0.6670	66.76	11.16	-0.00	1.000

ADVERSE PRESSURE GRADIENT (-0.275,0.)

RUN = 20573-1	UINF = 17.6	K =-0.594E-06	CF/2 = 0.00065	DELM = 2.411	DELH = 2.401
PLATE = 12	TWALL = 95.9	BETA = 7.171	ST = 0.00227	DEL1M = 0.861	DEL2H = 0.1690
X(IN) = 46.	DC = 33.663	BF = 0.000	PPLUS = 0.03555	DEL2M = 0.419	REH = 1549.
Z(IN) = 0.	DEL3 = 4.097	F = 0.00000	VOPLUS= 0.00000	REM = 3844.	GH = 2.900
POINTS= 43	TGAS = 67.0	BH = 0.000	REY.NO=0.468E 06	H = 2.053	GF = 20.050

I	Y	YPLUS	Y/DELM	Y/DC	U	UPLUS	UDE	UBAR	Y/DELH	Y/DEL3	T	TPLUS	TDE	TBAR
1	0.000	0.0	0.0000	0.00000	0.00	0.00	-39.12	0.000	0.0000	0.0000	95.86	0.00	-11.26	0.000
2	0.005	1.1	0.0021	0.00015	0.83	1.84	-37.28	0.047	0.0021	0.0012	92.31	1.39	-9.87	0.123
3	0.006	1.3	0.0025	0.00018	0.90	2.00	-37.12	0.051	0.0025	0.0015	91.97	1.52	-9.74	0.135
4	0.007	1.5	0.0029	0.00021	0.94	2.08	-37.03	0.053	0.0029	0.0017	91.63	1.65	-9.61	0.147
5	0.008	1.7	0.0033	0.00024	0.92	2.04	-37.08	0.052	0.0033	0.0020	91.12	1.85	-9.41	0.164
6	0.009	1.9	0.0037	0.00027	0.96	2.13	-36.99	0.054	0.0037	0.0022	90.82	1.97	-9.29	0.175
7	0.011	2.3	0.0046	0.00033	1.10	2.44	-36.68	0.062	0.0046	0.0027	89.89	2.33	-8.93	0.207
8	0.013	2.8	0.0054	0.00039	1.19	2.64	-36.48	0.067	0.0054	0.0032	89.46	2.50	-8.76	0.222
9	0.015	3.2	0.0062	0.00045	1.35	2.99	-36.12	0.077	0.0062	0.0037	88.75	2.78	-8.48	0.247
10	0.017	3.6	0.0071	0.00051	1.46	3.24	-35.88	0.083	0.0071	0.0041	88.21	2.99	-8.27	0.265
11	0.020	4.3	0.0083	0.00059	1.74	3.86	-35.26	0.099	0.0083	0.0049	87.12	3.41	-7.85	0.303
12	0.023	4.9	0.0095	0.00068	1.94	4.30	-34.81	0.110	0.0096	0.0056	86.26	3.75	-7.51	0.333
13	0.026	5.5	0.0108	0.00077	2.22	4.92	-34.19	0.126	0.0108	0.0063	85.26	4.14	-7.12	0.358
14	0.029	6.2	0.0120	0.00086	2.42	5.37	-33.75	0.137	0.0121	0.0071	84.55	4.42	-6.84	0.392
15	0.033	7.0	0.0137	0.00098	2.89	6.41	-32.71	0.164	0.0137	0.0081	83.89	4.68	-6.58	0.415
16	0.037	7.9	0.0153	0.00110	2.97	6.59	-32.53	0.168	0.0154	0.0090	83.18	4.95	-6.31	0.440
17	0.042	9.0	0.0174	0.00125	3.22	7.14	-31.98	0.183	0.0175	0.0103	82.30	5.30	-5.96	0.470
18	0.047	10.0	0.0195	0.00140	3.46	7.67	-31.44	0.196	0.0196	0.0115	81.91	5.45	-5.81	0.484
19	0.052	11.1	0.0216	0.00154	3.63	8.05	-31.07	0.206	0.0217	0.0127	81.06	5.78	-5.48	0.513
20	0.057	12.2	0.0236	0.00169	3.92	8.69	-30.42	0.222	0.0237	0.0139	80.44	6.02	-5.23	0.535
21	0.062	13.2	0.0257	0.00184	4.07	9.03	-30.09	0.231	0.0258	0.0151	79.94	6.22	-5.04	0.552
22	0.072	15.4	0.0299	0.00214	4.24	9.40	-29.71	0.240	0.0300	0.0176	79.52	6.38	-4.87	0.567
23	0.082	17.5	0.0340	0.00244	4.62	10.24	-28.87	0.262	0.0341	0.0200	78.66	6.72	-4.54	0.597
24	0.097	20.7	0.0402	0.00288	4.79	10.62	-28.49	0.272	0.0404	0.0237	78.36	6.84	-4.42	0.607
25	0.117	25.0	0.0485	0.00348	5.16	11.44	-27.67	0.293	0.0487	0.0286	77.65	7.11	-4.14	0.632
26	0.142	30.3	0.0589	0.00422	5.41	12.00	-27.12	0.307	0.0591	0.0347	77.01	7.36	-3.89	0.654
27	0.167	35.6	0.0693	0.00496	5.47	12.13	-26.99	0.310	0.0695	0.0408	76.62	7.52	-3.74	0.667
28	0.217	46.3	0.0900	0.00645	5.95	13.19	-25.92	0.337	0.0904	0.0530	75.92	7.79	-3.47	0.692
29	0.267	57.0	0.1107	0.00793	6.20	13.75	-25.37	0.351	0.1112	0.0652	75.34	8.02	-3.24	0.712
30	0.317	67.6	0.1315	0.00942	6.63	14.70	-24.41	0.376	0.1320	0.0774	74.98	8.16	-3.10	0.724
31	0.417	89.0	0.1729	0.01239	7.04	15.61	-23.51	0.399	0.1737	0.1018	74.22	8.45	-2.80	0.751
32	0.517	110.3	0.2144	0.01536	7.72	17.12	-22.00	0.438	0.2153	0.1262	73.60	8.70	-2.56	0.772
33	0.667	142.3	0.2766	0.01981	8.26	18.32	-20.80	0.468	0.2778	0.1628	72.77	9.02	-2.24	0.801
34	0.817	174.3	0.3388	0.02427	9.04	20.05	-19.07	0.512	0.3402	0.1994	72.11	9.28	-1.98	0.824
35	1.017	217.0	0.4218	0.03021	10.40	23.06	-16.05	0.590	0.4235	0.2482	71.25	9.61	-1.65	0.853
36	1.217	259.7	0.5047	0.03615	11.59	25.70	-13.42	0.657	0.5068	0.2970	70.48	9.91	-1.34	0.880
37	1.417	302.4	0.5877	0.04209	12.94	28.69	-10.42	0.734	0.5901	0.3459	69.90	10.14	-1.12	0.900
38	1.667	355.7	0.6914	0.04952	14.35	31.82	-7.30	0.813	0.6942	0.4069	69.00	10.49	-0.77	0.931
39	1.917	409.1	0.7951	0.05695	15.70	34.81	-4.30	0.890	0.7983	0.4679	68.48	10.69	-0.57	0.950
40	2.167	462.4	0.8987	0.06437	16.78	37.21	-1.91	0.951	0.9025	0.5289	67.73	10.99	-0.27	0.976
41	2.417	515.7	1.0024	0.07180	17.48	38.76	-0.35	0.991	1.0066	0.5899	67.29	11.16	-0.10	0.991
42	2.667	569.1	1.1061	0.07923	17.63	39.09	-0.02	0.999	1.1107	0.6509	67.01	11.27	0.01	1.001
43	2.917	622.4	1.2098	0.08665	17.64	39.12	0.00	1.000	1.2148	0.7120	67.03	11.26	-0.00	1.000

ADVERSE PRESSURE GRADIENT (-0.275,0.)

RUN	=	20573-2	UINF	=	17.1	K	=	-0.510E-06	CF/2	=	0.00076	DELM	=	3.109	DELH	=	2.845
PLATE	=	15	TWALL	=	96.8	BETA	=	6.224	ST	=	0.00223	DEL1M	=	1.044	DEL2H	=	0.1860
X(IN)	=	58.	DC	=	37.868	BF	=	0.000	PPLUS	=	0.02431	DEL2M	=	0.528	REH	=	1653.
Z(IN)	=	0.	DEL3	=	4.890	F	=	0.00000	VOPLUS	=	0.00000	REM	=	4695.	GH	=	2.937
POINTS	=	40	TGAS	=	67.2	BH	=	0.000	REY.NO	=	0.560E 06	H	=	1.977	GF	=	17.918

I	Y	YPLUS	Y/DELM	Y/DC	U	UPLUS	UDE	UBAR	Y/DELH	Y/DEL3	T	TPLUS	TDE	TBAR
1	0.000	0.0	0.0000	0.00000	0.00	0.00	-36.26	0.000	0.0000	0.0000	96.82	0.00	-12.37	0.000
2	0.005	1.1	0.0016	0.00013	0.83	1.76	-34.50	0.049	0.0018	0.0010	92.70	1.72	-10.64	0.139
3	0.006	1.3	0.0019	0.00016	0.85	1.80	-34.46	0.050	0.0021	0.0012	92.11	1.97	-10.40	0.159
4	0.007	1.6	0.0023	0.00018	0.91	1.93	-34.33	0.053	0.0025	0.0014	91.98	2.02	-10.34	0.164
5	0.008	1.8	0.0026	0.00021	0.93	1.97	-34.29	0.054	0.0028	0.0016	91.68	2.15	-10.22	0.174
6	0.009	2.0	0.0029	0.00024	1.07	2.27	-33.99	0.063	0.0032	0.0018	91.21	2.34	-10.02	0.190
7	0.010	2.2	0.0032	0.00026	1.06	2.25	-34.01	0.062	0.0035	0.0020	91.08	2.40	-9.97	0.194
8	0.012	2.7	0.0039	0.00032	1.16	2.46	-33.80	0.068	0.0042	0.0025	90.27	2.74	-9.63	0.221
9	0.014	3.1	0.0045	0.00037	1.28	2.71	-33.55	0.075	0.0049	0.0029	89.42	3.09	-9.27	0.250
10	0.016	3.6	0.0051	0.00042	1.55	3.28	-32.97	0.091	0.0056	0.0033	88.77	3.36	-9.00	0.272
11	0.019	4.2	0.0061	0.00050	1.63	3.45	-32.81	0.095	0.0067	0.0039	87.92	3.72	-8.65	0.301
12	0.022	4.9	0.0071	0.00058	2.04	4.32	-31.94	0.119	0.0077	0.0045	86.89	4.15	-8.22	0.335
13	0.027	6.0	0.0087	0.00071	2.26	4.79	-31.47	0.132	0.0095	0.0055	85.70	4.65	-7.72	0.376
14	0.032	7.1	0.0103	0.00085	2.73	5.79	-30.47	0.160	0.0112	0.0065	84.43	5.18	-7.19	0.419
15	0.037	8.2	0.0119	0.00098	3.07	6.51	-29.75	0.179	0.0130	0.0076	83.58	5.53	-6.83	0.447
16	0.042	9.3	0.0135	0.00111	3.51	7.44	-28.82	0.205	0.0148	0.0086	82.67	5.91	-6.45	0.478
17	0.052	11.6	0.0167	0.00137	3.73	7.90	-28.35	0.218	0.0183	0.0106	81.21	6.52	-5.84	0.527
18	0.062	13.8	0.0199	0.00164	4.14	8.77	-27.49	0.242	0.0218	0.0127	80.48	6.83	-5.54	0.552
19	0.077	17.1	0.0248	0.00203	4.56	9.66	-26.60	0.267	0.0271	0.0157	79.19	7.36	-5.00	0.595
20	0.097	21.6	0.0312	0.00256	4.97	10.53	-25.73	0.290	0.0341	0.0198	78.48	7.66	-4.70	0.619
21	0.122	27.2	0.0392	0.00322	5.21	11.04	-25.22	0.305	0.0429	0.0250	77.57	8.04	-4.32	0.650
22	0.172	38.3	0.0553	0.00454	5.59	11.85	-24.41	0.327	0.0605	0.0352	76.38	8.54	-3.82	0.690
23	0.222	49.4	0.0714	0.00586	5.97	12.65	-23.61	0.349	0.0780	0.0454	75.70	8.82	-3.54	0.713
24	0.322	71.7	0.1036	0.00850	6.36	13.48	-22.78	0.372	0.1132	0.0659	75.13	9.06	-3.30	0.733
25	0.422	93.9	0.1358	0.01114	6.83	14.47	-21.79	0.399	0.1483	0.0863	74.16	9.47	-2.90	0.765
26	0.572	127.3	0.1840	0.01511	7.44	15.77	-20.49	0.435	0.2011	0.1170	73.50	9.74	-2.62	0.788
27	0.722	160.7	0.2323	0.01907	7.85	16.64	-19.62	0.459	0.2538	0.1477	72.89	10.00	-2.36	0.808
28	0.922	205.2	0.2966	0.02435	8.74	18.52	-17.74	0.511	0.3241	0.1886	72.09	10.33	-2.03	0.835
29	1.172	260.9	0.3770	0.03095	9.86	20.90	-15.36	0.576	0.4120	0.2397	71.33	10.64	-1.72	0.861
30	1.422	316.5	0.4574	0.03755	11.04	23.40	-12.86	0.645	0.4998	0.2908	70.64	10.93	-1.43	0.884
31	1.672	372.2	0.5379	0.04415	11.82	25.05	-11.21	0.691	0.5877	0.3420	69.88	11.25	-1.11	0.910
32	1.922	427.8	0.6183	0.05076	13.37	28.33	-7.93	0.781	0.6756	0.3931	69.33	11.48	-0.88	0.928
33	2.172	483.5	0.6987	0.05736	14.36	30.43	-5.83	0.839	0.7635	0.4442	68.78	11.71	-0.66	0.947
34	2.422	539.1	0.7791	0.06396	15.45	32.74	-3.52	0.903	0.8513	0.4953	68.20	11.95	-0.41	0.966
35	2.672	594.8	0.8595	0.07056	16.22	34.37	-1.89	0.948	0.9392	0.5465	67.74	12.14	-0.22	0.982
36	2.922	650.4	0.9400	0.07716	16.70	35.39	-0.87	0.976	1.0271	0.5976	67.40	12.29	-0.08	0.994
37	3.172	706.1	1.0204	0.08376	17.02	36.07	-0.19	0.995	1.1150	0.6487	67.25	12.35	-0.02	0.999
38	3.422	761.7	1.1008	0.09037	17.11	36.26	0.00	1.000	1.2028	0.6999	67.17	12.38	0.02	1.001
39	3.672	817.4	1.1812	0.09697	17.08	36.20	-0.06	0.998	1.2907	0.7510	67.10	12.41	0.05	1.004
40	3.922	873.0	1.2616	0.10357	17.11	36.26	0.00	1.000	1.3786	0.8021	67.21	12.37	-0.00	1.000

ADVERSE PRESSURE GRADIENT (-0.275,0.)

RUN =	20573-3	UINF	= 16.5	K	=-0.454E-06	CF/2	= 0.00081	DELM	= 3.717	DELH	= 3.586
PLATE =	18	TWALL	= 96.5	BETA =	6.112	ST	= 0.00217	DEL1M	= 1.274	DEL2H	= 0.2366
X(IN) =	70.	DC	= 44.768	BF	= 0.000	PPLUS	= 0.01971	DEL2M	= 0.645	REH	= 2024.
Z(IN) =	0.	DEL3	= 6.440	F	= 0.00000	VOPLUS	= 0.00000	REM	= 5517.	GH	= 3.024
POINTS=	41	TGAS	= 67.3	BH	= 0.000	REY.NO	=0.642E 06	H	= 1.976	GF	= 17.356

I	Y	YPLUS	Y/DELM	Y/DC	U	UPLUS	UDE	UBAR	Y/DELH	Y/DEL3	T	TPLUS	TDE	TBAR
1	0.000	0.0	0.0000	0.00000	0.00	0.00	-35.14	0.000	0.0000	0.0000	96.55	0.00	-13.11	0.000
2	0.005	1.1	0.0013	0.00011	0.75	1.60	-33.54	0.046	0.0014	0.0008	93.01	1.59	-11.52	0.121
3	0.006	1.3	0.0016	0.00013	0.80	1.71	-33.44	0.049	0.0017	0.0009	92.73	1.71	-11.40	0.131
4	0.007	1.5	0.0019	0.00016	0.78	1.66	-33.48	0.047	0.0020	0.0011	92.20	1.95	-11.16	0.149
5	0.008	1.8	0.0022	0.00018	0.85	1.81	-33.33	0.052	0.0022	0.0012	91.96	2.06	-11.05	0.157
6	0.009	2.0	0.0024	0.00020	0.84	1.79	-33.35	0.051	0.0025	0.0014	91.71	2.17	-10.94	0.166
7	0.011	2.4	0.0030	0.00025	0.90	1.92	-33.22	0.055	0.0031	0.0017	91.05	2.47	-10.64	0.188
8	0.013	2.9	0.0035	0.00029	1.05	2.24	-32.90	0.064	0.0036	0.0020	90.35	2.78	-10.33	0.212
9	0.016	3.5	0.0043	0.00036	1.24	2.64	-32.50	0.075	0.0045	0.0025	89.41	3.20	-9.91	0.244
10	0.019	4.2	0.0051	0.00042	1.36	2.90	-32.24	0.083	0.0053	0.0030	88.51	3.61	-9.50	0.275
11	0.023	5.1	0.0062	0.00051	1.65	3.52	-31.62	0.100	0.0064	0.0036	87.32	4.14	-8.97	0.316
12	0.028	6.2	0.0075	0.00063	2.01	4.29	-30.86	0.122	0.0078	0.0043	85.99	4.74	-8.37	0.351
13	0.033	7.3	0.0089	0.00074	2.30	4.90	-30.24	0.140	0.0092	0.0051	84.95	5.21	-7.90	0.397
14	0.038	8.4	0.0102	0.00085	2.61	5.57	-29.58	0.158	0.0106	0.0059	84.22	5.53	-7.58	0.422
15	0.048	10.6	0.0129	0.00107	3.14	6.70	-28.45	0.191	0.0134	0.0075	82.69	6.22	-6.89	0.474
16	0.058	12.8	0.0156	0.00130	3.54	7.55	-27.59	0.215	0.0162	0.0090	81.41	6.79	-6.31	0.518
17	0.068	15.1	0.0183	0.00152	3.87	8.25	-26.89	0.235	0.0190	0.0106	80.38	7.26	-5.85	0.553
18	0.078	17.3	0.0210	0.00174	3.95	8.42	-26.72	0.240	0.0218	0.0121	79.91	7.47	-5.64	0.569
19	0.093	20.6	0.0250	0.00208	4.35	9.28	-25.87	0.264	0.0259	0.0144	79.18	7.80	-5.31	0.594
20	0.108	23.9	0.0291	0.00241	4.59	9.79	-25.36	0.279	0.0301	0.0168	78.70	8.01	-5.10	0.611
21	0.123	27.2	0.0331	0.00275	4.73	10.09	-25.06	0.287	0.0343	0.0191	78.07	8.29	-4.81	0.632
22	0.148	32.8	0.0398	0.00331	5.09	10.85	-24.29	0.309	0.0413	0.0230	77.38	8.60	-4.50	0.656
23	0.173	38.3	0.0465	0.00386	5.29	11.28	-23.86	0.321	0.0482	0.0269	76.77	8.88	-4.23	0.677
24	0.223	49.4	0.0600	0.00498	5.69	12.13	-23.01	0.345	0.0622	0.0346	76.28	9.10	-4.01	0.694
25	0.273	60.4	0.0734	0.00610	5.71	12.18	-22.97	0.346	0.0761	0.0424	75.71	9.35	-3.75	0.713
26	0.373	82.6	0.1004	0.00833	6.12	13.05	-22.09	0.371	0.1040	0.0579	74.88	9.73	-3.38	0.742
27	0.523	115.8	0.1407	0.01168	6.49	13.84	-21.30	0.394	0.1458	0.0812	74.14	10.06	-3.05	0.767
28	0.723	160.1	0.1945	0.01615	7.16	15.27	-19.87	0.434	0.2016	0.1123	73.35	10.41	-2.69	0.794
29	0.923	204.4	0.2483	0.02062	7.83	16.70	-18.45	0.475	0.2574	0.1433	72.84	10.64	-2.46	0.812
30	1.173	259.7	0.3156	0.02620	8.81	18.79	-16.36	0.535	0.3271	0.1822	71.98	11.02	-2.08	0.841
31	1.423	315.1	0.3828	0.03179	9.50	20.26	-14.88	0.576	0.3968	0.2210	71.44	11.27	-1.84	0.859
32	1.673	370.4	0.4501	0.03737	10.08	21.50	-13.65	0.612	0.4665	0.2598	70.88	11.52	-1.59	0.878
33	1.923	425.8	0.5174	0.04295	11.12	23.71	-11.43	0.675	0.5363	0.2986	70.37	11.75	-1.36	0.896
34	2.173	481.1	0.5846	0.04854	12.09	25.78	-9.36	0.734	0.6060	0.3374	69.93	11.95	-1.16	0.911
35	2.423	536.5	0.6519	0.05412	13.05	27.83	-7.31	0.792	0.6757	0.3763	69.41	12.18	-0.93	0.929
36	2.673	591.8	0.7191	0.05971	13.93	29.71	-5.44	0.845	0.7454	0.4151	68.97	12.38	-0.73	0.944
37	2.923	647.2	0.7864	0.06529	14.68	31.30	-3.84	0.891	0.8151	0.4539	68.48	12.59	-0.52	0.961
38	3.173	702.5	0.8536	0.07088	15.37	32.78	-2.37	0.933	0.8848	0.4927	68.23	12.71	-0.40	0.969
39	3.423	757.9	0.9209	0.07646	15.95	34.01	-1.13	0.968	0.9546	0.5316	67.83	12.89	-0.22	0.983
40	3.673	813.2	0.9882	0.08204	16.28	34.72	-0.43	0.988	1.0243	0.5704	67.51	13.03	-0.08	0.994
41	3.923	868.6	1.0554	0.08763	16.48	35.14	0.00	1.000	1.0940	0.6092	67.33	13.11	-0.00	1.000

C-3

ADVERSE PRESSURE GRADIENT (-0.275,-0.001)

RUN = 21573-1	UINF = 22.1	K =-0.946E-06	CF/2 = 0.00146	DELM = 0.964	DELH = 0.864
PLATE = 6	TWALL = 89.7	BETA = 1.794	ST = 0.00327	DEL1M = 0.239	DEL2H = 0.0694
X(IN) = 22.	DC = 6.254	BF = -0.683	PPLUS = 0.01688	DEL2M = 0.143	REH = 805.
Z(IN) = 0.	DEL3 = 1.459	F = -0.00100	VOPLUS= -0.02743	REM = 1658.	GH = 3.243
POINTS= 36	TGAS = 63.7	BH = -0.306	REY.NO=0.313E 06	H = 1.675	GF = 10.534

I	Y	YPLUS	Y/DELM	Y/DC	U	UPLUS	UDE	UBAR	Y/DELH	Y/DEL 3	T	TPLUS	TDE	TBAR
1	0.000	0.0	0.0000	0.00000	0.00	0.00	-26.13	0.000	0.0000	0.0000	89.71	0.00	-11.70	0.000
2	0.005	2.0	0.0052	0.00080	2.23	2.64	-23.49	0.101	0.0058	0.0034	84.54	2.33	-9.37	0.199
3	0.006	2.4	0.0062	0.00096	2.49	2.95	-23.18	0.113	0.0069	0.0041	84.22	2.48	-9.22	0.212
4	0.007	2.9	0.0073	0.00112	2.83	3.35	-22.78	0.128	0.0081	0.0048	83.69	2.71	-8.99	0.232
5	0.008	3.3	0.0083	0.00128	2.99	3.54	-22.59	0.135	0.0093	0.0055	83.11	2.98	-8.72	0.254
6	0.009	3.7	0.0093	0.00144	3.35	3.96	-22.17	0.152	0.0104	0.0062	82.63	3.19	-8.51	0.273
7	0.010	4.1	0.0104	0.00160	3.62	4.28	-21.85	0.164	0.0116	0.0069	82.17	3.40	-8.30	0.290
8	0.012	4.9	0.0124	0.00192	4.15	4.91	-21.22	0.188	0.0139	0.0082	81.04	3.91	-7.79	0.334
9	0.014	5.7	0.0145	0.00224	4.89	5.78	-20.35	0.221	0.0162	0.0096	80.13	4.32	-7.38	0.359
10	0.016	6.5	0.0166	0.00256	5.24	6.20	-19.93	0.237	0.0185	0.0110	79.49	4.61	-7.09	0.394
11	0.019	7.7	0.0197	0.00304	5.83	6.90	-19.23	0.264	0.0220	0.0130	78.48	5.06	-6.63	0.433
12	0.022	9.0	0.0228	0.00352	6.67	7.89	-18.24	0.302	0.0254	0.0151	77.57	5.47	-6.22	0.468
13	0.025	10.2	0.0259	0.00400	7.33	8.67	-17.46	0.332	0.0289	0.0171	76.76	5.84	-5.86	0.499
14	0.029	11.8	0.0301	0.00464	7.73	9.14	-16.99	0.350	0.0335	0.0199	75.94	6.21	-5.49	0.530
15	0.033	13.5	0.0342	0.00528	8.31	9.83	-16.30	0.376	0.0382	0.0226	75.32	6.48	-5.21	0.554
16	0.037	15.1	0.0384	0.00592	8.69	10.28	-15.85	0.393	0.0428	0.0254	74.88	6.68	-5.02	0.571
17	0.041	16.7	0.0425	0.00656	9.13	10.80	-15.33	0.413	0.0474	0.0281	74.29	6.95	-4.75	0.594
18	0.045	18.4	0.0467	0.00720	9.45	11.18	-14.95	0.428	0.0521	0.0309	73.71	7.21	-4.49	0.616
19	0.055	22.4	0.0570	0.00879	9.98	11.81	-14.32	0.452	0.0636	0.0377	73.02	7.52	-4.18	0.642
20	0.065	26.5	0.0674	0.01039	10.64	12.59	-13.54	0.482	0.0752	0.0446	72.39	7.80	-3.89	0.667
21	0.075	30.6	0.0778	0.01199	10.91	12.91	-13.22	0.494	0.0868	0.0514	71.99	7.98	-3.71	0.682
22	0.090	36.7	0.0933	0.01439	11.21	13.26	-12.87	0.507	0.1041	0.0617	71.37	8.26	-3.43	0.706
23	0.105	42.8	0.1089	0.01679	11.61	13.73	-12.40	0.526	0.1215	0.0720	70.91	8.47	-3.22	0.724
24	0.125	51.0	0.1296	0.01999	11.55	13.66	-12.47	0.523	0.1446	0.0857	70.41	8.70	-3.00	0.743
25	0.150	61.2	0.1555	0.02398	12.43	14.70	-11.43	0.563	0.1735	0.1028	69.90	8.93	-2.77	0.763
26	0.175	71.4	0.1815	0.02798	12.86	15.21	-10.92	0.582	0.2024	0.1200	69.42	9.14	-2.55	0.781
27	0.225	91.8	0.2333	0.03598	13.70	16.21	-9.92	0.620	0.2603	0.1543	68.76	9.44	-2.25	0.807
28	0.275	112.2	0.2852	0.04397	14.34	16.96	-9.17	0.649	0.3181	0.1885	68.12	9.73	-1.97	0.831
29	0.325	132.6	0.3370	0.05196	15.16	17.93	-8.20	0.686	0.3760	0.2228	67.54	9.99	-1.71	0.853
30	0.425	173.3	0.4407	0.06795	16.56	19.59	-6.54	0.750	0.4916	0.2914	66.52	10.45	-1.25	0.893
31	0.525	214.1	0.5444	0.08394	17.82	21.08	-5.05	0.807	0.6073	0.3599	65.78	10.78	-0.92	0.921
32	0.625	254.9	0.6481	0.09993	19.15	22.65	-3.48	0.867	0.7230	0.4285	65.11	11.08	-0.62	0.947
33	0.775	316.1	0.8036	0.12392	20.78	24.58	-1.55	0.941	0.8965	0.5313	64.26	11.47	-0.23	0.980
34	0.925	377.3	0.9591	0.14790	21.81	25.80	-0.33	0.987	1.0700	0.6341	63.82	11.67	-0.04	0.997
35	1.125	458.9	1.1665	0.17988	22.11	26.15	0.02	1.001	1.3014	0.7713	63.74	11.70	-0.00	1.000
36	1.325	540.4	1.3739	0.21186	22.09	26.13	0.00	1.000	1.5328	0.9084	63.73	11.70	-0.00	1.000

ADVERSE PRESSURE GRADIENT (-0.275,-0.001)

RUN =	21573-2	UINF	=	19.4	K	=	-0.705E-06	CF/2	=	0.00118	DELM	=	1.464	DELH	=	1.355
PLATE =	9	TWALL	=	89.9	BETA	=	2.503	ST	=	0.00298	DEL1M	=	0.410	DEL2H	=	0.1019
X(IN) =	34.	DC	=	11.955	BF	=	-0.874	PPLUS	=	0.01744	DEL2M	=	0.235	REH	=	1039.
Z(IN) =	0.	DEL3	=	2.193	F	=	-0.00103	VOPLUS	=	-0.03150	REM	=	2392.	GH	=	2.956
POINTS=	33	TGAS	=	63.9	BH	=	-0.346	REY.NO	=	0.398E 06	H	=	1.749	GF	=	12.475

I	Y	YPLUS	Y/DELM	Y/DC	U	UPLUS	UDE	UBAR	Y/DELH	Y/DEL3	T	TPLUS	TDE	TBAR
1	0.000	0.0	0.0000	0.00000	0.00	0.00	-29.14	0.000	0.0000	0.0000	89.85	0.00	-11.52	0.000
2	0.005	1.6	0.0034	0.00042	1.71	2.57	-26.57	0.088	0.0037	0.0023	84.82	2.23	-9.28	0.194
3	0.006	1.9	0.0041	0.00050	1.95	2.93	-26.21	0.100	0.0044	0.0027	84.26	2.48	-9.03	0.215
4	0.007	2.2	0.0048	0.00059	2.07	3.11	-26.03	0.107	0.0051	0.0032	83.82	2.68	-8.84	0.232
5	0.008	2.6	0.0055	0.00067	2.22	3.33	-25.80	0.114	0.0059	0.0036	83.46	2.84	-8.68	0.246
6	0.010	3.2	0.0068	0.00084	2.68	4.02	-25.11	0.138	0.0073	0.0046	82.68	3.18	-8.33	0.276
7	0.012	3.9	0.0082	0.00100	2.89	4.34	-24.80	0.149	0.0088	0.0055	81.79	3.58	-7.94	0.311
8	0.015	4.8	0.0102	0.00125	3.58	5.37	-23.76	0.184	0.0110	0.0068	80.69	4.07	-7.45	0.353
9	0.018	5.8	0.0123	0.00151	4.04	6.06	-23.07	0.208	0.0132	0.0082	79.64	4.53	-6.98	0.393
10	0.021	6.7	0.0143	0.00176	4.39	6.59	-22.55	0.226	0.0154	0.0096	78.82	4.90	-6.62	0.425
11	0.024	7.7	0.0164	0.00201	4.77	7.16	-21.98	0.246	0.0176	0.0109	78.01	5.25	-6.26	0.456
12	0.028	9.0	0.0191	0.00234	5.39	8.09	-21.05	0.278	0.0205	0.0128	77.25	5.59	-5.92	0.486
13	0.033	10.6	0.0225	0.00276	5.91	8.87	-20.27	0.304	0.0242	0.0150	76.43	5.96	-5.56	0.517
14	0.038	12.2	0.0260	0.00318	6.31	9.47	-19.67	0.325	0.0278	0.0173	75.68	6.29	-5.22	0.546
15	0.048	15.4	0.0328	0.00402	6.88	10.33	-18.81	0.354	0.0352	0.0219	74.46	6.83	-4.68	0.593
16	0.058	18.6	0.0396	0.00485	7.44	11.17	-17.97	0.383	0.0425	0.0264	73.95	7.06	-4.45	0.613
17	0.073	23.5	0.0499	0.00611	7.93	11.90	-17.23	0.409	0.0535	0.0333	73.03	7.47	-4.05	0.648
18	0.088	28.3	0.0601	0.00736	8.31	12.47	-16.66	0.428	0.0645	0.0401	72.44	7.72	-3.79	0.671
19	0.108	34.7	0.0738	0.00903	8.39	12.59	-16.54	0.432	0.0791	0.0492	71.95	7.94	-3.57	0.689
20	0.133	42.7	0.0909	0.01113	8.99	13.50	-15.64	0.463	0.0975	0.0606	71.29	8.23	-3.28	0.715
21	0.158	50.8	0.1079	0.01322	9.31	13.98	-15.16	0.480	0.1158	0.0720	70.90	8.41	-3.10	0.730
22	0.208	66.8	0.1421	0.01740	9.81	14.73	-14.41	0.505	0.1524	0.0948	70.34	8.66	-2.85	0.752
23	0.308	99.0	0.2104	0.02576	10.61	15.93	-13.21	0.547	0.2257	0.1404	69.17	9.17	-2.34	0.797
24	0.408	131.1	0.2787	0.03413	11.48	17.23	-11.90	0.591	0.2990	0.1860	68.37	9.53	-1.98	0.828
25	0.508	163.2	0.3470	0.04249	12.37	18.57	-10.57	0.637	0.3722	0.2316	67.72	9.82	-1.69	0.853
26	0.658	211.4	0.4495	0.05504	13.73	20.61	-8.53	0.707	0.4822	0.3000	66.82	10.22	-1.29	0.887
27	0.808	259.6	0.5520	0.06759	15.07	22.62	-6.52	0.776	0.5921	0.3684	66.06	10.55	-0.96	0.916
28	1.008	323.9	0.6886	0.08432	16.69	25.05	-4.08	0.860	0.7386	0.4596	65.24	10.92	-0.59	0.948
29	1.208	388.1	0.8252	0.10105	18.18	27.29	-1.85	0.937	0.8852	0.5508	64.55	11.23	-0.29	0.975
30	1.408	452.4	0.9619	0.11778	19.14	28.73	-0.41	0.986	1.0317	0.6420	64.04	11.45	-0.07	0.994
31	1.658	532.7	1.1327	0.13869	19.48	29.24	0.11	1.004	1.2149	0.7559	63.86	11.53	0.01	1.001
32	1.908	613.0	1.3034	0.15960	19.41	29.14	0.00	1.000	1.3981	0.8699	63.80	11.56	0.04	1.003
33	2.158	693.3	1.4742	0.18051	19.41	29.14	0.00	1.000	1.5813	0.9839	63.89	11.52	-0.00	1.000

ADVERSE PRESSURE GRADIENT (-0.275,-0.001)

RUN	=	21573-3	UINF	=	17.7	K	=	-0.570E-06	CF/2	=	0.00114	DELM	=	1.902	DELH	=	1.847
PLATE	=	12	TWALL	=	89.8	BETA	=	2.571	ST	=	0.00287	DEL1M	=	0.550	DEL2H	=	0.1326
X(IN)	=	46.	DC	=	16.330	BF	=	-0.907	PPLUS	=	0.01489	DEL2M	=	0.316	REH	=	1235.
Z(IN)	=	0.	DEL3	=	2.866	F	=	-0.00103	VOPLUS	=	-0.03207	REM	=	2939.	GH	=	2.822
POINTS	=	37	TGAS	=	64.0	BH	=	-0.359	REY.NO	=	0.475E 06	H	=	1.743	GF	=	12.649

I	Y	YPLUS	Y/DELM	Y/DC	U	UPLUS	UDE	UBAR	Y/DELH	Y/DEL3	T	TPLUS	TDE	TBAR
1	0.000	0.0	0.0000	0.00000	0.00	0.00	-29.67	0.000	0.0000	0.0000	89.82	0.00	-11.74	0.000
2	0.005	1.4	0.0026	0.00031	1.32	2.21	-27.46	0.074	0.0027	0.0017	85.41	2.00	-9.74	0.171
3	0.006	1.7	0.0032	0.00037	1.52	2.54	-27.13	0.086	0.0032	0.0021	85.27	2.07	-9.67	0.176
4	0.007	2.0	0.0037	0.00043	1.63	2.73	-26.95	0.092	0.0038	0.0024	84.85	2.26	-9.48	0.192
5	0.008	2.3	0.0042	0.00049	1.75	2.93	-26.74	0.099	0.0043	0.0028	84.29	2.51	-9.23	0.214
6	0.009	2.6	0.0047	0.00055	1.86	3.11	-26.56	0.105	0.0049	0.0031	83.95	2.67	-9.07	0.227
7	0.010	2.9	0.0053	0.00061	2.00	3.35	-26.33	0.113	0.0054	0.0035	83.51	2.87	-8.87	0.244
8	0.012	3.5	0.0063	0.00073	2.37	3.97	-25.71	0.134	0.0065	0.0042	82.79	3.19	-8.55	0.272
9	0.014	4.0	0.0074	0.00086	2.53	4.23	-25.44	0.143	0.0076	0.0049	82.09	3.51	-8.23	0.299
10	0.017	4.9	0.0089	0.00104	3.03	5.07	-24.60	0.171	0.0092	0.0059	81.06	3.98	-7.76	0.339
11	0.020	5.8	0.0105	0.00122	3.33	5.57	-24.10	0.188	0.0108	0.0070	80.06	4.43	-7.30	0.378
12	0.024	6.9	0.0126	0.00147	3.95	6.61	-23.06	0.223	0.0130	0.0084	79.26	4.80	-6.94	0.409
13	0.028	8.1	0.0147	0.00171	4.46	7.46	-22.21	0.252	0.0152	0.0098	78.17	5.29	-6.44	0.451
14	0.033	9.5	0.0173	0.00202	4.94	8.27	-21.41	0.279	0.0179	0.0115	77.25	5.71	-6.03	0.486
15	0.038	11.0	0.0200	0.00233	5.30	8.87	-20.80	0.299	0.0206	0.0133	76.32	6.13	-5.60	0.522
16	0.043	12.4	0.0226	0.00263	5.65	9.46	-20.22	0.319	0.0233	0.0150	75.64	6.44	-5.29	0.549
17	0.053	15.3	0.0279	0.00325	6.03	10.09	-19.58	0.340	0.0287	0.0185	74.68	6.88	-4.86	0.586
18	0.063	18.2	0.0331	0.00386	6.62	11.08	-18.59	0.373	0.0341	0.0220	74.00	7.19	-4.55	0.612
19	0.073	21.0	0.0384	0.00447	6.83	11.43	-18.24	0.385	0.0395	0.0255	73.37	7.48	-4.26	0.637
20	0.088	25.4	0.0463	0.00539	7.28	12.18	-17.49	0.411	0.0476	0.0307	72.73	7.77	-3.97	0.661
21	0.108	31.1	0.0568	0.00661	7.51	12.57	-17.10	0.424	0.0585	0.0377	72.06	8.07	-3.66	0.687
22	0.133	38.3	0.0699	0.00814	7.82	13.09	-16.59	0.441	0.0720	0.0464	71.58	8.29	-3.45	0.706
23	0.158	45.5	0.0831	0.00968	8.13	13.61	-16.07	0.459	0.0855	0.0551	71.17	8.48	-3.26	0.722
24	0.208	60.0	0.1093	0.01274	8.49	14.21	-15.46	0.479	0.1126	0.0726	70.44	8.80	-2.93	0.750
25	0.258	74.4	0.1356	0.01580	8.85	14.81	-14.86	0.499	0.1397	0.0900	69.98	9.01	-2.72	0.768
26	0.308	88.8	0.1619	0.01886	9.19	15.38	-14.29	0.518	0.1667	0.1075	69.60	9.19	-2.55	0.782
27	0.408	117.6	0.2145	0.02498	9.52	15.93	-13.74	0.537	0.2209	0.1423	68.90	9.50	-2.23	0.809
28	0.558	160.8	0.2933	0.03417	10.49	17.56	-12.12	0.592	0.3021	0.1947	68.13	9.85	-1.88	0.839
29	0.708	204.1	0.3722	0.04335	11.41	19.10	-10.58	0.644	0.3833	0.2470	67.45	10.16	-1.57	0.866
30	0.908	261.7	0.4773	0.05560	12.69	21.24	-8.44	0.716	0.4916	0.3168	66.75	10.48	-1.25	0.893
31	1.158	333.8	0.6087	0.07091	14.09	23.58	-6.09	0.795	0.6269	0.4040	65.87	10.88	-0.85	0.927
32	1.408	405.8	0.7401	0.08622	15.52	25.97	-3.70	0.875	0.7622	0.4912	65.17	11.20	-0.54	0.954
33	1.658	477.9	0.8715	0.10153	16.79	28.10	-1.57	0.947	0.8976	0.5784	64.51	11.50	-0.24	0.979
34	1.908	549.9	1.0029	0.11684	17.57	29.41	-0.27	0.991	1.0329	0.6657	64.15	11.66	-0.08	0.993
35	2.158	622.0	1.1343	0.13215	17.77	29.74	0.07	1.002	1.1682	0.7529	63.98	11.74	-0.00	1.000
36	2.408	694.1	1.2657	0.14745	17.78	29.76	0.08	1.003	1.3036	0.8401	63.98	11.74	-0.00	1.000
37	2.658	766.1	1.3971	0.16276	17.73	29.67	0.00	1.000	1.4389	0.9273	63.98	11.74	-0.00	1.000

ADVERSE PRESSURE GRADIENT (-0.275,-0.001)

RUN	=	21973-1	UINF	=	17.0	K	=	-0.488E-06	CF/2	=	0.00108	DELM	=	2.324	DELH =	2.151
PLATE	=	15	TWALL	=	90.9	BETA	=	2.554	ST	=	0.00280	DEL1M	=	0.631	DEL2H =	0.1436
X(IN)	=	58.	DC	=	19.230	BF	=	-0.948	PPLUS	=	0.01382	DEL2M	=	0.375	REH =	1327.
Z(IN)	=	0.	DEL3	=	3.147	F	=	-0.00102	VOPLUS	=	-0.03262	REM	=	3351.	GH =	2.770
POINTS	=	42	TGAS	=	65.1	BH	=	-0.364	REY.NO	=	0.563E 06	H	=	1.681	GF =	12.351

I	Y	YPLUS	Y/DELM	Y/DC	U	UPLUS	UDE	UBAR	Y/DELH	Y/DEL3	T	TPLUS	TDE	TBAR
1	0.000	0.0	0.0000	0.00000	0.00	0.00	-30.48	0.000	0.0000	0.0000	90.89	0.00	-11.72	0.000
2	0.005	1.3	0.0022	0.00026	1.18	2.12	-28.36	0.069	0.0023	0.0016	87.87	1.37	-10.35	0.117
3	0.006	1.6	0.0026	0.00031	1.27	2.28	-28.20	0.075	0.0028	0.0019	87.55	1.51	-10.20	0.129
4	0.007	1.9	0.0030	0.00036	1.35	2.42	-28.06	0.080	0.0033	0.0022	87.13	1.71	-10.01	0.146
5	0.008	2.2	0.0034	0.00042	1.49	2.67	-27.81	0.088	0.0037	0.0025	86.73	1.89	-9.83	0.161
6	0.009	2.4	0.0039	0.00047	1.62	2.91	-27.57	0.095	0.0042	0.0029	86.43	2.02	-9.69	0.173
7	0.011	3.0	0.0047	0.00057	1.79	3.21	-27.27	0.105	0.0051	0.0035	85.66	2.37	-9.34	0.202
8	0.013	3.5	0.0056	0.00068	2.05	3.68	-26.80	0.121	0.0060	0.0041	84.76	2.78	-8.93	0.237
9	0.015	4.0	0.0065	0.00078	2.36	4.24	-26.25	0.139	0.0070	0.0048	84.07	3.09	-8.62	0.264
10	0.017	4.6	0.0073	0.00088	2.66	4.78	-25.71	0.157	0.0079	0.0054	83.35	3.42	-8.29	0.292
11	0.020	5.4	0.0086	0.00104	3.14	5.64	-24.85	0.185	0.0093	0.0064	82.28	3.91	-7.81	0.333
12	0.023	6.2	0.0099	0.00120	3.51	6.30	-24.18	0.207	0.0107	0.0073	81.48	4.27	-7.44	0.364
13	0.027	7.3	0.0116	0.00140	3.92	7.04	-23.45	0.231	0.0126	0.0086	80.45	4.74	-6.98	0.404
14	0.032	8.6	0.0138	0.00166	4.42	7.93	-22.55	0.260	0.0149	0.0102	79.10	5.35	-6.36	0.456
15	0.037	10.0	0.0159	0.00192	4.92	8.83	-21.65	0.290	0.0172	0.0118	78.13	5.79	-5.92	0.494
16	0.042	11.3	0.0181	0.00218	5.40	9.69	-20.79	0.318	0.0195	0.0133	77.30	6.16	-5.55	0.526
17	0.047	12.7	0.0202	0.00244	5.68	10.20	-20.29	0.335	0.0219	0.0149	76.46	6.55	-5.17	0.559
18	0.052	14.0	0.0224	0.00270	5.95	10.68	-19.80	0.350	0.0242	0.0165	76.21	6.66	-5.05	0.568
19	0.057	15.3	0.0245	0.00296	6.29	11.29	-19.19	0.370	0.0265	0.0181	75.64	6.92	-4.79	0.590
20	0.067	18.0	0.0288	0.00348	6.57	11.79	-18.69	0.387	0.0312	0.0213	74.93	7.24	-4.47	0.618
21	0.077	20.7	0.0331	0.00400	6.96	12.49	-17.99	0.410	0.0358	0.0245	74.38	7.49	-4.22	0.639
22	0.092	24.8	0.0396	0.00478	7.02	12.60	-17.88	0.413	0.0428	0.0292	73.72	7.79	-3.92	0.665
23	0.107	28.8	0.0460	0.00556	7.37	13.23	-17.25	0.434	0.0497	0.0340	73.17	8.04	-3.67	0.686
24	0.127	34.2	0.0547	0.00660	7.69	13.80	-16.68	0.453	0.0590	0.0404	72.72	8.24	-3.47	0.704
25	0.152	40.9	0.0654	0.00790	8.02	14.40	-16.08	0.472	0.0707	0.0483	72.21	8.47	-3.24	0.723
26	0.177	47.6	0.0762	0.00920	8.23	14.77	-15.71	0.485	0.0823	0.0562	71.81	8.66	-3.05	0.739
27	0.227	61.1	0.0977	0.01180	8.55	15.35	-15.13	0.504	0.1055	0.0721	71.35	8.86	-2.85	0.756
28	0.277	74.6	0.1192	0.01440	8.75	15.71	-14.77	0.515	0.1288	0.0880	70.78	9.12	-2.59	0.778
29	0.377	101.5	0.1622	0.01960	9.23	16.57	-13.91	0.544	0.1753	0.1198	70.16	9.40	-2.31	0.802
30	0.477	128.4	0.2053	0.02481	9.72	17.45	-13.03	0.572	0.2218	0.1516	69.72	9.60	-2.11	0.819
31	0.627	168.8	0.2698	0.03261	10.25	18.40	-12.08	0.604	0.2915	0.1992	69.00	9.93	-1.78	0.847
32	0.827	222.6	0.3559	0.04301	11.14	20.00	-10.48	0.656	0.3845	0.2628	68.40	10.20	-1.51	0.871
33	1.027	276.4	0.4420	0.05341	11.85	21.27	-9.21	0.698	0.4775	0.3264	67.72	10.51	-1.20	0.897
34	1.227	330.3	0.5280	0.06381	12.94	23.23	-7.25	0.762	0.5705	0.3899	67.22	10.74	-0.98	0.916
35	1.427	384.1	0.6141	0.07421	13.80	24.77	-5.71	0.813	0.6635	0.4535	66.69	10.98	-0.74	0.937
36	1.677	451.4	0.7217	0.08721	14.94	26.82	-3.66	0.880	0.7797	0.5329	66.05	11.27	-0.45	0.961
37	1.927	518.7	0.8293	0.10021	15.84	28.44	-2.05	0.933	0.8960	0.6123	65.55	11.49	-0.22	0.981
38	2.177	586.0	0.9369	0.11321	16.64	29.87	-0.61	0.980	1.0122	0.6918	65.29	11.61	-0.10	0.991
39	2.427	653.3	1.0444	0.12621	16.93	30.39	-0.09	0.997	1.1284	0.7712	65.05	11.72	0.00	1.000
40	2.677	720.6	1.1520	0.13921	16.99	30.50	0.02	1.001	1.2447	0.8507	64.99	11.75	0.03	1.003
41	2.927	787.8	1.2596	0.15221	17.01	30.54	0.05	1.002	1.3609	0.9301	65.03	11.73	0.01	1.001
42	3.177	855.1	1.3672	0.16521	16.98	30.48	0.00	1.000	1.4771	1.0096	65.06	11.72	-0.00	1.000

ADVERSE PRESSURE GRADIENT (-0.275,-0.001)

RUN =	21973-2	UINF =	16.9	K =	-0.438E-06	CF/2 =	0.00116	DELM =	2.712	DELH =	2.533
PLATE =	18	TWALL =	90.8	BETA =	2.362	ST =	0.00272	DEL1M =	0.706	DEL2H =	0.1813
X(IN) =	70.	DC =	20.735	BF =	-0.854	PPLUS =	0.01110	DEL2M =	0.434	REH =	1605.
Z(IN) =	0.	DEL3 =	3.879	F =	-0.00099	VOPLUS=	-0.03050	REM =	3846.	GH =	2.749
POINTS=	40	TGAS =	65.2	BH =	-0.364	REY.NO=	0.664E 06	H =	1.625	GF =	11.299

I	Y	YPLUS	Y/DELM	Y/DC	U	UPLUS	UDE	UBAR	Y/DELH	Y/DEL3	T	TPLUS	TDE	TBAR
1	0.000	0.0	0.0000	0.00000	0.00	0.00	-29.38	0.000	0.0000	0.0000	90.79	0.00	-12.52	0.000
2	0.005	1.4	0.0018	0.00024	1.34	2.34	-27.04	0.080	0.0019	0.0013	86.58	2.06	-10.46	0.154
3	0.006	1.7	0.0022	0.00029	1.51	2.63	-26.74	0.090	0.0023	0.0015	86.28	2.20	-10.31	0.176
4	0.007	1.9	0.0026	0.00034	1.67	2.91	-26.46	0.099	0.0027	0.0018	86.00	2.34	-10.17	0.187
5	0.008	2.2	0.0029	0.00039	1.75	3.05	-26.32	0.104	0.0031	0.0021	85.48	2.60	-9.92	0.207
6	0.009	2.5	0.0033	0.00043	1.85	3.23	-26.15	0.110	0.0035	0.0023	85.22	2.72	-9.79	0.218
7	0.011	3.0	0.0041	0.00053	2.22	3.87	-25.50	0.132	0.0043	0.0028	84.56	3.05	-9.47	0.243
8	0.013	3.6	0.0048	0.00063	2.39	4.17	-25.21	0.142	0.0050	0.0034	83.89	3.37	-9.14	0.270
9	0.015	4.2	0.0055	0.00072	2.73	4.76	-24.62	0.162	0.0058	0.0039	83.05	3.78	-8.73	0.302
10	0.016	4.4	0.0059	0.00077	3.09	5.39	-23.99	0.183	0.0062	0.0041	82.46	4.07	-8.44	0.325
11	0.021	5.8	0.0077	0.00101	3.57	6.22	-23.15	0.212	0.0081	0.0054	81.62	4.48	-8.03	0.358
12	0.026	7.2	0.0096	0.00125	4.12	7.18	-22.19	0.245	0.0101	0.0067	80.23	5.16	-7.35	0.413
13	0.031	8.6	0.0114	0.00150	4.61	8.04	-21.34	0.274	0.0120	0.0080	79.34	5.60	-6.91	0.447
14	0.036	10.0	0.0133	0.00174	4.92	8.58	-20.80	0.292	0.0139	0.0093	78.48	6.02	-6.49	0.481
15	0.041	11.4	0.0151	0.00198	5.37	9.36	-20.01	0.319	0.0159	0.0106	77.59	6.46	-6.06	0.516
16	0.046	12.8	0.0170	0.00222	5.76	10.04	-19.33	0.342	0.0178	0.0119	76.95	6.77	-5.74	0.541
17	0.051	14.1	0.0188	0.00246	6.12	10.67	-18.71	0.363	0.0197	0.0131	76.59	6.95	-5.57	0.555
18	0.061	16.9	0.0225	0.00294	6.45	11.24	-18.13	0.383	0.0236	0.0157	75.46	7.50	-5.01	0.599
19	0.071	19.7	0.0262	0.00342	7.03	12.26	-17.12	0.417	0.0275	0.0183	74.86	7.79	-4.72	0.623
20	0.086	23.8	0.0317	0.00415	7.17	12.50	-16.88	0.426	0.0333	0.0222	73.91	8.26	-4.25	0.660
21	0.101	28.0	0.0372	0.00487	7.64	13.32	-16.06	0.453	0.0391	0.0260	73.37	8.52	-3.99	0.681
22	0.121	33.5	0.0446	0.00584	7.80	13.60	-15.78	0.463	0.0468	0.0312	73.08	8.66	-3.85	0.692
23	0.146	40.5	0.0538	0.00704	8.09	14.10	-15.27	0.430	0.0565	0.0376	72.65	8.87	-3.64	0.709
24	0.171	47.4	0.0630	0.00825	8.44	14.71	-14.66	0.501	0.0662	0.0441	72.12	9.13	-3.38	0.729
25	0.221	61.3	0.0815	0.01066	8.58	14.96	-14.42	0.509	0.0856	0.0570	71.63	9.37	-3.14	0.748
26	0.321	89.0	0.1183	0.01548	9.03	15.74	-13.63	0.536	0.1243	0.0828	70.74	9.80	-2.71	0.783
27	0.421	116.7	0.1552	0.02030	9.71	16.93	-12.45	0.576	0.1630	0.1085	70.33	10.00	-2.51	0.799
28	0.571	158.3	0.2105	0.02754	9.95	17.35	-12.03	0.591	0.2211	0.1472	69.58	10.37	-2.14	0.829
29	0.721	199.9	0.2658	0.03477	10.61	18.50	-10.88	0.630	0.2791	0.1859	68.94	10.68	-1.83	0.854
30	0.921	255.3	0.3396	0.04442	10.99	19.16	-10.22	0.652	0.3566	0.2374	68.53	10.89	-1.62	0.870
31	1.171	324.6	0.4317	0.05648	12.05	21.01	-8.37	0.715	0.4533	0.3019	67.86	11.21	-1.30	0.896
32	1.421	393.9	0.5239	0.06853	12.86	22.42	-6.96	0.763	0.5501	0.3663	67.33	11.47	-1.04	0.917
33	1.671	463.2	0.6161	0.08059	13.88	24.20	-5.18	0.824	0.6469	0.4308	66.84	11.71	-0.80	0.935
34	1.921	532.5	0.7082	0.09265	14.66	25.56	-3.82	0.870	0.7437	0.4952	66.35	11.95	-0.56	0.955
35	2.171	601.8	0.8004	0.10470	15.63	27.25	-2.13	0.928	0.8405	0.5597	65.99	12.13	-0.39	0.969
36	2.421	671.1	0.8926	0.11676	16.15	28.15	-1.22	0.958	0.9373	0.6241	65.63	12.30	-0.21	0.983
37	2.671	740.4	0.9848	0.12882	16.66	29.04	-0.33	0.989	1.0340	0.6886	65.36	12.44	-0.08	0.994
38	2.921	809.7	1.0769	0.14087	16.79	29.27	-0.10	0.996	1.1308	0.7530	65.20	12.52	0.00	1.000
39	3.171	879.0	1.1691	0.15293	16.84	29.36	-0.02	0.999	1.2276	0.8175	65.19	12.52	0.00	1.000
40	3.421	948.3	1.2613	0.16499	16.85	29.38	0.00	1.000	1.3244	0.8819	65.20	12.52	-0.00	1.000

ADVERSE PRESSURE GRADIENT (-0.275,-0.001)

RUN = 21973-3	UINF = 15.8	K =-0.413E-06	CF/2 = 0.00121	DELM = 3.368	DELH = 3.357
PLATE = 21	TWALL = 90.6	BETA = 2.576	ST = 0.00259	DEL1M = 0.903	DEL2H = 0.2330
X(IN) = 82.	DC = 26.015	BF = -0.830	PPLUS = 0.00987	DEL2M = 0.540	REH = 1940.
Z(IN) = 0.	DEL3 = 5.395	F = -0.00100	VOPLUS= -0.03021	REM = 4494.	GH = 2.918
POINTS= 40	TGAS = 65.0	BH = -0.386	REY.NO=0.724E 06	H = 1.672	GF = 11.582

I	Y	YPLUS	Y/DELM	Y/DC	U	UPLUS	UDE	UBAR	Y/DELH	Y/DEL3	T	TPLUS	TDE	TBAR
1	0.000	0.0	0.0000	0.00000	0.00	0.00	-28.81	0.000	0.0000	0.0000	90.58	0.00	-13.40	0.000
2	0.005	1.3	0.0015	0.00019	1.06	1.93	-26.88	0.067	0.0015	0.0009	87.06	1.85	-11.56	0.138
3	0.006	1.6	0.0018	0.00023	1.13	2.06	-26.75	0.071	0.0018	0.0011	86.96	1.90	-11.50	0.142
4	0.007	1.9	0.0021	0.00027	1.21	2.20	-26.61	0.076	0.0021	0.0013	86.56	2.11	-11.29	0.157
5	0.008	2.1	0.0024	0.00031	1.28	2.33	-26.48	0.081	0.0024	0.0015	86.16	2.32	-11.08	0.173
6	0.010	2.7	0.0030	0.00038	1.49	2.71	-26.10	0.094	0.0030	0.0019	85.58	2.62	-10.78	0.196
7	0.012	3.2	0.0036	0.00046	1.76	3.20	-25.60	0.111	0.0036	0.0022	84.93	2.96	-10.44	0.221
8	0.015	4.0	0.0045	0.00058	2.02	3.68	-25.13	0.128	0.0045	0.0028	84.01	3.45	-9.96	0.257
9	0.018	4.8	0.0053	0.00069	2.30	4.19	-24.62	0.145	0.0054	0.0033	83.30	3.82	-9.58	0.285
10	0.022	5.8	0.0065	0.00085	2.78	5.06	-23.75	0.176	0.0066	0.0041	82.03	4.48	-8.92	0.335
11	0.027	7.2	0.0080	0.00104	3.40	6.19	-22.62	0.215	0.0080	0.0050	80.73	5.17	-8.23	0.385
12	0.032	8.5	0.0095	0.00123	3.57	6.50	-22.31	0.226	0.0095	0.0059	79.77	5.67	-7.73	0.423
13	0.037	9.8	0.0110	0.00142	4.07	7.41	-21.40	0.257	0.0110	0.0069	78.87	6.14	-7.26	0.458
14	0.042	11.2	0.0125	0.00161	4.39	7.99	-20.82	0.277	0.0125	0.0078	77.99	6.60	-6.80	0.493
15	0.047	12.5	0.0140	0.00181	4.79	8.72	-20.09	0.303	0.0140	0.0087	77.29	6.97	-6.43	0.520
16	0.052	13.8	0.0154	0.00200	5.16	9.39	-19.42	0.326	0.0155	0.0096	76.93	7.16	-6.24	0.534
17	0.062	16.5	0.0184	0.00238	5.55	10.10	-18.71	0.351	0.0185	0.0115	76.25	7.52	-5.88	0.561
18	0.077	20.5	0.0229	0.00296	5.96	10.85	-17.96	0.377	0.0229	0.0143	75.23	8.05	-5.35	0.601
19	0.092	24.4	0.0273	0.00354	6.20	11.28	-17.52	0.392	0.0274	0.0171	74.39	8.49	-4.91	0.634
20	0.112	29.8	0.0332	0.00431	6.67	12.14	-16.67	0.421	0.0334	0.0208	74.37	8.50	-4.90	0.634
21	0.137	36.4	0.0407	0.00527	6.88	12.52	-16.29	0.435	0.0408	0.0254	73.47	8.97	-4.42	0.670
22	0.162	43.0	0.0481	0.00623	7.11	12.94	-15.87	0.449	0.0483	0.0300	72.94	9.25	-4.15	0.690
23	0.212	56.3	0.0629	0.00815	7.31	13.30	-15.50	0.462	0.0632	0.0393	72.10	9.69	-3.70	0.723
24	0.262	69.6	0.0778	0.01007	7.74	14.09	-14.72	0.489	0.0780	0.0486	71.59	9.96	-3.44	0.743
25	0.362	96.2	0.1075	0.01392	7.92	14.41	-14.39	0.500	0.1078	0.0671	70.93	10.31	-3.09	0.769
26	0.512	136.1	0.1520	0.01968	8.48	15.43	-13.38	0.536	0.1525	0.0949	70.25	10.66	-2.74	0.795
27	0.712	189.2	0.2114	0.02737	9.05	16.47	-12.34	0.572	0.2121	0.1320	69.41	11.10	-2.30	0.828
28	0.912	242.3	0.2707	0.03506	9.54	17.36	-11.45	0.603	0.2717	0.1691	68.98	11.33	-2.07	0.845
29	1.162	308.8	0.3450	0.04467	10.45	19.02	-9.79	0.660	0.3461	0.2154	68.34	11.66	-1.74	0.870
30	1.412	375.2	0.4192	0.05428	10.80	19.65	-9.15	0.682	0.4206	0.2617	67.82	11.93	-1.46	0.890
31	1.662	441.6	0.4934	0.06389	11.98	21.80	-7.01	0.757	0.4951	0.3081	67.45	12.13	-1.27	0.905
32	1.912	508.1	0.5676	0.07350	12.52	22.78	-6.02	0.791	0.5696	0.3544	67.09	12.32	-1.08	0.919
33	2.162	574.5	0.6418	0.08311	13.22	24.06	-4.75	0.835	0.6440	0.4008	66.61	12.57	-0.83	0.938
34	2.412	640.9	0.7161	0.09272	13.94	25.37	-3.44	0.881	0.7185	0.4471	66.31	12.73	-0.67	0.950
35	2.662	707.4	0.7903	0.10233	14.60	26.57	-2.24	0.922	0.7930	0.4934	65.99	12.89	-0.51	0.962
36	2.912	773.8	0.8645	0.11194	15.11	27.50	-1.31	0.955	0.8674	0.5398	65.73	13.03	-0.37	0.972
37	3.162	840.2	0.9387	0.12155	15.49	28.19	-0.62	0.979	0.9419	0.5861	65.40	13.20	-0.20	0.985
38	3.412	906.6	1.0129	0.13116	15.71	28.59	-0.22	0.992	1.0164	0.6325	65.24	13.29	-0.12	0.991
39	3.662	973.1	1.0871	0.14077	15.78	28.72	-0.09	0.997	1.0908	0.6788	65.09	13.37	-0.04	0.997
40	3.912	1039.5	1.1614	0.15038	15.83	28.81	0.00	1.000	1.1653	0.7251	65.02	13.40	-0.00	1.000

ADVERSE PRESSURE GRADIENT (-0.275,-0.002)

RUN	=	30473-1	UINF	=	21.8	K	=	-0.953E-06	CF/2	=	0.00221	DEL4	=	0.840	DELH =	0.755
PLATE	=	6	TWALL	=	89.2	BETA	=	0.891	ST	=	0.00375	DEL1M	=	0.180	DEL2H =	0.0581
X(IN)	=	22.	DC	=	3.841	BF	=	-0.902	PPLUS	=	0.00919	DEL2M	=	0.115	REH =	664.
Z(IN)	=	0.	DEL3	=	1.217	F	=	-0.00199	VOPLUS	=	-0.04435	REM	=	1312.	GH =	3.315
POINTS	=	33	TGAS	=	64.5	BH	=	-0.531	REY.NO	=	0.309E 06	H	=	1.573	GF =	7.756

I	Y	YPLUS	Y/DELM	Y/DC	U	UPLUS	UDE	UBAR	Y/DELH	Y/DEL3	T	TPLUS	TDE	TBAR
1	0.000	0.0	0.0000	0.00000	0.00	0.00	-21.29	0.000	0.0000	0.0000	89.16	0.00	-12.53	0.000
2	0.005	2.5	0.0060	0.00130	3.02	2.95	-18.34	0.138	0.0066	0.0041	83.45	2.90	-9.62	0.232
3	0.006	3.0	0.0071	0.00156	3.39	3.31	-17.98	0.155	0.0079	0.0049	83.03	3.11	-9.41	0.249
4	0.007	3.5	0.0083	0.00182	3.75	3.66	-17.63	0.172	0.0093	0.0058	82.39	3.44	-9.08	0.275
5	0.008	4.0	0.0095	0.00208	4.05	3.95	-17.33	0.186	0.0106	0.0066	81.88	3.70	-8.82	0.295
6	0.009	4.5	0.0107	0.00234	4.49	4.38	-16.90	0.206	0.0119	0.0074	81.48	3.90	-8.62	0.311
7	0.011	5.5	0.0131	0.00286	5.19	5.07	-16.22	0.238	0.0146	0.0090	80.44	4.43	-8.09	0.354
8	0.013	6.4	0.0155	0.00338	5.83	5.69	-15.60	0.267	0.0172	0.0107	79.61	4.85	-7.67	0.387
9	0.015	7.4	0.0179	0.00391	6.48	6.32	-14.96	0.297	0.0199	0.0123	78.59	5.37	-7.15	0.429
10	0.017	8.4	0.0202	0.00443	7.11	6.94	-14.35	0.326	0.0225	0.0140	77.83	5.76	-6.75	0.460
11	0.019	9.4	0.0226	0.00495	7.54	7.36	-13.93	0.346	0.0252	0.0156	77.33	6.01	-6.51	0.480
12	0.021	10.4	0.0250	0.00547	7.98	7.79	-13.50	0.366	0.0278	0.0173	76.67	6.35	-6.17	0.507
13	0.024	11.9	0.0286	0.00625	8.57	8.36	-12.92	0.393	0.0318	0.0197	75.92	6.72	-5.80	0.537
14	0.029	14.4	0.0345	0.00755	9.48	9.25	-12.03	0.435	0.0384	0.0238	74.78	7.30	-5.22	0.583
15	0.034	16.9	0.0405	0.00885	10.08	9.84	-11.45	0.462	0.0450	0.0279	74.00	7.70	-4.82	0.615
16	0.039	19.3	0.0464	0.01015	10.61	10.36	-10.93	0.486	0.0516	0.0320	73.54	7.93	-4.59	0.633
17	0.049	24.3	0.0583	0.01276	11.41	11.14	-10.15	0.523	0.0649	0.0403	72.70	8.36	-4.16	0.667
18	0.059	29.2	0.0703	0.01536	11.79	11.51	-9.78	0.541	0.0781	0.0485	71.75	8.84	-3.68	0.706
19	0.074	36.7	0.0881	0.01927	12.36	12.06	-9.22	0.567	0.0980	0.0608	71.19	9.13	-3.39	0.729
20	0.099	49.1	0.1179	0.02578	13.10	12.79	-8.50	0.601	0.1311	0.0813	70.29	9.59	-2.93	0.765
21	0.124	61.5	0.1476	0.03229	13.60	13.27	-8.01	0.624	0.1642	0.1019	69.76	9.86	-2.66	0.787
22	0.149	73.8	0.1774	0.03879	13.93	13.60	-7.69	0.639	0.1973	0.1224	69.16	10.16	-2.36	0.811
23	0.174	86.2	0.2072	0.04530	14.41	14.06	-7.22	0.661	0.2304	0.1429	68.83	10.32	-2.20	0.824
24	0.224	111.0	0.2667	0.05832	15.07	14.71	-6.58	0.691	0.2966	0.1840	68.19	10.65	-1.87	0.850
25	0.274	135.8	0.3263	0.07134	15.82	15.44	-5.85	0.725	0.3628	0.2251	67.62	10.94	-1.58	0.873
26	0.374	185.4	0.4453	0.09738	17.20	16.79	-4.50	0.789	0.4952	0.3072	66.76	11.38	-1.14	0.908
27	0.474	234.9	0.5644	0.12341	18.45	18.01	-3.28	0.846	0.6276	0.3894	66.09	11.72	-0.81	0.935
28	0.624	309.3	0.7430	0.16247	20.14	19.66	-1.63	0.923	0.8262	0.5126	65.20	12.17	-0.36	0.971
29	0.774	383.6	0.9216	0.20152	21.39	20.88	-0.41	0.981	1.0248	0.6358	64.68	12.44	-0.09	0.993
30	0.924	458.0	1.1002	0.24058	21.85	21.33	0.04	1.002	1.2234	0.7591	64.49	12.53	-0.00	1.000
31	1.124	557.1	1.3384	0.29265	21.86	21.34	0.05	1.002	1.4882	0.9234	64.44	12.55	0.03	1.002
32	1.324	656.2	1.5765	0.34472	21.86	21.34	0.05	1.002	1.7530	1.0877	64.53	12.51	-0.02	0.998
33	1.524	755.3	1.8146	0.39679	21.81	21.29	0.00	1.000	2.0178	1.2520	64.50	12.53	-0.00	1.000

ADVERSE PRESSURE GRADIENT (-0.275,-0.002)

RUN =	30473-2	UINF =	19.2	K =	-0.716E-06	CF/2 =	0.00185	DELM =	1.249	DELH =	1.178
PLATE =	9	TWALL =	89.2	BETA =	1.160	ST =	0.00347	DEL1M =	0.298	DEL2H =	0.0859
X(IN) =	34.	DC =	6.919	BF =	-1.103	PPLUS =	0.00901	DEL2M =	0.185	REH =	865.
Z(IN) =	0.	DEL3 =	1.808	F =	-0.00204	VOPLUS=	-0.04968	REM =	1868.	GH =	3.037
POINTS=	35	TGAS =	64.5	BH =	-0.588	REY.NO=	0.393E 06	H =	1.604	GF =	8.758

I	Y	YPLUS	Y/DELM	Y/DC	U	UPLUS	UDE	UBAR	Y/DELH	Y/DEL3	T	TPLUS	TDE	TBAR
1	0.000	0.0	0.0000	0.00000	0.00	0.00	-23.26	0.000	0.0000	0.0000	89.23	0.00	-12.39	0.000
2	0.005	2.0	0.0040	0.00072	2.52	3.05	-20.20	0.131	0.0042	0.0028	83.57	2.83	-9.55	0.229
3	0.006	2.4	0.0048	0.00087	2.70	3.27	-19.99	0.141	0.0051	0.0033	83.22	3.01	-9.38	0.243
4	0.007	2.8	0.0056	0.00101	2.86	3.46	-19.79	0.149	0.0059	0.0039	82.79	3.23	-9.16	0.250
5	0.008	3.2	0.0064	0.00116	3.08	3.73	-19.52	0.160	0.0068	0.0044	82.45	3.40	-8.99	0.274
6	0.009	3.6	0.0072	0.00130	3.27	3.96	-19.29	0.170	0.0076	0.0050	82.24	3.50	-8.89	0.283
7	0.011	4.4	0.0088	0.00159	3.65	4.42	-18.83	0.190	0.0093	0.0061	81.47	3.89	-8.50	0.314
8	0.013	5.2	0.0104	0.00188	4.15	5.03	-18.23	0.216	0.0110	0.0072	80.60	4.32	-8.07	0.349
9	0.015	6.0	0.0120	0.00217	4.61	5.58	-17.67	0.240	0.0127	0.0083	79.88	4.68	-7.70	0.378
10	0.018	7.2	0.0144	0.00260	5.21	6.31	-16.95	0.271	0.0153	0.0100	78.79	5.23	-7.16	0.422
11	0.021	8.4	0.0168	0.00304	5.93	7.18	-16.07	0.309	0.0178	0.0116	77.88	5.69	-6.70	0.459
12	0.024	9.6	0.0192	0.00347	6.37	7.72	-15.54	0.332	0.0204	0.0133	76.97	6.14	-6.25	0.496
13	0.027	10.8	0.0216	0.00390	6.80	8.24	-15.02	0.354	0.0229	0.0149	76.35	6.45	-5.93	0.521
14	0.031	12.4	0.0248	0.00448	7.28	8.82	-14.44	0.379	0.0263	0.0171	75.63	6.81	-5.57	0.550
15	0.036	14.4	0.0288	0.00520	7.88	9.54	-13.71	0.410	0.0306	0.0199	74.95	7.15	-5.23	0.577
16	0.041	16.4	0.0328	0.00593	8.12	9.84	-13.42	0.423	0.0348	0.0227	74.28	7.49	-4.90	0.604
17	0.051	20.4	0.0408	0.00737	8.86	10.73	-12.52	0.461	0.0433	0.0282	73.35	7.95	-4.44	0.642
18	0.061	24.4	0.0489	0.00882	9.28	11.24	-12.02	0.483	0.0518	0.0337	72.73	8.26	-4.12	0.667
19	0.076	30.3	0.0609	0.01098	9.78	11.85	-11.41	0.509	0.0645	0.0420	72.04	8.61	-3.78	0.695
20	0.091	36.3	0.0729	0.01315	10.11	12.25	-11.01	0.527	0.0773	0.0503	71.44	8.91	-3.48	0.719
21	0.111	44.3	0.0889	0.01604	10.31	12.49	-10.77	0.537	0.0942	0.0614	70.98	9.14	-3.25	0.737
22	0.136	54.3	0.1089	0.01966	10.69	12.95	-10.31	0.557	0.1155	0.0752	70.34	9.46	-2.93	0.763
23	0.161	64.3	0.1289	0.02327	11.01	13.34	-9.92	0.573	0.1367	0.0890	70.01	9.62	-2.76	0.777
24	0.211	84.3	0.1690	0.03049	11.48	13.90	-9.35	0.598	0.1791	0.1167	69.33	9.96	-2.42	0.804
25	0.261	104.2	0.2090	0.03772	12.02	14.56	-8.70	0.626	0.2216	0.1443	68.81	10.23	-2.16	0.825
26	0.361	144.2	0.2891	0.05217	12.78	15.48	-7.78	0.666	0.3065	0.1996	68.12	10.57	-1.81	0.853
27	0.461	184.1	0.3692	0.06663	13.61	16.48	-6.77	0.709	0.3914	0.2549	67.44	10.91	-1.47	0.881
28	0.611	244.0	0.4893	0.08830	14.90	18.05	-5.21	0.776	0.5187	0.3379	66.59	11.34	-1.05	0.915
29	0.761	303.9	0.6094	0.10998	16.19	19.61	-3.65	0.843	0.6461	0.4208	65.97	11.65	-0.74	0.940
30	0.911	363.8	0.7296	0.13166	17.35	21.01	-2.24	0.904	0.7734	0.5038	65.39	11.94	-0.45	0.963
31	1.111	443.7	0.8897	0.16057	18.65	22.59	-0.67	0.971	0.9433	0.6144	64.82	12.22	-0.17	0.986
32	1.311	523.5	1.0499	0.18947	19.17	23.22	-0.04	0.998	1.1131	0.7250	64.54	12.36	-0.03	0.998
33	1.511	603.4	1.2101	0.21838	19.26	23.33	0.07	1.003	1.2829	0.8356	64.48	12.39	-0.00	1.000
34	1.711	683.3	1.3702	0.24728	19.20	23.26	0.00	1.000	1.4527	0.9462	64.46	12.40	0.01	1.001
35	1.911	763.1	1.5304	0.27619	19.20	23.26	0.00	1.000	1.6225	1.0568	64.48	12.39	-0.00	1.000

ADVERSE PRESSURE GRADIENT (-0.275,-0.002)

RUN = 30473-3	UINF = 17.6	K =-0.583E-06	CF/2 = 0.00178	DELM = 1.631	DELH = 1.554
PLATE = 12	TWALL = 88.9	BETA = 1.192	ST = 0.00341	DEL1M = 0.392	DEL2H = 0.1106
X(IN) = 46.	DC = 9.310	BF = -1.154	PPLUS = 0.00779	DEL2M = 0.247	REH = 1024.
Z(IN) = 0.	DEL3 = 2.291	F = -0.00205	VOPLUS= -0.05091	REM = 2283.	GH = 2.867
POINTS= 32	TGAS = 64.4	BH = -0.601	REY.NO=0.472E 06	H = 1.591	GF = 8.817

I	Y	YPLUS	Y/DELM	Y/DC	U	UPLUS	UDE	UBAR	Y/DELH	Y/DEL3	T	TPLUS	TDE	TBAR
1	0.000	0.0	0.0000	0.00000	0.00	0.00	-23.73	0.000	0.0000	0.0000	88.85	0.00	-12.36	0.000
2	0.005	1.8	0.0031	0.00054	1.84	2.47	-21.25	0.104	0.0032	0.0022	84.43	2.23	-10.13	0.181
3	0.006	2.2	0.0037	0.00064	2.10	2.82	-20.90	0.119	0.0039	0.0026	83.95	2.47	-9.88	0.200
4	0.007	2.5	0.0043	0.00075	2.22	2.99	-20.74	0.126	0.0045	0.0031	83.42	2.74	-9.62	0.222
5	0.009	3.2	0.0055	0.00097	2.63	3.54	-20.19	0.149	0.0058	0.0039	82.66	3.13	-9.23	0.253
6	0.011	4.0	0.0067	0.00118	3.08	4.14	-19.58	0.175	0.0071	0.0048	81.72	3.60	-8.76	0.291
7	0.013	4.7	0.0080	0.00140	3.44	4.63	-19.10	0.195	0.0084	0.0057	81.06	3.93	-8.42	0.318
8	0.016	5.8	0.0098	0.00172	3.90	5.25	-18.48	0.221	0.0103	0.0070	80.25	4.34	-8.01	0.351
9	0.021	7.6	0.0129	0.00226	4.86	6.54	-17.19	0.276	0.0135	0.0092	78.47	5.24	-7.11	0.424
10	0.026	9.4	0.0159	0.00279	5.71	7.68	-16.05	0.324	0.0167	0.0114	77.16	5.90	-6.45	0.478
11	0.031	11.2	0.0190	0.00333	6.31	8.49	-15.24	0.358	0.0200	0.0135	76.17	6.40	-5.95	0.518
12	0.036	13.0	0.0221	0.00387	6.79	9.13	-14.59	0.385	0.0232	0.0157	75.34	6.82	-5.53	0.552
13	0.041	14.8	0.0251	0.00440	7.02	9.44	-14.28	0.398	0.0264	0.0179	74.64	7.18	-5.18	0.581
14	0.051	18.4	0.0313	0.00548	7.72	10.38	-13.34	0.438	0.0328	0.0223	73.49	7.76	-4.60	0.628
15	0.061	22.0	0.0374	0.00655	8.42	11.32	-12.40	0.477	0.0393	0.0266	72.93	8.04	-4.32	0.650
16	0.071	25.6	0.0435	0.00763	8.44	11.35	-12.37	0.478	0.0457	0.0310	72.22	8.39	-3.96	0.679
17	0.086	31.0	0.0527	0.00924	8.80	11.84	-11.89	0.499	0.0554	0.0375	71.59	8.71	-3.64	0.705
18	0.101	36.4	0.0619	0.01085	9.20	12.37	-11.35	0.522	0.0650	0.0441	71.18	8.92	-3.44	0.722
19	0.116	41.8	0.0711	0.01246	9.29	12.49	-11.23	0.527	0.0747	0.0506	70.77	9.13	-3.23	0.738
20	0.141	50.8	0.0865	0.01515	9.53	12.82	-10.91	0.540	0.0908	0.0616	70.33	9.35	-3.01	0.756
21	0.166	59.8	0.1018	0.01783	9.82	13.21	-10.52	0.557	0.1069	0.0725	69.95	9.54	-2.81	0.772
22	0.216	77.8	0.1325	0.02320	10.27	13.81	-9.91	0.582	0.1390	0.0943	69.45	9.79	-2.56	0.792
23	0.316	113.8	0.1938	0.03394	10.73	14.43	-9.29	0.608	0.2034	0.1379	68.67	10.19	-2.17	0.824
24	0.416	149.8	0.2551	0.04468	11.31	15.21	-8.51	0.641	0.2678	0.1816	68.07	10.49	-1.86	0.849
25	0.516	185.8	0.3165	0.05542	11.81	15.88	-7.84	0.670	0.3321	0.2253	67.59	10.73	-1.62	0.868
26	0.666	239.8	0.4084	0.07154	12.88	17.32	-6.40	0.730	0.4287	0.2907	66.96	11.05	-1.30	0.894
27	0.816	293.8	0.5004	0.08765	13.78	18.53	-5.19	0.781	0.5252	0.3562	66.46	11.31	-1.05	0.915
28	1.016	365.8	0.6231	0.10913	14.97	20.13	-3.59	0.849	0.6540	0.4435	65.83	11.62	-0.74	0.940
29	1.216	437.8	0.7457	0.13061	15.98	21.49	-2.23	0.906	0.7827	0.5308	65.25	11.91	-0.44	0.964
30	1.416	509.9	0.8684	0.15210	16.94	22.78	-0.94	0.960	0.9114	0.6181	64.79	12.15	-0.21	0.983
31	1.666	599.9	1.0217	0.17895	17.55	23.60	-0.12	0.995	1.0724	0.7273	64.47	12.31	-0.05	0.996
32	1.916	689.9	1.1750	0.20580	17.64	23.73	0.00	1.000	1.2333	0.8364	64.37	12.36	-0.00	1.000

ADVERSE PRESSURE GRADIENT (-0.275,-0.002)

RUN = 30473-4	UINF = 17.0	K =-0.495E-06	CF/2 = 0.00187	DEL4 = 1.875	DELH = 1.822
PLATE = 15	TWALL = 88.9	BETA = 0.991	ST = 0.00334	DEL1M = 0.419	DEL2H = 0.1294
X(IN) = 58.	DC = 9.693	BF = -1.076	PPLUS = 0.00613	DEL2M = 0.272	REH = 1155.
Z(IN) = 0.	DEL3 = 2.684	F = -0.00201	VOPLUS= -0.04867	REM = 2430.	GH = 2.922
POINTS= 38	TGAS = 64.5	BH = -0.602	REY.NO=0.562E 06	H = 1.539	GF = 8.099

I	Y	YPLUS	Y/DELM	Y/DC	U	UPLUS	UDE	UBAR	Y/DELH	Y/DEL3	T	TPLUS	TDE	TBAR
1	0.000	0.0	0.0000	0.00000	0.00	0.00	-23.14	0.000	0.0000	0.0000	88.89	0.00	-12.94	0.000
2	0.005	1.8	0.0027	0.00052	1.62	2.20	-20.93	0.095	0.0027	0.0019	85.13	1.99	-10.95	0.154
3	0.006	2.1	0.0032	0.00062	1.81	2.46	-20.67	0.106	0.0033	0.0022	84.80	2.17	-10.77	0.167
4	0.007	2.5	0.0037	0.00072	1.98	2.69	-20.44	0.116	0.0038	0.0026	84.34	2.41	-10.53	0.186
5	0.008	2.8	0.0043	0.00083	2.18	2.97	-20.17	0.128	0.0044	0.0030	84.09	2.54	-10.39	0.197
6	0.009	3.2	0.0048	0.00093	2.32	3.16	-19.98	0.136	0.0049	0.0034	83.67	2.77	-10.17	0.214
7	0.011	3.9	0.0059	0.00113	2.72	3.70	-19.44	0.160	0.0060	0.0041	82.82	3.22	-9.72	0.249
8	0.013	4.6	0.0069	0.00134	3.09	4.20	-18.93	0.182	0.0071	0.0048	82.12	3.59	-9.35	0.277
9	0.015	5.3	0.0080	0.00155	3.42	4.65	-18.48	0.201	0.0082	0.0056	81.35	4.00	-8.94	0.309
10	0.018	6.4	0.0096	0.00186	4.25	5.78	-17.36	0.250	0.0099	0.0067	80.31	4.55	-8.39	0.352
11	0.021	7.5	0.0112	0.00217	4.61	6.27	-16.87	0.271	0.0115	0.0078	79.35	5.06	-7.88	0.391
12	0.025	8.9	0.0133	0.00258	5.21	7.09	-16.05	0.306	0.0137	0.0093	77.92	5.82	-7.12	0.450
13	0.030	10.7	0.0160	0.00309	5.99	8.15	-14.99	0.352	0.0165	0.0112	77.08	6.26	-6.67	0.484
14	0.035	12.5	0.0187	0.00361	6.67	9.07	-14.06	0.392	0.0192	0.0130	76.01	6.83	-6.10	0.528
15	0.040	14.2	0.0213	0.00413	6.98	9.49	-13.64	0.410	0.0220	0.0149	75.38	7.17	-5.77	0.554
16	0.050	17.8	0.0267	0.00516	7.73	10.51	-12.62	0.454	0.0274	0.0186	74.04	7.88	-5.06	0.609
17	0.060	21.4	0.0320	0.00619	8.19	11.14	-12.00	0.481	0.0329	0.0224	73.20	8.32	-4.61	0.643
18	0.070	24.9	0.0373	0.00722	8.68	11.81	-11.33	0.510	0.0384	0.0261	72.62	8.63	-4.31	0.667
19	0.085	30.3	0.0453	0.00877	8.88	12.08	-11.06	0.522	0.0467	0.0317	71.88	9.02	-3.92	0.697
20	0.105	37.4	0.0560	0.01083	9.34	12.70	-10.43	0.549	0.0576	0.0391	71.22	9.37	-3.57	0.724
21	0.125	44.5	0.0667	0.01290	9.57	13.02	-10.12	0.563	0.0686	0.0466	70.80	9.59	-3.34	0.741
22	0.150	53.4	0.0800	0.01547	9.81	13.34	-9.79	0.577	0.0823	0.0559	70.31	9.85	-3.08	0.761
23	0.175	62.3	0.0933	0.01805	9.98	13.57	-9.56	0.587	0.0960	0.0652	69.95	10.04	-2.89	0.776
24	0.225	80.1	0.1200	0.02321	10.28	13.98	-9.15	0.604	0.1235	0.0838	69.54	10.26	-2.68	0.793
25	0.325	115.7	0.1733	0.03353	10.73	14.59	-8.54	0.631	0.1784	0.1211	68.66	10.73	-2.21	0.829
26	0.425	151.3	0.2267	0.04385	11.27	15.33	-7.81	0.663	0.2333	0.1583	68.30	10.92	-2.02	0.844
27	0.575	204.7	0.3067	0.05932	11.90	16.19	-6.95	0.700	0.3156	0.2142	67.65	11.26	-1.67	0.870
28	0.725	258.1	0.3867	0.07479	12.47	16.96	-6.18	0.733	0.3979	0.2701	67.07	11.57	-1.36	0.894
29	0.925	329.3	0.4934	0.09543	13.49	18.35	-4.79	0.793	0.5077	0.3446	66.53	11.86	-1.08	0.916
30	1.125	400.5	0.6000	0.11606	14.24	19.37	-3.77	0.837	0.6175	0.4191	65.96	12.16	-0.77	0.940
31	1.325	471.7	0.7067	0.13669	15.27	20.77	-2.37	0.898	0.7272	0.4936	65.55	12.38	-0.56	0.956
32	1.525	543.0	0.8134	0.15733	15.88	21.60	-1.54	0.934	0.8370	0.5681	65.18	12.57	-0.37	0.972
33	1.725	614.2	0.9200	0.17796	16.60	22.58	-0.56	0.976	0.9468	0.6426	64.84	12.75	-0.19	0.986
34	1.925	685.4	1.0267	0.19859	16.92	23.01	-0.12	0.995	1.0565	0.7171	64.62	12.87	-0.07	0.995
35	2.175	774.4	1.1600	0.22438	17.10	23.26	0.12	1.005	1.1938	0.8102	64.52	12.92	-0.02	0.999
36	2.425	863.4	1.2934	0.25017	17.08	23.23	0.10	1.004	1.3310	0.9034	64.47	12.95	0.01	1.001
37	2.675	952.4	1.4267	0.27597	17.07	23.22	0.08	1.004	1.4682	0.9965	64.53	12.92	-0.02	0.998
38	2.925	1041.4	1.5601	0.30176	17.01	23.14	0.00	1.000	1.6054	1.0896	64.49	12.94	-0.00	1.000

ADVERSE PRESSURE GRADIENT (-0.275,-0.002)

RUN	=	30573-5	UINF	=	16.6	K	=-0.429E-06	CF/2	=	0.00191	DELM	=	2.138	DELH	= 2.325
PLATE	=	18	TWALL	=	89.5	BETA	= 0.908	ST	=	0.00325	DEL1M	=	0.467	DEL2H	= 0.1504
X(IN)	=	70.	DC	=	10.685	BF	= -1.044	PPLUS	=	0.00515	DEL2M	=	0.310	REH	= 1301.
Z(IN)	=	0.	DEL3	=	3.121	F	= -0.00199	VOPLUS	=	-0.04774	REM	=	2678.	GH	= 2.812
POINTS	=	39	TGAS	=	64.6	BH	= -0.612	REY.NO	=	0.649E 06	H	=	1.507	GF	= 7.702

I	Y	YPLUS	Y/DELM	Y/DC	U	UPLUS	UDE	UBAR	Y/DELH	Y/DEL3	T	TPLUS	TDE	TBAR
1	0.000	0.0	0.0000	0.00000	0.00	0.00	-22.90	0.000	0.0000	0.0000	89.47	0.00	-13.43	0.000
2	0.005	1.7	0.0023	0.00047	1.58	2.19	-20.72	0.095	0.0022	0.0016	85.37	2.21	-11.22	0.165
3	0.006	2.1	0.0028	0.00056	1.79	2.48	-20.43	0.108	0.0026	0.0019	85.12	2.35	-11.08	0.175
4	0.007	2.4	0.0033	0.00066	2.03	2.81	-20.09	0.123	0.0030	0.0022	84.74	2.55	-10.88	0.190
5	0.008	2.8	0.0037	0.00075	2.17	3.00	-19.90	0.131	0.0034	0.0026	84.21	2.84	-10.59	0.211
6	0.010	3.5	0.0047	0.00094	2.62	3.63	-19.28	0.158	0.0043	0.0032	83.50	3.22	-10.21	0.240
7	0.012	4.2	0.0056	0.00112	2.87	3.97	-18.93	0.173	0.0052	0.0038	82.73	3.64	-9.79	0.271
8	0.014	4.9	0.0065	0.00131	3.19	4.41	-18.49	0.193	0.0060	0.0045	82.02	4.02	-9.41	0.299
9	0.017	5.9	0.0079	0.00159	3.76	5.20	-17.70	0.227	0.0073	0.0054	81.05	4.54	-8.89	0.338
10	0.021	7.3	0.0098	0.00197	4.46	6.17	-16.73	0.269	0.0090	0.0067	79.73	5.26	-8.17	0.391
11	0.026	9.0	0.0122	0.00243	5.46	7.56	-15.35	0.330	0.0112	0.0083	78.60	5.87	-7.56	0.437
12	0.031	10.8	0.0145	0.00290	5.94	8.22	-14.68	0.359	0.0133	0.0099	77.47	6.48	-6.95	0.482
13	0.036	12.5	0.0168	0.00337	6.38	8.83	-14.07	0.385	0.0155	0.0115	76.40	7.05	-6.38	0.525
14	0.041	14.3	0.0192	0.00384	6.92	9.58	-13.33	0.418	0.0176	0.0131	75.58	7.50	-5.93	0.558
15	0.046	16.0	0.0215	0.00431	7.15	9.89	-13.01	0.432	0.0198	0.0147	74.90	7.86	-5.57	0.585
16	0.051	17.8	0.0238	0.00477	7.59	10.50	-12.40	0.459	0.0219	0.0163	74.32	8.18	-5.25	0.609
17	0.061	21.2	0.0285	0.00571	8.07	11.17	-11.73	0.488	0.0262	0.0195	73.56	8.59	-4.84	0.639
18	0.071	24.7	0.0332	0.00664	8.33	11.53	-11.38	0.503	0.0305	0.0228	72.85	8.97	-4.46	0.667
19	0.086	29.9	0.0402	0.00805	8.99	12.44	-10.46	0.543	0.0370	0.0276	72.19	9.32	-4.11	0.694
20	0.101	35.2	0.0472	0.00945	9.18	12.70	-10.20	0.555	0.0434	0.0324	71.72	9.58	-3.85	0.713
21	0.121	42.1	0.0566	0.01132	9.28	12.84	-10.06	0.561	0.0520	0.0388	70.91	10.01	-3.42	0.745
22	0.146	50.8	0.0683	0.01366	9.54	13.20	-9.70	0.576	0.0628	0.0468	70.65	10.15	-3.28	0.756
23	0.171	59.5	0.0800	0.01600	9.79	13.55	-9.35	0.592	0.0735	0.0548	70.28	10.35	-3.08	0.771
24	0.221	76.9	0.1033	0.02068	10.24	14.17	-8.73	0.619	0.0950	0.0708	69.64	10.70	-2.73	0.796
25	0.321	111.7	0.1501	0.03004	10.34	14.31	-8.59	0.625	0.1381	0.1029	68.87	11.11	-2.32	0.827
26	0.421	146.5	0.1969	0.03940	10.98	15.19	-7.71	0.663	0.1811	0.1349	68.55	11.29	-2.14	0.840
27	0.571	198.7	0.2670	0.05344	11.37	15.73	-7.17	0.687	0.2456	0.1830	67.64	11.78	-1.65	0.877
28	0.721	251.0	0.3372	0.06748	11.96	16.55	-6.35	0.723	0.3101	0.2310	67.39	11.91	-1.52	0.887
29	0.921	320.6	0.4307	0.08619	12.79	17.70	-5.20	0.773	0.3961	0.2951	66.93	12.16	-1.27	0.905
30	1.121	390.2	0.5242	0.10491	13.48	18.65	-4.25	0.815	0.4821	0.3592	66.46	12.42	-1.01	0.924
31	1.321	459.8	0.6177	0.12363	14.06	19.46	-3.45	0.850	0.5681	0.4233	65.94	12.70	-0.73	0.945
32	1.521	529.4	0.7113	0.14235	14.70	20.34	-2.56	0.888	0.6542	0.4874	65.72	12.81	-0.62	0.954
33	1.721	599.0	0.8048	0.16107	15.38	21.28	-1.62	0.929	0.7402	0.5515	65.30	13.04	-0.39	0.971
34	1.921	668.6	0.8983	0.17978	15.88	21.98	-0.93	0.960	0.8262	0.6156	64.99	13.21	-0.23	0.983
35	2.171	755.6	1.0152	0.20318	16.46	22.78	-0.12	0.995	0.9337	0.6957	64.93	13.24	-0.19	0.986
36	2.421	842.7	1.1321	0.22658	16.61	22.99	0.08	1.004	1.0412	0.7758	64.75	13.34	-0.10	0.993
37	2.671	929.7	1.2490	0.24997	16.61	22.99	0.08	1.004	1.1488	0.8559	64.64	13.40	-0.04	0.997
38	2.921	1016.7	1.3659	0.27337	16.64	23.03	0.12	1.005	1.2563	0.9360	64.76	13.33	-0.10	0.992
39	3.171	1103.7	1.4828	0.29677	16.55	22.90	0.00	1.000	1.3638	1.0162	64.57	13.43	-0.00	1.000

ADVERSE PRESSURE GRADIENT (-0.275,-0.002)

RUN	= 30573-6	UINF	= 15.8	K	=-0.376E-06	CF/2	= 0.00190	DELM	= 2.644	DELH	= 2.596
PLATE	= 21	TWALL	= 89.8	BETA	= 0.944	ST	= 0.00318	DEL1M	= 0.578	DEL2H	= 0.1703
X(IN)	= 82.	DC	= 13.277	BF	= -1.065	PPLUS	= 0.00455	DEL2M	= 0.382	REH	= 1403.
Z(IN)	= 0.	DEL3	= 3.687	F	= -0.00202	VOPLUS	= -0.04859	REM	= 3144.	GH	= 2.877
POINTS	= 40	TGAS	= 64.8	BH	= -0.635	REY.NO	= 0.717E 06	H	= 1.515	GF	= 7.805

I	Y	YPLUS	Y/DELM	Y/DC	U	UPLUS	UDE	UBAR	Y/DELH	Y/DEL3	T	TPLUS	TDE	TBAR
1	0.000	0.0	0.0000	0.00000	0.00	0.00	-22.96	0.000	0.0000	0.0000	89.82	0.00	-13.70	0.000
2	0.005	1.7	0.0019	0.00038	1.37	1.99	-20.96	0.087	0.0019	0.0014	86.31	1.92	-11.78	0.140
3	0.006	2.0	0.0023	0.00045	1.49	2.17	-20.79	0.094	0.0023	0.0016	85.87	2.16	-11.54	0.158
4	0.007	2.3	0.0026	0.00053	1.59	2.31	-20.64	0.101	0.0027	0.0019	85.44	2.39	-11.30	0.175
5	0.008	2.6	0.0030	0.00060	1.70	2.47	-20.48	0.108	0.0031	0.0022	85.35	2.44	-11.25	0.178
6	0.009	3.0	0.0034	0.00068	1.88	2.74	-20.22	0.119	0.0035	0.0024	85.31	2.46	-11.23	0.180
7	0.011	3.6	0.0042	0.00083	2.03	2.96	-20.00	0.129	0.0042	0.0030	84.28	3.03	-10.67	0.221
8	0.013	4.3	0.0049	0.00098	2.36	3.44	-19.52	0.150	0.0050	0.0035	83.58	3.41	-10.29	0.249
9	0.016	5.3	0.0061	0.00121	2.89	4.21	-18.75	0.183	0.0062	0.0043	82.53	3.98	-9.71	0.291
10	0.019	6.3	0.0072	0.00143	3.30	4.80	-18.15	0.209	0.0073	0.0052	81.70	4.44	-9.26	0.324
11	0.022	7.3	0.0083	0.00166	3.81	5.55	-17.41	0.242	0.0085	0.0060	80.80	4.93	-8.77	0.360
12	0.026	8.6	0.0098	0.00196	4.40	6.41	-16.55	0.279	0.0100	0.0071	79.55	5.61	-8.08	0.410
13	0.031	10.2	0.0117	0.00233	4.99	7.26	-15.69	0.316	0.0119	0.0084	78.44	6.22	-7.47	0.454
14	0.036	11.9	0.0136	0.00271	5.44	7.92	-15.04	0.345	0.0139	0.0098	77.53	6.72	-6.98	0.490
15	0.041	13.6	0.0155	0.00309	5.92	8.62	-14.34	0.375	0.0158	0.0111	76.61	7.22	-6.47	0.527
16	0.046	15.2	0.0174	0.00346	6.40	9.32	-13.64	0.406	0.0177	0.0125	76.04	7.53	-6.16	0.550
17	0.056	18.5	0.0212	0.00422	7.01	10.20	-12.75	0.445	0.0216	0.0152	74.83	8.19	-5.50	0.598
18	0.066	21.8	0.0250	0.00497	7.14	10.39	-12.56	0.453	0.0254	0.0179	73.80	8.76	-4.94	0.639
19	0.081	26.8	0.0306	0.00610	7.87	11.46	-11.50	0.499	0.0312	0.0220	72.92	9.24	-4.46	0.674
20	0.096	31.7	0.0363	0.00723	8.22	11.97	-10.99	0.521	0.0370	0.0260	72.25	9.60	-4.09	0.701
21	0.116	38.3	0.0439	0.00874	8.29	12.07	-10.89	0.526	0.0447	0.0315	71.61	9.95	-3.75	0.726
22	0.141	46.6	0.0533	0.01062	8.66	12.61	-10.35	0.549	0.0543	0.0382	71.11	10.22	-3.47	0.746
23	0.166	54.9	0.0628	0.01250	8.85	12.88	-10.07	0.561	0.0640	0.0450	70.73	10.43	-3.26	0.761
24	0.216	71.4	0.0817	0.01627	9.20	13.39	-9.56	0.583	0.0832	0.0586	70.08	10.78	-2.91	0.787
25	0.316	104.4	0.1195	0.02380	9.56	13.92	-9.04	0.606	0.1217	0.0857	69.38	11.17	-2.53	0.815
26	0.416	137.5	0.1573	0.03133	10.00	14.56	-8.40	0.634	0.1603	0.1128	69.16	11.29	-2.41	0.824
27	0.566	187.1	0.2141	0.04263	10.34	15.05	-7.90	0.656	0.2181	0.1535	68.35	11.73	-1.96	0.856
28	0.716	236.6	0.2708	0.05393	10.87	15.82	-7.13	0.689	0.2759	0.1942	67.79	12.04	-1.66	0.879
29	0.916	302.7	0.3465	0.06899	11.55	16.81	-6.14	0.732	0.3529	0.2484	67.65	12.11	-1.58	0.884
30	1.166	385.4	0.4410	0.08782	12.20	17.76	-5.20	0.774	0.4492	0.3162	66.89	12.53	-1.16	0.915
31	1.416	468.0	0.5356	0.10665	12.84	18.69	-4.27	0.814	0.5456	0.3840	66.41	12.79	-0.90	0.934
32	1.666	550.6	0.6301	0.12548	13.59	19.78	-3.17	0.862	0.6419	0.4518	66.07	12.98	-0.72	0.948
33	1.916	633.2	0.7247	0.14431	14.13	20.57	-2.39	0.896	0.7382	0.5196	65.65	13.21	-0.49	0.964
34	2.166	715.9	0.8193	0.16314	14.94	21.75	-1.21	0.947	0.8345	0.5874	65.40	13.34	-0.36	0.974
35	2.416	798.5	0.9138	0.18197	15.43	22.46	-0.49	0.978	0.9308	0.6552	65.23	13.44	-0.26	0.981
36	2.666	881.1	1.0084	0.20080	15.63	22.75	-0.20	0.991	1.0272	0.7230	64.91	13.61	-0.09	0.994
37	2.916	963.7	1.1029	0.21963	15.74	22.91	-0.04	0.998	1.1235	0.7908	64.81	13.67	-0.03	0.998
38	3.166	1046.4	1.1975	0.23846	15.82	23.03	0.07	1.003	1.2198	0.8586	64.78	13.68	-0.02	0.999
39	3.416	1129.0	1.2920	0.25729	15.77	22.96	0.00	1.000	1.3161	0.9264	64.70	13.73	0.03	1.002
40	3.666	1211.6	1.3866	0.27612	15.77	22.96	0.00	1.000	1.4124	0.9942	64.75	13.70	-0.00	1.000

ADVERSE PRESSURE GRADIENT (-0.275,-0.004)

RUN = 31173-1	UINF = 21.5	K =-0.947E-06	CF/2 = 0.00329	DELM = 0.646	DELH = 0.514
PLATE = 6	TWALL = 77.4	BETA = 0.342	ST = 0.00504	DEL1M = 0.102	DEL2H = 0.0313
X(IN) = 22.	DC = 1.773	BF = -1.244	PPLUS = 0.00502	DEL2M = 0.071	REH = 366.
Z(IN) = 0.	DEL3 = 0.571	F = -0.00409	VOPLUS= -0.07467	REM = 834.	GH = 3.048
POINTS= 33	TGAS = 53.3	BH = -0.812	REY.NO=0.315E 06	H = 1.423	GF = 5.134

I	Y	YPLUS	Y/DELM	Y/DC	U	UPLUS	UDE	UBAR	Y/DELH	Y/DEL3	T	TPLUS	TDE	TBAR
1	0.000	0.0	0.0000	0.00000	0.00	0.00	-17.44	0.000	0.0000	0.0000	77.38	0.00	-11.38	0.000
2	0.005	3.1	0.0077	0.00282	4.75	3.85	-13.59	0.221	0.0097	0.0088	70.17	3.41	-7.96	0.300
3	0.006	3.7	0.0093	0.00338	5.23	4.24	-13.20	0.243	0.0117	0.0105	69.54	3.71	-7.66	0.326
4	0.007	4.3	0.0108	0.00395	5.95	4.83	-12.61	0.277	0.0136	0.0123	68.78	4.07	-7.30	0.358
5	0.008	4.9	0.0124	0.00451	6.21	5.04	-12.40	0.289	0.0156	0.0140	68.15	4.37	-7.01	0.384
6	0.009	5.6	0.0139	0.00508	6.61	5.36	-12.08	0.307	0.0175	0.0158	67.65	4.60	-6.77	0.405
7	0.010	6.2	0.0155	0.00564	7.22	5.86	-11.58	0.336	0.0194	0.0175	66.95	4.93	-6.44	0.434
8	0.012	7.4	0.0186	0.00677	7.97	6.47	-10.98	0.371	0.0233	0.0210	66.18	5.30	-6.07	0.466
9	0.014	8.6	0.0217	0.00790	8.84	7.17	-10.27	0.411	0.0272	0.0245	65.13	5.79	-5.58	0.509
10	0.016	9.9	0.0248	0.00903	9.58	7.77	-9.67	0.446	0.0311	0.0280	64.26	6.20	-5.17	0.545
11	0.018	11.1	0.0279	0.01015	10.32	8.37	-9.07	0.480	0.0350	0.0315	63.41	6.61	-4.76	0.581
12	0.020	12.4	0.0310	0.01128	10.89	8.83	-8.61	0.507	0.0389	0.0351	62.83	6.88	-4.49	0.605
13	0.023	14.2	0.0356	0.01297	11.58	9.39	-8.05	0.539	0.0447	0.0403	61.94	7.30	-4.07	0.642
14	0.026	16.1	0.0402	0.01467	12.09	9.81	-7.63	0.562	0.0505	0.0456	61.17	7.67	-3.70	0.674
15	0.030	18.5	0.0464	0.01692	12.83	10.41	-7.03	0.597	0.0583	0.0526	60.13	8.16	-3.21	0.717
16	0.035	21.6	0.0542	0.01974	13.33	10.81	-6.63	0.620	0.0680	0.0613	59.70	8.36	-3.01	0.735
17	0.040	24.7	0.0619	0.02256	13.80	11.19	-6.25	0.642	0.0778	0.0701	59.31	8.55	-2.82	0.751
18	0.045	27.8	0.0697	0.02538	14.14	11.47	-5.97	0.658	0.0875	0.0789	58.73	8.82	-2.55	0.776
19	0.055	34.0	0.0851	0.03102	14.55	11.80	-5.64	0.677	0.1069	0.0964	58.03	9.15	-2.22	0.804
20	0.070	43.2	0.1084	0.03948	15.15	12.29	-5.15	0.705	0.1361	0.1227	57.43	9.43	-1.94	0.829
21	0.085	52.5	0.1316	0.04795	15.59	12.65	-4.79	0.725	0.1652	0.1490	57.03	9.62	-1.75	0.846
22	0.100	61.8	0.1548	0.05641	15.80	12.82	-4.62	0.735	0.1944	0.1753	56.67	9.79	-1.58	0.861
23	0.120	74.1	0.1858	0.06769	16.25	13.18	-4.26	0.756	0.2333	0.2103	56.21	10.01	-1.36	0.880
24	0.170	105.0	0.2632	0.09589	16.95	13.75	-3.69	0.788	0.3304	0.2980	55.66	10.27	-1.10	0.903
25	0.220	135.9	0.3406	0.12410	17.64	14.31	-3.13	0.820	0.4276	0.3856	55.12	10.53	-0.84	0.926
26	0.320	197.6	0.4954	0.18050	18.81	15.26	-2.18	0.875	0.6220	0.5609	54.39	10.87	-0.50	0.956
27	0.420	259.4	0.6502	0.23691	19.81	16.07	-1.37	0.921	0.8164	0.7362	53.87	11.12	-0.26	0.977
28	0.520	321.2	0.8050	0.29332	20.65	16.75	-0.69	0.960	1.0108	0.9114	53.55	11.27	-0.10	0.991
29	0.620	382.9	0.9598	0.34972	21.22	17.21	-0.23	0.987	1.2051	1.0867	53.35	11.37	-0.01	0.999
30	0.720	444.7	1.1146	0.40613	21.47	17.42	-0.02	0.999	1.3995	1.2620	53.27	11.40	0.03	1.002
31	0.920	568.2	1.4242	0.51894	21.51	17.45	0.01	1.000	1.7883	1.6125	53.21	11.43	0.06	1.005
32	1.120	691.7	1.7338	0.63176	21.51	17.45	0.01	1.000	2.1770	1.9631	53.29	11.40	0.02	1.002
33	1.320	815.3	2.0434	0.74457	21.50	17.44	0.00	1.000	2.5658	2.3136	53.33	11.38	-0.00	1.000

ADVERSE PRESSURE GRADIENT (-0.275,-0.004)

RUN =	31173-2	UINF =	19.0	K =	-0.708E-06	CF/2 =	0.00329	DELM =	0.886	DELH =	0.699
PLATE =	9	TWALL =	77.8	BETA =	0.323	ST =	0.00485	DEL1M =	0.146	DEL2H =	0.0382
X(IN) =	34.	DC =	2.542	BF =	-1.266	PPLUS =	0.00375	DEL2M =	0.104	REH =	394.
Z(IN) =	0.	DEL3 =	0.735	F =	-0.00417	VOPLUS=	-0.07611	REM =	1072.	GH =	3.095
POINTS=	34	TGAS =	53.4	BH =	-0.860	REY.NO=	0.402E 06	H =	1.404	GF =	5.015

I	Y	YPLUS	Y/DELM	Y/DC	U	UPLUS	UDE	UBAR	Y/DELH	Y/DEL3	T	TPLUS	TDE	TBAR
1	0.000	0.0	0.0000	0.00000	0.00	0.00	-17.43	0.000	0.0000	0.0000	77.76	0.00	-11.83	0.000
2	0.005	2.7	0.0056	0.00197	3.84	3.52	-13.90	0.202	0.0072	0.0068	70.81	3.38	-8.45	0.286
3	0.006	3.3	0.0068	0.00236	4.24	3.89	-13.54	0.223	0.0086	0.0082	70.36	3.60	-8.23	0.304
4	0.007	3.8	0.0079	0.00275	4.68	4.29	-13.13	0.246	0.0100	0.0095	69.56	3.99	-7.84	0.337
5	0.008	4.4	0.0090	0.00315	4.95	4.54	-12.89	0.261	0.0114	0.0109	69.24	4.14	-7.68	0.350
6	0.009	4.9	0.0102	0.00354	5.27	4.83	-12.59	0.277	0.0129	0.0122	68.79	4.36	-7.46	0.359
7	0.011	6.0	0.0124	0.00433	5.98	5.48	-11.94	0.315	0.0157	0.0150	67.67	4.91	-6.92	0.415
8	0.013	7.1	0.0147	0.00511	6.61	6.06	-11.36	0.348	0.0186	0.0177	66.96	5.25	-6.57	0.444
9	0.015	8.2	0.0169	0.00590	7.14	6.55	-10.88	0.376	0.0215	0.0204	66.16	5.64	-6.18	0.477
10	0.017	9.3	0.0192	0.00669	7.97	7.31	-10.12	0.419	0.0243	0.0231	65.21	6.11	-5.72	0.516
11	0.020	10.9	0.0226	0.00787	8.59	7.88	-9.55	0.452	0.0286	0.0272	64.31	6.54	-5.29	0.553
12	0.023	12.6	0.0260	0.00905	9.33	8.56	-8.87	0.491	0.0329	0.0313	63.28	7.04	-4.79	0.595
13	0.027	14.7	0.0305	0.01062	9.98	9.15	-8.27	0.525	0.0386	0.0367	62.26	7.54	-4.29	0.637
14	0.032	17.5	0.0361	0.01259	10.74	9.85	-7.58	0.565	0.0458	0.0435	61.34	7.99	-3.84	0.675
15	0.037	20.2	0.0418	0.01456	11.12	10.20	-7.23	0.585	0.0529	0.0503	60.56	8.37	-3.46	0.707
16	0.042	22.9	0.0474	0.01652	11.60	10.64	-6.79	0.611	0.0601	0.0571	60.05	8.61	-3.21	0.728
17	0.047	25.6	0.0531	0.01849	11.98	10.99	-6.44	0.631	0.0672	0.0639	59.55	8.86	-2.97	0.749
18	0.057	31.1	0.0644	0.02242	12.13	11.13	-6.30	0.638	0.0815	0.0775	58.61	9.31	-2.51	0.787
19	0.072	39.3	0.0813	0.02832	12.90	11.83	-5.59	0.679	0.1030	0.0979	57.91	9.66	-2.17	0.816
20	0.087	47.5	0.0982	0.03422	13.35	12.24	-5.18	0.703	0.1245	0.1183	57.48	9.87	-1.96	0.834
21	0.107	58.4	0.1208	0.04209	13.56	12.44	-4.99	0.714	0.1531	0.1455	57.12	10.04	-1.79	0.849
22	0.132	72.0	0.1491	0.05193	13.90	12.75	-4.68	0.732	0.1888	0.1795	56.58	10.30	-1.52	0.871
23	0.157	85.7	0.1773	0.06176	14.07	12.90	-4.52	0.741	0.2246	0.2135	56.27	10.45	-1.37	0.884
24	0.207	113.0	0.2337	0.08143	14.38	13.19	-4.24	0.757	0.2961	0.2815	55.84	10.66	-1.17	0.901
25	0.257	140.2	0.2902	0.10110	15.05	13.80	-3.62	0.792	0.3677	0.3495	55.27	10.94	-0.89	0.924
26	0.307	167.5	0.3467	0.12077	15.40	14.12	-3.30	0.811	0.4392	0.4175	55.06	11.04	-0.79	0.933
27	0.407	222.1	0.4596	0.16011	16.09	14.76	-2.67	0.847	0.5823	0.5535	54.49	11.32	-0.51	0.957
28	0.507	276.6	0.5725	0.19944	16.83	15.44	-1.99	0.886	0.7253	0.6894	54.26	11.43	-0.40	0.966
29	0.607	331.2	0.6854	0.23878	17.56	16.11	-1.32	0.924	0.8684	0.8254	53.92	11.60	-0.23	0.980
30	0.757	413.1	0.8548	0.29779	18.45	16.92	-0.50	0.971	1.0830	1.0294	53.52	11.79	-0.04	0.996
31	0.907	494.9	1.0242	0.35680	18.87	17.31	-0.12	0.993	1.2976	1.2334	53.35	11.87	0.04	1.003
32	1.107	604.0	1.2500	0.43547	19.00	17.43	0.00	1.000	1.5837	1.5054	53.29	11.90	0.07	1.006
33	1.307	713.2	1.4759	0.51415	18.93	17.36	-0.06	0.996	1.8698	1.7773	53.20	11.94	0.11	1.009
34	1.507	822.3	1.7017	0.59282	19.00	17.43	0.00	1.000	2.1560	2.0493	53.43	11.83	-0.00	1.000

ADVERSE PRESSURE GRADIENT (-0.275,-0.004)

RUN =	31173-3	UINF =	17.4	K =	-0.577E-06	CF/2 =	0.00322	DELM =	1.059	DELH =	0.915
PLATE =	12	TWALL =	77.7	BETA =	0.283	ST =	0.00471	DEL1M =	0.167	DEL2H =	0.0551
X(IN) =	46.	DC =	2.951	BF =	-1.278	PPLUS =	0.00316	DEL2M =	0.119	REH =	520.
Z(IN) =	0.	DEL3 =	1.012	F =	-0.00411	VOPLUS=	-0.07587	REM =	1124.	GH =	2.906
POINTS=	36	TGAS =	53.5	BH =	-0.873	REY.NO=	0.481E 06	H =	1.405	GF =	5.083

I	Y	YPLUS	Y/DELM	Y/DC	U	UPLUS	UDE	UBAR	Y/DELH	Y/DEL3	T	TPLUS	TDE	TBAR
1	0.000	0.0	0.0000	0.00000	0.00	0.00	-17.63	0.000	0.0000	0.0000	77.66	0.00	-12.04	0.000
2	0.005	2.5	0.0047	0.00169	2.80	2.84	-14.79	0.161	0.0055	0.0049	72.36	2.65	-9.39	0.220
3	0.006	3.0	0.0057	0.00203	3.02	3.06	-14.57	0.174	0.0066	0.0059	71.91	2.87	-9.17	0.238
4	0.007	3.5	0.0066	0.00237	3.35	3.40	-14.24	0.193	0.0076	0.0069	71.36	3.14	-8.89	0.261
5	0.008	4.0	0.0076	0.00271	3.62	3.67	-13.96	0.208	0.0087	0.0079	70.83	3.41	-8.63	0.283
6	0.009	4.4	0.0085	0.00305	3.96	4.02	-13.62	0.228	0.0098	0.0089	70.48	3.58	-8.45	0.298
7	0.011	5.4	0.0104	0.00373	4.62	4.68	-12.95	0.266	0.0120	0.0109	69.39	4.13	-7.91	0.343
8	0.013	6.4	0.0123	0.00441	5.32	5.39	-12.24	0.306	0.0142	0.0129	68.29	4.68	-7.36	0.389
9	0.015	7.4	0.0142	0.00508	5.87	5.95	-11.68	0.338	0.0164	0.0148	67.36	5.14	-6.89	0.427
10	0.018	8.9	0.0170	0.00610	6.70	6.79	-10.84	0.385	0.0197	0.0178	66.15	5.75	-6.29	0.477
11	0.021	10.4	0.0198	0.00712	7.39	7.49	-10.14	0.425	0.0229	0.0208	65.06	6.29	-5.74	0.523
12	0.024	11.9	0.0227	0.00813	8.20	8.31	-9.32	0.472	0.0262	0.0237	64.36	6.64	-5.39	0.552
13	0.027	13.3	0.0255	0.00915	8.69	8.81	-8.82	0.500	0.0295	0.0267	63.64	7.00	-5.04	0.581
14	0.031	15.3	0.0293	0.01051	9.21	9.34	-8.29	0.530	0.0339	0.0306	62.68	7.48	-4.56	0.621
15	0.035	17.3	0.0330	0.01186	9.68	9.81	-7.82	0.557	0.0382	0.0346	61.90	7.87	-4.17	0.653
16	0.040	19.8	0.0378	0.01356	10.25	10.39	-7.24	0.589	0.0437	0.0395	61.05	8.29	-3.74	0.689
17	0.045	22.2	0.0425	0.01525	10.68	10.83	-6.80	0.614	0.0492	0.0445	60.41	8.61	-3.42	0.715
18	0.055	27.2	0.0519	0.01864	11.25	11.41	-6.23	0.647	0.0601	0.0544	59.63	9.00	-3.03	0.748
19	0.065	32.1	0.0614	0.02203	11.46	11.62	-6.01	0.659	0.0710	0.0643	58.80	9.42	-2.62	0.782
20	0.080	39.5	0.0755	0.02711	11.96	12.13	-5.51	0.688	0.0874	0.0791	58.14	9.75	-2.29	0.810
21	0.095	46.9	0.0897	0.03220	12.32	12.49	-5.14	0.708	0.1038	0.0939	57.73	9.95	-2.08	0.827
22	0.115	56.8	0.1086	0.03897	12.45	12.62	-5.01	0.716	0.1256	0.1137	57.29	10.17	-1.86	0.845
23	0.140	69.1	0.1322	0.04745	12.72	12.90	-4.74	0.731	0.1530	0.1384	56.83	10.40	-1.63	0.864
24	0.165	81.5	0.1558	0.05592	12.98	13.16	-4.47	0.746	0.1803	0.1631	56.58	10.53	-1.51	0.874
25	0.215	106.2	0.2030	0.07286	13.29	13.48	-4.16	0.764	0.2349	0.2125	56.20	10.72	-1.32	0.890
26	0.315	155.5	0.2974	0.10675	13.91	14.10	-3.53	0.800	0.3441	0.3114	55.57	11.03	-1.00	0.916
27	0.415	204.9	0.3919	0.14064	14.40	14.60	-3.03	0.828	0.4534	0.4103	55.11	11.26	-0.78	0.935
28	0.515	254.3	0.4863	0.17453	14.94	15.15	-2.48	0.859	0.5626	0.5091	54.71	11.46	-0.58	0.952
29	0.615	303.7	0.5807	0.20842	15.52	15.74	-1.90	0.892	0.6719	0.6080	54.45	11.59	-0.45	0.962
30	0.765	377.7	0.7224	0.25926	16.18	16.41	-1.23	0.930	0.8358	0.7563	54.09	11.77	-0.27	0.977
31	0.915	451.8	0.8640	0.31010	16.82	17.05	-0.58	0.967	0.9997	0.9045	53.79	11.92	-0.12	0.990
32	1.115	550.5	1.0528	0.37788	17.37	17.61	-0.02	0.999	1.2182	1.1023	53.57	12.03	-0.01	0.999
33	1.315	649.3	1.2417	0.44566	17.48	17.72	0.09	1.005	1.4367	1.3000	53.53	12.05	0.01	1.001
34	1.515	748.0	1.4305	0.51344	17.45	17.69	0.06	1.003	1.6552	1.4977	53.55	12.04	-0.00	1.000
35	1.715	846.8	1.6194	0.58122	17.42	17.66	0.03	1.002	1.8737	1.6954	53.51	12.06	0.02	1.002
36	1.915	945.9	1.8083	0.64900	17.39	17.63	0.00	1.000	2.0922	1.8931	53.55	12.04	-0.00	1.000

ADVERSE PRESSURE GRADIENT (-0.275,-0.004)

RUN =	31173-4	UINF =	16.8	K =	-0.494E-06	CF/2 =	0.00327	DELM = 1.243	DELH = 0.914
PLATE =	15	TWALL =	77.6	BETA =	0.248	ST =	0.00471	DEL1M = 0.180	DEL2H = 0.0516
X(IN) =	58.	DC =	3.150	BF =	-1.254	PPLUS =	0.00264	DEL2M = 0.133	REH = 470.
Z(IN) =	0.	DEL3 =	0.968	F =	-0.00410	VOPLUS=	-0.07500	REM = 1211.	GH = 3.061
POINTS=	35	TGAS =	54.0	BH =	-0.870	REY.NO=	0.574E 06	H = 1.356	GF = 4.592

I	Y	YPLUS	Y/DELM	Y/DC	U	UPLUS	UDE	UBAR	Y/DELH	Y/DEL3	T	TPLUS	TDE	TBAR
1	0.000	0.0	0.0000	0.00000	0.00	0.00	-17.49	0.000	0.0000	0.0000	77.62	0.00	-12.14	0.000
2	0.005	2.4	0.0040	0.00159	3.01	3.13	-14.36	0.179	0.0055	0.0052	72.25	2.76	-9.38	0.227
3	0.006	2.9	0.0048	0.00190	3.01	3.13	-14.36	0.179	0.0066	0.0062	72.09	2.84	-9.30	0.234
4	0.007	3.4	0.0056	0.00222	3.26	3.39	-14.10	0.194	0.0077	0.0072	71.65	3.07	-9.07	0.253
5	0.008	3.9	0.0064	0.00254	3.57	3.71	-13.78	0.212	0.0088	0.0083	71.09	3.35	-8.78	0.276
6	0.009	4.3	0.0072	0.00286	3.95	4.11	-13.38	0.235	0.0099	0.0093	70.53	3.64	-8.50	0.300
7	0.011	5.3	0.0088	0.00349	4.59	4.77	-12.72	0.273	0.0120	0.0114	69.71	4.06	-8.07	0.335
8	0.013	6.3	0.0105	0.00413	5.28	5.49	-12.00	0.314	0.0142	0.0134	68.67	4.60	-7.54	0.379
9	0.016	7.7	0.0129	0.00508	6.06	6.30	-11.19	0.360	0.0175	0.0165	67.47	5.21	-6.92	0.429
10	0.019	9.1	0.0153	0.00603	7.00	7.28	-10.21	0.416	0.0208	0.0196	66.19	5.87	-6.27	0.484
11	0.022	10.6	0.0177	0.00698	7.71	8.02	-9.47	0.458	0.0241	0.0227	65.21	6.38	-5.76	0.525
12	0.025	12.0	0.0201	0.00794	8.13	8.45	-9.03	0.483	0.0274	0.0258	64.29	6.85	-5.29	0.564
13	0.028	13.5	0.0225	0.00889	8.85	9.20	-8.29	0.526	0.0306	0.0289	63.70	7.15	-4.99	0.589
14	0.032	15.4	0.0257	0.01016	9.14	9.50	-7.98	0.543	0.0350	0.0331	62.64	7.69	-4.45	0.633
15	0.037	17.8	0.0298	0.01175	9.90	10.29	-7.19	0.589	0.0405	0.0382	62.22	7.91	-4.23	0.651
16	0.042	20.2	0.0338	0.01333	10.40	10.81	-6.67	0.618	0.0460	0.0434	61.12	8.47	-3.66	0.698
17	0.052	25.0	0.0418	0.01651	10.90	11.33	-6.15	0.648	0.0569	0.0537	60.12	8.99	-3.15	0.740
18	0.062	29.9	0.0499	0.01968	11.23	11.68	-5.81	0.668	0.0679	0.0641	59.30	9.41	-2.73	0.775
19	0.072	34.7	0.0579	0.02286	11.69	12.15	-5.33	0.695	0.0788	0.0744	58.92	9.60	-2.53	0.791
20	0.087	41.9	0.0700	0.02762	11.92	12.39	-5.09	0.709	0.0952	0.0899	58.26	9.94	-2.19	0.819
21	0.102	49.1	0.0820	0.03238	12.30	12.79	-4.70	0.731	0.1117	0.1054	57.86	10.15	-1.99	0.836
22	0.122	58.7	0.0981	0.03873	12.54	13.04	-4.45	0.746	0.1335	0.1261	57.45	10.36	-1.78	0.853
23	0.147	70.8	0.1182	0.04667	12.72	13.22	-4.26	0.756	0.1609	0.1519	57.03	10.58	-1.56	0.871
24	0.172	82.8	0.1384	0.05460	12.80	13.31	-4.18	0.761	0.1883	0.1778	56.77	10.71	-1.43	0.882
25	0.222	106.9	0.1786	0.07048	13.05	13.57	-3.92	0.776	0.2430	0.2294	56.27	10.97	-1.17	0.903
26	0.322	155.1	0.2590	0.10222	13.55	14.09	-3.40	0.806	0.3525	0.3328	55.83	11.19	-0.95	0.922
27	0.472	227.3	0.3797	0.14984	14.15	14.71	-2.78	0.841	0.5167	0.4878	55.19	11.52	-0.62	0.949
28	0.622	299.5	0.5003	0.19746	14.75	15.34	-2.15	0.877	0.6809	0.6428	54.89	11.67	-0.47	0.961
29	0.772	371.8	0.6210	0.24508	15.33	15.94	-1.55	0.911	0.8451	0.7978	54.45	11.90	-0.24	0.980
30	0.922	444.0	0.7416	0.29270	15.89	16.52	-0.97	0.945	1.0093	0.9528	54.20	12.03	-0.11	0.991
31	1.122	540.3	0.9025	0.35619	16.47	17.12	-0.36	0.979	1.2282	1.1595	54.06	12.10	-0.04	0.997
32	1.322	636.6	1.0634	0.41968	16.77	17.44	-0.05	0.997	1.4471	1.3662	53.87	12.20	0.06	1.005
33	1.522	732.9	1.2243	0.48318	16.82	17.49	0.00	1.000	1.6660	1.5729	53.81	12.23	0.09	1.007
34	1.722	829.2	1.3851	0.54667	16.83	17.50	0.01	1.001	1.8850	1.7796	53.88	12.19	0.05	1.004
35	1.922	925.5	1.5460	0.61016	16.82	17.49	0.00	1.000	2.1039	1.9863	53.98	12.14	-0.00	1.000

ADVERSE PRESSURE GRADIENT (-0.275,-0.004)

RUN	=	31173-5	UINF	=	16.2	K	=	-0.437E-06	CF/2	=	0.00342	DELM	=	1.416	DELH	=	1.145
PLATE	=	18	TWALL	=	77.7	BETA	=	0.212	ST	=	0.00454	DEL1M	=	0.189	DEL2H	=	0.0671
X(IN)	=	70.	DC	=	3.229	BF	=	-1.194	PPLUS	=	0.00218	DEL2M	=	0.143	REH	=	591.
Z(IN)	=	0.	DEL3	=	1.229	F	=	-0.00409	VOPLUS	=	-0.07315	REM	=	1255.	GH	=	2.733
POINTS	=	35	TGAS	=	53.8	BH	=	-0.901	REY.NO	=	0.660E 06	H	=	1.325	GF	=	4.194

I	Y	YPLUS	Y/DELM	Y/DC	U	UPLUS	UDE	UBAR	Y/DELH	Y/DEL3	T	TPLUS	TDE	TBAR
1	0.000	0.0	0.0000	0.00000	0.00	0.00	-17.09	0.000	0.0000	0.0000	77.69	0.00	-12.89	0.000
2	0.005	2.4	0.0035	0.00155	3.28	3.45	-13.63	0.202	0.0044	0.0041	71.45	3.36	-9.53	0.251
3	0.006	2.9	0.0042	0.00186	3.68	3.87	-13.21	0.227	0.0052	0.0049	70.71	3.76	-9.13	0.292
4	0.007	3.3	0.0049	0.00217	4.03	4.24	-12.84	0.248	0.0061	0.0057	70.22	4.02	-8.86	0.312
5	0.008	3.8	0.0056	0.00248	4.32	4.55	-12.54	0.266	0.0070	0.0065	69.82	4.24	-8.65	0.329
6	0.010	4.8	0.0071	0.00310	4.86	5.12	-11.97	0.299	0.0087	0.0081	68.96	4.70	-8.18	0.365
7	0.012	5.7	0.0085	0.00372	5.51	5.80	-11.29	0.339	0.0105	0.0098	68.07	5.18	-7.70	0.402
8	0.014	6.7	0.0099	0.00434	5.89	6.20	-10.89	0.363	0.0122	0.0114	67.23	5.64	-7.25	0.437
9	0.016	7.6	0.0113	0.00496	6.46	6.80	-10.29	0.398	0.0140	0.0130	66.61	5.97	-6.92	0.463
10	0.019	9.0	0.0134	0.00588	7.25	7.63	-9.45	0.447	0.0166	0.0155	65.62	6.50	-6.38	0.505
11	0.022	10.5	0.0155	0.00681	7.84	8.25	-8.83	0.483	0.0192	0.0179	64.70	7.00	-5.89	0.543
12	0.025	11.9	0.0177	0.00774	8.30	8.74	-8.35	0.511	0.0218	0.0203	64.04	7.35	-5.54	0.570
13	0.029	13.8	0.0205	0.00898	8.76	9.22	-7.86	0.540	0.0253	0.0236	63.12	7.85	-5.04	0.609
14	0.033	15.7	0.0233	0.01022	9.32	9.81	-7.28	0.574	0.0288	0.0269	62.62	8.12	-4.77	0.630
15	0.038	18.1	0.0268	0.01177	9.81	10.33	-6.76	0.604	0.0332	0.0309	61.76	8.58	-4.31	0.666
16	0.043	20.4	0.0304	0.01332	10.29	10.83	-6.25	0.634	0.0375	0.0350	61.10	8.94	-3.95	0.693
17	0.048	22.8	0.0339	0.01487	10.52	11.08	-6.01	0.648	0.0419	0.0391	60.44	9.29	-3.60	0.721
18	0.058	27.6	0.0410	0.01796	11.07	11.66	-5.43	0.682	0.0506	0.0472	59.60	9.74	-3.14	0.756
19	0.068	32.3	0.0480	0.02106	11.28	11.88	-5.21	0.695	0.0593	0.0553	58.92	10.11	-2.78	0.784
20	0.083	39.5	0.0586	0.02570	11.57	12.18	-4.91	0.713	0.0724	0.0676	58.22	10.49	-2.40	0.814
21	0.098	46.6	0.0692	0.03035	11.79	12.41	-4.67	0.726	0.0855	0.0798	57.79	10.72	-2.17	0.832
22	0.118	56.1	0.0833	0.03654	12.13	12.77	-4.32	0.747	0.1030	0.0960	57.39	10.94	-1.95	0.848
23	0.143	68.0	0.1010	0.04429	12.42	13.08	-4.01	0.765	0.1248	0.1164	57.01	11.14	-1.75	0.864
24	0.168	79.9	0.1186	0.05203	12.54	13.20	-3.89	0.773	0.1466	0.1367	56.79	11.26	-1.63	0.873
25	0.218	103.6	0.1539	0.06751	12.87	13.55	-3.54	0.793	0.1902	0.1774	56.35	11.50	-1.39	0.892
26	0.318	151.2	0.2245	0.09848	13.14	13.83	-3.25	0.810	0.2775	0.2588	55.85	11.77	-1.12	0.913
27	0.418	198.7	0.2952	0.12945	13.55	14.27	-2.82	0.835	0.3647	0.3402	55.41	12.00	-0.88	0.931
28	0.568	270.0	0.4011	0.17591	13.97	14.71	-2.38	0.861	0.4956	0.4623	55.04	12.20	-0.68	0.947
29	0.718	341.4	0.5070	0.22236	14.38	15.14	-1.95	0.886	0.6265	0.5844	54.81	12.32	-0.57	0.956
30	0.918	436.4	0.6482	0.28430	15.03	15.82	-1.26	0.926	0.8010	0.7472	54.41	12.54	-0.35	0.973
31	1.118	531.5	0.7894	0.34624	15.59	16.41	-0.67	0.961	0.9755	0.9100	54.04	12.74	-0.15	0.988
32	1.318	626.6	0.9306	0.40818	15.94	16.78	-0.31	0.982	1.1500	1.0728	53.74	12.90	0.01	1.001
33	1.518	721.7	1.0719	0.47012	16.20	17.06	-0.03	0.998	1.3245	1.2356	53.76	12.89	0.00	1.000
34	1.718	816.8	1.2131	0.53206	16.25	17.11	0.02	1.001	1.4990	1.3983	53.76	12.89	-0.00	1.000
35	1.918	911.9	1.3543	0.59400	16.23	17.09	0.00	1.000	1.6735	1.5611	53.76	12.89	-0.00	1.000

ADVERSE PRESSURE GRADIENT (-0.275,-0.004)

RUN =	31173-6	UINF =	15.4	K =	-0.396E-06	CF/2 =	0.00334	DELM = 1.591	DELH = 1.111
PLATE =	21	TWALL =	77.8	BETA =	0.216	ST =	0.00446	DEL1M = 0.219	DEL2H = 0.0586
X(IN) =	82.	DC =	3.782	BF =	-1.203	PPLUS =	0.00205	DEL2M = 0.164	REH = 489.
Z(IN) =	0.	DEL3 =	1.185	F =	-0.00402	VOPLUS=	-0.07274	REM = 1364.	GH = 3.395
POINTS=	38	TGAS =	54.1	BH =	-0.901	REY.NO=	0.725E 06	H = 1.336	GF = 4.347

I	Y	YPLUS	Y/DELM	Y/DC	U	UPLUS	UDE	UBAR	Y/DELH	Y/DEL3	T	TPLUS	TDE	TBAR
1	0.000	0.0	0.0000	0.00000	0.00	0.00	-17.30	0.000	0.0000	0.0000	77.79	0.00	-12.96	0.000
2	0.005	2.2	0.0031	0.00132	2.36	2.65	-14.65	0.153	0.0045	0.0042	73.05	2.60	-10.36	0.201
3	0.006	2.7	0.0038	0.00159	2.48	2.79	-14.51	0.161	0.0054	0.0051	72.80	2.74	-10.22	0.211
4	0.007	3.1	0.0044	0.00185	2.79	3.14	-14.16	0.181	0.0063	0.0059	72.28	3.02	-9.94	0.233
5	0.008	3.6	0.0050	0.00212	3.04	3.42	-13.88	0.198	0.0072	0.0068	71.79	3.29	-9.67	0.254
6	0.009	4.0	0.0057	0.00238	3.23	3.63	-13.67	0.210	0.0081	0.0076	71.57	3.41	-9.55	0.263
7	0.010	4.5	0.0063	0.00264	3.26	3.66	-13.63	0.212	0.0090	0.0084	71.38	3.52	-9.44	0.271
8	0.012	5.3	0.0075	0.00317	3.55	3.99	-13.31	0.231	0.0108	0.0101	70.94	3.76	-9.20	0.290
9	0.014	6.2	0.0088	0.00370	3.94	4.43	-12.87	0.256	0.0126	0.0118	70.31	4.10	-8.86	0.316
10	0.017	7.6	0.0107	0.00450	4.79	5.38	-11.92	0.311	0.0153	0.0143	68.77	4.95	-8.01	0.382
11	0.020	8.9	0.0126	0.00529	5.57	6.26	-11.04	0.362	0.0180	0.0169	67.92	5.41	-7.55	0.418
12	0.024	10.7	0.0151	0.00635	6.34	7.13	-10.17	0.412	0.0216	0.0203	66.66	6.10	-6.85	0.471
13	0.029	12.9	0.0182	0.00767	7.21	8.10	-9.19	0.468	0.0261	0.0245	65.00	7.01	-5.94	0.541
14	0.034	15.1	0.0214	0.00899	8.03	9.03	-8.27	0.522	0.0306	0.0287	64.07	7.52	-5.43	0.580
15	0.039	17.4	0.0245	0.01031	8.53	9.59	-7.71	0.554	0.0351	0.0329	62.89	8.16	-4.79	0.630
16	0.044	19.6	0.0277	0.01163	9.21	10.35	-6.95	0.598	0.0396	0.0371	62.02	8.64	-4.32	0.667
17	0.049	21.8	0.0308	0.01296	9.42	10.59	-6.71	0.612	0.0441	0.0414	61.25	9.06	-3.89	0.699
18	0.054	24.0	0.0339	0.01428	9.76	10.97	-6.33	0.634	0.0486	0.0456	60.80	9.31	-3.65	0.718
19	0.064	28.5	0.0402	0.01692	10.20	11.47	-5.83	0.663	0.0576	0.0540	59.93	9.79	-3.17	0.755
20	0.074	32.9	0.0465	0.01957	10.59	11.90	-5.40	0.688	0.0666	0.0625	59.37	10.10	-2.86	0.779
21	0.084	37.4	0.0528	0.02221	10.86	12.21	-5.09	0.706	0.0756	0.0709	58.76	10.43	-2.53	0.805
22	0.099	44.1	0.0622	0.02618	11.07	12.44	-4.86	0.719	0.0891	0.0836	58.45	10.60	-2.36	0.818
23	0.114	50.8	0.0717	0.03014	11.43	12.85	-4.45	0.743	0.1026	0.0962	58.18	10.75	-2.21	0.829
24	0.139	61.9	0.0874	0.03676	11.65	13.10	-4.20	0.757	0.1252	0.1173	57.55	11.09	-1.86	0.856
25	0.164	73.0	0.1031	0.04337	11.75	13.21	-4.09	0.763	0.1477	0.1384	57.13	11.32	-1.63	0.874
26	0.214	95.3	0.1345	0.05659	11.94	13.42	-3.88	0.776	0.1927	0.1806	56.78	11.52	-1.44	0.889
27	0.314	139.8	0.1974	0.08303	12.23	13.75	-3.55	0.795	0.2827	0.2650	56.16	11.86	-1.10	0.915
28	0.414	184.3	0.2602	0.10947	12.66	14.23	-3.07	0.823	0.3728	0.3494	55.70	12.11	-0.85	0.934
29	0.564	251.1	0.3545	0.14914	13.01	14.62	-2.68	0.845	0.5078	0.4760	55.30	12.33	-0.63	0.951
30	0.714	317.9	0.4488	0.18880	13.44	15.11	-2.19	0.873	0.6429	0.6026	54.96	12.51	-0.44	0.966
31	0.914	406.9	0.5745	0.24168	13.95	15.68	-1.62	0.906	0.8230	0.7714	54.64	12.69	-0.27	0.979
32	1.114	496.0	0.7002	0.29457	14.43	16.22	-1.08	0.938	1.0030	0.9403	54.37	12.83	-0.13	0.990
33	1.314	585.0	0.8260	0.34745	14.73	16.56	-0.74	0.957	1.1831	1.1091	54.21	12.92	-0.04	0.997
34	1.514	674.1	0.9517	0.40034	15.14	17.02	-0.28	0.984	1.3632	1.2779	54.06	13.00	0.04	1.003
35	1.714	763.1	1.0774	0.45323	15.39	17.30	0.00	1.000	1.5433	1.4467	54.08	12.99	0.03	1.003
36	1.914	852.1	1.2031	0.50611	15.38	17.29	-0.01	0.999	1.7234	1.6155	53.92	13.08	0.12	1.009
37	2.164	963.4	1.3603	0.57222	15.37	17.28	-0.02	0.999	1.9485	1.8265	54.04	13.02	0.05	1.004
38	2.414	1074.8	1.5174	0.63832	15.39	17.30	0.00	1.000	2.1736	2.0375	54.14	12.96	-0.00	1.000

E-5. Reynolds stress tensor components (isothermal)

The runs are tabulated below and they were all taken at plate 18, x 70 in. See also 9.3 for symbol explanation

Date	m	F
062473	0	0
050973	-0.275	0
051673	-0.275	-0.001
052373	-0.275	-0.002
052973	-0.275	-0.004

Special Nomenclature

Symbol	Explanation	Unit
UTAU	Friction velocity, $U_\infty \sqrt{C_f/2}$	ft/sec
DEL	Momentum boundary layer thickness, δ	in
U'	RMS value of longitudinal velocity fluctuation, $\sqrt{\overline{u'^2}}$	ft/sec
V'	RMS value of normal velocity fluctuation, $\sqrt{\overline{v'^2}}$	ft/sec
W'	RMS value of tangential velocity fluctuation, $\sqrt{\overline{w'^2}}$	ft/sec
Q	Turbulent kinetic energy, $\overline{u'^2} + \overline{v'^2} + \overline{w'^2}$	ft^2/sec^2
UV	Correlation between u' and v' (shear stress), $\overline{u'v'}$	ft^2/sec^2
RUV	Correlation coefficient, $-\overline{u'v'} \Big/ \sqrt{\overline{u'^2}}\sqrt{\overline{v'^2}}$	-

REYNOLDS STRESS TENSOR COMPONENTS (ISOTHERMAL)
FLAT PLATE (0.,0.)

DATE= 62473
UINF= 31.60 FT/SEC
CF/2=0.00181
UTAU= 1.344

Y	Y/DEL	YPLUS	U	UPLUS	U'/UTAU	V'/UTAU	W'/UTAU	Q/UTAU**2	-UV/UTAU**2	RUV	UV/Q
0.072	0.056	49.5	18.88	14.04	2.113	1.069	1.557	8.030	0.969	0.429	0.121
0.082	0.064	56.4	19.35	14.39	2.031	1.078	1.492	7.513	0.977	0.446	0.130
0.102	0.080	70.1	19.82	14.74	1.971	1.116	1.495	7.367	0.969	0.441	0.132
0.132	0.103	90.7	20.69	15.39	1.897	1.133	1.469	7.041	0.977	0.455	0.139
0.182	0.143	125.1	21.41	15.93	1.860	1.048	1.382	6.467	0.915	0.469	0.142
0.282	0.221	193.8	23.13	17.20	1.726	1.181	1.407	6.352	0.907	0.445	0.143
0.382	0.299	262.6	23.79	17.70	1.651	1.086	1.317	5.641	0.820	0.457	0.145
0.582	0.456	400.0	26.74	19.89	1.517	1.109	1.298	5.218	0.752	0.447	0.144
0.782	0.613	537.5	27.78	20.66	1.272	0.992	1.143	3.908	0.572	0.453	0.146
1.082	0.848	743.7	30.30	22.54	0.907	0.664	0.734	1.804	0.251	0.416	0.139
1.282	1.005	881.1	31.23	23.23	0.566	0.438	0.398	0.671	0.085	0.344	0.127

REYNOLDS STRESS TENSOR COMPONENTS (ISOTHERMAL)
ADVERSE PRESSURE GRADIENT (-0.275,0.)

DATE= 50973
UINF= 16.13 FT/SEC
CF/2=0.00081
UTAU= 0.459

Y	Y/DEL	YPLUS	U	UPLUS	U'/UTAU	V'/UTAU	W'/UTAU	Q/UTAU**2	-UV/UTAU**2	RUV	UV/Q
0.069	0.019	16.2	3.72	8.10	3.652	1.080	2.272	19.664	1.134	0.287	0.058
0.089	0.024	20.9	4.13	9.00	3.368	1.534	2.493	19.910	1.357	0.263	0.068
0.129	0.035	30.3	4.49	9.78	3.216	1.601	2.561	19.464	1.348	0.262	0.069
0.199	0.054	46.7	5.27	11.48	2.995	1.918	2.545	19.123	1.599	0.278	0.084
0.299	0.080	70.2	5.64	12.29	2.931	2.034	2.652	19.759	1.727	0.290	0.087
0.499	0.134	117.1	6.12	13.33	3.057	2.330	2.716	22.155	2.510	0.352	0.113
0.799	0.215	187.5	6.74	14.68	3.246	2.489	2.827	24.722	2.980	0.369	0.121
1.209	0.325	283.7	7.95	17.32	3.451	2.863	3.186	30.260	3.981	0.403	0.132
1.905	0.513	447.1	10.63	23.16	3.684	3.199	3.695	37.458	5.196	0.441	0.139
2.909	0.783	682.7	14.07	30.65	2.840	2.804	3.024	25.073	3.459	0.434	0.138

REYNOLDS STRESS TENSOR COMPONENTS (ISOTHERMAL)
ADVERSE PRESSURE GRADIENT (-0.275,-0.001)

DATE= 51673
UINF= 16.28 FT/SEC
CF/2=0.00116
UTAU= 0.554

Y	Y/DEL	YPLUS	U	UPLUS	U'/UTAU	V'/UTAU	W'/UTAU	Q/UTAU**2	-UV/UTAU**2	RUV	UV/Q
0.069	0.025	19.7	6.35	11.45	2.788	0.655	1.740	11.231	0.755	0.413	0.067
0.089	0.033	25.4	6.74	12.16	2.693	0.701	1.757	10.831	0.816	0.433	0.075
0.119	0.044	33.9	7.30	13.17	2.614	0.946	1.738	10.747	1.005	0.407	0.094
0.159	0.059	45.4	7.67	13.83	2.479	1.166	1.829	10.851	1.083	0.375	0.100
0.209	0.077	59.6	7.99	14.41	2.372	1.328	1.891	10.965	1.197	0.380	0.109
0.309	0.114	88.1	8.56	15.44	2.365	1.454	1.983	11.641	1.311	0.381	0.113
0.409	0.151	116.7	8.90	16.05	2.420	1.535	1.972	12.100	1.454	0.392	0.120
0.609	0.225	173.7	9.44	17.03	2.531	1.613	2.070	13.293	1.734	0.425	0.130
0.909	0.335	259.3	10.56	19.04	2.663	1.900	2.264	15.827	2.153	0.426	0.136
1.409	0.520	401.9	12.52	22.58	2.741	1.902	2.470	17.229	2.488	0.477	0.144
1.900	0.701	541.9	14.11	25.45	2.433	1.728	2.099	13.313	1.935	0.460	0.145
2.409	0.888	687.1	15.51	27.97	1.653	1.318	1.348	6.287	0.914	0.420	0.145

REYNOLDS STRESS TENSOR COMPONENTS (ISOTHERMAL)
ADVERSE PRESSURE GRADIENT (-0.275,-0.002)

DATE= 52373
UINF= 16.37 FT/SEC
CF/2=0.00191
UTAU= 0.715

Y	Y/DEL	YPLUS	U	UPLUS	U'/UTAU	V'/UTAU	W'/UTAU	Q/UTAU**2	-UV/UTAU**2	RUV	UV/Q
0.069	0.032	25.4	8.07	11.28	2.083	0.673	1.398	6.746	0.533	0.380	0.079
0.088	0.041	32.4	8.62	12.05	1.987	0.819	1.390	6.549	0.529	0.326	0.081
0.128	0.060	47.1	9.18	12.83	1.817	0.851	1.419	6.041	0.569	0.368	0.094
0.198	0.093	72.9	9.60	13.42	1.671	1.030	1.394	5.799	0.608	0.353	0.105
0.298	0.139	109.7	10.17	14.22	1.642	1.115	1.437	6.004	0.717	0.392	0.119
0.398	0.186	146.5	10.63	14.86	1.660	1.211	1.472	6.389	0.830	0.413	0.130
0.598	0.280	220.1	11.42	15.96	1.718	1.342	1.568	7.211	0.961	0.417	0.133
0.798	0.373	293.7	12.21	17.07	1.751	1.341	1.641	7.561	1.024	0.436	0.135
0.998	0.467	367.3	12.80	17.89	1.768	1.337	1.623	7.549	1.055	0.446	0.140
1.248	0.584	459.3	13.52	18.90	1.718	1.248	1.543	6.887	1.002	0.468	0.146
1.498	0.701	551.3	14.49	20.25	1.569	1.181	1.436	5.920	0.879	0.474	0.149
1.902	0.890	700.0	15.60	21.81	1.153	0.924	0.975	3.134	0.422	0.396	0.135

REYNOLDS STRESS TENSOR COMPONENTS (ISOTHERMAL)
ADVERSE PRESSURE GRADIENT (-0.275,-0.004)

DATE = 52973
UINF = 16.54 FT/SEC
CF/2=0.00342
UTAU= 0.967

Y	Y/DEL	YPLUS	U	UPLUS	U'/UTAU	V'/UTAU	W'/UTAU	Q/UTAU**2	-UV/UTAU**2	RUV	UV/Q
0.069	0.049	34.1	11.38	11.77	1.414	0.498	0.913	3.080	0.215	0.305	0.070
0.089	0.063	44.0	11.79	12.19	1.279	0.537	0.885	2.707	0.200	0.291	0.074
0.119	0.084	58.8	12.33	12.75	1.128	0.646	0.896	2.492	0.238	0.327	0.096
0.149	0.105	73.7	12.40	12.82	1.049	0.550	0.846	2.119	0.215	0.372	0.101
0.199	0.141	98.4	12.64	13.07	0.953	0.671	0.855	2.090	0.249	0.389	0.119
0.299	0.211	147.9	13.04	13.48	0.907	0.631	0.807	1.873	0.228	0.398	0.122
0.399	0.282	197.3	13.40	13.85	0.877	0.689	0.826	1.927	0.262	0.433	0.136
0.599	0.423	296.2	14.15	14.63	0.871	0.668	0.798	1.842	0.261	0.448	0.142
0.799	0.564	395.1	14.71	15.21	0.834	0.623	0.738	1.627	0.243	0.467	0.149
0.999	0.706	494.0	15.37	15.89	0.746	0.566	0.655	1.305	0.193	0.458	0.148
1.299	0.917	642.4	16.19	16.74	0.496	0.440	0.434	0.627	0.087	0.397	0.138

E-6. Velocity and temperature fluctuation profiles

The runs are tabulated below and they were all taken at plate 18, x = 70 in. See also 9.3 for symbol explanation.

Date	m	F
041473	0	0
050273	-0.275	0
051773	-0.275	-0.001
052173	-0.275	-0.002
060373	-0.275	-0.004

It should be noted that when the calibration curves are not reliable (low velocities), no tabulation is provided. This justifies the blanks in the tables.

Special Nomenclature

Symbol	Explanation	Unit
TW-TINF	Wall to free stream temperature differences	F
STANTON	Stanton number	-
UTAU	Friction velocity, $U_\infty \sqrt{C_f/2}$	ft/sec
TTAU	$(T_o - T_\infty)\sqrt{C_f/2}$ /ST	°F
U'	RMS value of longitudinal velocity fluctuation, $\sqrt{\overline{u'^2}}$	ft/sec
T'	RMS value of temperature fluctuation, $\sqrt{\overline{t'^2}}$	°F
T'RAW	Raw value of T'	°F
R-FUNC	Eq 7.17	-

VELOCITY AND TEMPERATURE FLUCTUATION PROFILES
FLAT PLATE (0.,0.)   PLATE 18

DATE = 41473
UINF = 31.60 FT/SEC
TW-TINF= 24.5 F
CF/2 =0.00181
STANTON=0.00200
UTAU = 1.344
TTAU = 1.152

Y	Y/DELM	Y/DELH	YPLUS	U'	U'/UTAU	T'RAW	T'	T'/TTAU	R-FUNC
0.006	0.005	0.004	3.8	2.20	1.64	0.92	1.09	0.94	1.27
0.013	0.010	0.009	8.2	3.07	2.28	1.38	1.61	1.40	1.19
0.018	0.014	0.013	11.4	3.40	2.53	1.56	1.81	1.58	1.17
0.023	0.018	0.016	14.6	3.52	2.62	1.64	1.90	1.65	1.16
0.028	0.022	0.020	17.7	3.48	2.59	1.67	1.93	1.67	1.13
0.033	0.026	0.023	20.9	3.42	2.54	1.67	1.92	1.67	1.11
0.038	0.030	0.027	24.1	3.31	2.46	1.64	1.89	1.64	1.10
0.052	0.041	0.037	32.9	3.11	2.31	1.55	1.78	1.55	1.09
0.062	0.049	0.044	39.2	2.95	2.19	1.49	1.71	1.48	1.08
0.072	0.056	0.051	45.6	2.84	2.11	1.45	1.66	1.44	1.07
0.082	0.064	0.058	51.9	2.73	2.03	1.41	1.62	1.40	1.06
0.102	0.080	0.072	64.6	2.65	1.97	1.34	1.53	1.33	1.08
0.132	0.103	0.093	83.5	2.55	1.90	1.26	1.44	1.25	1.11
0.182	0.143	0.128	115.2	2.50	1.86	1.18	1.35	1.17	1.16
0.282	0.221	0.199	178.5	2.32	1.73	1.09	1.24	1.08	1.17
0.382	0.299	0.270	241.8	2.22	1.65	1.04	1.18	1.03	1.17
0.582	0.456	0.411	368.4	2.04	1.52	0.94	1.07	0.93	1.20
0.882	0.691	0.622	558.3	1.55	1.15	0.80	0.91	0.79	1.07
1.082	0.848	0.764	684.9	1.22	0.91	0.60	0.68	0.59	1.12
1.282	1.005	0.905	811.4	0.76	0.57	0.53	0.60	0.52	0.79

VELOCITY AND TEMPERATURE FLUCTUATION PROFILES
ADVERSE PRESSURE GRADIENT (-0.275,0.)   PLATE 18

DATE = 50273
UINF = 16.13 FT/SEC
TW-TINF= 31.0 F
CF/2 =0.00081
STANTON=0.00217
UTAU = 0.459
TTAU = 2.364

Y	Y/DELM	Y/DELH	YPLUS	U'	U'/UTAU	T'RAW	T'	T'/TTAU	R-FUNC
0.006	0.002	0.002	1.3			0.63	0.78	0.33	
0.011	0.003	0.003	2.4			0.99	1.22	0.52	
0.016	0.004	0.004	3.4			1.52	1.87	0.79	
0.021	0.006	0.006	4.5			2.10	2.57	1.09	
0.026	0.007	0.007	5.6			2.39	2.91	1.23	
0.031	0.008	0.009	6.6			2.63	3.19	1.35	
0.036	0.010	0.010	7.7			2.80	3.38	1.43	
0.045	0.012	0.013	9.6			2.99	3.59	1.52	
0.055	0.015	0.015	11.8	1.74	3.79	3.06	3.69	1.56	1.77
0.065	0.017	0.018	13.9	1.69	3.68	3.05	3.67	1.55	1.73
0.085	0.023	0.024	18.2	1.55	3.38	2.95	3.54	1.50	1.65
0.118	0.032	0.033	25.3	1.50	3.27	2.72	3.25	1.38	1.73
0.148	0.040	0.041	31.7	1.42	3.09	2.56	3.06	1.29	1.75
0.198	0.053	0.055	42.5	1.38	3.01	2.31	2.75	1.16	1.88
0.248	0.067	0.069	53.2	1.35	2.94	2.14	2.55	1.08	1.99
0.298	0.080	0.083	63.9	1.35	2.94	1.95	2.32	0.98	2.19
0.398	0.107	0.111	85.3	1.38	3.01	1.77	2.10	0.89	2.47
0.498	0.134	0.139	106.8	1.40	3.05	1.62	1.92	0.81	2.74
0.698	0.188	0.195	149.7	1.47	3.20	1.44	1.70	0.72	3.25
0.998	0.268	0.278	214.0	1.54	3.35	1.27	1.50	0.64	3.86
1.498	0.403	0.418	321.2	1.65	3.59	1.10	1.29	0.55	4.81
1.920	0.517	0.535	411.7	1.69	3.68	0.99	1.16	0.49	5.50
2.420	0.651	0.675	518.9	1.54	3.35	0.92	1.07	0.45	5.41
2.920	0.786	0.814	626.2	1.29	2.81	0.82	0.95	0.40	5.10
3.420	0.920	0.954	733.4	0.80	1.74	0.66	0.76	0.32	3.94
3.920	1.055	1.093	840.6	0.36	0.78	0.37	0.43	0.18	3.17

VELOCITY AND TEMPERATURE FLUCTUATION PROFILES
ADVERSE PRESSURE GRADIENT (-0.275,-0.001) PLATE 18

DATE = 51773
UINF = 16.28 FT/SEC
TW-TINF= 25.6 F
CF/2 =0.00116
STANTON=0.00272
UTAU = 0.554
TTAU = 2.044

Y	Y/DELM	Y/DELH	YPLUS	U'	U'/UTAU	T'RAW	T'	T'/TTAU	R-FUNC
0.006	0.002	0.002	1.6			0.52	0.64	0.31	
0.008	0.003	0.003	2.1			0.64	0.78	0.38	
0.011	0.004	0.004	2.9			0.92	1.11	0.54	
0.014	0.005	0.005	3.7			1.15	1.38	0.68	
0.018	0.007	0.007	4.8			1.42	1.70	0.83	
0.023	0.008	0.009	6.1	1.56	2.81	1.64	1.98	0.97	2.12
0.028	0.010	0.011	7.4	1.64	2.96	1.90	2.28	1.12	1.94
0.038	0.014	0.015	10.0	1.65	2.98	2.35	2.80	1.37	1.59
0.048	0.018	0.019	12.7	1.64	2.96	2.34	2.77	1.36	1.59
0.058	0.021	0.022	15.3	1.61	2.90	2.36	2.79	1.37	1.55
0.069	0.025	0.027	18.2	1.55	2.80	2.30	2.72	1.33	1.54
0.089	0.033	0.034	23.5	1.49	2.69	2.16	2.55	1.25	1.58
0.119	0.044	0.046	31.4	1.45	2.62	1.99	2.34	1.14	1.67
0.159	0.059	0.062	42.0	1.37	2.47	1.76	2.07	1.01	1.78
0.209	0.077	0.081	55.2	1.32	2.38	1.55	1.82	0.89	1.95
0.309	0.114	0.120	81.6	1.31	2.36	1.32	1.55	0.76	2.28
0.409	0.151	0.158	108.0	1.34	2.42	1.18	1.38	0.68	2.61
0.609	0.225	0.236	160.8	1.41	2.54	1.01	1.18	0.58	3.22
0.909	0.335	0.352	240.0	1.48	2.67	0.87	1.01	0.50	3.93
1.159	0.427	0.449	306.0	1.55	2.80	0.78	0.91	0.44	4.61
1.409	0.520	0.545	372.0	1.52	2.74	0.71	0.82	0.40	4.97
1.909	0.704	0.739	504.0	1.36	2.45	0.59	0.68	0.33	5.37
2.409	0.888	0.933	636.1	0.92	1.66	0.47	0.54	0.27	4.57
2.909	1.073	1.126	768.1	0.37	0.67	0.26	0.30	0.15	3.33
3.420	1.261	1.324	903.0	0.18	0.32	0.07	0.08	0.04	6.01

VELOCITY AND TEMPERATURE FLUCTUATION PROFILES
ADVERSE PRESSURE GRADIENT (-0.275,-0.002) PLATE 18

DATE = 52173
UINF = 16.37 FT/SEC
TW-TINF= 23.8 F
CF/2 =0.00191
STANTON=0.00325
UTAU = 0.715
TTAU = 1.770

Y	Y/DELM	Y/DELH	YPLUS	U'	U'/UTAU	T'RAW	T'	T'/TTAU	R-FUNC
0.006	0.003	0.003	2.0			0.89	1.08	0.61	
0.010	0.005	0.004	3.4			0.92	1.11	0.63	
0.014	0.007	0.006	4.8	1.35	1.89	1.20	1.45	0.82	1.68
0.018	0.008	0.008	6.1	1.42	1.98	1.47	1.76	1.00	1.45
0.023	0.011	0.010	7.8	1.51	2.11	1.73	2.06	1.17	1.32
0.028	0.013	0.012	9.5	1.53	2.14	1.85	2.20	1.24	1.26
0.038	0.018	0.016	12.9	1.60	2.24	2.06	2.43	1.38	1.19
0.048	0.022	0.021	16.4	1.61	2.25	2.08	2.45	1.38	1.19
0.069	0.032	0.030	23.5	1.49	2.08	1.97	2.31	1.31	1.16
0.088	0.041	0.038	30.0	1.42	1.98	1.83	2.14	1.21	1.20
0.128	0.060	0.055	43.6	1.30	1.82	1.61	1.88	1.06	1.25
0.198	0.093	0.085	67.5	1.20	1.68	1.31	1.53	0.86	1.42
0.298	0.139	0.128	101.5	1.17	1.64	1.09	1.27	0.72	1.66
0.398	0.186	0.171	135.6	1.19	1.66	0.95	1.11	0.63	1.94
0.598	0.280	0.257	203.7	1.23	1.72	0.81	0.94	0.53	2.36
0.798	0.373	0.343	271.9	1.25	1.75	0.72	0.84	0.47	2.70
0.998	0.467	0.429	340.0	1.27	1.78	0.65	0.75	0.43	3.04
1.248	0.584	0.537	425.2	1.23	1.72	0.57	0.66	0.37	3.37
1.498	0.701	0.644	510.3	1.12	1.57	0.51	0.59	0.33	3.43
1.920	0.898	0.826	654.1	0.81	1.13	0.41	0.47	0.27	3.09
2.428	1.136	1.044	827.2	0.30	0.42	0.21	0.24	0.14	2.24

VELOCITY AND TEMPERATURE FLUCTUATION PROFILES
ADVERSE PRESSURE GRADIENT (-0.275,-0.004) PLATE 18

DATE = 60373
UINF = 16.54 FT/SEC
TW-TINF = 23.0 F
CF/2 =0.00342
STANTON=0.00454
UTAU = 0.967
TTAU = 1.786

Y	Y/DELM	Y/DELH	YPLUS	U'	U'/UTAU	T'RAW	T'	T'/TTAU	R-FUNC
0.006	0.004	0.005	2.7	0.92	0.95	0.65	0.78	0.44	1.59
0.010	0.007	0.009	4.6	1.09	1.13	0.91	1.09	0.61	1.35
0.014	0.010	0.012	6.4	1.25	1.29	1.16	1.38	0.77	1.22
0.018	0.013	0.016	8.2	1.39	1.44	1.38	1.63	0.91	1.15
0.023	0.016	0.020	10.5	1.51	1.56	1.61	1.89	1.05	1.07
0.028	0.020	0.024	12.8	1.57	1.62	1.70	1.99	1.12	1.06
0.038	0.027	0.033	17.4	1.56	1.61	1.81	2.12	1.18	0.99
0.048	0.034	0.042	22.0	1.53	1.58	1.78	2.08	1.16	0.99
0.069	0.049	0.060	31.6	1.37	1.42	1.63	1.90	1.06	0.97
0.089	0.063	0.078	40.8	1.24	1.28	1.44	1.67	0.94	1.00
0.119	0.084	0.104	54.5	1.09	1.13	1.24	1.44	0.81	1.02
0.149	0.105	0.130	68.2	1.01	1.04	1.08	1.25	0.70	1.09
0.199	0.141	0.174	91.1	0.92	0.95	0.89	1.03	0.58	1.20
0.299	0.211	0.261	136.9	0.88	0.91	0.70	0.81	0.45	1.46
0.399	0.282	0.348	182.7	0.85	0.88	0.59	0.68	0.38	1.68
0.599	0.423	0.523	274.3	0.84	0.87	0.47	0.54	0.30	2.08
0.799	0.564	0.697	365.9	0.81	0.84	0.39	0.45	0.25	2.42
0.999	0.706	0.872	457.5	0.72	0.74	0.33	0.38	0.21	2.55
1.299	0.917	1.134	594.9	0.48	0.50	0.24	0.28	0.15	2.34
1.499	1.059	1.308	686.5	0.30	0.31	0.17	0.20	0.11	2.06

E-7. Turbulent Prandtl numbers

The runs are tabulated below and they were all taken at plate 18, x 70 in. See also 9.5 for symbol explanation.

Date	m	F
060473	0	0
050873	-0.275	0
051573	-0.275	-0.001
052273	-0.275	-0.002
053173	-0.275	-0.004

Special Nomenclature

Symbol	Explanation	Unit
VT	Normal velocity-temperature correlation, $\overline{v't'}$	ft. F/sec
VTPLUS	$\overline{v't'}/u_\tau T_t$	
PRT	Turbulent Prandtl number	-
VT/V'T'	Correlation coefficient, $\overline{v't'}/\sqrt{\overline{v'^2}}\,\sqrt{\overline{t'^2}}$	-
Q'	Square root of the turbulent kinetic energy, Q	ft/sec

TURBULENT PRANDTL NUMBER
FLAT PLATE(0.,0.) PLATE 18

DATE = 60473
UINF = 31.60 FT/SEC
TW-TINF= 24.8 F
CF/2 =0.00181
STANTON=0.00200
UTAU = 1.344
TTAU = 1.166

Y	Y/DELM	Y/DELH	YPLUS	VTPLUS	PRT	VT/V'T'	VT/Q'T'	UV	VT
0.072	0.056	0.051	45.7	0.931	0.95	0.612	0.231	-1.750	1.459
0.082	0.064	0.058	52.0	0.963	0.93	0.643	0.253	-1.750	1.510
0.102	0.080	0.072	64.7	0.886	1.01	0.605	0.249	-1.750	1.388
0.132	0.103	0.093	83.7	0.904	0.99	0.646	0.276	-1.750	1.417
0.182	0.143	0.128	115.5	0.928	0.88	0.765	0.315	-1.730	1.455
0.282	0.221	0.199	178.9	0.797	0.97	0.635	0.297	-1.660	1.249
0.382	0.299	0.270	242.3	0.803	0.85	0.731	0.334	-1.570	1.259
0.582	0.456	0.411	369.2	0.634	0.95	0.623	0.302	-1.360	0.993
0.782	0.613	0.552	496.1	0.511	0.88	0.626	0.314	-1.030	0.801
1.082	0.848	0.764	686.4	0.327	0.61	0.843	0.417	-0.450	0.512
1.282	1.005	0.905	813.3	0.125	0.54	0.555	0.297	-0.150	0.196

TURBULENT PRANDTL NUMBER
ADVERSE PRESSURE GRADIENT(-0.275,0.) PLATE 18

DATE = 50873
UINF = 16.13 FT/SEC
TW-TINF= 31.0 F
CF/2 =0.00081
STANTON=0.00217
UTAU = 0.459
TTAU = 2.364

Y	Y/DELM	Y/DELH	YPLUS	VTPLUS	PRT	VT/V'T'	VT/Q'T'	UV	VT
0.089	0.024	0.025	19.1	0.315	2.28	0.139	0.048	-0.255	0.342
0.129	0.035	0.036	27.7	0.417	1.84	0.193	0.070	-0.290	0.452
0.199	0.054	0.055	42.7	0.594	1.32	0.266	0.117	-0.340	0.645
0.299	0.080	0.083	64.1	0.785	1.09	0.393	0.180	-0.390	0.852
0.499	0.134	0.139	107.0	1.047	0.81	0.553	0.274	-0.485	1.136
0.799	0.215	0.223	171.3	0.968	0.92	0.564	0.282	-0.630	1.050
1.209	0.325	0.337	259.3	1.104	0.86	0.646	0.336	-0.840	1.198
1.905	0.513	0.531	408.5	1.030	0.66	0.656	0.343	-1.095	1.118
2.909	0.783	0.811	623.8	0.974	0.33	0.864	0.484	-0.730	1.057

TURBULENT PRANDTL NUMBER
ADVERSE PRESSURE GRADIENT(-0.275,-0.001) PLATE 18

DATE = 51573
UINF = 16.28 FT/SEC
TW-TINF= 25.6 F
CF/2 =0.00116
STANTON=0.00272
UTAU = 0.554
TTAU = 2.044

Y	Y/DELM	Y/DELH	YPLUS	VTPLUS	PRT	VT/V'T'	VT/Q'T'	UV	VT
0.069	0.025	0.027	18.2	0.315	1.32	0.361	0.071	-0.260	0.357
0.089	0.033	0.034	23.5	0.403	1.10	0.461	0.098	-0.280	0.457
0.119	0.044	0.046	31.4	0.514	0.88	0.475	0.137	-0.300	0.583
0.159	0.059	0.062	42.0	0.428	1.11	0.362	0.128	-0.330	0.485
0.209	0.077	0.081	55.2	0.410	1.23	0.347	0.139	-0.360	0.465
0.309	0.114	0.120	81.6	0.485	1.11	0.440	0.188	-0.400	0.550
0.409	0.151	0.158	108.0	0.532	1.10	0.514	0.227	-0.450	0.603
0.609	0.225	0.236	160.8	0.581	1.08	0.624	0.276	-0.530	0.659
0.909	0.335	0.352	240.0	0.593	1.18	0.632	0.302	-0.660	0.672
1.409	0.520	0.545	372.0	0.602	1.06	0.789	0.361	-0.760	0.682
1.909	0.701	0.736	501.7	0.525	0.81	0.913	0.433	-0.600	0.595
2.409	0.888	0.933	636.1	0.326	0.54	0.935	0.491	-0.280	0.369

TURBULENT PRANDTL NUMBER
ADVERSE PRESSURE GRADIENT(-0.275,-0.002) PLATE 18

DATE = 52273
UINF = 16.37 FT/SEC
TW-TINF= 23.8 F
CF/2 =0.00191
STANTON=0.00325
UTAU = 0.715
TTAU = 1.770

Y	Y/DELM	Y/DELH	YPLUS	VTPLUS	PRT	VT/V'T'	VT/Q'T'	UV	VT
0.069	0.032	0.030	23.5	0.274	1.26	0.312	0.081	-0.262	0.347
0.088	0.041	0.038	30.0	0.374	0.93	0.377	0.121	-0.271	0.473
0.128	0.060	0.055	43.6	0.490	0.71	0.541	0.188	-0.290	0.620
0.198	0.093	0.085	67.5	0.466	0.82	0.523	0.224	-0.322	0.590
0.298	0.139	0.128	101.5	0.405	1.04	0.507	0.230	-0.367	0.513
0.398	0.186	0.171	135.6	0.340	1.28	0.448	0.215	-0.410	0.431
0.598	0.280	0.257	203.7	0.355	1.35	0.499	0.249	-0.492	0.450
0.798	0.373	0.343	271.9	0.359	1.28	0.564	0.275	-0.524	0.455
0.998	0.467	0.429	340.0	0.389	1.20	0.686	0.334	-0.540	0.492
1.248	0.584	0.537	425.2	0.385	0.98	0.828	0.394	-0.513	0.488
1.498	0.701	0.644	510.3	0.318	0.97	0.808	0.392	-0.450	0.403
1.902	0.890	0.818	648.0	0.213	0.65	0.869	0.454	-0.216	0.270

TURBULENT PRANDTL NUMBER
ADVERSE PRESSURE GRADIENT(-0.275,-0.004) PLATE 18

DATE = 53173
UINF = 16.54 FT/SEC
TW-TINF= 23.0 F
CF/2 =0.00342
STANTON=0.00454
UTAU = 0.967
TTAU = 1.786

Y	Y/DELM	Y/DELH	YPLUS	VTPLUS	PRT	VT/V'T'	VT/Q'T'	UV	VT
0.069	0.049	0.060	31.6	0.140	1.21	0.264	0.075	-0.201	0.242
0.089	0.063	0.078	40.8	0.150	1.17	0.298	0.097	-0.211	0.259
0.119	0.084	0.104	54.5	0.166	1.07	0.319	0.131	-0.220	0.287
0.149	0.105	0.130	68.2	0.151	1.21	0.391	0.148	-0.227	0.260
0.199	0.141	0.174	91.1	0.151	1.24	0.389	0.181	-0.235	0.260
0.299	0.211	0.261	136.9	0.150	1.25	0.524	0.242	-0.242	0.259
0.399	0.282	0.348	182.7	0.157	1.18	0.600	0.298	-0.245	0.272
0.599	0.423	0.523	274.3	0.175	1.02	0.869	0.427	-0.244	0.303
0.799	0.564	0.697	365.9	0.138	1.18	0.878	0.429	-0.226	0.238
0.999	0.706	0.872	457.5	0.116	1.13	0.961	0.476	-0.186	0.200
1.299	0.917	1.134	594.9	0.069	0.82	0.999	0.555	-0.081	0.119